National Research Council Canada
Astronomy Technology Program

FEASIBILITY STUDY REPORT FOR THE NEXT GENERATION CFHT: II. TECHNICAL

Author: Kei Szeto

Date: 2012-11-23

Revision 2.2

TABLE OF CONTENTS

LIST OF FIGURES

LIST OF TABLES

ACRONYMS AND ABBREVIATIONS

ADC	Atmospheric Dispersion Corrector
AO	Adaptive optics
AR	Anti-Reflective
CCD	Charge Coupled Device
CFD	Computational Fluid Dynamics
CFHT	Canada-France-Hawaii Telescope
DSL	Dynamic Structures Limited
EE	Ensquared Energy or Encircled Energy
FOV	Field Of View
ELT	Extremely Large Telescope
FWHM	Full Width at Half Maximum
HIA	Herzberg Institute of Astrophysics
ICD	Interface Control Document
IQ	Image Quality
IR	Infrared
M1	Primary Mirror
M2	Secondary Mirror
M3	Tertiary Mirror
ngCFHT	Next Generation Canada-France-Hawaii Telescope
MIR	Mid-Infrared
NIR	Near-Infrared
NRC	National Research Council of Canada
OAP	Off-Axis Parabola
PSD	Power Spectral Density
PFS	Prime Focus Spectrograph
PSF	Point-Spread Function
QE	Quantum Efficiency
RMS	Root Mean Square
ROM	Order of Magnitude
RSS	Root Sum Square
SNR	Signal-to-Noise Ratio
TBD	To Be Determined
VPH	Volume Phase Holographic
WFC	Wide Field Corrector
WFE	Wavefront Error
WFOS	Wide Field Optical Spectrograph
WFS	Wavefront Sensor

EXECUTIVE SUMMARY

The next generation Canada-France-Hawaii Telescope (ngCFHT) is a proposed redevelopment of the existing 3.6m telescope to upgrade to a 10m-class facility with a mandate for dedicated spectroscopic observations. The science cases for such a facility are described in an accompanying document, *Feasibility Study Report for the Next Generation CFHT: I. Science,* and are used to set top level technical requirements. The science requires that ngCFHT have a 10-m aperture primary with a field of view of order 1.5 square degrees and good image quality. In a single set-up, it obtains spectra for up to 3200 objects simultaneously with complete coverage from 370-1300nm at a spectral resolution of R=2000. It also operates at higher spectral resolutions of R=6500 and R=20000, with up to 800 objects obtained simultaneously in two selectable grating dependent optical wavelength windows at the highest resolution setting.

We further ensure that the redevelopment process will not disturb the ground beyond what has already been done (this includes minimizing work at the summit by reusing the telescope and enclosure piers), and the new facility will stay within the current space envelope defined by CFHT. Technical and programmatic studies were initiated to explore the feasibility of constructing such a facility on the current CFHT site, and this report provides a summary of these studies and their main conclusions. The full reports are included as Appendices.

Studies were contracted to Dynamic Structures Limited, who constructed the CFHT telescope and enclosure, to investigate the load capacities of the existing telescope and enclosure piers and determine if they could support the new ngCFHT facility while meeting relevant design codes, and determine whether the new structure could be fully contained within the existing space envelope. The enclosure configuration is based on the Calotte design, selected due to its structural and operational efficiency, and its compactness. Results from DSL demonstrate that the ngCFHT facility will be able to successfully re-use the existing piers and meet design codes. In the case of telescope pier, no deficiency has been identified; in the case of the enclosure pier, new bracings should be added (a process that does not involve disturbing the exterior cladding). The entire ngCFHT enclosure will be able to match the existing CFHT envelope dimensions.

The optical designs for the major optical subsystems – telescope, feed optics and spectrograph(s) – have been investigated to ensure that they are fully demonstrated with existing technologies, are practical, and are affordable. For the telescope optical design, a wide field corrector and atmospheric dispersion corrector are additionally incorporated into the designs. A single mirror design is preferred both for its low risk and high throughput relative to two and three mirror options. All lenses are less than 1.2m diameter to ensure availability, and vignetting is shown to be zero on axis and be a maximum of 13% at the edge of the field. Options exist to reduce this value further. Numerous options exist for the feed optics, and high efficiency is achievable for the fiber-feed across the wavelength range, particularly if efforts are made to minimise the required length of the fiber. Note that the fiber-positioning technology has not been examined as part of these studies; the feasibility of this important subcomponent is currently being demonstrated in developments for other spectroscopic projects (e.g., the Subaru Prime Focus Spectrograph; PFS).

Several highly-multiplexed spectrograph designs are currently in development, particularly for operation at lower spectral resolutions. In order to provide the most stringent tests on the feasibility of the combination of spectral resolutions, wavelength windows and multiplexing required for ngCFHT, we develop a concept for a single instrument capable of all the observing modes. Particular focus is placed on high resolutions since here the technical challenges are greatest. The design that is presented is for a triple-resolution spectrograph that operates on the principal of pupil-slicing. This technique offers the flexibility to switch between different observing modes efficiently and which provides good performance in terms of image quality and throughput. In this design, two identical spectrographs are required to obtain the required multiplexing, and the throughput of the instrument is estimated to be 50% at peak (including optics and detectors). Alternative designs include the use of multiple spectrographs that operate at separate spectral resolutions, and we additionally consider the specific case of a PFS-style design for the low resolution mode.

A programmatic study was conducted by DSL to determine the cost and schedule for the CFHT deconstruction, structural retro-fit and ngCFHT construction. Work completed to date shows that the cost and telescope construction downtime, with a general contingency of 20%, are estimated to be USD68.2M and 33 months, respectively. Furthermore a study is ongoing by the WindEEE Research Institute to examine the aero-thermal characteristics of the ngCFHT dome in order to ensure dome-effects do not degrade the exquisite image quality that the Mauna Kea site provides. Results from the full report will be made publicly available soon after the completion of the preliminary study in November 2012.

Cost estimates are continually revised based on information available to date. The full cost of the design and construction of ngCFHT is currently estimated to be USD206.3M.

The feasibility studies summarized in this document and presented in the Appendices show that ngCFHT is technically viable and can be designed and constructed based on existing technologies. These findings should be used as a basis to advance the ngCFHT project to a full Conceptual Design Phase that involves all stakeholders.

1 THE NGCFHT CONCEPT

The Next Generation Canada-France-Hawaii Telescope is a concept to replace the existing 3.6m telescope with a 10m-class telescope on the same pier and within the same three-dimensional envelope. It will be equipped with a dedicated wide-field multi-object spectrograph capable of obtaining thousands of spectra simultaneously over a large field of view, at a range of spectral resolutions and operating over a very broad optical-near infrared wavelength range. This new and unique spectroscopic facility will fill the gap in optical-infrared capabilities that has emerged as a result of many new and proposed ambitious photometric and astrometric surveys for which there is currently no means of obtaining equivalently ambitious spectroscopic follow-up. ngCFHT will be the natural complement to these studies in the next decade. It will further enable independent transformational scientific programs that require large amounts of telescope time, in fields as diverse as the mapping of the interstellar medium, stellar astrophysics, near field cosmology and Gaia follow-up, extragalactic astronomy, and the nature of dark matter and dark energy.

An accompanying science report document *Feasibility Study Report for the Next Generation CFHT: I. Science* details the results from the science impact study of the proposed facility, and includes examples of the transformational science programs that ngCFHT will perform. This includes a discussion of top level science requirements and possible survey strategies. We refer the reader to this document for more details of all aspects of the scientific development of this concept.

In parallel with the scientific development, a feasibility study was initiated to address the key technical aspects and programmatic challenges of the ngCFHT concept, and to determine the achievability of the science requirements. Results from this study are detailed in this document.

1.1 Top level Requirements and Scope of the Feasibility Study

A summary of the science requirements that were developed is reproduced in Table 1 based on the science considerations detailed in the aforementioned science report. Importantly, additional requirements emerge as a result of the fact that ngCFHT will represent a “reusing” of a pre-existing facility. Thus, in order to facilitate the technical feasibility studies, the baseline ngCFHT configuration was considered within the context provided by the Office of Mauna Kea Management Mauna Kea Science Reserve Master Plan. Here, the redevelopment of CFHT is classified as a Type I facility development. In order to best adhere to the guidelines in this document and the principles that it encapsulates, additional constraints on the new ngCFHT facility are adopted:

- It will not disturb the ground beyond what has already been done
- It will stay within the current CFHT space envelope
- Work at the summit will be minimized by reusing the telescope and enclosure piers

Table 1. ngCFHT science requirements

	ISM	Stellar Astrophysics		Milky Way / Galactic Archaeology			Local Group		Nearby galaxies	
Parameter	*3D mapping*	*Time domain*	*Rare objects*	*Chemodynamics of the stellar halo*	*Disk evolution*	*Bulge science*	*Global chemodynamics of M31/M33*	*Structure of dwarf galaxies*	*Structure of DM halos*	*Rich clusters*
Spectral resolutions	≥ 20000	≥ 20000	~ 20000	6000, 20000	6000, 20000	≥ 20000	6000	6000	2000	2000
Magnitude limit (AB) §	g=16	g=16	g=19.5	g=21.5, 19.5	g=21.5, 19.5	g=18	g=23	g=23	i=22	r=22
Wavelength range (µm)	0.38 - 0.88	0.37 - 0.95	0.37 - 0.89	0.37 - 0.90	0.37 - 0.90	0.37 - 0.90	0.4 - 0.95	0.4 - 0.95	0.37 - 1.3	0.37 - 1.3
(complete wavelength coverage required?)										
Target density (# / sq. degree)	~500	1300	rare *	~500 ♮	$> 10^4$	>1000	~ 1000s	~ 1000s	1400	$\sim 10^4$
Survey area (sq. degrees)	5000 - 10000	~ 100	10000	10000	10000	~ 200	350	1 <--> 10	1000	30
# science objects	$> 10^6$	$> 10^5$	n x 10^6 *	n x 10^6	n x 10^6	$> 10^5$	n x 10^5	n x 10^3	5 x 10^5	20 cluster fields
Velocity accuracy (km/s)	n/a	*0.15 (goal)*	< 2	< 2	< 2	< 2	< 5	< 5	15 - 30	15 - 30
Survey synergies	Gaia, multi-wavelength surveys	Kepler, Gaia, AAT/HERMES, SDSS, PS1 ...		Gaia, SDSS, PS1, AAT/HERMES, LSST...large number of current and upcoming photometric+spectroscopic surveys			Dedicated pre-imaging surveys (e.g. CFHT MegaCam, Subaru HSC...)		eRosita, PS1, ASKAP, GAMA, GALEX, LSST, Euclid...	
Other notes	Early-type stars preferred	Time resolved spectroscopy of Kepler fields (115 sq. degrees)		RV accuracy to match that of Gaia transverse velocities at the faint end. Extension to NIR and higher resolution desirable for bulge science			Foreground contamination likely high in outer regions of galaxies (identify using gravity sensitive features)		Study of nearest galaxies (e.g., Virgo cluster) could additionally use R ~ 6000	

	Galaxy Evolution			IGM		QSOs / AGN		Cosmology	
Parameter	*Environment*	*Clustering/halo models*	*Epoch of formation*	*Lyman alpha forest*	*DLAs*	*Clustering*	*Reverberation mapping*	*BAO/RSD*	*Cosmological clusters*
Spectral resolutions	2000	2000	2000	2000 - 20000	2000 - 20000	2000	≤ 2000	2000	2000
Magnitude limit (AB) §	i=23.5	i=24.25	i=26	B ~ 20	i ~ 19.5	i=23.5	g=22.95	g=23.7	i=23.5
Wavelength range (µm)	0.37 - 1.3	0.37 - 1.3	0.37 - 1.3	0.37 - 1.3	0.37 - 1.3	0.37 - 1.3	0.37 - 1.3	0.37 - 1.3	0.37 - 1.3
(complete wavelength coverage required?)	yes	yes	yes	desirable	desirable	desirable	desirable	yes	yes
Target density (# / sq. degree)	~3 x 10^4	~8 x 10^4	> 10^5	1 - 10s	few	~200	~ 350	tracer dependant	>10^4
Survey area (sq. degrees)	4300	100	1.5	1000 - 10000	1000 - 10000	4300	1.5	10000	~750
# science objects	~ 7 x 10^5	~ 2 x 10^6	~ 30000	~ 1000	~1000s	~ 5 x 10^5	~ 500	n x 10^6	~ 500 clusters
Velocity accuracy (km/s)	resolution limited	resolution limited	resolution limited	n/a	n/a	resolution limited	resolution limited	resolution limited	resolution limited
Survey synergies	SDSS, LSST, PS1, DES, Euclid, DEEP2, zCOSMOS,...			SDSS, VLT UVES, Keck HIRES, ...		SDSS, CFHTLS, Plank, Herschel, SKA pathfinders, Chandra, eRosita, Gaia, ...		eRosita, PS1, Euclid, LSST, ASKAP, Planck...	
Other notes	Study galaxies over seven different epochs between 0.5 < z < 1.5 each with the same statistical power as SDSS			High resolution for chemical abundance analysis; see also Cosmology/BAO		Deep field same as for Galaxy Evolution study? High resolution also useful (absorbers, AGN feedback)		BAO calculations can be made for multiple source populations (LRGs, ELGs, Lyα forest, QSOs...)	

§ magnitude limits that drive facility requirements (bold, red font) correspond to SNR = 5 - 10 (point source detection limit)

* rare objects (e.g., white dwarfs) will be a small fraction of the number of stars targetted in a single field (e.g., expect ~8 white dwarfs per NFCFHT field of view)

♮ measured at the North Galactic Cap for g ≤ 21

Combining these principles with the high level science requirements that have emerged from the science report leads to the top level baseline technical requirements for ngCFHT detailed in

Table 2. These requirements form the basis for the scope and trade studies described in this report.

Table 2. Top level baseline requirements

Aperture	10 m (segmented)
Field of View (FOV)	1.5 deg^2 (hexagonal)
Wavelength Range	370 to 1300 nm
Telescope Image Quality (†)	EE80D < 0.45" (FWHM ~ 0.3")
Total System Throughput (*)	>25% over 90% of the wavelength range >30% peak (goal)
Number of Fibers	3,200 (low + medium resolution) 800 (high resolution)
Spectral Resolution	R2,000 (370-1300 nm) R6,500 (370−510 nm & 770−910 nm) R20,000 (420-620 nm)

(†)refers to the telescope optical quality without atmospheric or dome/mirror seeing, as seen at fiber entrance, but including nominal image quality, residual atmospheric dispersion, manufacturing, alignment and control errors. This value will be convolved with the observed seeing profile to give the total object PSF. A conversion factor from EE80D and FWHM assume a Gaussian profile.
(*)includes telescope optics, wide field corrector optics, ADC optics, geometrical vignetting, fiber train, spectrograph optics, and detectors. No entrance losses (strongly seeing dependent) or atmospheric extinction (zenith dependent) are taken into account. When multiplied by these two last factors, the observed flux can be computed.

Examination of the above requirements and constraints resulted in the identification of six technical study areas and two programmatic areas that together set the scope of the feasibility study. Specifically, these are:

i. Determination of load capacity of telescope pier
ii. Determination of load capacity of enclosure pier
iii. Definition of telescope and enclosure configuration
iv. Development of telescope and "feed" optics
v. Development of spectrograph feasibility design
vi. Prediction of aero-thermal performance
vii. Facility redevelopment study (programmatic)
viii. Cost estimate summary (programmatic)

The following baseline ngCFHT facility configuration is utilized to facilitate the technical studies:

- "Keck-like" 10m segmented mirror telescope structure
- Subaru "PFS-like" fiber-fed system with multi-object pickoffs at telescope prime focus and spectrograph(s) located within the telescope pier
- Calotte style enclosure matching the exterior dimensions of the current CFHT dome

In this report, information of the technical studies is organized into three parts capturing the key findings and highlights. Each of the detailed feasibility reports is included in full as appendices (Table 3):

- Appendices A & B summarize the finding and recommendations of the load capacity studies, and proposes the basic facility configuration for the telescope and enclosure compatible with the redevelopment principles;
- Appendices C & D describe the optical design studies conducted for the facility, and includes (i) the telescope system optical configuration (ii) fiber-feed and spectrograph concepts along with the design space explored with alternate designs considered (including redeployment of the Subaru Prime Focus Spectrograph, PFS)
- Appendix E describes the planned aero-thermal work using computational fluid dynamic simulation to determine the feasibility of the proposed enclosure configuration based on the velocity and temperature profiles within the dome under median observing conditions.

The programmatic study to evaluate the cost and schedule of the redevelopment of the CFHT facility is underway. The revitalization study is composed of three separate steps:

- Deconstruction of the CFHT facility
- Structural retrofit of the telescope and enclosure piers
- Construction of the ngCFHT facility

The detailed report of the programmatic study is attached in Appendix F (Table 3) and the findings are summarized in this report and incorporated in the preliminary cost estimate for the overall ngCFHT facility.

The final section of this report summarizes suggestions for future work that have been identified as a result of this feasibility study.

Table 3. Guide to the Appendices

Study Area	Appendix
Determination of load capacity of telescope pier	APPENDIX A. NEXT GENERATION CANADA-FRANCE-HAWAII TELESCOPE PIER BUILDING EVALUATION
Determination of load capacity of enclosure pier	APPENDIX B. NGCFHT TELESCOPE AND ENCLOSURE CONFIGURATION AND OUTER PIER CAPACITY STUDY
Definition of telescope and enclosure configuration	APPENDIX B. NGCFHT TELESCOPE AND ENCLOSURE CONFIGURATION AND OUTER PIER CAPACITY STUDY
Development of telescope and “feed” optics	APPENDIX C. NGCFHT TELESCOPE OPTICAL DESIGN
Development of spectrograph feasibility design	APPENDIX D. NGCFHT SPECTROGRAPH OPTICAL DESIGN
Prediction of aero-thermal performance	APPENDIX E. NGCFHT VENT SYSTEM CFD STUDY STATEMENT OF WORK
Facility redevelopment study	APPENDIX F. PROGRAMMATIC STUDY FOR UPGRADE OF TELESCOPE
Supplemental information	APPENDIX G. NGCFHT PRELIMINARY OPTICAL DESIGN CONCEPTS FOR THE 2010 CFHT USERS MEETING IN TAIPEI

2 FEASIBILITY OF REUSING THE TELESCOPE AND ENCLOSURE PIERS

APPENDIX A. NEXT GENERATION CANADA-FRANCE-HAWAII-TELESCOPE PIER BUILDING EVALUATION
APPENDIX B. NGCFHT TELESCOPE AND ENCLOSURE CONFIGURATION AND OUTER PIER CAPACITY STUDY

To adhere to the principles of the Office of Mauna Kea Management Mauna Kea Science Reserve Master Plan, it is important that any redevelopment of CFHT does not disturb the ground any more than has already been done, and that ngCFHT remains within the same three dimensional envelope as CFHT. Thus it is key to ensure that ngCFHT is able to utilise the same telescope and enclosure piers as CFHT. Given the proposed baseline configuration, the objective of the load capacity studies is to determine the feasibility to reuse the piers to support the new facility by evaluating the load bearing capacity of the existing CFHT telescope and enclosure piers based on modern design codes.

Specifically, the following design codes were utilized to determine the design loads and engineering requirements for the existing concrete telescope pier and steel enclosure pier (Figure 1):

- *ASCE-7, Minimum Design Loads of Buildings and Other Structures,* American Society of Civil Engineers, Reston, (2010)
- *ACI 318-08, Building Code Requirements for Structural Concrete and Commentary,* American Concrete Institute, Farmington Hills (2008)
- *AISC 360-05, Specification for Structural Steel Buildings,* American Institute of Steel Construction, Chicago (2005)

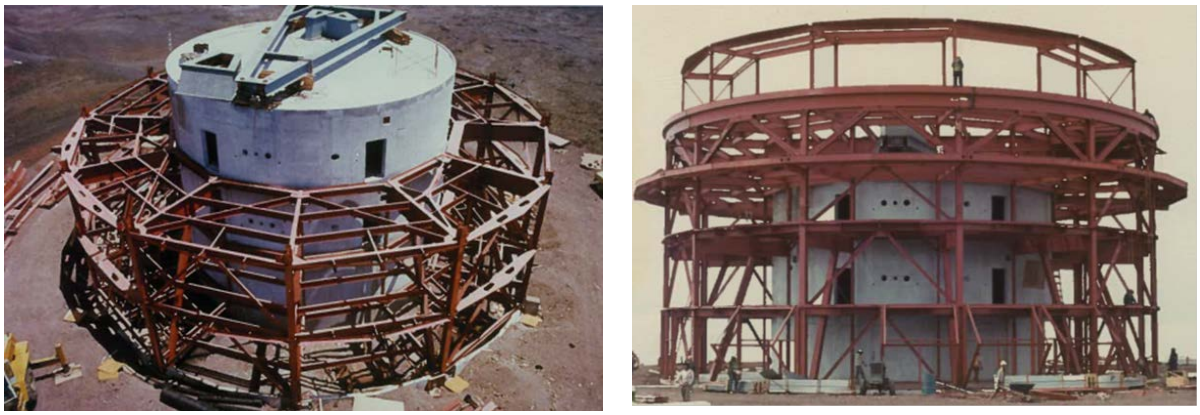

Figure 1. Canada France Hawaii Telescope pier under construction – the inner cylindrical concrete building is the telescope pier and the outer ring steel structure is the enclosure pier.

For the purpose of the load capacity studies, the basic telescope configuration assumed is a 10 m diameter f/2 segmented primary mirror. The height of the telescope from the M1 vertex to the top is 19.4m, including the length of the wide field corrector and prime focus components of the spectrograph (Figure 2). In the baseline design it is assumed the

telescope design is similar to the 10 m Keck telescope minus the tertiary mirror and Nasmyth platforms.

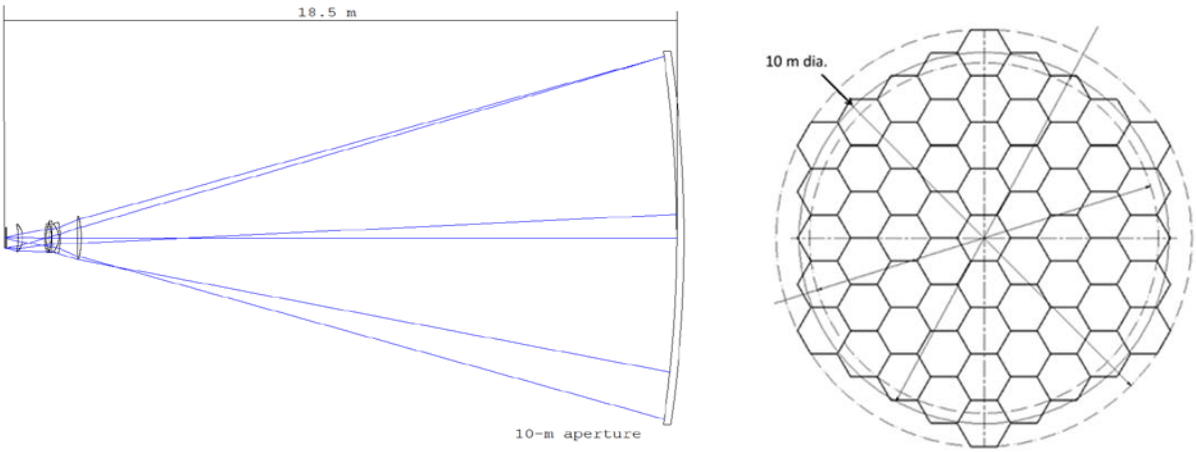

Figure 2. Telescope configuration assumed for the load capacity studies – optical design without spectrograph (left) and primary mirror layout with 60 hexagonal segments of 1.44 m in size (right).

The enclosure configuration is based on the Calotte design. The Calotte design is selected due to its structural and operational efficiency[1] and its compactness provides the best possible match to the existing enclosure size and mass than a conventional dome with the same 10 m aperture opening. The proposed enclosure configuration also incorporates realistic space allowances for interior insulation and the mechanical systems required for dome rotation and servicing of the M1 segments and spectrograph components at prime focus (Figure 3).

[1] The Thirty Meter Telescope Project has conducted extensive comparative studies among alternate enclosure designs: Calotte, dome-shutter (CFHT and Keck), and carousel (Subaru), and selected the Calotte design based on its structural efficiency, construction considerations and operating costs.

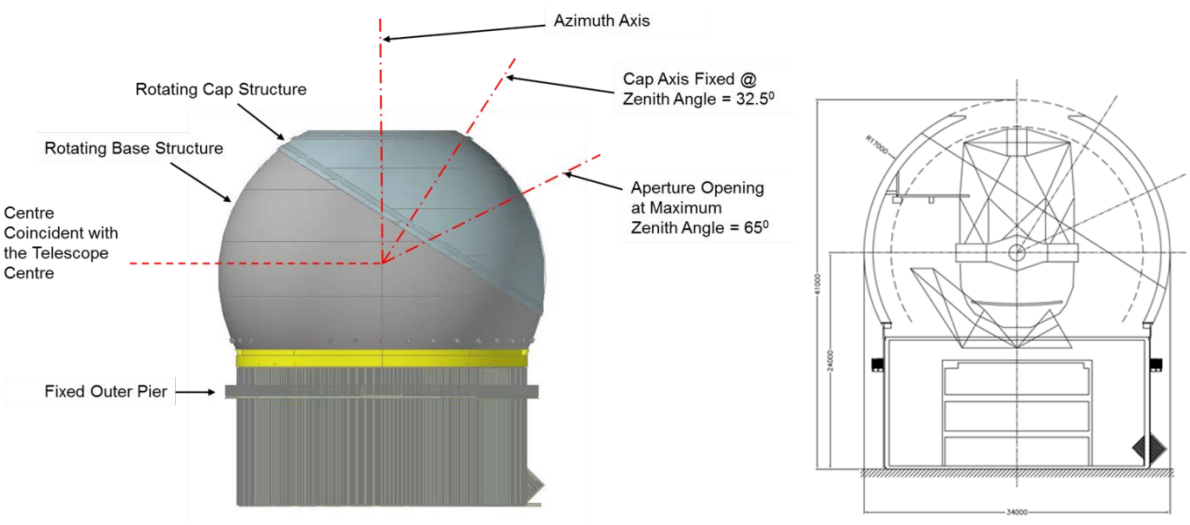

Figure 3. Enclosure configuration shown at zenith pointing – mechanical bogie and drive systems facilitate base and cap rotations allowing the enclosure to point from 0° to 65° zenith (left) and cross section view of the enclosure showing a 1 m wall thickness, including interior insulation, and the enclosure mounted crane system for servicing of telescope subsystems during operation (right).

2.1 Load analyses

For the load analysis, the structural components and mass of the existing piers were derived from the original CFHT construction drawings. The new telescope mass is estimated to be 270 tons (the same as the Keck telescope), and this is a 6% increase from the current mass. The combined telescope and pier system mass is 1,613 tons. The estimated enclosure mass is 510 tons, a 32% increase from the current mass. The combined enclosure and pier system mass is 1,403 tons.

Each combined structural system was modeled separately in the SAP2000 finite element analysis (FEA) software. Spring elements were incorporated to represent the soil stiffness and the mechanical connections between the supported (telescope or enclosure) mass and the pier (Figure 4). The spring element stiffnesses were selected to account for the dynamic interactions in the model analysis for the seismic load assessments.

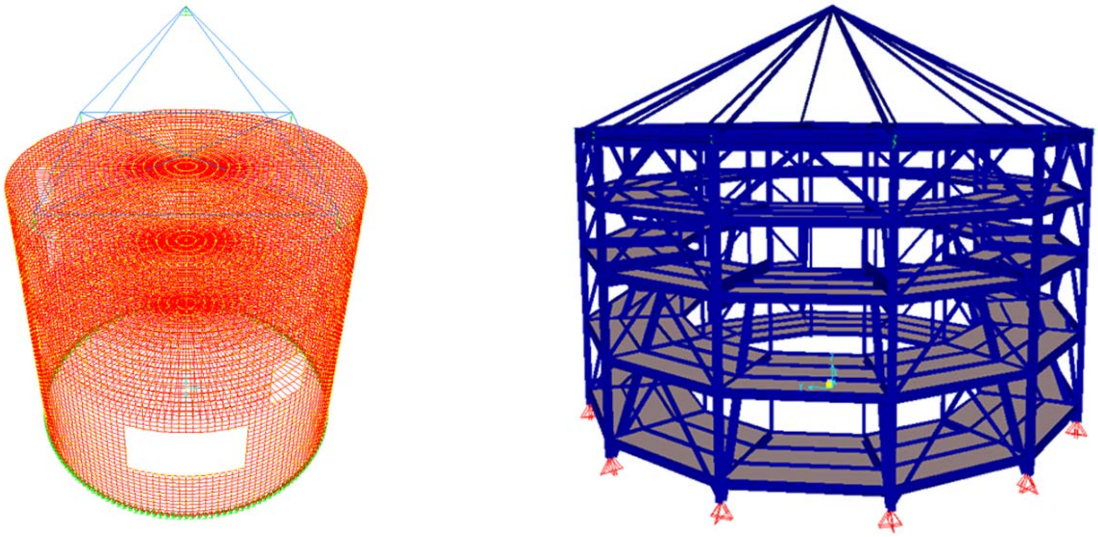

Figure 4. Finite element models – telescope pier system with the telescope represented as a lumped mass at the correct centre-of-gravity (CG) position located by a beam element frame and connected to the inner pier through spring elements (left); similarly the enclosure is also represented as a lumped mass at the correct CG position located by a pyramidal frame and connected to the outer pier through spring elements (right).

Generally, the load capacities of the piers were determined based on load cases with dead, live, seismic and environmental loads and their combinations specified according to the design codes. However, environmental loads (snow, ice and wind) were applied to the enclosure pier analysis only.

2.2 Results

Based on the load conditions, the capacity of each structural element was verified. Table 4 summarizes the findings of the load capacity studies. For the telescope pier, all elements including the soil[2] meet the load requirements of the new telescope. For the enclosure pier, all elements except the bracing meet the load requirements.

Table 4. Summary findings of the pier capacity studies

Telescope Pier		Enclosure Pier		Comment
Wall	√	Beam	√	Meet all load combinations
Slab	√	Column	√	Meet all load combinations
Footing	√	Footing	√	Meet all load combinations
Soil	√			Although the soil bearing capacity under earthquake loads is exceeded by 33%, the dynamic nature of these loadings allows an increase of capacity by one-third[2]
		Soil	√	Meet all load combinations
		Bracing	X	Seismic capacity is 24% of requirement

The enclosure pier bracing does not meet the increased seismic requirements in the newer design codes. However, cost effective options are available to reinforce the pier without

[2] See Appendix F for detail

altering the exterior appearance. The reinforcement option is outlined in the facility redevelopment process discussed in Section 5.1.

2.3 Geometry of the proposed facility configuration

Figure 5 shows the cross section views, based on actual CAD models of the ngCFHT and CFHT facilities and confirms that a Keck-size telescope and Calotte enclosure will fit on both of the the existing piers respectively. Figure 5 also compares the external dimensions of the new enclosure against the current enclosure. Presently, the proposed enclosure is about 7% taller and 3% larger in diameter. With further optimization of the telescope and enclosure geometries, we are confident that the new enclosure can be reduced to match the current enclosure dimensions, if necessary. For example, an f/1.83 segmented primary mirror is proposed in the telescope system optical design section (in contrast to the f/2 design assumed for this study) that will shorten the length of the telescope structure and the height of the enclosure.

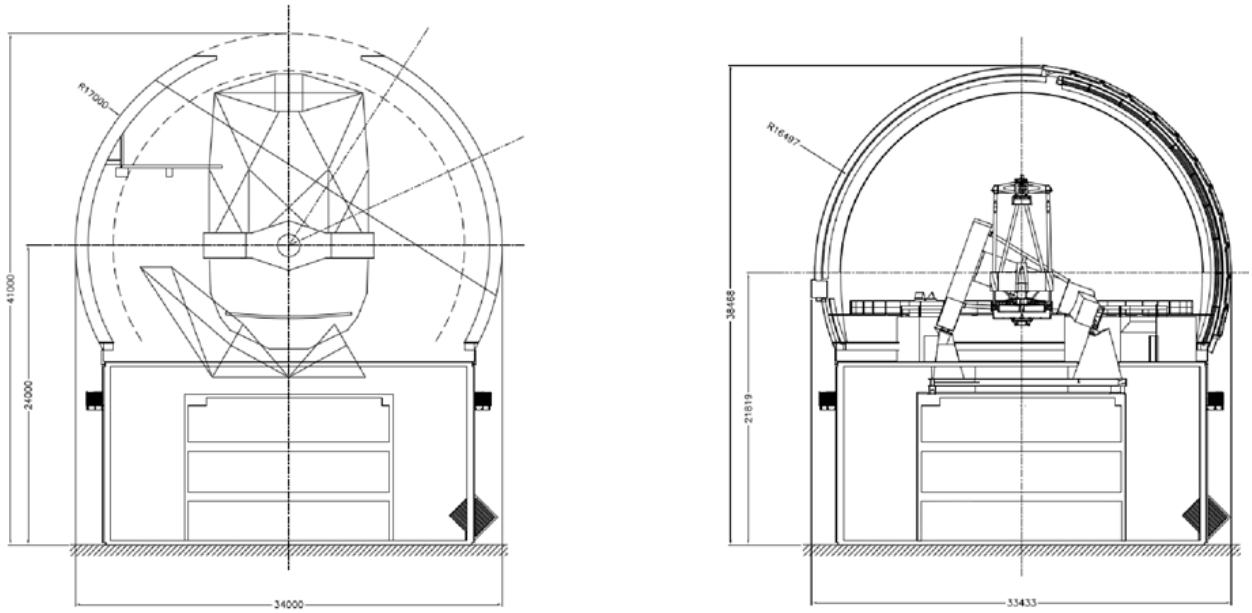

Figure 5. Cross section views and exterior dimensions of the proposed ngCFHT facility (left) and current CFHT facility (right).

2.4 Summary

The load capacity studies did not identify major deficiencies that require significant structural modifications or dimensional mismatch indicating that the proposed ngCFHT facility is geometrically incompatible with the current piers. From the feasibility standpoint, we conclude that the current telescope and enclosure piers are able to accommodate the new ngCFHT facility, structurally and geometrically. In further development of the ngCFHT project, the reinforcement options for the piers should be examined further, in addition to optimising the enclosure dimensions for the finalised telescope design.

3 DEVELOPMENT OF FEASIBLE OPTICAL DESIGNS

The objectives of the optical design studies are to assess the feasibility of optical designs that meet the performance requirements for the telescope, fiber-feed and spectrograph. In particular, we want to determine the current level of technologies involved, including programmatic considerations such as availability of potential vendors and cost/schedule risks associated with supply and fabrication.

This section summarises feasibility design considerations for the three main optical subsystems:

- Telescope optical configuration (Section 3.1)
- Fibre feed (Section 3.2)
- Spectrograph optical design (Section 3.3)

3.1 Telescope optical configuration

APPENDIX C. NGCFHT TELESCOPE OPTICAL DESIGN

The goal of this study is to determine the optimal telescope configuration that best meets requirements and is able to fit within the enclosure with minimal programmatic risks. We adopt a comparative approach and consider a single-mirror configuration (Figure 6), a two-mirror design (Figure 7) and a three-mirror design (Figure 8). This approach allows us to explore the design space and understand the strength and limitations of each configuration, and to eliminate design solutions that are unworkable. We incorporate additional optics into each design to produce a telescope system that efficiently feeds fibers across the telescope focal plane. Specifically, we consider

- A wide field corrector (WFC) to maintain image quality and telecentricity and to reimage the input beam to the required fiber-feed input focal ratio
- An atmospheric dispersion corrector (ADC) to maintain the requisite image size given the wide wavelength bandwidth

The feasibility studies intentionally leveraged and adopted existing optical design work of similar astronomical systems for the ngCFHT facility. The optical design requirements and considerations adopted to direct the telescope design are:

- Average image quality <0.45 arcsec EE80 diameter at all zenith angles
- Maximum zenith angle: 60°
- Residual dispersion after ADC correction <0.2 arcsec
- Telecentric fiber feed
- Small field curvature allowed as a design parameter to facilitate optical system optimization

3.1.1 Single-mirror configuration

The focal ratio of the telescope primary mirror design is f/1.83 in order to comply with the enclosure height limits which restricts the f-ratio to <f/2. Both WFC and ADC optics are incorporated in the telescope system optical design to maximize performance. The configuration is a “4+2” lens design (Figure 6), which is a simplified design over the

Subaru Hyper-Suprime Cam corrector, with four powered elements for field correction and two elements for atmospheric correction. The optic performance of field correctors with four, five and six powered elements was analyzed and compared in the design study; the four-element design was found to be optimal in terms of image quality, cost and complexity. The ADC lens pair provides correction with a lateral shift of <30 mm at the maximum zenith angle of 60°.

In order to ensure the availability of quality lens blanks, a conservative maximum lens diameter of 1.2 m was considered. Asphericity, if required, was allowed on one side of the lenses only, with maximum aspherical departure up to few mm, as successfully proven on Subaru's Hyper Suprime-Cam wide field corrector lenses.

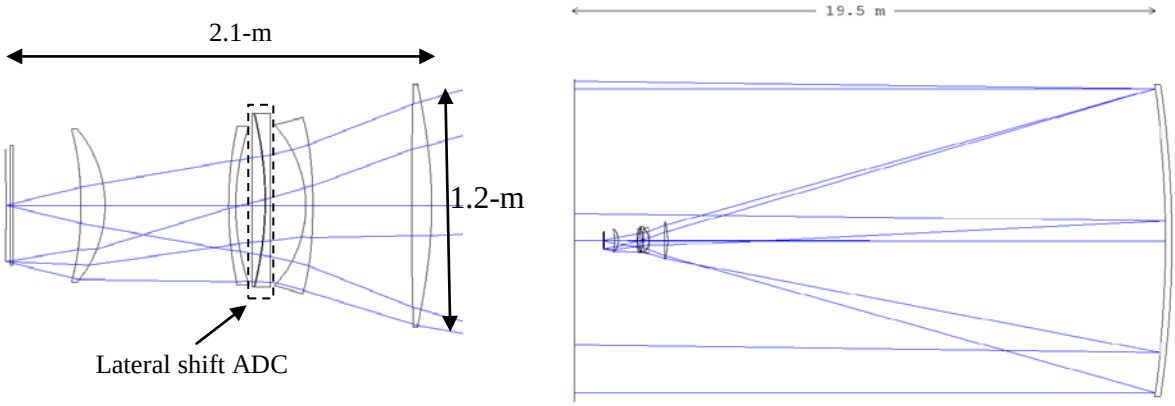

Figure 6. Single-mirror design with f/1.83 10 m diameter M1, WFC and ADC.

Fused silica is the preferred lens material for most of the lenses as large blanks with good homogeneity are available. Moreover, this material provides high transmission over the whole wavelength range. In order to reduce cost but maintain UV transmittance, i-line glasses are assumed. However, their performance in the NIR needs to be ratified based on the overall science requirements before the WFC glass choice can be finalised.

With the conservative 1.2 m diameter constraint, vignetting increases linearly from zero on-axis to 13% at the edge of the field. By increasing the maximum diameter to 1.35 m for the first lens element the vignetting can be reduced to 0% at the edge of the field.

3.1.2 Two-mirror configuration

The motivations for considering the two-mirror design are the advantages of compact telescope height, simplified field corrector optics and shorter fiber-feed length for the spectrograph as the focal plane is located closer to the primary mirror (Figure 7).

The two-mirror design uses a 10 m diameter segmented primary mirror and a convex hyperbolic secondary mirror with a circular clear aperture of 2.4 m. The lens design is a "3+2" configuration with a three-element field corrector and a two-element counter-rotating ADC incorporated between the 2nd and 3rd corrector lens elements. All refractive elements are less than 1.2 m in diameter.

The spectrograph fiber-feed can be routed through either the hole of the primary mirror to the bench mounted spectrograph location or along the elevation axis to two "Nasmyth-like platforms" on the side of the telescope, where the spectrographs could be installed. This alternative location would enable a short fiber length that would maximize UV throughput. A considerable drawback with this two mirror configuration, however, is the obscuration generated by the secondary mirror and the associated support structure, which is expected to be 13% over the telescope aperture.

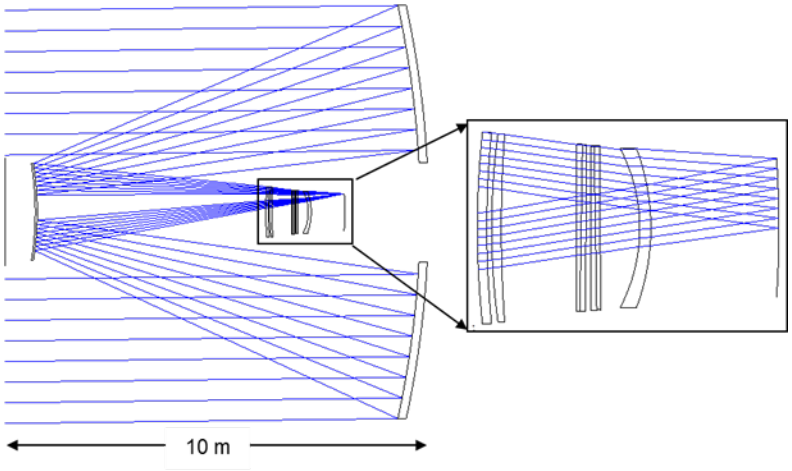

Figure 7. Two-mirror design with 10 m diameter M1, 2.4 m diameter M2, WFC and ADC - a very compact telescope length of 10 m is attained.

3.1.3 Three-mirror configuration[3]

The motivation for the investigation of the three-mirror design is to examine an alternative optical design where the field of view is not governed by the size of refractive corrective optics but only by the optical aberrations. A three mirror anastigmat (Figure 8) design was explored with the LSST design as the starting point, but without incorporating an ADC design at the focal plane behind the secondary mirror. To maintain practicality for mirror fabrication, this concept assumed the same LSST mirror polishing process by which two curvatures are generated on the same 8.36 m diameter mirror substrate. The central obstruction of this configuration is 4m so the effective unobstructed aperture is only 7.34 m. The small aperture imposes major limitations on system throughout and scientific efficiency.

Due the latter, the three-mirror configuration is not considered a contender for the ngCFHT. However, it does have a respectable A-Omega value of 207 m^{2}-deg^{2} and could be scientifically compelling for others astronomy programs, but not for ngCFHT.

[3] The three-mirror design is described in Appendix G. ngCFHT Preliminary Optical Design Concepts for the 2010 CFHT users meeting in Taipei.

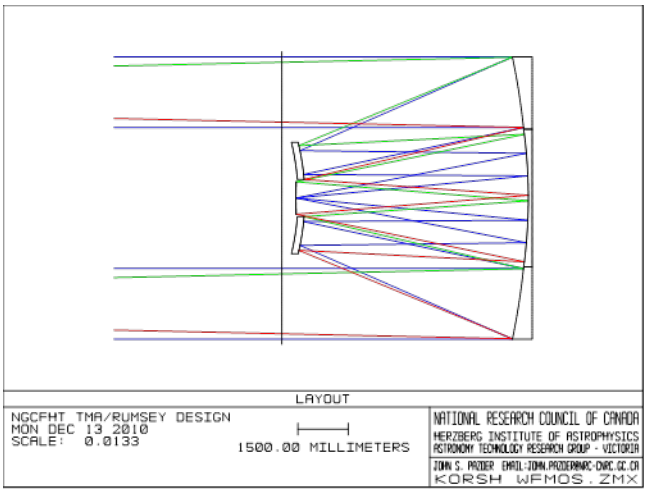

Figure 8. Three-mirror design with 8.36 m diameter M1 but this design is not considered a contender.

3.1.4 Additional optical items considered

The feasibility of additional optical items was examined, namely the primary mirror segment size, reflective mirror coating and anti-reflection coating.

3.1.4.1 Primary mirror segment

A hexagonal 1.45 m (corner to corner) size segment is adopted for the 10 m segmented M1. Technical feasibility of produced M1 segment economically and efficiently has been demonstrated by the current ELT projects such that we can leverage on their segment development work.

3.1.4.2 Available Coatings

For optimal UV throughput, aluminum coating is preferred for the mirror even though the average reflectivity over the wavelength range is lower than the Gemini's protected silver coating. A Solgel/MgF2 anti-reflection coating with reflectivity <1% is available for the refractive optical elements.

Further trade study is required to finalize the specifics on mirror coating which will be based on scientific and operational considerations. Regardless of the final selection, technologies for deposition of both reflective coatings and anti-reflection coating are feasible and well established.

3.1.5 Summary of telescope optical design

The primary design parameters and performance characteristics of the two feasible telescope optical designs (the one and two mirror systems) are summarized in Table 5.

Table 5. Properties of the two telescope optical designs.

Design	Aperture Size, m	Overall F-Ratio	Plate Scale, arcsec/mm	FoV, deg^2	Vignetting, %	EE80 diam. (*), arcsec	Comment
One-Mirror	M1: 10	f/2.1	102	1.5	0% on-axis 13% max off-axis	<0.35 @ 0° zenith <0.45 @ 60° zenith	Average over the FoV
Two-Mirror	M1: 10 M2: 2.4	f/3.6	175	1.4	13% constant across the telescope aperture	<0.22 @ 0° zenith <0.39 @ 60° zenith	% vignetting based on a central obscuration of 3.6 m dia.

*Image quality includes telescope optics, WFC and ADC residual.

The equivalent effective telescope collecting area accounting for transmission losses due to mirror reflections, lens and prism internal absorption, air-glass reflections, and telescope vignetting are compared in Figure 9 for the first two telescope configurations examined. Based on the effective collecting area achieved, the baseline one-mirror design is preferred by virtue of its higher overall efficiency. Moreover because of the additional large secondary mirror system, the two-mirror design is considered undesirable due to the added cost and the associated fabrication risks when compared with the single-mirror design.

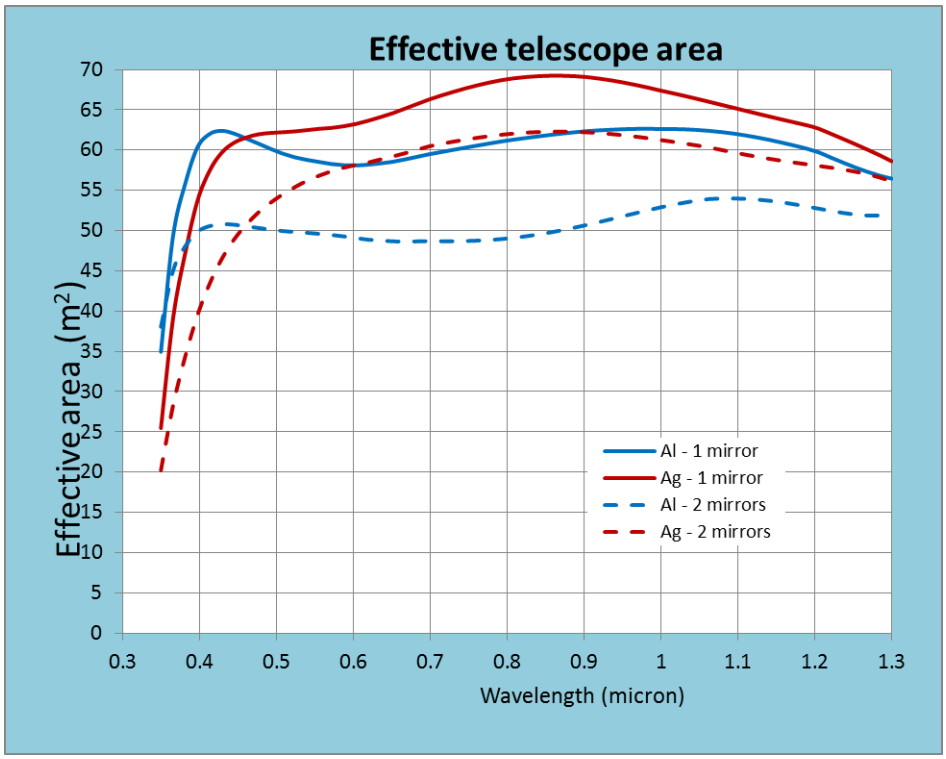

Figure 9. Comparison of equivalent telescope collection area delivered for the two telescope configurations discounted for all losses in the telescope optical system.

3.2 Fiber-feed system

3.2.1 Fiber diameter

The diameter of the fiber projected on the sky should be well matched to the typical astronomical source diameter in arcseconds. While larger fibers sample a larger fraction of light from the source, they also sample a larger amount of flux from the sky. The increasing sky flux is particularly problematic for faint targets. Figure 10 demonstrates this by showing the relative Signal-to-Noise Ratio (SNR) obtained as a function of projected fiber diameter for two different IQ conditions, for point-source targets of different luminosities relative to the sky. Here, the only contributions to the S/N are from the target and the sky. Fiber diameters of less than 1 arcsecond are ideal for observing faint targets while taking advantage of the excellent seeing conditions possible on Mauna Kea. Larger fibers are better suited for bright targets and/or poorer seeing conditions and for extended sources. Note that Figure 10 does not incorporate losses due to possible positioning errors.

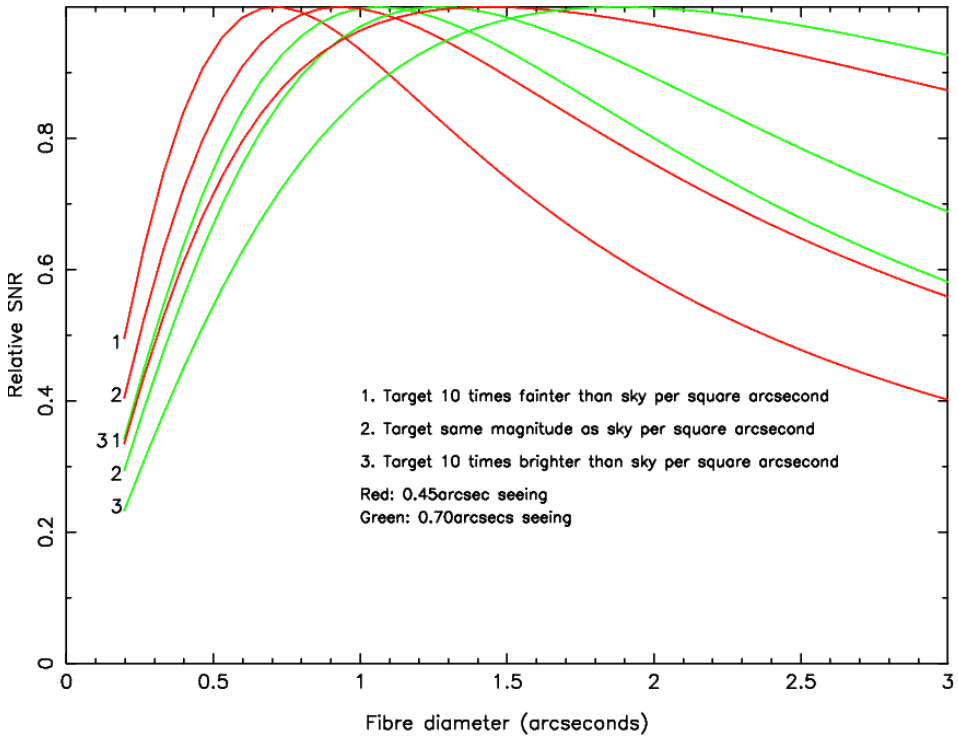

Figure 10. Relative signal to noise ratio vs. fiber diameter.

In Section 3.3, we investigate a spectrograph design concept to examine the overall feasibility of the combination of multiplexing, wavelength range and spectral resolution required by the ngCFHT science considerations. One of the most demanding aspects of this design is obtaining the high resolution observing mode. With this consideration in mind, we proceed with the rest of this feasibility study with 0.9arcsec fibers; this is a reasonable choice based on the considerations described above, and it facilitates obtaining the highest resolution modes. The final value of the fiber diameter that is adopted may be larger, to make it better suited to median seeing conditions and/or extended (extragalactic) sources. We anticipate that the spectrograph design presented could be modified to operate with a large fiber diameter, and that other concepts could be developed as appropriate. As a baseline to demonstrate general feasibility, the current choice of fiber diameter is reasonable.

3.2.2 Fiber transmission

The primary design consideration for the fiber-feed to the spectrograph is to maximize throughput over the wavelength range required. The major contributors specific to fiber throughput losses are focal ratio degradation (FRD) and internal absorption. Consultations with one of the leading fiber vendors, Polymicro Technologies, recommended maintaining an input beam f-ratio of slower than f/2.3 for conventional fiber in order to minimize FRD loss. However, custom fibers are available from Polymicro Technologies to accommodate input f-ratio as fast as f/1.85 without significant FRD effect.

In addition, good UV throughput is feasible using the Polymicro FBP fiber which offers excellent throughput over a broad wavelength band. Figure 11 shows the Polymicro FBP

fiber transmission for different fiber lengths over the wavelength range required. In order to minimize overall transmission loss, it is desirable to keep the fiber-feed length to <50 m (with a goal of <35 m). We conclude that there will be several feasible options for the ngCFHT fiber feed that ensure good or excellent throughput across the desired wavelength range.

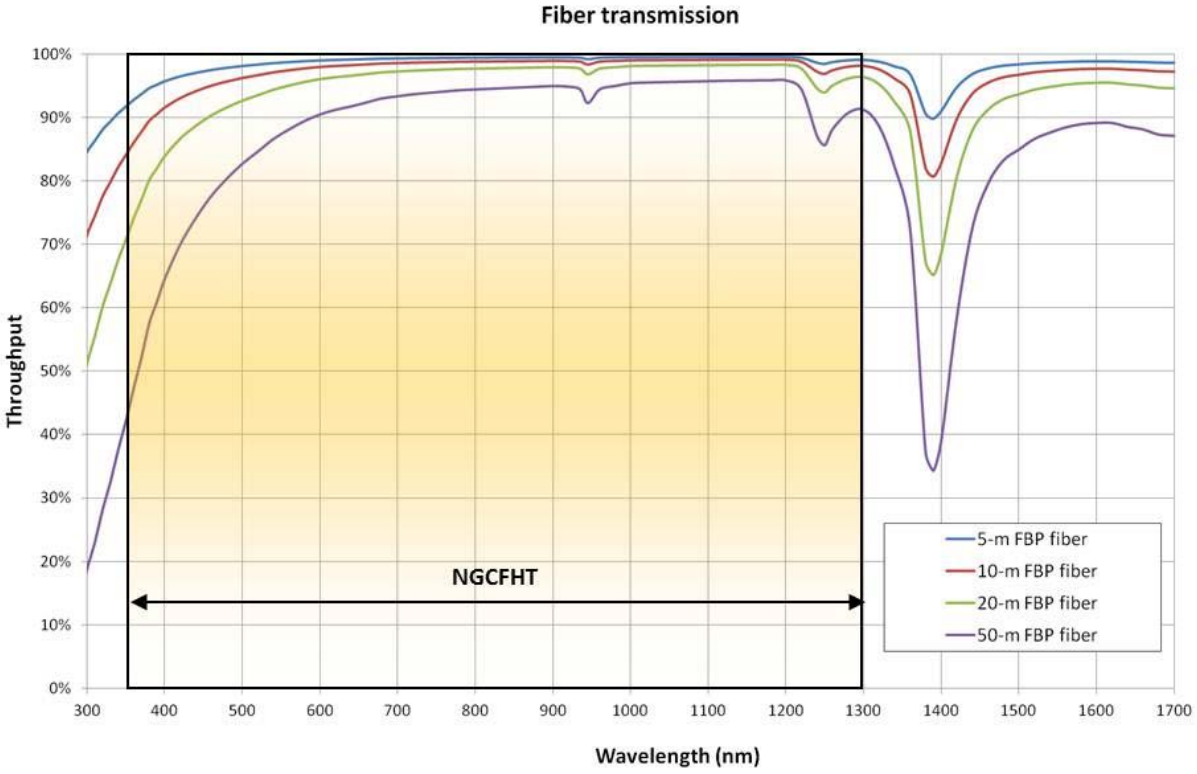

Figure 11. Polymicro FBP fiber transmission for different fiber-feed lengths across the ngCFHT wavelength range.

3.3 Fiber-fed spectrograph

The objective of the fiber-fed spectrograph study is to demonstrate the design and feasibility of the bench mounted spectrograph. Several highly multiplexed spectrograph designs have been or are being developed (e.g. Subaru/PFS, AAT/HERMES, 4MOST). The combination of the multiplexing, wavelength coverage and spectral resolutions required for ngCFHT are a particular challenge. Several design solutions exist; for example three independent spectrographs, each designed to work at a specific resolution; two spectrographs, where one works at double-resolution; or a single spectrograph that operates at all three resolution settings. We note that several double-resolution spectrograph designs have been developed and can likely be adapted for use on ngCFHT. In this respect, we consider in Section 3.4 the feasibility of redeploying the complete PFS system, including the Prime Focus Unit, for ngCFHT. We also consider redeploying only the PFS spectrograph (if the PFS is adopted for the R2,000 mode then a separate double-resolution spectrograph will be required for the R6,500 and R20,000 modes).

Given the range of spectrograph designs that have been and are being considered for other projects, and to robustly demonstrate the feasibility of the spectroscopic

requirements, we consider the design solution that offers the most stringent and unique technical challenges, namely a spectrograph that can operate in all three observing modes. In order to facilitate development of the highest resolution mode, we adopt 0.9 arcsec fibres at this stage of development, as described in Section 3.2.

We have not considered the prime focus components in our feasibility study. These are key components, but other spectrographic projects, such as PFS and LAMOST, have designed comparable fiber-feed positioner systems that demonstrate their feasibility.

3.3.1 Bench Mounted spectrograph

APPENDIX D. NGCFHT SPECTROGRAPH OPTICAL DESIGN

The goal of the triple-resolution spectrograph concept is to achieve three switchable resolution modes for Nx4 objects as dictated by the top level requirement, where N= 800. In fact, our triple-resolution design enables four switchable modes:

- Low Resolution (LR) Mode with maximum multiplexing of Nx4 objects at ~R2,000 resolution with full wavelength coverage between 370 to 1,300 nm
- High resolution (HR) Mode at maximum ~R20,000 resolution for N objects with two selectable λ/7 wavelengths regions in the visible only (370 – 1,000 nm)
- "Bonus" Medium Resolution full-Coverage (MR-FC) Mode for N objects at ~R6,500 resolution with full wavelength coverage in the visible only (370 – 1,000 nm)
- Medium Resolution High-Multiplexing (MR-HM) Mode for Nx4 objects at ~R6,500 resolution with two windows of λ/7 over two central wavelengths in the visible (with NIR spectra at low resolution available)

The pupil slicing technique is selected for the triple-resolution spectrograph design as it offers the flexibility to switch between the requisite observing modes efficiently and provides good performances in terms of image quality (IQ), spectral resolution and throughput. The spectrograph design that uses four sliced sub-pupils is illustrated schematically in Figure 12. The choice of wavelength regions that are to be available depends on the grating selection, and so should be investigated during subsequent design phases.

The four resolution modes are generated by switching mechanisms that deploy in combinations either a prism-plate or an anamorphoser and the low resolution or high resolution gratings (Table 6). The fiber-feed unit delivers either N or Nx4 objects (illuminated fibers) by adjusting the locations of fiber positioners at the telescope focal plane or at the entrance to the spectrograph.

As shown in Figure 13 and Figure 14, light exits the fiber-feed through relay optics which projects an intermediate focal plane on the first switchable element (the prism-plate or anamorphoser) and then through the collimator onto the pupil slicer. Then light from each "slice" is directed into one of the four identical channels and further separated into three optical arms by beam splitters into three wavelength ranges: blue, red and NIR. Depending on the resolution mode desired, the spectra are dispersed using either the low

or high resolution gratings deployed by the second switching mechanisms. The optics and detector in each arm are optimized according to wavelength range to maximize efficiency.

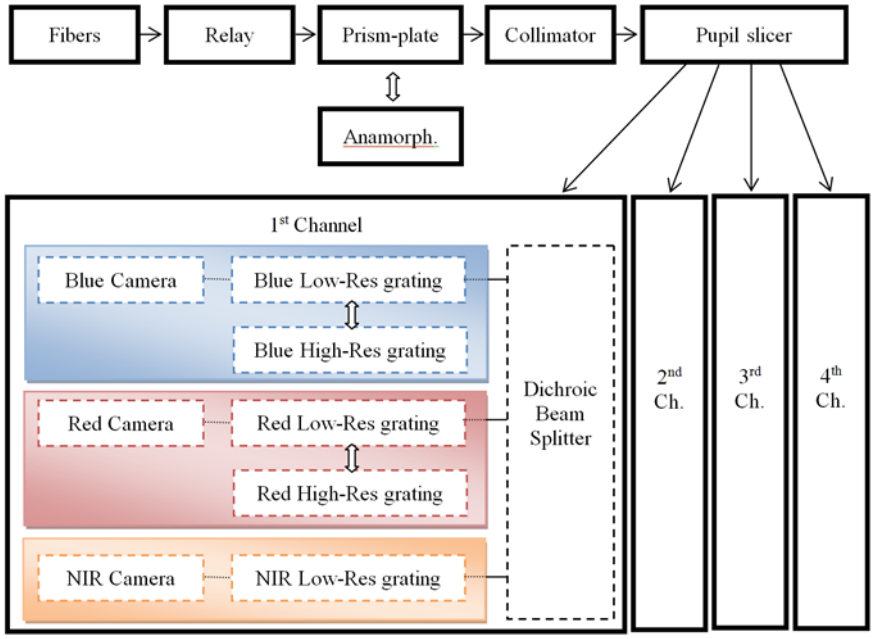

Figure 12. Schematic diagram of the spectrograph showing light entering the relay optics at the top-left.

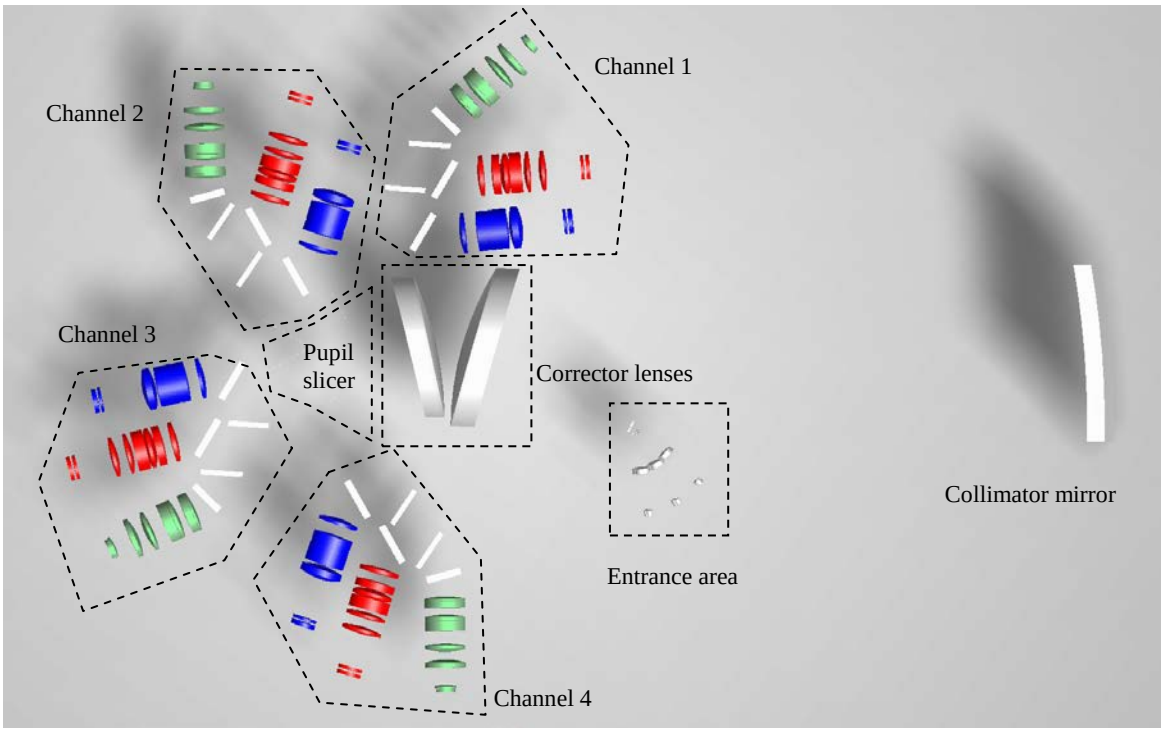

Figure 13. Top view of the spectrograph optical elements.

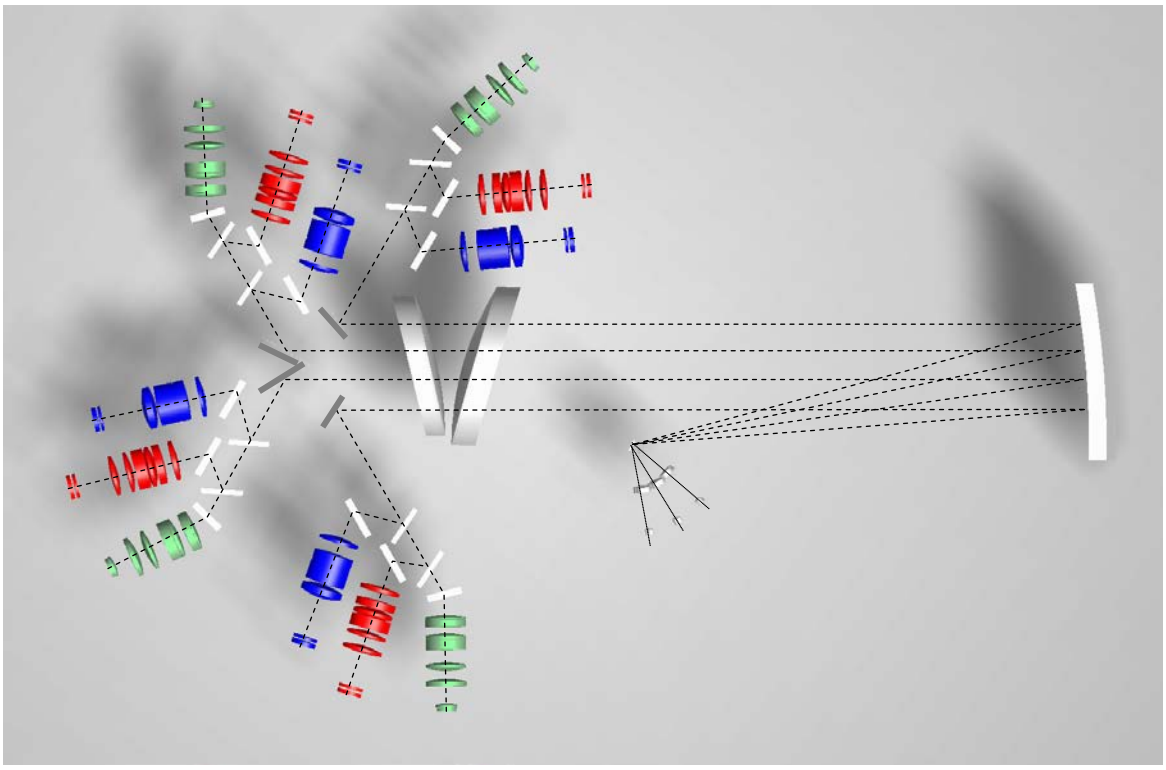

Figure 14. Top view the spectrograph optics showing light exiting the relay optics at the lower-right.

The characteristics of each resolution mode and combinations of optical elements used are tabulated in Table 6.

Table 6. Characteristics of the four resolution modes

Mode	Resolution in visible (Blue + Red arms)	Resolution in NIR arm	Simultaneous Coverage	# of Objects	Deployable Optical Elements Combination
LR	2,000	2,000	Full	Nx4	Prism-plate with Low-Res grating
HR	20,000	NA	Two windows of λ/7 in visible[4]	N	Anamorphoser with High-Res grating
MR-FC	6,500	NA	Full (visible only)	N	Anamorphoser with Low-Res grating
MR-HM	6,500	2,000	Two windows of λ/7 in visible4	Nx4	Prism-plate with High-Res grating

The anamorphoser is used with N-object fiber inputs and it elongates the pupil by a factor of four in the spectral direction and effectively reduces the spectral width of the image by the same effect (Figure 15). By pupil slicing, each fiber will produce 4 identical images, each one corresponding to a different sub-pupil. Therefore light collected in each fiber

[4] Defined by grating selection

produces four sets of identical spectra in the spectrograph, one per each channel, and the spectra are "recombined and readout" by customized data reduction software.[5]

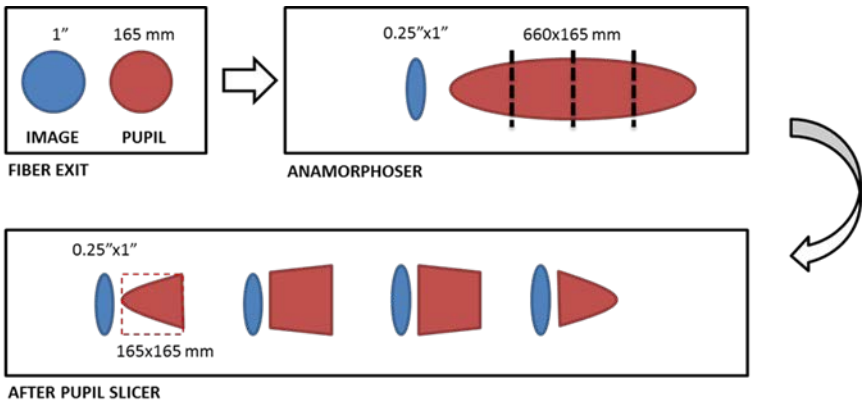

Figure 15. The anamorphoser elongates the pupil and it is sliced four times by the pupil slicer thus the same fiber "slit" is transmitted into all four channels.

The four-time anamorphic magnification is introduced by a cylindrical microlens with a cylindrical aspheric entrance surface and a toroidal exit surface. The anamorphoser is manufactured by standard technologies used in the semiconductor industry such as photolithography, resist processing and reactive ion etching. These technologies allow a very accurate shaping of the lens profile and a precise positioning of the lenses. The physical layout of the anamorphoser is shown in Figure 16.

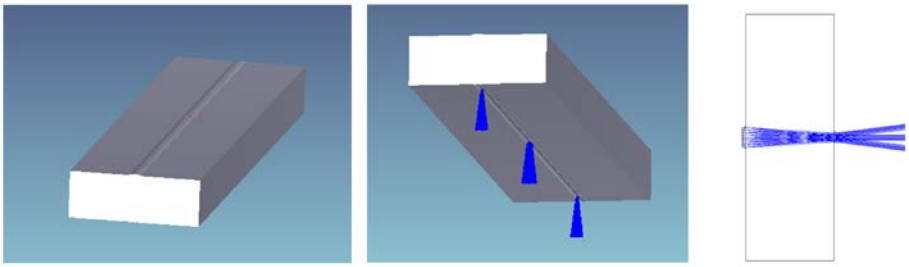

Figure 16. Physical layout of the anamorphoser (left) with light paths through the anamorphoser, shown as blue rays (middle and right).

A total internal reflection prism-plate is used with Nx4-object fiber inputs to direct light from each fiber to a single channel only, i.e. each fiber produces a unique set of spectra in the spectrograph (Figure 17). The effective slit width is wider than in the "pupil-slicing" mode providing a lower resolution, but the number of observed fibers provides a four-time gain in multiplexing.

The physical layout of the prism-plate is shown in Figure 18. The prism-plate tilts the chief ray of each fiber into the appropriate sub-pupil positions when exiting the prism-plate.

[5]This approach will result in a higher read-noise contribution for the high resolution mode. Science targets for the high resolution mode, however, are sufficiently bright that this is not expected to impact science performance.

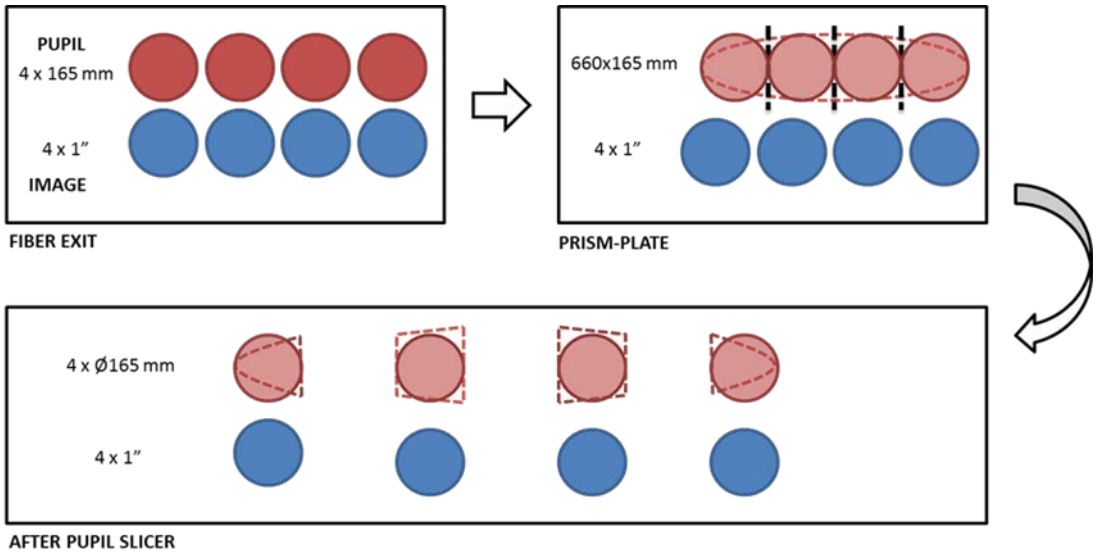

Figure 17. The prism-plate projects four circular pupils of adjacent fibers and they are not affected by the pupil slicer thus each fiber "slit" is transmitted into a single channel only. A comparison projection of the anamorphoser "elongated" pupil (dashed line) is also shown.

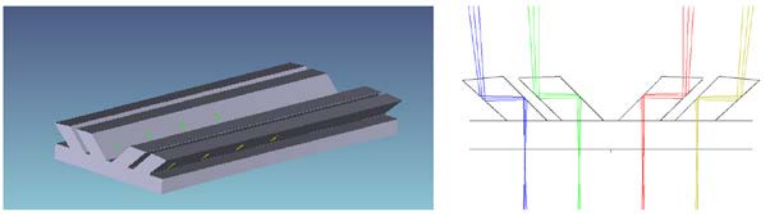

Figure 18. Physical layout of prism-plate (left) and it tilts the chief ray of four adjacent fibers, shown as different colours, into the proper pupil positions corresponding to the four-channel layout in the spectrograph (right).

3.3.2 Spectrograph Optical Design Trade Study

Given the top level parameters such as the telescope aperture, wavelength coverage, spectrograph resolutions and their corresponding wavelength ranges, a trade study was conducted to determine the optimal (yet interrelated) values for the number of objects, detector sizes and simultaneous wavelength coverage for all resolution modes. For the parametric trade study, practical considerations were applied to ensure that the overall design is balanced and achieves consistency at the sub-system level in terms of technical challenges, feasibility and attainability, including camera size and f-ratio, detectors, VPH gratings, dichroic beam splitters, etc.

For the HR mode, additional trades were examined for different combinations of slices and anamorphic factors before selecting the "4x4" configuration, i.e. four-times anamorphism by four-slice, as the spectrograph baseline.

The main characteristics of the baseline triple-resolution spectrograph are listed in Table 7 and the detailed characteristics of the different resolution modes achieved can be found in Appendix D. ngCFHT Spectrograph Optical Design.

Two spectrographs are needed in order to meet the number of objects in the top level requirements (~3,600 objects in LR and ~900 objects in MR and HR modes will likely be attained in this design).

Table 7. Main triple-resolution spectrograph characteristics.

Parameter	Value	Note
Fiber diameter	0.9”	*(150 um at F/3.5)*
Resolving power	2000 6500 20000	*LR mode* *MR-FC & MR-HM modes* *HR mode*
Spectral bandwidth	370 – 1300 nm	
Simultaneous coverage	Full (370-1300 nm) Full (370-850 nm) 2 selectable regions λ/7[6]	*LR mode* *MR-FC mode* *HR & MR-HM modes*
Spectral Sampling	10 pixel 4.5 pixel 2.5 pixel	*Visible arms, LR & MR-HM modes* *NIR arm, LR & MR-HM modes* *Visible arms, HR & MR-FC modes*
Interspectra separation	7 pixel 3 pixel	*Visible arms* *NIR arms*
Number of objects	1800 ± 10% 450 ± 10%	*LR & MR-HM modes* *HR & MR-FC modes*
Detectors	9kx9k, 10um CCD (8X) 4kx4k, 15um FPA (4X)	*Visible arms* *NIR arm*
Efficiency	50% ± 5% (at peak)	*Spectrograph optics + detectors*

3.3.3 Performance

The fundamental performance of the triple-resolution spectrograph design in meeting the top level requirements is demonstrated by its image quality as expressed in EE80 encircled energy and overall system throughput according to the selectable wavelength windows in the HR mode and the total wavelength coverage in the LR mode.

3.3.3.1 Selectable wavelength windows in HR mode

In the HR mode, there are selectable wavelength regions in the blue and red arms. The central wavelengths and the corresponding bandwidth values within each arm should be investigated based on science requirements during subsequent design phases. For this phase, we demonstrated feasibility by adopting uniformly spaced wavelength regions that are set by available gratings.

[6] Defined by grating selection

3.3.3.2 Wavelength windows in LR mode

The wavelength coverage for the three arms: blue, red and NIR, expressed in terms of central wavelengths and bandwidths are listed in Table 8.

Table 8. Wavelength windows in LR mode.

Wavelength region	Central wavelength (nm)	Bandwidth (nm)
LR BLUE	465	370-560
LR RED	696	552-844
LR NIR	1048	836-1260

3.3.3.3 Image quality

A provisional IQ budget was developed to guide the design process of the different optical subsystems based on the EE80 diameter projected on the detector focal selected. The spectrograph design is optimized for the highest resolving power needed in the HR mode. The total IQ budget is 0.23” in the HR mode and 0.3” in the LR mode.

Representative plots of the HR and LR mode EE80 diameter maps for the red arm of the four spectrograph channels are plotted in Figure 19. The results show feasibility in the design to meet the top level IQ requirement while having leaving sufficient margin to accommodate for real-world considerations such as manufacturing and alignment tolerances. Future design refinement and optimization shall ensure that the final IQ requirements are met.

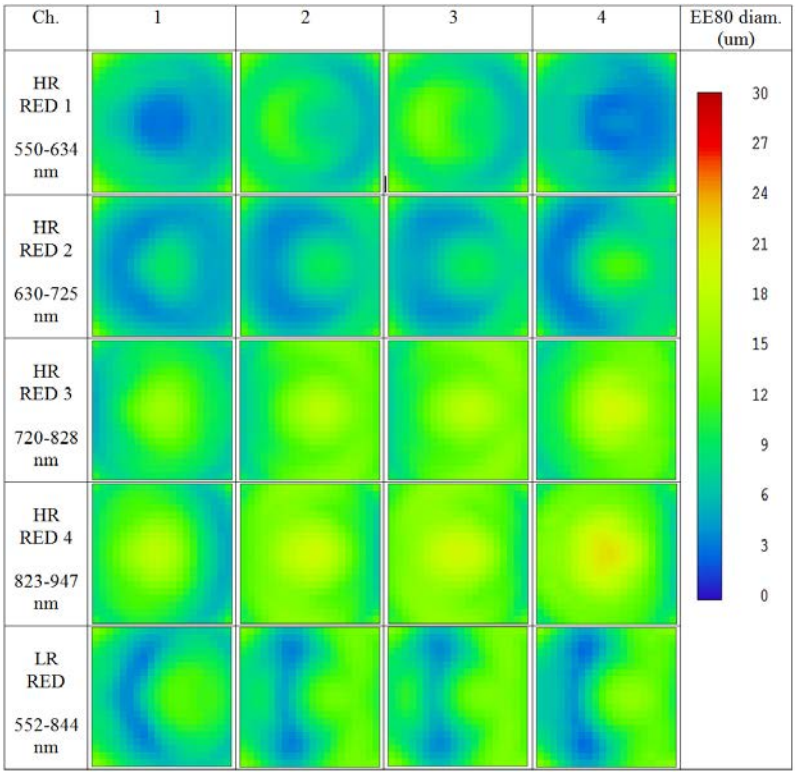

Figure 19. Spectrograph red arm EE80 diameter map.

3.3.3.4 Overall system throughput

The predicted system throughput including allowances for telescope optics, WFC, ADC, fiber-feed, spectrograph optics and detector efficiency is plotted in Figure 20 over the operating wavelength range. The system throughput is within the top level requirements.

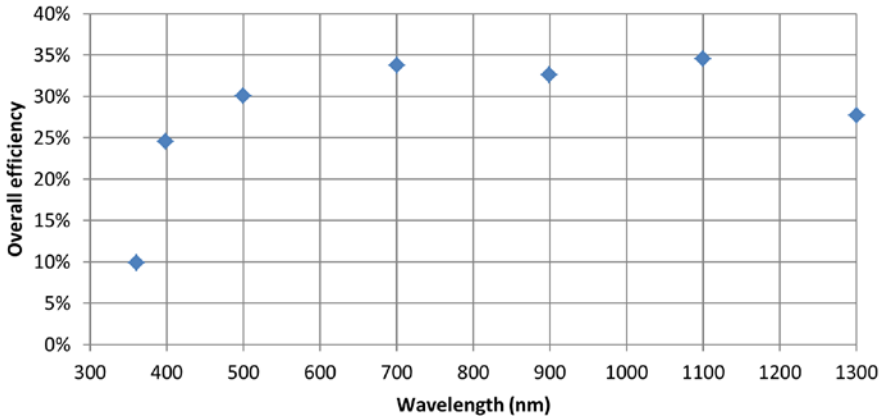

Figure 20. Overall system throughput curve with allowances for telescope optics, WFC, ADC, fiber-feed, spectrographic optics and detector efficiency.

3.4 Feasibility of the Subaru PFS design for ngCFHT

In addition to considering the triple resolution spectrograph design solution, it is sensible to consider alternative concepts, e.g. multiple spectrographs that operate at single resolution settings. In this context, there is an exciting synergy with the Subaru PFS facility. The PFS design is being developed based on many of the same science considerations that motivate the low-resolution mode of ngCFHT, and it is scheduled to be in operation on Mauna Kea towards the end of this decade. It is desirable, therefore, to consider whether it is feasible to deploy this instrument on the ngCFHT, since this would represent an exciting opportunity for highly multiplexed spectroscopy.

The PFS consists of three main subsystems: a prime focus fiber positioner unit, fiber-feed system with 1.1" diameter fibers and four R2,000 spectrograph units at 600 objects capacity each, 2,400 objects in total. Two feasible scenarios are considered, therefore, that represent different deployment option:

- Full employment of the PFS design with all three subsystems
- Partial employment with the spectrograph design only

The first case utilizes all three subsystems of the PFS, by adapting the ngCFHT telescope structure design to match the current PFS interfaces. The second case incorporates the spectrographs into a new fiber positioner unit and fiber-feed system. This provides flexibility to optimize science performance by cloning one more spectrographs (to meet the multiplexing requirement for ngCFHT) and adjusting the fiber diameters of the fiber-feed system to match the spectrograph resolutions. In both cases, additional spectrograph(s) would be required for the MR/HR modes.

Table 9 summarizes the characteristics of LR spectrographic capabilities according to the two scenarios. Due to the difference on telescope diameter, the Subaru PFS fiber diameter corresponds to 0.9" in terms of sky aperture which is the same value adopted for the triple-resolution spectrograph design. For the second case, options exist to have two sets of fiber diameters to optimize fiber input efficiency between the LR and MR/HR modes, i.e. a new 1.1" fiber diameter fiber-feed for the LR mode and redeploying the PFS at 0.9" fiber diameter for the MR/HR modes. Of course, this would require additional study to determine how best to deal with multiple sets of fibres.

As summarized in, the full deployment of PFS will result in a smaller FOV and lower number of objects than the top level requirements. These considerations and their impact upon the science capabilities must be traded against potentially exciting gains in programmatic and collaborative areas, as well as in terms of developing a coherent observatory system for Mauna Kea. Additional study and development is required to determine the full cost and benefits between the options of deploying the PFS (or certain subsystems) against other design solutions such as the triple-resolution spectrograph.

Table 9. Characteristics of the low resolution spectrograph with redeployment of PFS

Deployment Scenario	FOV	Fiber Diameter	Resolution	# of Objects	Comment
Full PFS	1°	0.9”	2,000	2,400	Direct adoption
Spectrographs only with new fiber positioner unit and fiber-feed system	1.5°	1.1”[C1]	~1,500[C2]	3,000[C3]	C1. New fiber-feed C2. 20-25% reduction in resolution due to increase in telescope aperture from 8m to 10m C3. By adding 600 extra fibers and one cloned spectrograph

3.5 Summary

Based on the feasibility studies, we conclude that there are viable options to develop a LR/MR/HR spectrographic system. The prime focus components are fully demonstrated by existing designs and the new triple-resolution spectrograph design illustrates one feasible option for the fiber-fed spectrograph, with other options including a low resolution spectrograph such as PFS working with a MR/HR double-resolution spectrograph design.

4 AERO-THERMAL PERFORMANCE

APPENDIX E. NGCFHT VENT SYSTEM CFD STUDY STATEMENT OF WORK

The objective of the aero-thermal study is to determine if the proposed enclosure configuration has sufficient ventilation to mitigate local seeing effect to ensure excellent image quality. Unlike the TMT Calotte enclosure design, which uses passive ventilation for dome flushing and aperture flaps to minimize telescope wind shake (Figure 21), the baseline ngCFHT design uses active ventilation produced by fan-driven floor vent and does not incorporate aperture flaps. This is a result of the desire to simplify the ngCFHT design to minimize the size and life-cycle cost of the enclosure and to maximize reliability by not having mechanically deployable vent doors and aperture flaps which require regular maintenance, additional equipment, and walkways for access and handling.

A computational fluid dynamics (CFD) study is underway to evaluate aero-thermal performance of the baseline enclosure design. The CFD study compares the relative performance of the ngCFHT enclosure with passive (Figure 22) and active ventilation. The comparison of performance is evaluated by ways of flow profiles, temperature variations and distributions inside the enclosure, specifically along the optical path and near the top-end, under different operating conditions. Moreover, the actual aero-thermal performance will be assessed qualitatively by using the knowledge base established by the TMT project which has conducted extensive CFD studies along with field validations.

The CFD study is conducted by the WindEEE Research Institute at the University of Western Ontario. The scope of work of the aero-thermal study is attached in Appendix E. ngCFHT Vent System CFD Study Statement of Work.

Preliminary findings of the CFD study are expected by the end 2012 and will be made immediately available.

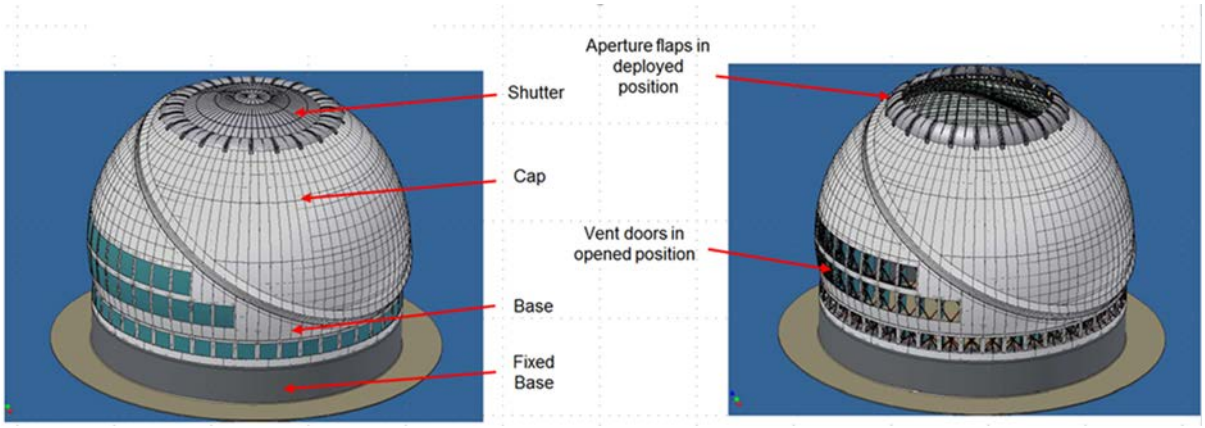

Figure 21. TMT Calotte enclosure with vent doors and aperture flaps. The vent doors provide passive ventilation for dome flushing to minimize seeing effect and the aperture flaps minimize turbulence and flow entrainment at the telescope top-end by deflect the high velocity flow away from the aperture.

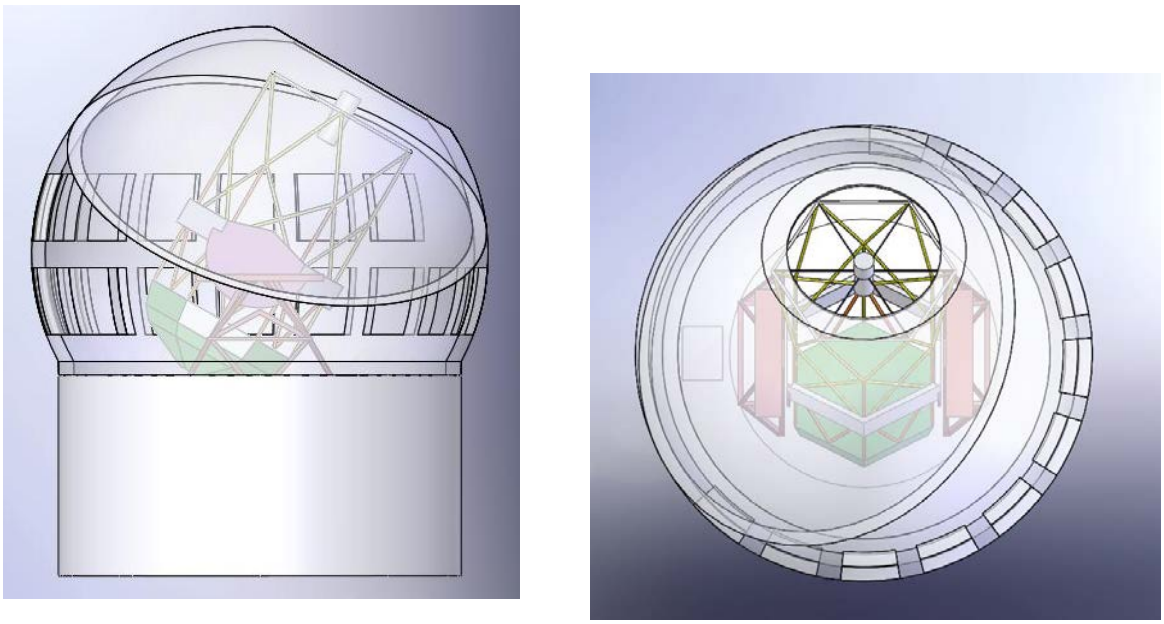

Figure 22. ngCFHT CFD model with telescope at 30° zenith – side view showing passive vent doors (left); top view showing the rectangular floor vent opening at the nine o'clock position on the floor (right).

5 FACILITY REDEVELOPMENT STUDY

APPENDIX F. PROGRAMMATIC STUDY FOR UPGRADE OF TELESCOPE STRUCTURE AND ENCLOSURE

5.1 Scope and construction sequence

The facility redevelopment study is a programmatic study to determine the time and cost required for the deconstruction of the existing CFHT facility and the construction of the new ngCFHT facility. Three separate steps are required in order to complete the facility redevelopment process and to determine the relevant cost and schedule estimates:

- Deconstruction of the CFHT facility
- Structural retrofit of the enclosure pier to support the ngCFHT facility
- Construction of the ngCFHT facility

Dynamic Structures Ltd. (DSL) led this study and has produced cost and schedule estimates for each stage. The DSL study includes the cost and schedule of the redevelopment tasks of the enclosure and telescope structural and mechanical systems. However, the study does not include activities associated with the telescope optics, instruments and general purpose facility equipment for air handling, coolant and electrical distribution etc. It is assumed that these will be performed independently by the ngCFHT project.

DSL is well qualified for this work as they have extensive experience in the design and construction of existing telescope structures and enclosures on the Mauna Kea summit including the CFHT, Gemini, Keck and Subaru observatories. More recently, DSL led the TMT telescope structure system design up to the post-conceptual stage. Currently, DSL is the prime vendor responsible for the TMT enclosure system which has passed final design review and in the pre-construction stage. As part of the TMT work, DSL prepared detailed cost and schedule estimates and on-site construction plan for both telescope and enclosure systems for major project reviews. The findings of these reviews have been positive such that panels of international experts acknowledged the accuracy and quality of DSL's cost and schedule estimates in all areas of design, fabrication, and on-site construction, with insight into the local conditions such as equipment availability, warehousing, overtime and insurance[7] according to the Hawaiian labour rules and regulations.

Using the CFHT site topology (Figure 23), existing CFHT drawings (Figure 24), construction plans developed for the TMT enclosure and telescope systems, and consultation with personnel involved in previous construction projects on Mauna Kea, including the original CFHT, DSL developed task-based bottom-up cost and schedule estimates for the redevelopment process. The cost estimate includes the design and manufacturing costs, imported and local labour costs, and equipment costs including cranes and lifts, temporary falsework support, transportation, safety equipment, consumables, staging and shipping logistics etc.

[7] Typical worker's compensation insurance rate for high altitude iron worker is 30% of the hourly labour cost.

The deconstruction sequence is in reverse order of the original construction sequence. The schedule is based on using a temporary crane attached to the enclosure to facilitate dismantling of the telescope structural components. Removal of the enclosure structural components is done by the 250 ton hydraulic mobile crane (Figure 23) afterward. The size and weight of every crane lift is determined from the original construction drawings to ensure safety.

The structural retrofit work is conducted concurrently with the deconstruction work by sharing lifting equipment. Access to the braces of the enclosure pier is from the outside by cutting through the exterior siding. Temporary weather protection and structural support will be provided in order to replace existing bracing with stronger bracings. Fire retardant and insulation matching the existing installation will be applied to all new structural elements.

The construction sequences including manufacturing are similar to those developed for the TMT project; however, factory trial assembly of main structural components is planned for the telescope system only. Construction of the ngCFHT is separated into two phases. In the first phase, the enclosure construction starts immediately after deconstruction of the existing enclosure and telescope. The second phase of telescope construction begins once the enclosure is secured when telescope parts can be lifted safely into the interior through the enclosure aperture using the mobile crane. The telescope erection is accomplished by using a combination of falsework, mobile gantry crane and the enclosure crane.

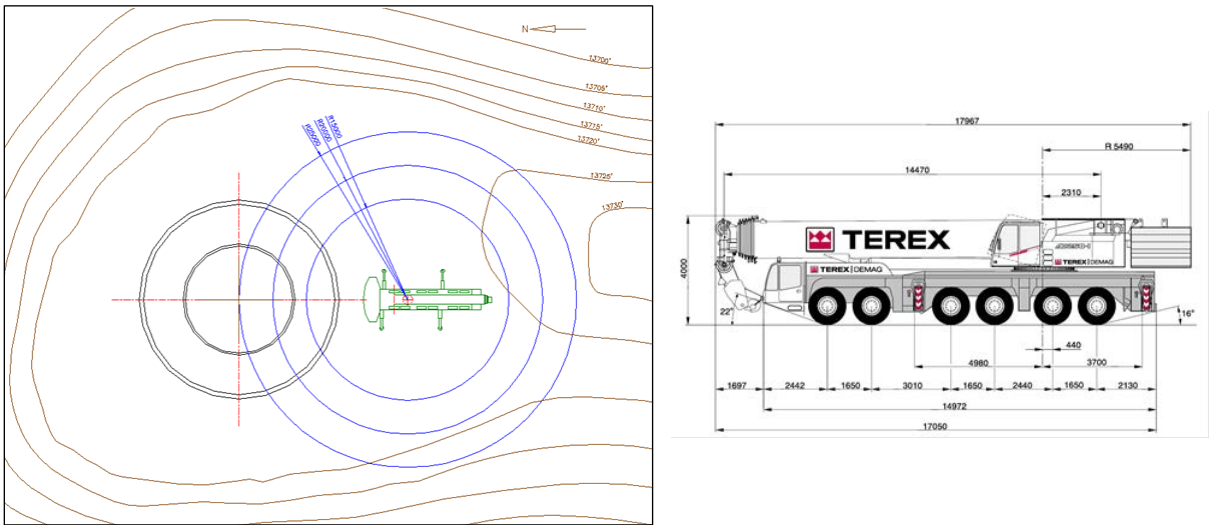

Figure 23. Plan view of the mobile construction crane location set-up next to CFHT pier (left) and 250 ton hydraulic mobile crane dimensions (right).

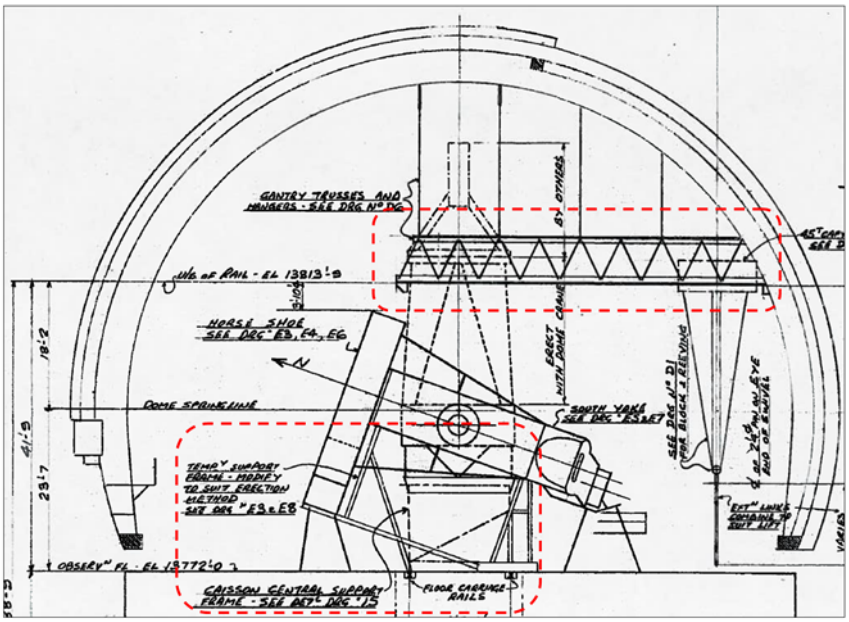

Figure 24. Excerpt of the original CFHT telescope structure erection drawing.

5.2 Estimated cost and schedule for redevelopment

The estimated redevelopment cost breakdown is shown in Table 10 along with the schedule summary. The labour component includes cost increases associated with working at high altitude including an inefficiency factor of 62.5%, i.e. the same work will take 1.6 times longer at the summit than sea level, and a worker's compensation insurance premium of 30% of the hourly rate. However, the costs associated with the redevelopment of the facility equipment within the CFHT piers, disposal of existing CFHT facility, site preparation for crane access and provision of site facilities such as toilets and first-aid at the summit are not part of the DSL redevelopment cost estimate: it is assumed that these will be carried out by the ngCFHT project.

The total redevelopment cost in US dollars is $68,191,381 with 15% DSL profit and 20% contingency and the total redevelopment schedule is five and a half years including design and manufacturing, and the actual "telescope downtime" is less than three years.

Table 10. Redevelopment cost estimate including contingency.

PHASE	Cost	Year 1				Year 2				Year 3				Year 4				Year 5			
	[2012 USD]	Q1	Q2	Q3	Q4	Q1	Q2	Q3	Q4	Q1	Q2	Q3	Q4	Q1	Q2	Q3	Q4	Q1	Q2	Q3	Q4
Design - Enclosure	$ 11,979,880																				
Manufacture - Enclosure																					
Design - Telescope	$ 14,719,699																				
Manufacture - Telescope																					
Deconstruction - Telescope	$ 6,602,690																				
Deconstruction - Enclosure																					
Outer Pier Upgrade	$ 2,688,556																				
Construction - Enclosure	$ 32,200,556																				
Construction - Telescope																					
Total	**$ 68,191,381**																				

6 COST ESTIMATE SUMMARIES TO DATE

In parallel, working with CFHT, we plan to identify additional tasks associated with the tasks excluded in the DSL study and produce cost and schedule estimates of the same. Currently, this cost is represented in the row Facility Redevelopment & Commissioning in Table 11. Once this is complete then the total cost will be revised and consolidated in Table 11 prior to the March 2013 ngCFHT workshop.

The basis of estimate in Table 11 documents the different methodologies used to derive the costs. They vary from order-of-magnitude (ROM), parametric, extrapolation, DSL study and engineer's estimate. The parametric cost is derived by scaling the existing cost estimate of similar projects. The extrapolation cost is a weighted cost of two or more sources. In general, the DSL costs used are either bottom-up estimate performed specifically for ngCFHT or parametric cost based on DSL's past project experience. The engineer's estimate is bottom-up cost estimate using a top level work breakdown structure.

Table 11. Cost Summary of the ngCFHT facility

Item	Cost Estimate ($M)	Basis of Estimate
Design and management	$10M	ROM estimate with using personnel from current CFHT and partner countries
M1 optics	$10M	Parametric cost based on ELT estimate
M1 support system	$5M	Parametric cost based on ELT estimate
Wide field corrector	$5M	Engineer's estimate
Software and control	$10M	Extrapolation from ELT estimate and CFHT historical cost
30% Contingency	$12M	
Sub-total	$52M	

Removal of 3.6m telescope and dome	$6.6M	DSL study with 15% profit and 20% contingency but excluding additional facility decommissioning and disposal costs
Enclosure pier structural upgrade	$2.7M	DSL study with 15% profit and 30% contingency
Telescope structure	$30.8M	Parametric costs from DSL study using TMT cost estimates With the $32M construction cost divided equally Include 15% DSL profit and 20% contingency
Enclosure	$28.1M[8]	
Facility redevelopment & commissioning	$10M	ROM budgetary estimate
Spectrograph system	$76.1M	Includes 20% contingency $50.1M for two triple-resolution spectrographs based on Engineer's estimate including detector systems, control and data reduction software $26M parametric cost based on WMFOS estimate for the prime focus unit and fiber-feed system
Total	$206.3M	

[8] Cost includes CFHT style mechanical vent doors

7 CONCLUSIONS OF FEASIBILITY STUDY

The findings from the technical studies show that it is feasible to develop a ngCFHT facility with telescope and enclosure compatible with the geometry and load capacities of the current piers. Optical designs for the telescope and spectrograph that will meet the top level science requirements are also feasible. More specifically, at the subsystem-level:

- A single-mirror 10 m segmented mirror telescope can be accommodated on the current pier with minimal modification to the foundation soil
- A Calotte enclosure can be accommodated on the current pier with minimal modification to the structure and with considerations for the Office of Mauna Kea Management Comprehensive Management Plan
- Technologies for the mirror segment fabrication and segment support system are now mature, based on the development work for the ELT projects
- High efficiency fiber and optical systems are now practical
- Several options exist for the spectrograph, including a versatile innovative triple-resolution design

Based upon these findings, a formal Conceptual Design Study for ngCFHT should be initiated. This will include:

- Integrating systems engineering practices to refine and delineate the science requirements into system and subsystem design requirements to guide the conceptual engineering and design activities, and to derive performance budgets (based on the overall system performance requirements) to evaluate and validate design objectives;
- Developing selection criteria and conducting down-select studies to finalize the ngCFHT facility configuration among alternate design solutions. The facility configuration includes the telescope and enclosure configuration, layout for fiber routes and spectrograph locations, and general arrangement for the optical, mechanical and electrical facilities required for efficient operation, safe service and maintenance of the Observatory;
- Identifying and assessing major technical and programmatic risk areas to facilitate the design trade process;
- Incorporating value engineering techniques to enable objective assessment of design trades that balances performance against programmatic risks in the areas of technology, cost and schedule;
- Defining the modifications required to utilize the CFHT telescope and enclosure piers;
- Completing conceptual design for all major systems and subsystems, including:
    - Telescope structure system
    - Enclosure structure system
    - Segmented primary mirror, WFC and ADC

  - Prime focus system including the fiber positioner, fiber handling unit, acquisition and guide system, calibration unit and de-rotator
  - Fiber-feed management system
  - Spectrograph system with design solutions among the various options (e.g., single, dual or triple-resolution spectrograph solutions)
- Refining the facility redevelopment study to capture all the associated cost components in order to refine the overall project cost and schedule estimates

In summary, the feasibility study for ngCFHT has demonstrated that the scientific vision and requirements developed in the *Feasibility Study Report for the Next Generation CFHT: I. Science* is technically viable and can be designed and constructed based on existing technologies. The formalized Conceptual Design study should involve all potential partners in the production of an end-to-end design for the spectrographic facility that meets the technical requirements and represents the optimal combination of performance, cost and risk. It will be the fundamental step in realizing the scientific potential of ngCFHT.

APPENDIX A. NEXT GENERATION CANADA-FRANCE-HAWAII TELESCOPE PIER BUILDING EVALUATION

Next Generation Canada-France-Hawaii Telescope Pier Building Evaluation

Report Prepared by Mathieu Angers

University of British Columbia

&

Empire Dynamic Structure

15 August 2011

Executive summary

Canada-France-Hawaii Telescope (CFHT) mandated a research group from University of British Columbia (UBC) and engineers from Empire Dynamic Structures (EDS) to evaluate the possibility to have the current pier building supporting a new telescope design, mass and geometry. The pier having been designed in 1974, it is necessary to verify if the structure meets the new Codes requirements, mostly regarding the seismic design and analysis of structures. The CFHT is located on Mauna Kea volcano in Hawaii. The current 3.6 m telescope is wished to be replaced by possibly a 10 or 12 m segmented mirror instrument. From the plans and information furnished by the CFHT, the pier walls, slabs, footings and soil capacities are evaluated according to the American Concrete Institute code and compared to the forces induced by the loads defined in the International Building Code. In order to have a realistic evaluation of the forces in the pier building, a telescope frame idealization is used following EDS recommendations. A static equivalent method is employed for the seismic analysis and the IBC furnishes the design spectrum for Mauna Kea.

- The bending moment and shear capacities are high enough to resist the forces. The required steel reinforcement in the walls and slabs of the pier building are comparable to the one found in the current structure and are judged to be sufficient.
- The foundation structural resistance is also evaluated and is satisfactory. The differential settlements have to be kept less than 10 mm. It is evaluated they are of approximately 3.8 mm.
- The soil allowable bearing capacity of 191 kPa under dead and live load is satisfactory; the pressure induced by the footing is equal to the capacity. The bearing pressure for earthquake load combinations is 254 kPa. Because of the transient nature of this type of loading an increase in the bearing capacity can be assumed. The capacity is considered to be high enough.
- The soil parameters having been evaluated in 1973 and pressures surpassing the capacity in some cases, we recommend for further design to have a geotechnical consultant completing a soil and foundation evaluation.

Table of content

1. Scope

The purpose of this document is to present the methodology, results and recommendations of the CFHT pier building structural and geotechnical evaluation. The CFHT observatory is located on Mauna Kea, in Hawaii. A new generation telescope replacing the current one is wished to be installed on the existing pier building. The structure having been designed in 1974, it is wanted to know if the current structure, foundations and soil meet the requirements of current building codes and if it can support the new telescope geometry and mass. The study is based on the information, plans and reports from the original design furnished by the CFHT. This study is the first of a series that will define the baseline configuration of the telescope structure and enclosure system for the Next Generation CFHT instrument.

Figure 1: Current CFHT on Mauna Kea Volcano, Hawaii (CFHT).

2. Background

The CFHT observatory has been in function since 1979 and is located in Hawaii on the dormant volcano, Mauna Kea, at an altitude of 4200 meter. The telescope hosted by the CFHT observatory is a world-class 3.6 m optical/infrared telescope. The CFHT wants to replace the current instrument and according to Grundmann (1997), “It is the opinion of this committee that recent advances in optical and infrared astronomy have been primarily the consequence of improved capabilities in angular resolution, light-gathering power and the ability to conduct observations in non-traditional wavelength regimes. While the CFHT has served its users well by setting the technical standard in these areas, we believe that the "long term" facility needs of the three communities would be best

served by replacing the existing 3.6 m telescope with a segmented mirror instrument of 12-16 m aperture on the same site (possibly using the same pier)". To replace the current telescope, it is wished to evaluate if the existing pier can be safely reused.

In order to assess the current building, a preliminary draft design for the possible telescope frame was done by Dr. Michael Gedig from EDS. This draft was used to represent the telescope, its supporting frame, bearings and ring girder on the pier structure. His work was based on Grundmann report (1997) that "identifies the largest telescope which could reasonably be installed making use of the existing pier". A 12 to 15 m segmented mirror telescope was studied and Grundmann (1997) came to the conclusion that a 12 m telescope would be the maximum size the current structure could hold because of the current pier and dome track dimension and design. In addition, he states that a 10 m segmented mirror telescope would be best for the current installations.

3. Structure description

3.1 Geometry

The pier building is a 3 storey reinforced concrete cylindrical pier structure. It has a 16.3 m diameter and is 14.4 m high. The walls are 304.8 mm thick over its whole height. The slabs of the first and second storey are hollow slab and 711 mm thick. The voids in the slabs are rectangular and have 914 x 914 x 356 mm dimensions. The top slab is a 304.8 mm thick slab. The first storey is 6.3 m high with an opening of 5.8 m wide and 3.2 mm high. The second and third storeys are 4.0 m high and have 3 openings of 1020 x 2080 mm and one opening of 1800 x 2080 mm each. The foundation is a ring footing of 610 mm thickness and 2240 mm width. Please refer to the plans for more details.

Figure 2: CFHT Pier building during the dome support construction (CFHT).

Materials

Concrete compressive strength is 20.7 MPa and the elasticity modulus is evaluated to be 21 525 MPa according to the ACI. The reinforcing bars have a yielding strength of 413 MPa and an elasticity modulus of 200 000 MPa.

Soil

Soil data is taken from the Foundation Investigation Report prepared by Dames & Moore, (1973). The maximum soil pressure is 191 kPa. Design Criteria & Basis of Calculations for Concrete Telescope Support states "Dames & Moores believes the maximum safe bearing pressure under the central pier slab on unfortified soil to be 4000 psf, from the standpoint of bearing capacity and differential settlement of less than 100 mm". The footing top is located 2.5 m below the soil surface. The soil under the foundation consists of "sand and gravel size volcanic ash and cinders with occasional clinkers up to 152 mm. The ash is similar to furnace slag", (Dames & Moore, 1973). The density of such soil varies from 700 kg/m^3 to 2300 kg/m^3, (Dames & Moore, 1973). In the calculation, an average of 1800 kg/m^3 is assumed for simplicity.

Telescope frame

The telescope steel frame was modeled following the recommendation of Dr. Michael Gedig from EDS. The location of the telescope center of gravity is 7.0 meter over the top slab of the pier structure. Its mass is attached to the pier via truss frame elements forming a pyramidal structure. This pyramidal frame is connected to the pier with 4 linear spring elements that represent the stiffness of the hydraulic bearings sitting on the azimuth track and ring girder. The sections of the frame members were determined by keeping the dead load deflection of the pyramidal frame under 5 mm. The bearing stiffnesses were evaluated in function of the periods of vibration of the frame. The first mode of the frame has to have a period equal to 0.25 second and the higher modes have to have periods over 0.25 second, but not so high the pier stiffness increases too much. Each spring has a radial (K_r), tangential (K_t) and vertical (K_v) stiffness. The height of the telescope over the pier top surface (H) is 7.0 m. The azimuth track radius (R) is the one of the pier building, 8.15 m. The four bearings are spaced equally of a distance (B) and placed over the azimuth track. The mass (M) of the telescope is approximated to 270 000 kg compared to 255 000 kg for the old telescope.

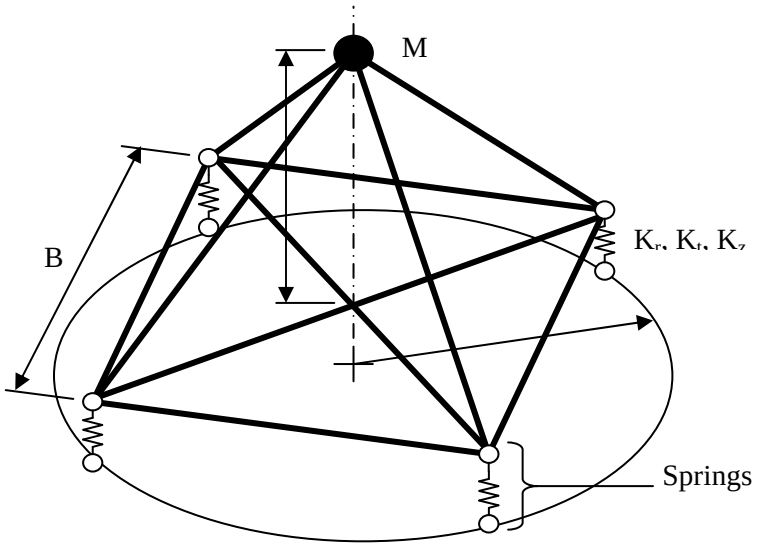

Figure 3: Idealization of the telescope frame, bearings and ring girder (Michael Gedig, EDS).

The ring girder and azimuth track were modeled as rigid beam elements connected to the pier wall. These are modeled to not overly stiffen the structure and, to distribute the forces more uniformly to the pier in order to avoid stress concentration. Figure 4 presents a possible design for the azimuth track and ring girder.

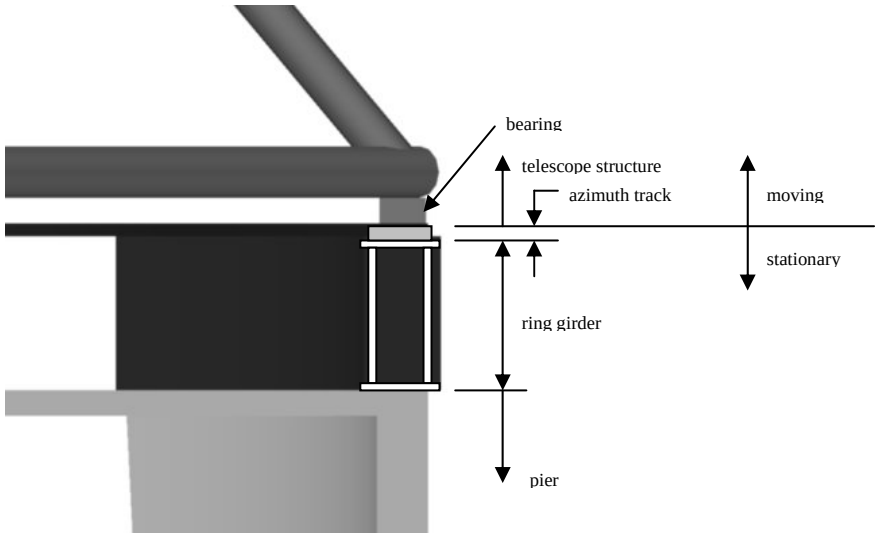

Figure 4: Connection of the telescope frame to the pier building detail (Michael Gedig, EDS).

The telescope model which will be connected to the pier structure is plotted in figure 5 with its frame, springs and rigid ring girder elements.

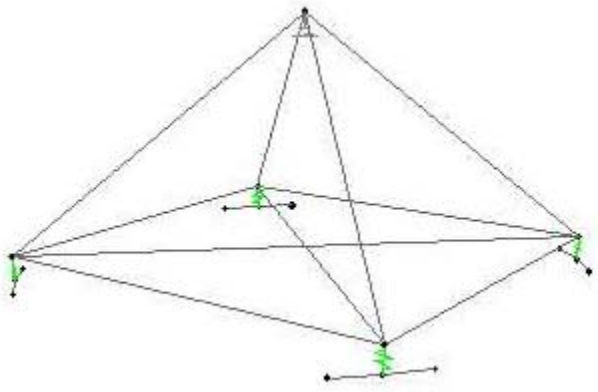

Figure 5: SAP2000 telescope frame, bearings and supports model.

4. Methodology and assumptions

4.1 Building codes and design philosophy

The structure forces, reactions and displacements induced in the different members due to the load cases and combinations first need to be computed. The loads and design requirements are defined by the International Building Code (IBC) and American Society of Civil Engineers 7 - Minimum Design Loads of Buildings and Other Structures (ASCE 7), the regulation in force in Hawaii. These forces are then compared to the capacities of the different components that are evaluated according to the American Concrete Institute code (ACI). Two design philosophies are used for design. The structural and footing design is done using limit state design (LSD) and the soil foundation is designed using allowable stress design (ASD). LSD insures that the different limit states are respected, for example the bending capacity of a beam, assuming a certain probability of rupture. The security associated with the limit state is dependent on the variability of the resistance and of the loads. Factors are applied to the loads and capacities to achieve that goal. ASD philosophy is to make sure the service loads are under the elastic limit, limit that is reduced by a factor of safety. The safety factor for foundation design is usually 3.

4.2 Load cases

The loads to which the structure is submitted are the dead, live and seismic loads. Wind loads were ignored because the enclosure covering the pier is isolated from the pier. The dead load includes the self weight of the structure, and telescope mass. The live loads are the equipment and people loads.

The live load values were taken from the “Design Criteria & Basis of calculations for Concrete Telescope Support”.

4.3 Seismic analysis

The IBC and ASCE-7 define different procedures to do a seismic analysis of a structure. They depend on the level of precision required and on the structure particularities. The structure being a regular and low height building, the static equivalent method is used because of its simplicity and understanding of the behavior induced by this type of loading. The static equivalent method represents an earthquake loading by a pattern of forces pushing laterally on the vertical axis of the structure. The first lateral period of the structure gives the spectral acceleration of the structure from the design spectrum. The design spectrum is dependent on the location of the structure and defined by the IBC. It is also function of the soil class on which the structure is sitting. The soil is evaluated to be a soil class C. It was determined with the shear wave velocities for the different layers of soil given in the Foundation Investigation Report, (Dames & Moore, 1973). The design spectrum is for a 2% occurrence in 50 years earthquake (2500 years return period). The response spectrum is interpolated from the spectral acceleration at 0.2 seconds and at 1 second. The damping is assumed to be 5%. The design spectrum accounting for a soil class C and 5 % damping is shown in figure 6.

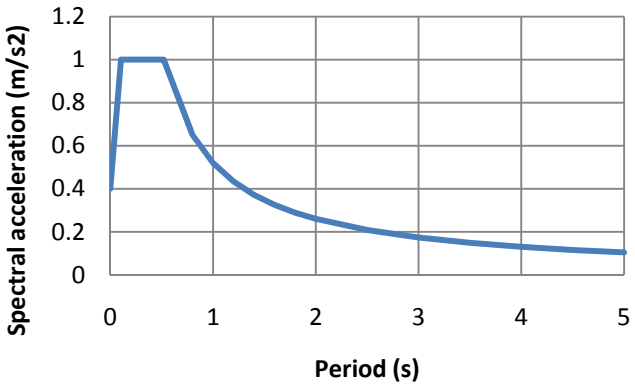

Figure 6: Design response spectrum for Mauna Kea, Hawaii, soil class C and damping ratio of 5%.

The elastic base shear is then evaluated in function of the total weight of the structure. This shear is distributed at each degree of freedom of the model in function of the mass at each of these DOFs. Then the elastic forces are reduced because of the ductility and overstrength of the structural system.

The circular concrete pier structure is assumed to act as a normal concrete shear walls. The force reduction factor for this type of structural system is 4.0 as stated in the IBC.

4.4 Load combinations

For the design of the pier walls, slabs and footings limit state design is used. The dead load (D), live load (L) and earthquake load (E) are factored and then combined according to the IBC requirements.

1.4D

1.2D+1.6L

(0.9-0.2)D+1E

(1.2+0.2)D+1E+0.5L

The combinations that include earthquake loads have a portion of their dead load added or removed to account for vertical vibration. The seismic loads are applied with different orientations on the structure. The forces, reactions and displacements are evaluated assuming the structure to remain in its elastic range. The forces induced by these factored loads are compared to the factored capacities.

The design of the foundation is done using allowable stress design. Different load combinations are used and vertical vibration can be neglected as stated in the ASCE-7:

1D

1D+1L

1D+0.7E

1D+0.525E+0.75L

0.6D+0.7E

The pressure induced by these loads under the footing is compared to the bearing capacity on which a safety factor was applied.

4.5 Structure modeling

The structure is modeled in the structural analysis software SAP2000. The ACI and IBC codes are implemented in the program. The concrete walls and slabs are modeled as shell elements and the supports take into account the soil and foundation stiffness and are modeled as spring elements. Figure 7 present the SAP2000 finite element model of the pier and telescope structures.

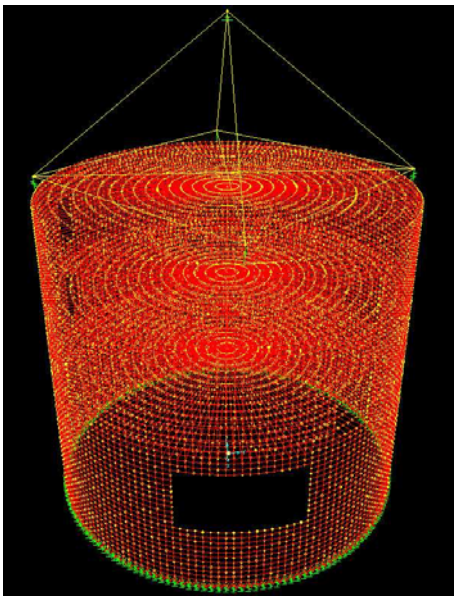

Figure 7: SAP2000 pier and telescope frame finite element model.

It is also important to make sure the SAP2000 finite element modeling is done properly. It needs to behave as the real structure and the displacement and forces have to be well approximated. To do so, a simpler model of the structure is used representing the structure as single frame elements to model the pier. Weights of the walls are incorporated in the self-weight of the walls and the slab weight and telescope mass are lumped at each storey. The telescope frame is modeled as one frame element that provides the same displacement under a horizontal load as the complete telescope frame. The displacements at each floor, the mode shapes and modal periods, as well as the base reactions give really close results to for the more complex model under the same load combinations. These results provide the confidence that the modeling has been done correctly.

Figure 8: SAP2000 pier and telescope frame simplified model.

5. Analysis

5.1 Bending capacity

The structure has to be able to resist the maximum bending moment induced by the earthquake loads. The bending capacity can be assumed as the ultimate bending capacity (M_n) (when bars start breaking), or the bending cracking point (M_{cr}), (point where concrete cracks in tension). For the current problem, it is wished to have the pier behaving elastically, so the cracking point will be assumed as the capacity. The factored maximum bending moment (M_u) was determined from the 4 DOFs model. The capacity was evaluated with Response 2000, software developed at University of Toronto by Dr. Bentz and Collins (2000). With this software, it is possible to evaluate the moment-curvature curve of a reinforced concrete section. The walls of the structure with the vertical reinforcement were modeled and the curve plotted in figure 9. The capacity is function of the tension cracking strength, the inertia of the section, radius, the area and the axial load. The first portion is a straight line until the cracking of the concrete occurs. The tensile strength of the concrete is taken as a conservative value of 1.49 MPa. After cracking, it is the steel that resists the tension forces in the section. The capacity keeps increasing until the steel starts to yield. Finally, the capacity increases because of steel strain hardening. To obtain conservative results, the axial load is assumed as the dead load.

The bending moment is 54 110 kN.m and is smaller than the evaluated cracking bending moment of 142 843 kN.m and the ultimate bending moment of 240 114 kN.m. The yielding moment is 193 259 kN.m.

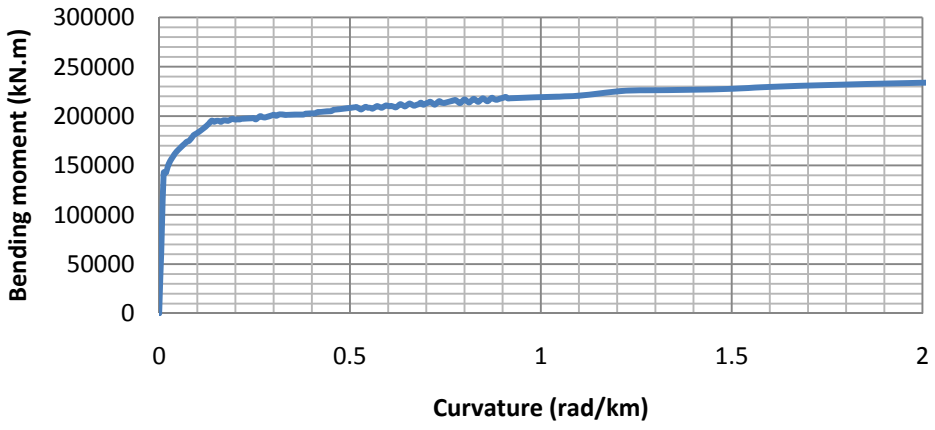

Figure 9: Moment-curvature function for the pier structure section.

The induced moment is 38% of the bending moment cracking point. It is concluded that the structure remains elastic at its base when subjected to earthquake loads, which is the wished behavior.

5.2 Shear capacity

5.2.1 Method 1

The horizontal forces in the pier building walls also have to be checked. These horizontal forces are called shear forces. Shear forces (V_u) in reinforced concrete structure is resisted by the shear capacity (V_n) that is constituted of a steel portion (V_s) and a concrete portion (V_c). The steel contribution is given by the horizontal steel in the walls. The first method used is derived from the ACI 371R "Guide for the analysis, design, and construction of concrete-pedestal water towers". It assumes that the shear is resisted on two straight parallel walls at different sections height. For sections without openings, the shear force at that height is equally distributed in each wall. At sections where openings are present, the shear force is distributed in function of the center of rigidity. Figure 10 presents the procedure.

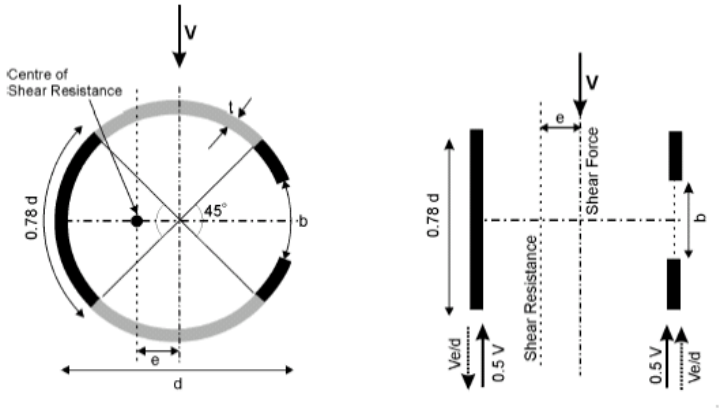

Figure 10: Shear forces distribution diagram in the walls of the pier structure (ACI 371R).

The capacity at the base of the pier and at the openings is evaluated and compared to the shear forces induced by the earthquake loads. The concrete contribution of the capacity is determined with a conservative equation from the ACI 318. In order to obtain a conservative evaluation of the capacity, it is assumed that the axial force would not contribute in an increase of the capacity. The shear forces for each section are obtained from the 4 DOFs model. Capacities are checked at the base because it is where the shear force is the highest and at the opening because of the different

distribution of forces. According to the ACI 318, the shear capacity needs to be decreased by a factor of 0.75.

Table 1: Shear capacity and forces check.

	Shear force kN	Shear capacity kN	Factored shear capacity kN	Ratio
Pier base	3 856			
Wall 1	1 928	5 280	3 960	0.48
Wall 2	1 928	5 280	3 960	0.48
Main opening center	3 763			
Wall 1	1 364	5 280	3 960	0.34
Wall 2 (opening)	2 398	3 004	2 253	1.06

It is observed that the shear capacity at the base is sufficient and that at the openings height, the ratio of capacity over force is slightly over 1.0. Because of the conservative assumption of the concrete contribution and of the low 0.75 capacity reduction factor, it is assumed that the shear capacity is sufficient.

5.2.2 Method 2

The shear capacity is also checked using a different approach to confirm the results of the first method. The SAP2000 finite element model is used and the tangential horizontal forces at each node of the structure's walls are compared to the capacity of the section each of the node covers. The shear forces envelope is plotted on the structure model in figure 11.

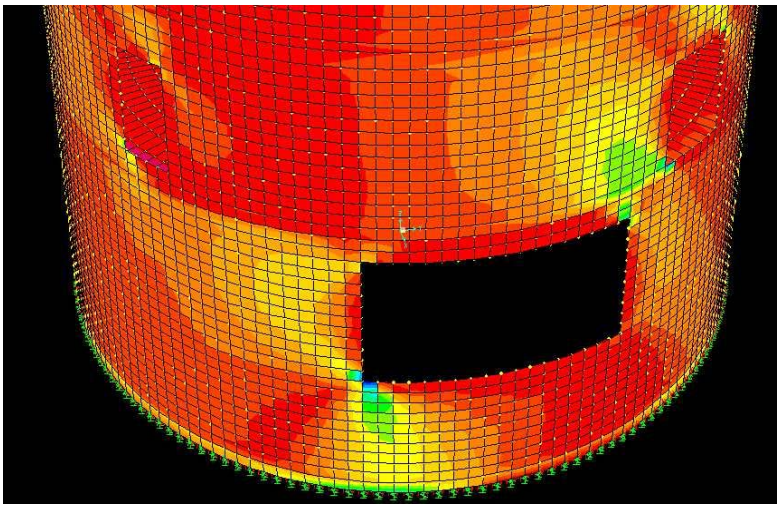

Figure 11: Shear forces envelope in the pier structure under earthquake loading.

Nodes are placed every 304.8 mm and the capacity is the summation of the concrete and steel contribution over that length. The concrete contribution is in this case amplified by the axial force present at each node. The axial force is here taken into account because this axial force can be evaluated precisely with the FEM model. The capacity at each node is compared with the forces for the different load combinations and earthquake orientations. The capacity is again reduced by a factor of 0.75 as recommended by the ACI 318. Each load combination for each section is checked. The forces are lower than the factored capacities in almost every case. Only a few nodes are slightly over the capacity, ratios between 1.0 and 1.3. This is observed at the openings corner. Because of the stress redistribution after cracking, it is assumed the shear capacity is sufficient for the pier walls.

5.3 Steel reinforcement design check

Ratios of steel reinforcement for the walls and the slabs also have to be verified. The method used is the one implemented in SAP2000 and is based on Brondum-Nielsen, (1974) and Marti, (1990). The structure was modeled with shell elements. When applying loads, these shell elements develop membrane forces (f_{11}, f_{22} and f_{12}), flexural moments (m_{11}, m_{22} and m_{12}), and shear forces (V_{13} and V_{23}) components. This design method assumes the shell to be constituted of three layers. Two steel reinforcement outer layers and one concrete core layer. This is often called a “sandwich model”. The outer layers take the moments and membrane forces and the core takes the out of plane shear forces.

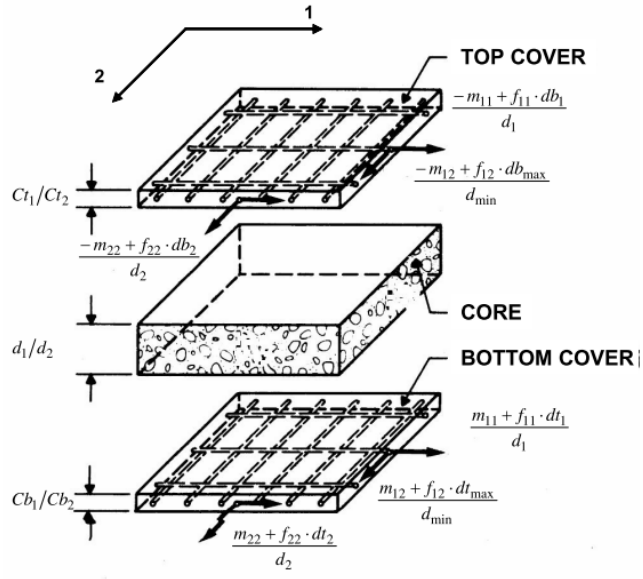

Figure 12: Shell forces and layers for steel design (CSI Berkley, 2006).

The six resultant forces cited earlier are transformed in pure membrane forces (N_{11}, N_{22} and N_{12}). These forces are then transformed in design forces (N_{des}) in 1 and 2 directions for the top and bottom layers. They are obtained from Brondum-Nielsen, (1974), equations. The design forces can then be transformed in steel area ratios, principal compressive forces and principal compressive stresses. For more detail on the procedure, please refer to "Concrete Shell Reinforcement Design Technical Note and Design Information", (2006). The steel ratios are computed using a reduction factor of 0.9. Using this method, the steel ratios in the one and two directions and for the top and bottom layers are evaluated for the slabs and walls for the different load combinations.

The steel present in the top slab and in the first and second storey slabs are sufficient. The required steel ratio over the present steel ratio is under 1.0 for each slab section, for 1 and 2 directions and top and bottom.

The walls were more complex to analysis because of stress concentration due to the slab connections and openings. The structure is first checked without any openings and the required ratios were lower or slightly over the steel ratios present in the structure. The structure is also analyzed with the openings. Stress concentration around the openings and the different forces distributions are observed. The ratios of required steel are a bit higher than the present steel, but not excessively. It is assumed the steel ratios are acceptable because of stress redistribution when cracking occurs and because of the strain hardening after yielding of the bars.

The minimum reinforcements are also checked. ACI 371R gives recommendation on the amount of horizontal and vertical steel there should at least be in the pier walls. In high seismic zones, the ratio of steel should be higher than 0.0025 in both directions, there should be two layers of steel in both directions and the ratio of vertical steel should be higher than the horizontal one. The vertical steel ratio is 0.0033 and the horizontal ratio is 0.0023. For flexural members, the ratio of vertical steel should be equal or higher than 0.0033. The required horizontal steel ratio of steel is just slightly over the one found in the structure and the vertical steel requirement is met. The steel ratios are assumed to be sufficient.

5.4 Openings

The small openings were assumed to be sufficiently reinforced and to not redistribute the stresses in the structure significantly. The main first floor opening capacity is checked in the next sections.

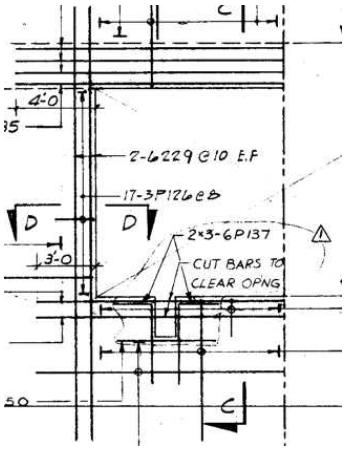

Figure 13: Reinforcement detail of the first storey opening (Plan 3516-0000-4200-4).

5.4.1 Top and bottom of the opening

It is wished to know if the main opening top has enough horizontal steel to resist the maximum bending moment. The required amount of steel is evaluated with ACI 371R requirements. The area of steel should be 808 mm^2 over a height of 914 mm according to the calculations. The amount of steel present on top over a height of 711 mm is 2272 mm^2. The load is assumed for this method to be equally distributed. It is not the case for the telescope load but, because of the important distance between the opening and the bearings of the telescope, the load is assumed to be equally distributed. This was confirmed by checking the forces distribution of the Finite element model. The required amount of steel for the bottom of the opening is the same as for the top and the area of steel present is 1420 mm^2.

5.4.2 Sides of the opening

The sides of the main opening capacities also needed to be checked. They are assumed to perform as columns and ACI 318 is used for this case. Recommendations of the ACI 371R are also followed for the loads to apply and the width of the column. The design of the column was made with SAP2000 which has a design function implemented. The capacity ratio is 0.367. It is concluded that there is capacity left in the columns besides the main opening.

5.5 Footing structural capacity

The structural capacity of the footings also needs to be checked. The shear capacity and flexural capacities have to exceed the forces at the supports due to the different load combinations. The foundation cross section evaluated is shown in the next figure.

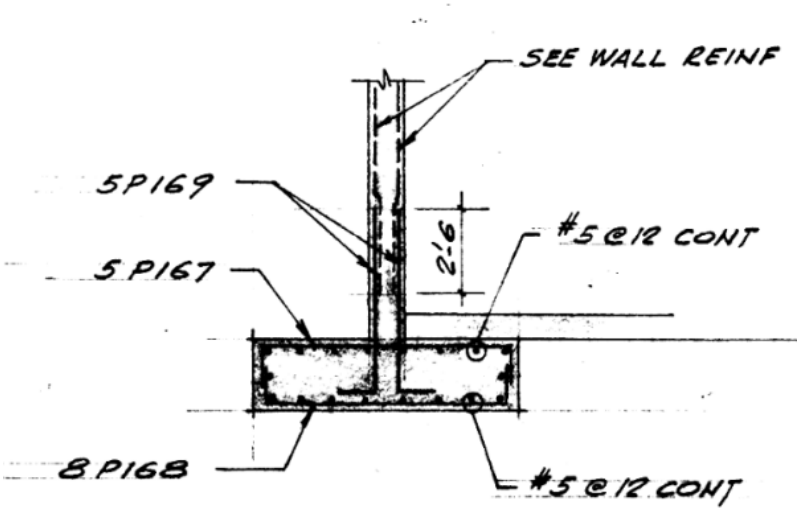

Figure 14: Foundation cross section and reinforcement detail.

First, the vertical shear capacity of the footing was checked. The results indicate that the shear capacity is high enough and resists the forces induced by all load combinations.

It is also required to evaluate the bending capacity of the footing. It is done checking if there is enough flexural reinforcement in it. The required ratios of reinforcement are evaluated for each load combination at each section. These ratios are all smaller than the steel ratios present in the structure. The footing is considered to have enough shear and flexural capacity.

5.6 Settlements

The "Final Investigation Report" by Dames & Moore (1974) states that the differential settlement should be kept less than 10 mm. The settlements are evaluated using the plate bearing deflection curves. Because precipitations are really low as well as the water level, the deformations are assumed to be elastic only. The pressures from the finite element model for the load case D + L are used. The maximum pressure found around the ring footing is 194 kPa and the minimum pressure is 153 kPa. To obtain conservative results the maximum deflection is evaluated with Test #2 and the minimum deflection is calculated with Test #1. The maximum deflection is approximately 4.1 mm and the minimum 0.5 mm. This gives a differential settlement of 3.6 mm. To achieve a 10 mm settlement, a pressure of 343 MPa is required.

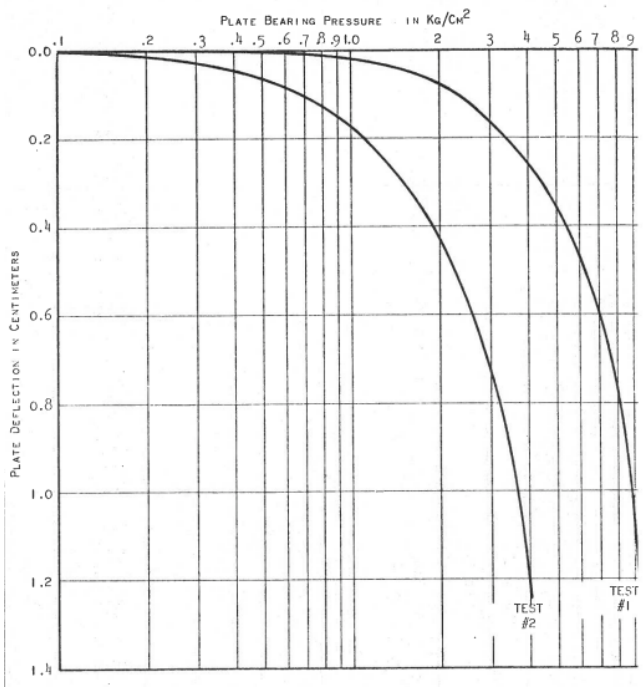

Figure 15: Plate bearing deflection curves (Dames & Moore, 1974)

It is concluded that the differential settlements are not an issue here even if it can be observed on figure 15 that there is important variability in the results of the two tests. More tests could be done to determine if the present results are reliable and representative of the soil in place. More refined methods exist to evaluate the differential settlements, but more detailed data of the soil in place is required.

5.7 Soil capacity

The allowable stress design load combinations applied to the pier building induce forces at the base of the structure. These forces are resisted by the footings that distribute them to the soil. A bigger area of foundation results in a lower pressure applied to the soil. The pressure distributed by the footing at each node of the modeled structure is compared to the capacity of the soil of 191 kPa. The vertical force and the moment induce pressure. The moment is transformed in a force being applied with an eccentricity (e) and an equivalent pressure is calculated and compared to the bearing capacity. For the load combinations D and D + L, the maximum ratios of pressure over capacity are 0.91 and 1.02.

For the load combinations including earthquake loads, the maximum pressure found has a ratio of 1.33. Coduto, (2001) states that geotechnical engineers usually increase the bearing capacity of soils by 33% for load combinations with earthquake loads. This is permitted for 4 reasons. The shear strength of soils under high rate loading is higher than during sustained loading resulting in a greater bearing capacity. Also, lower factor of safety can be tolerated because of the rare nature of earthquake events. Under transitory loading, settlements are generally smaller. Larger settlements can be tolerated under rare events because people are going to accept some cracking or minor distress. Because of the variability of the soils, it is not every soil type that will present that type of behavior. Increasing the bearing capacity by 33% is not recommended anymore in the recent codes.

The soil under dead and live load can bear the pressure distributed by the footings. Considering there is a certain safety factor for the bearing capacity, it is acceptable. For the earthquake combinations, if a 33% increase in the bearing capacity is taken, the design could be considered as safe. But to do so, advice from geotechnical experts having studied the site conditions is required.

If the capacity is judged to be insufficient, some solutions can be envisaged to solve the problem. An easy way to decrease the pressure induced by the footing is to increase its width. In the case of the pier building, because of the presence of the dome structure around the pier, it is only possible to increase the footing width inside the pier. Also, because of the restrained space and equipment in place, it may be complicated to execute.

An laternate solution would be to reinforce the soil bearing capacity with post-grouting piles through drilled holes. It consists of drilling a 100 mm hole in the foundation and soil and inserting a 50 mm diameter steel pipe that reaches the bearing stratum. The space between the hole and the pipe is filled with sand and grouting is inserted in the pipe and around the footing and pipe. The problem with this option is again the restrained space to drill and the fact that the bearing stratum may be far away from the surface. Other avenues can be studied to reinforce the soil.

It should be noted that Dames & Moore (1973) recommended that the footing should at least be 3.0 m wide and that the soil should have been strengthen with cement grouting under the foundation in drilled holes. The current footing is 2.24 m and the soil has not been reinforced to our knowledge. This may explain why the capacity is a bit too low under earthquake load combinations.

6. Conclusion

The upgrade of the current Canada-France-Hawaii telescope from a 3.6 m to a possibly 10-12 m telescope raised various questions. The first step was to assure that the current concrete pier structure can support the geometry and mass of the new telescope. Also, the pier having been designed in 1974, the Codes have evolved since then, mostly regarding the seismic design and analysis of structures. The pier building of the CFHT was analyzed for the next generation telescope according to the current requirements for structural design. A description of the structure, foundation and soil was first done. Then a methodology was developed to evaluate the capacity of the different members and loads applied on them. The International Building Code and the American Concrete Institute code were used for that purpose. Seismic analysis was performed using the equivalent static method and the design spectrum specific to Mauna Kea. A draft version of a frame was designed and placed on top of the pier that represents the telescope static and dynamic behavior. The shear capacity, bending capacity, steel reinforcement, foundation capacity and soil capacity were evaluated. They were then compared to the forces and steel in place.

- The walls, slabs and footings are judged to have a sufficient structural capacity.
- The differential settlements are evaluated to be less than 10 mm. The soil allowable bearing capacity under dead and live load is sufficient; the pressure induced by the footing is equal to the capacity.
- Although the required bearing capacity is 254 kPa for earthquake load combinations, the nominal bearing capacity under seismic loading can be increased to account for the transient nature of the loading, permitting to assess the bearing capacity as sufficient.
- If the new generation CFHT is planned to be built, a geotechnical investigation should be done to revaluate the soil parameters and foundations capacity.

References

ACI 318-08. (2008). “Building Code Requirements for Structural Concrete and Commentary”. American Concrete Institute, Farmington Hills, Michigan, USA.

ACI 371R-98. (1998). “Guide for the Analysis, Design, and Construction of Concrete-Pedestal Water Towers”. American Concrete Institute, Farmington Hills, Michigan, USA.

American Society of Civil Engineers, (2010). “Minimum Design Loads of Buildings and Other Structures – ASCE 7”. Reston Virginia, USA.

Bentz E. and Collins M.P. (2000), “Response-2000, Version 1.0.5, Reinforced Concrete Sectional Analysis using the Modified Compression Field Theory”. University of Toronto, Ontario, Canada.

Coduto, D.P. (2001). “Foundation Design – Principles and Practices”. Prentice-Hall, Upper Saddle River, new jersey, USA.

Durgesh, C. R. and Bhumika, S.. (2004). “Seismic design of Concrete Pedestal Supported Tanks”. 13th World Conference on Earthquake Engineering. Vancouver, B.C., Canada, Paper No. 230 .

Dames and Moore, (1973). “Foundation Investigation Report”. Hawaii, USA.

Dames and Moore, (1974), “Final Investigation Report”, Hawaii, USA.

IBC. (2003). “International Building Code”. International Code Council, Country Club Hills, Illinois, USA.

Grundmann, W., et al. (1997). A Canada-France-Hawaii 12-16m Telescope Study.

Pillai, S. U., Marie-Anne Erki, and D. W. Kirk. (2008). “Reinforced Concrete Design”. Toronto, Ontario, Canada.

SAP2000, Computers and Structures, Inc., Berkley. (2009). “Structural Analysis Program”. Version 14. Berkley. California, USA.

SAP2000, Computers and Structures, Inc., Berkley. (2006). “Concrete Shell Reinforcement Design Technical Note and Design Information”. Berkley, California, USA.

APPENDIX B. NGCFHT TELESCOPE AND ENCLOSURE CONFIGURATION AND OUTER PIER CAPACITY STUDY

ngCFHT Telescope and Enclosure Configuration and Outer Pier Capacity Study

Dynamic Structures Ltd. &

University of British Columbia

January 2012

Revision History

Version	Date	Comments
1	Dec 22, 2011	Initial release
2	Jan 20, 2012	Information on ngCFHT telescope concept
3	Jan 30, 2012	Revisions based on review meeting

Table of Contents

List of Tables

List of Figures

Introduction

This report summarizes the results of a study on the Next Generation Canada-France-Hawaii Telescope (ngCFHT). The work was conducted from October to December 2011. This is the third phase of development work carried out by DSL and UBC on the ngCFHT project. The first was the telescope pier capacity study done by UBC. The second was DSL's work on defining the telescope mass properties and modeling of the azimuth track interface for the first study.

There are two primary objectives of the present work phase:

- The first objective is to develop an ngCFHT system with the telescope and calotte enclosure configuration meeting the dimensional constraints of the current CFHT inner and outer piers and site considerations. The goal is to develop a new telescope and enclosure system with the calotte enclosure matching the three dimensional volume of the current CFHT enclosure while accommodating a new and fully functional 10 m class segmented mirror telescope within the interior space. The telescope and enclosure configuration should include realistic space allocations for the telescope azimuth journal and its structural interface with the inner pier, enclosure wall thickness with realistic structural member dimensions, and enclosure bogies and their structural interfaces with the outer pier. Additional outcomes are the mass, centre of gravity (CG), mass moment of inertia estimates of the telescope and enclosure. The new ngCFHT system should have sufficient details to allow for a ROM cost estimate.
- The second objective of this study is to determine the load capacity, statically and dynamically, of the current enclosure foundation and pier based on the latest structural design codes and including all environmental loads. The outcome is to determine if the current CFHT outer pier has sufficient load capacity for the calotte enclosure configuration.

Statement of Work: Based on the site and as-built information, and design and functional parameters:

1. Develop a conceptual ngCFHT telescope and enclosure system compatible to the current CFHT geometry
2. Determine the load carrying capacity of the current enclosure foundation and pier
3. Provide recommendations to retrofit the enclosure pier should its capacity deemed to insufficient
4. Provide assessments of the suitability of the current telescope foundation/pier and enclosure foundation/pier for future upgrade and potential dynamic interactions

1. Concept Design

The goal of the concept design is to develop a new enclosure and telescope system. This should match the space envelope of the current observatory as closely as possible, including realistic space allocations for structural and mechanical subsystems

1.1 Requirements

The following summarizes the requirements on the concept design of the enclosure and telescope system.

- General
  - The goal of ngCFHT is to preserve existing aspects of the CFHT observatory as much as possible. Preserving the overall observatory space envelope will facilitate the permitting process. Reusing the inner and outer piers is beneficial for cost and schedule considerations.
- Optical configuration:
  - The primary mirror is an f/2 segmented 10 m diameter mirror
  - The distance from primary mirror to image plane is 17.9m (see Figure 1). The space envelope for the fibre position system and telescope guide camera is an additional 1.5m for a total distance of 19.4m from the primary mirror vertex to the top of the telescope
  - The enclosure will provide a clear zenith angle observing range from 0 degrees to 65 degrees. The telescope will be able to point to 90 degrees to facilitate maintenance of the top end components.
- Handling requirements: A dome-mounted crane (or cranes) will handle the M1 segments and the prime focus components. The top end components can be modular such that they stack together. A piece size of 1 m dia. X 0.5 m thick and 500 kg is assumed.

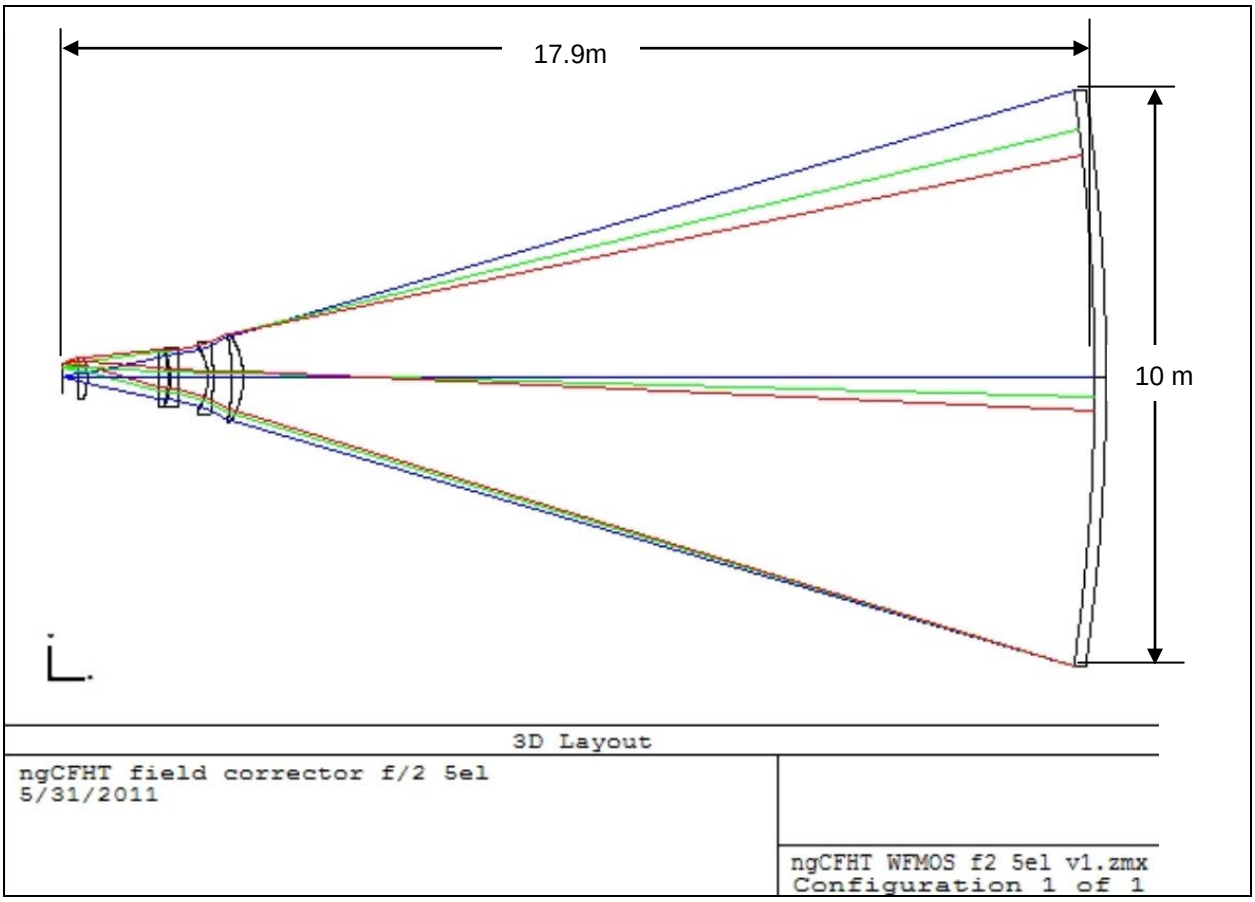

Figure 1: Optical configuration of ngCFHT

1.2 Enclosure Concept

A calotte configuration for the enclosure was selected due to its compact design and structural efficiency. These features give it the best possibility of matching the existing enclosure size and mass, which would allow the existing enclosure pier to be utilized. Figure 2 below shows a CAD model of the existing CFHT enclosure and telescope. Figure 3 shows the proposed ngCFHT calotte enclosure.

Figure 2: Existing CFHT Enclosure and Telescope

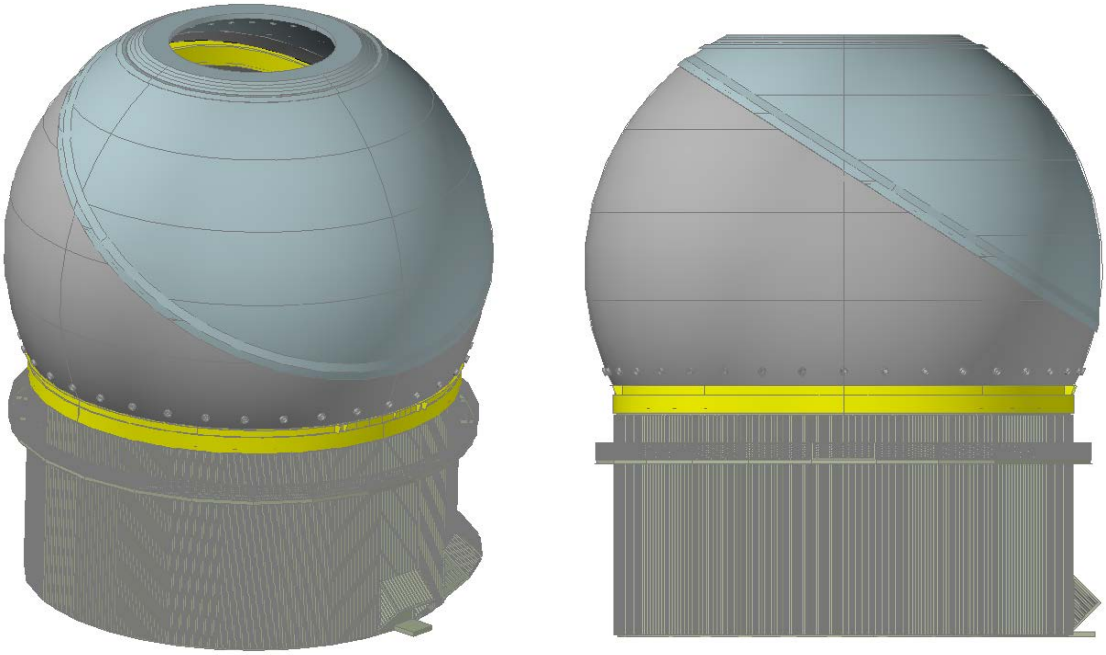

Figure 3: Proposed ngCFHT calotte enclosure

1.2.1 Geometry

The dimensions of the proposed ngCFHT enclosure are shown in Figure 4 below. A telescope sweep radius of 14.0m is assumed. The inside radius of the dome is set at 16.0m (inside of the dome insulation) and the outside radius is set at 17.0m. A goal of the design is to reuse the existing rotating ring girder and azimuth bogie system if possible. Since the sphere of the dome must therefore intersect the existing ring girder, this determines the approximate height of the elevation axis, which is presently set to 24.0m above grade. There is some opportunity to reduce this if necessary by using a variable radius on the dome so that the elevation axis can be lowered, and the dome sphere will still intersect azimuth ring girder. Figure 5 shows a comparison of the proposed ngCFHT enclosure dimensions to the existing CFHT enclosure dimensions.

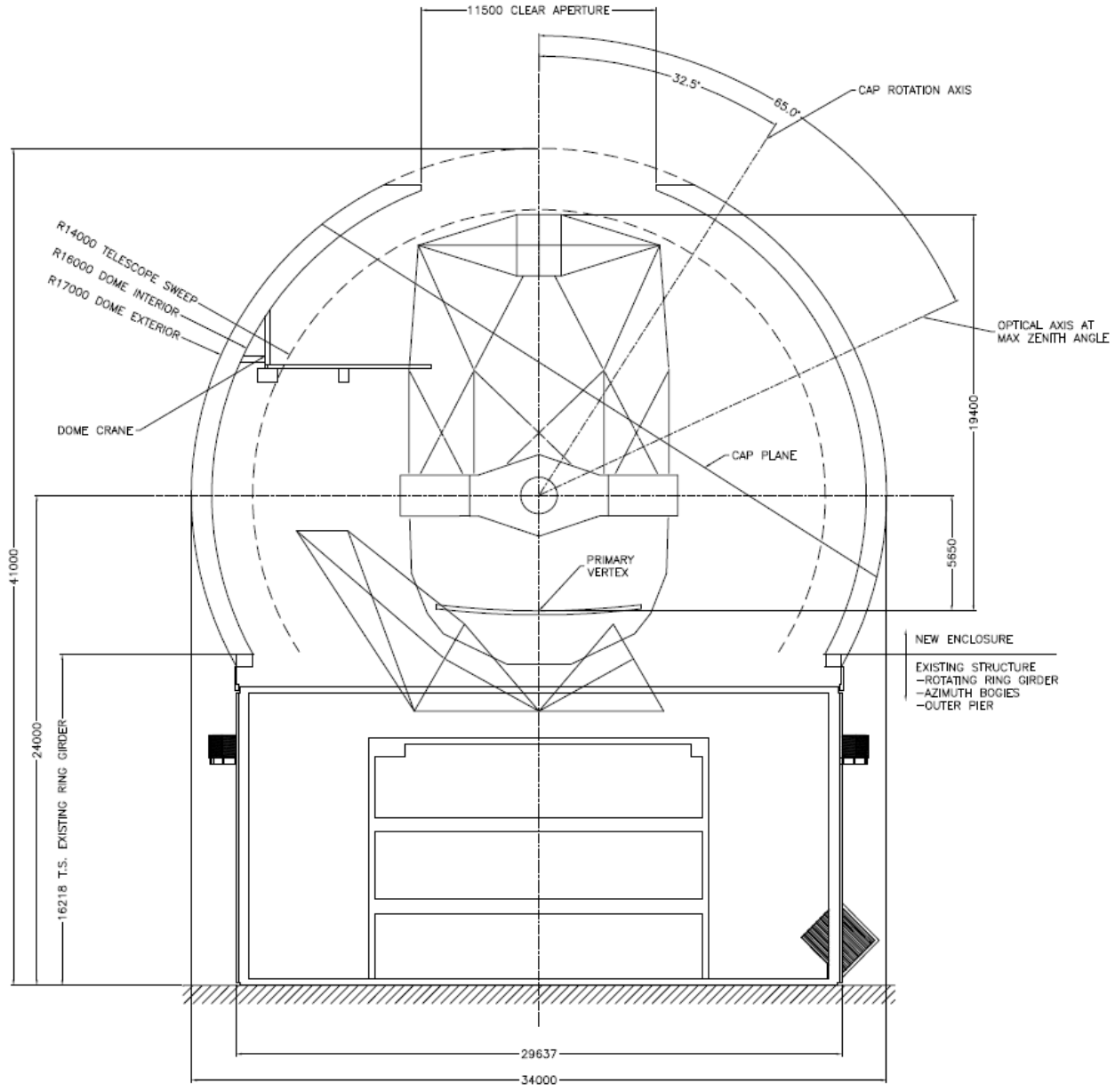

Figure 4: Dimensions of proposed ngCFHT enclosure

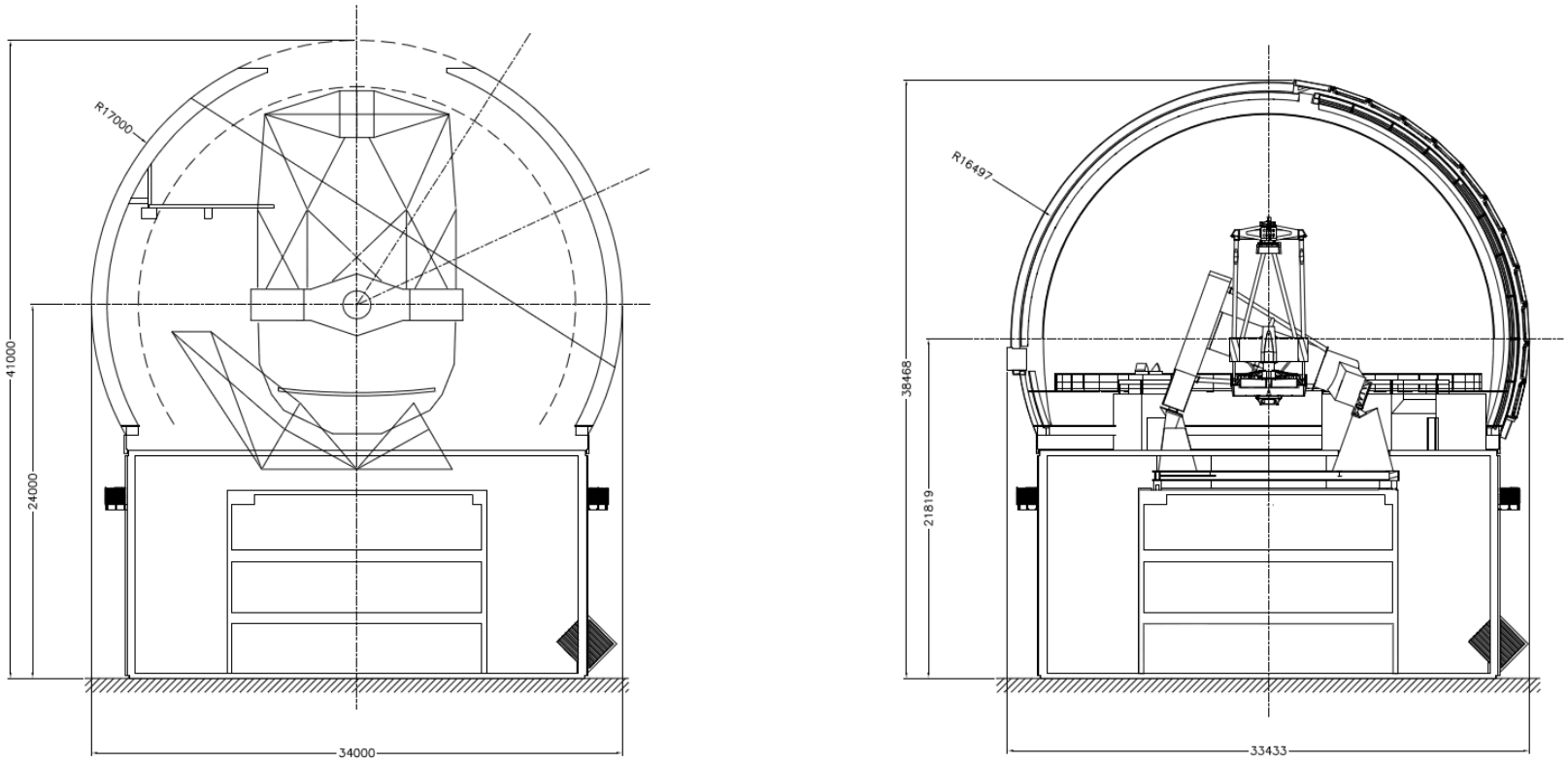

Figure 5: Comparison of ngCFHT enclosure dimensions (left) to existing CFHT enclosure dimensions (right)

1.2.2 Shutter

The shutter concept for the ngCFHT is shown in Figure 6 below. The geometry of the enclosure permits a fixed shutter concept to be used, where the shutter (shown in blue in Figure 6) is a cantilevered extension of the base structure. The aperture is closed by rotating the aperture over top of the shutter. This approach eliminates the need for additional major mechanisms to open and close the shutter.

In the closed position, a locking mechanism is likely required to secure the aperture to the shutter at points around its perimeter. A sealing mechanism would also be required to seal the interface. An inflatable seal is a possible solution here and has been proposed and prototyped for TMT.

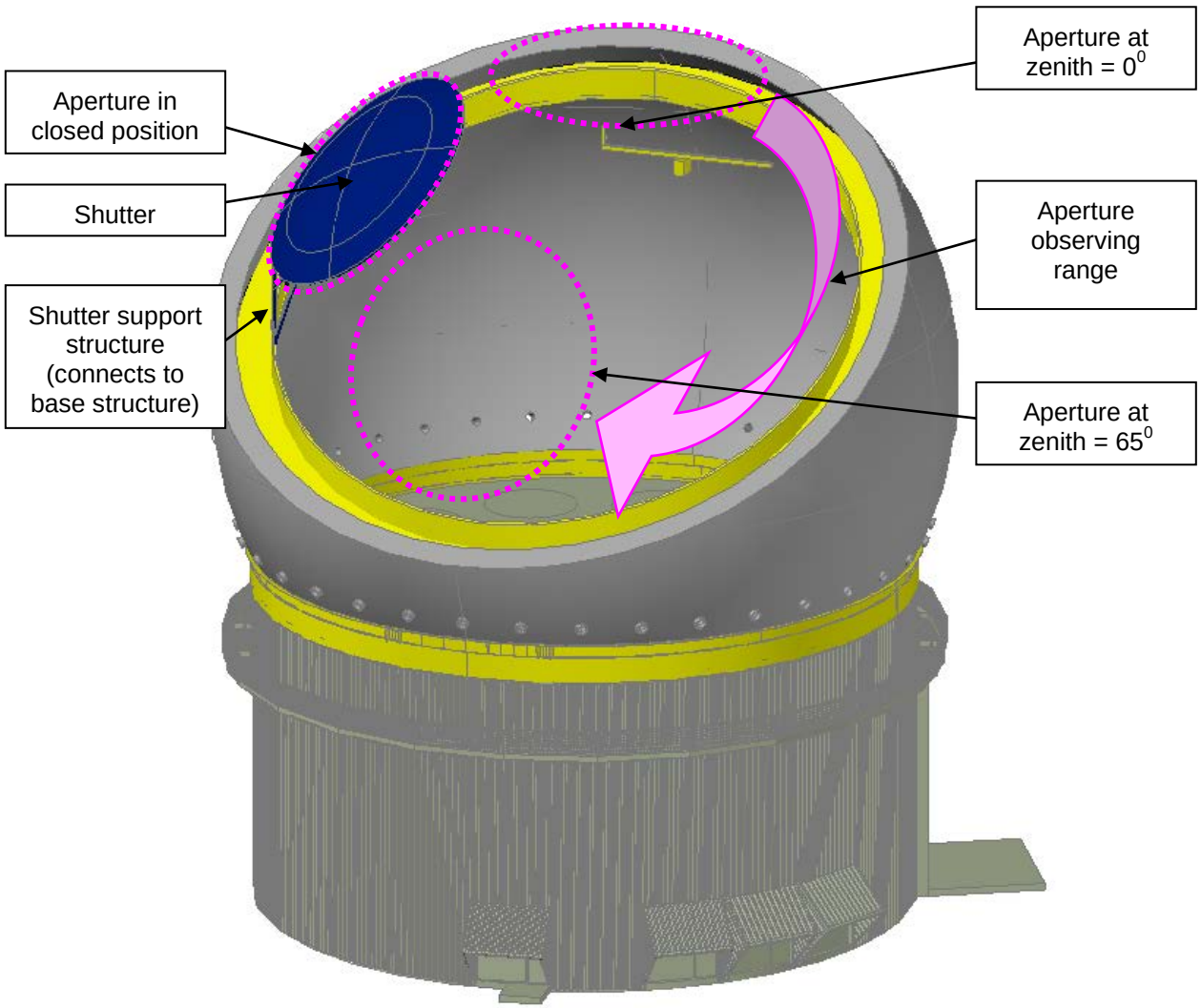

Figure 6: Shutter concept (cap is removed to show shutter, aperture indicated by dotted lines)

Since the shutter is located on the inside of the dome when open, the shutter would need to be clear of large accumulations of snow and ice prior to opening. The center of the shutter is sloped at 45deg relative to horizontal, so much of the snow should shed naturally. Ice and snow accumulation could be mitigated by pointing the shutter downwind during storms. Ice and snow shedding could be enhanced by adding a heating system if necessary. Once the enclosure is opened, any run-off from residual snow or ice on the shutter could be controlled by a gutter system around the shutter perimeter.

Access to the perimeter of the shutter is likely required to inspect the locking mechanisms and seals. If possible, it is desirable that the access would all be located inside the dome such that the exterior of the dome is kept free of walkways, ladders, and other protrusions that would accumulate snow and ice.

1.2.3 Structure

The basic structural elements include ring girders at the circular mechanical interfaces, and a rib structure for the spherical portions of the structure. Cladding is provided by a welded steel plate skin. The basic structural approach is similar to that used on the existing CFHT dome, and other domes such as Keck and Gemini.

1.2.4 Mechanisms

The major mechanisms are the azimuth bogie and drive system, and the cap bogie and drive system. It is intended that the existing azimuth bogie and drive system can be reused, but this will need to be verified in further design studies. Designs for the cap bogie and drive system have been well developed for TMT. The cap bogies are distributed around the perimeter of the inclined cap plane. The cap drives consist of a rack and roller pinion drive system located at the lowest point of the inclined cap plane. The drive system is similar to that used on the existing CFHT shutter.

1.2.5 Environmental Control

1.2.5.1 Insulation

It is assumed the dome will be insulated. Sandwich panels with aluminum skins and expanded polystyrene core are commercially available with thicknesses from 4” to 10”. These provide a cost effective solution, and can provide good insulation to a spherical dome if proper connection details are specified.

1.2.5.2 Vents

No ventilation specifications have been developed at this point. Options exist to ventilate the interstitial space of the enclosure (as on the existing CFHT dome) and also to passively ventilate the entire dome interior via large ventilation openings (as on Gemini). For the TMT calotte design, commercially available roll-up doors with high wind load ratings were proposed for the ventilation doors. A secondary set of insulated doors provides the thermal break when the doors are closed. This approach could be used on the ngCFHT calotte also. For practicality reasons, it is preferred to only locate the ventilation openings on the base portion of the enclosure (below the inclined bearing).

1.2.5.3 Flaps

Aperture flaps are wind-deflecting features around the perimeter of the aperture, which are used to reduce wind speeds around the telescope top end during observing. Aperture flaps were deemed to be necessary for the TMT calotte to reduce wind speeds. On a site such as Mauna Kea that is subject to snow and ice storms, the flaps must be retractable such that they do not accumulate an excessive amount of snow and ice during storms. This requires additional mechanical and access complexity. For the ngCFHT dome it is assumed that aperture flaps will not be required.

1.2.6 Handling

A dome-mounted handling crane may be used to handle the primary mirror segments and also components at the telescope top-end. A crane similar to the Keck segment handling crane is proposed. The handling of the primary mirror segments generally requires large crane reach and low capacity, whereas the handling of the top end components may require higher capacity but shorter reach. Thus it may be beneficial to provide two separate cranes to serve these two basic functions.

1.3 Enclosure Loads

Assumed environmental survival loads are tabulated below.

Table 1: Environmental loads for survivability requirements

Description	Value	Notes/assumptions
Wind – shutter closed	78 m/s	3sec gust @ 10m, 50 year return
Wind – shutter open	35 m/s	3sec gust @ 10m
Snow	150 kg/m^2	
Ice	68 kg/m^2	
Seismic – lateral spectral acceleration	0.5g	See section 2.2.2.6 below for details
Temperature	-16ºC / +30 ºC	

1.4 Telescope Concept

The telescope structure and mechanical concept can largely be derived from the Keck telescopes, which are also 10m diameter segmented alt-az telescopes. The primary baseline for the optical design for the telescope has been outlined above and as these are nearly identical to the twin Kecks the structure and mechanical systems will be of similar capacity.

There are a few major differences between the Keck telescopes and the ngCFHT proposal due to the nature of the instrumentation and data focal plane proposed. These differences significantly reduce the side and rear space requirements for the support structure on the telescope azimuth however as they are not driving factors in the telescope envelope no savings is realized in the telescope rotational sweep. The telescope sweep envelope is governed by the elevation sweep of the telescope optical assembly itself. This sweep is identified in Figure 4 above. The space savings between the Keck design and the ngcCFHT arise from the removal of the two Nasmyth Platforms and the rear Cassegrain Platform which are not required for the proposed optical design. The removal of these three structures will allow a significant reduction in the rotating mass of the Azimuth structure and related reduction in the size of the drives required.

Mechanically the telescope structure has two rotational axis; the Elevation axis which is located at what would be the Nasmyth level and the Azimuth axis which is at the bottom of the telescope support structure. The rotational elements of the Elevation axis are a pair of conventional bearings that, although custom ordered, are available from several suppliers. The Azimuth Bearing is a custom designed oil bearing. The sizing of this bearing could be slightly smaller than the current Keck design due to the savings in mass noted above. The two drive systems are designed to be friction systems and these are stable designs with identified deficiencies. A future option could be to look at alternate drive methods such as integral direct drive or Linear Induction Motors. Advances in encoder technology since the production of the Keck telescopes have allowed for higher resolution for positioning and control.

The last area of consideration is the Secondary cage and its related mechanical systems. These are largely a fall-out of the operational requirements of the instrumentation and must be designed in concert with those constraints. At the very minimum, methods for focusing and instrumentation need to be included.

2. Existing Enclosure Pier Evaluation

The goal of the existing enclosure pier evaluation is to provide an evaluation of the possible reusing of the current enclosure pier and foundation for future upgrade and potential dynamic interactions. This section presents in details the procedure used to perform the assessment of the outer pier as well as the analysis results and conclusions.

The structure is first described in detail. Following that, the methodology and modeling assumptions are presented. Finally, the analysis results and design checks that were performed to assess the structure are reviewed.

2.1 Structure description

This section of the report presents a detailed review of the structure and foundation components. It characterizes the geometry and structural configuration of the outer steel frame pier, footings and dome idealization. The material properties and soil information of the site are also described.

2.1.1.1 Geometry and structural configuration

The outer pier covers the inner concrete pier building supporting the telescope as shown in Figure 7. The outer pier building is a 5 storey steel structure of an overall height of 14.9 m and of an outer diameter of 28.8 m. The 1st level is referred as the ground level and the 5th level as the observation level. The inner diameter is of 16.8 m and there is a spacing of 76 mm between the inner concrete pier and the outer steel pier.

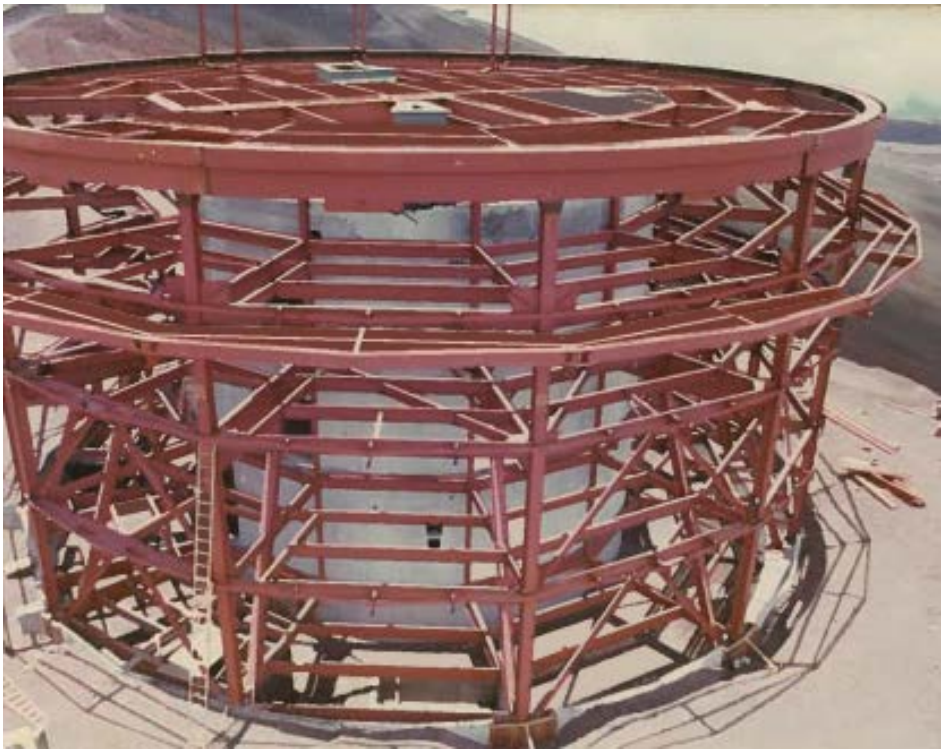

Figure 7: Outer pier framing during its construction

The structure is divided in 12 bays along its perimeter. Each column is numbered from 1 to 12. For each level and each bay, the typical bay framing is drawn. Figure 8 to Figure 12 show the plan view of the different levels. The main opening of the outer pier is located at the ground level between columns 1 and 12.

The x-axis is perpendicular to the opening and the y-axis parallel to the opening. The z-axis is in the vertical direction.

The third level has horizontal bracings joining the tangential beams together. The observation floor has a framing at its center. The beams in the x-direction on the center of the observation level are composite beams, this means that they act in a composite way with the concrete slab on top of it.

Concrete slabs cover the floor framings, the ground, second, third and fourth slabs are 64 mm thick and the observation level slab is 250 mm thick. The slab is continuous around the perimeter of the ground floor and no slab is present between columns 1 and 12 for the higher levels.

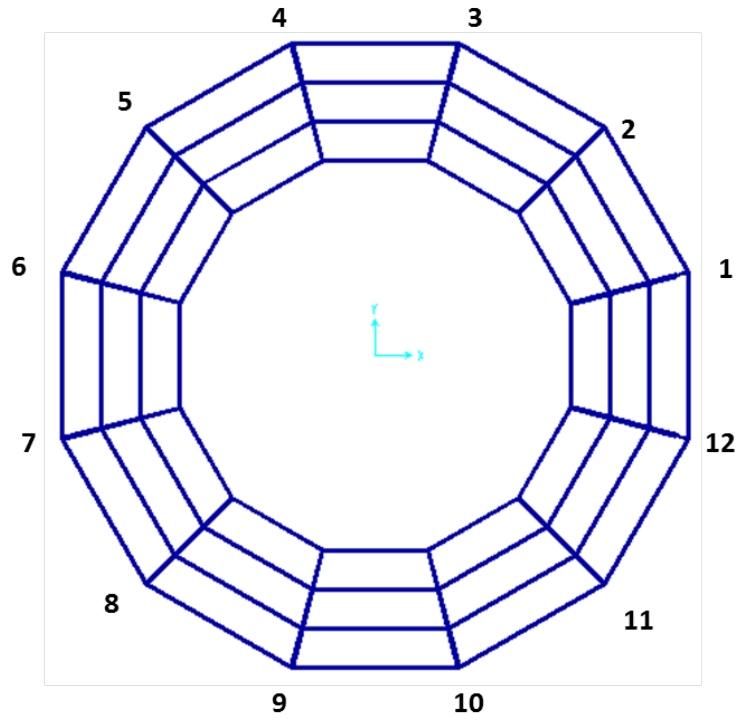

Figure 8: Ground level plan

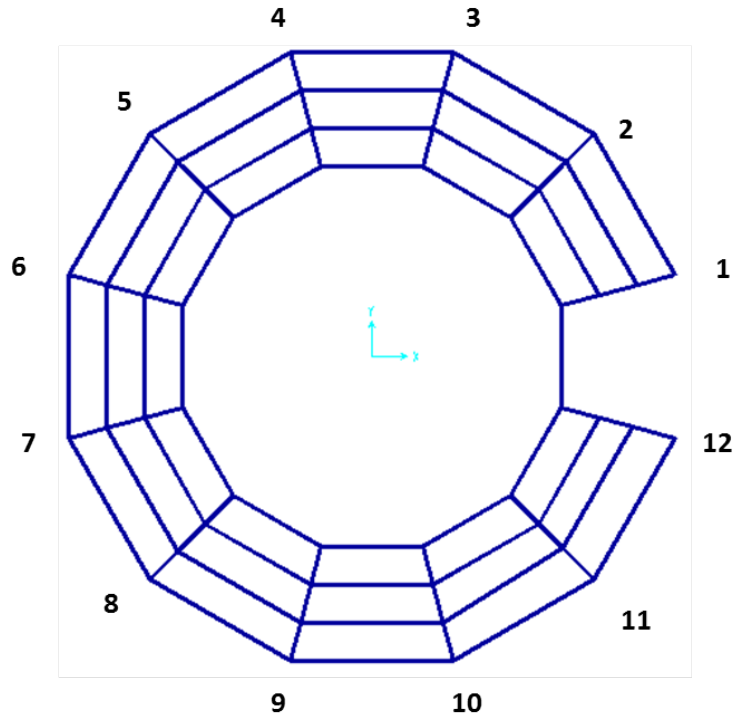

Figure 9: Second level plan

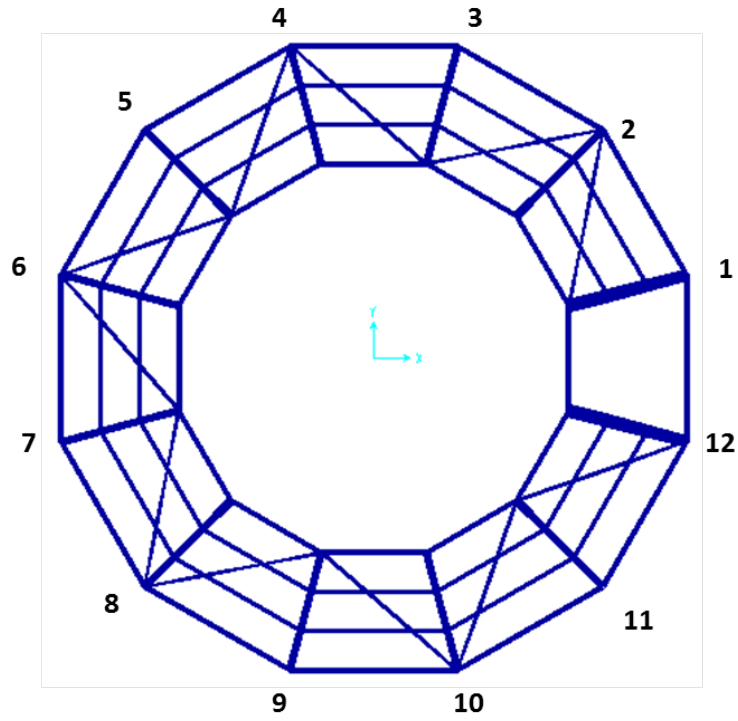

Figure 10: Third level plan

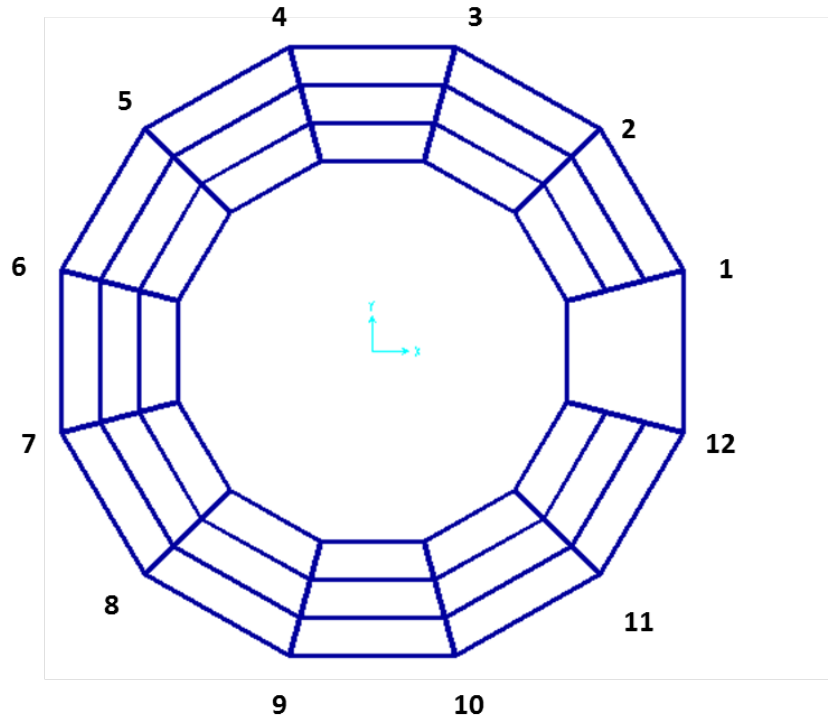

Figure 11: Fourth level plan

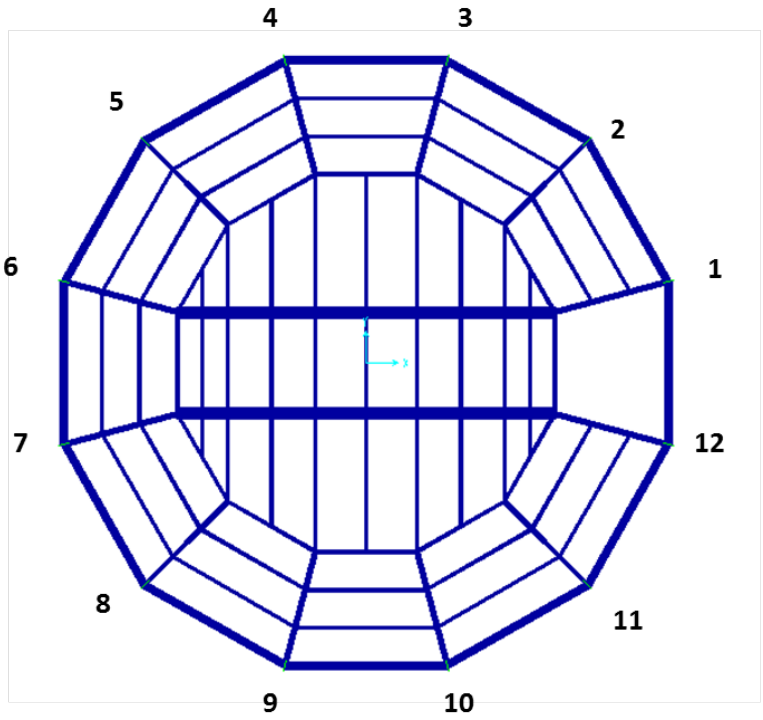

Figure 12: Fifth level plan with wide welded flange section

The height from the footing top to the ground level is 0.77 m and the interstorey height for the second and third levels is 3.91 m and 4.01 m, respectively. For both the fourth and observation levels, the interstorey height is 3.09 m. The fifth level is the observation level and a balcony is located on its slab. The balcony is not shown on the drawings. The dome is placed on top of the observation level on the external ring girder.

The vertical load on the observatory level is distributed to the levels below using both inner and outer columns. The load is then carried by the diagonal columns and the outer columns to the foundation. The tension hangers support the ground and second levels and are attached to the beams of the third level. Figure 13 presents the outer perimeter of the pier structure, and Figure 14 displays the inner perimeter of the pier structure.

The bracings are chevron types and are the elements resisting the lateral loads applied to the structure. The bays are braced at each bay for the top level and every two bays for the lower ones.

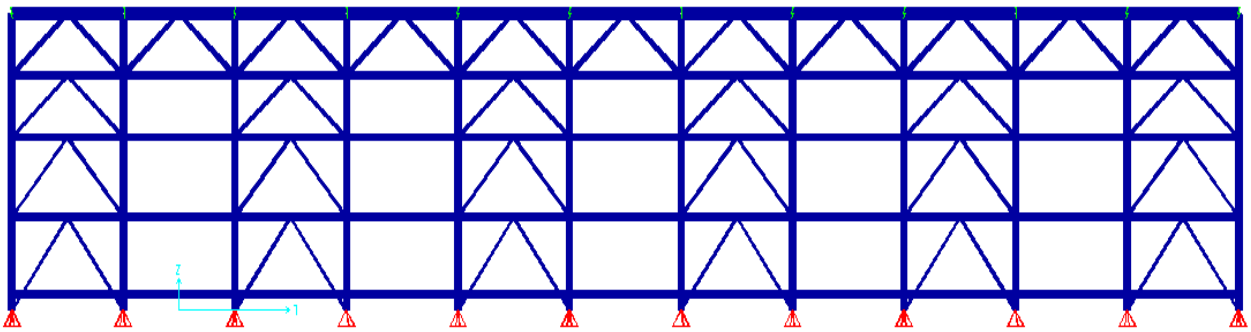

Figure 13: Outer perimeter of the outer pier structure

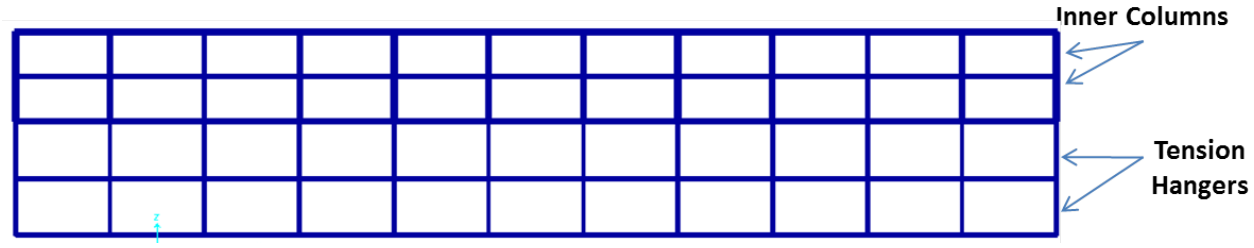

Figure 14: Inner perimeter of the outer pier structure

Diagonal columns are run continuously from the pinned support at the foundation to the third level beams as shown in the next figure.

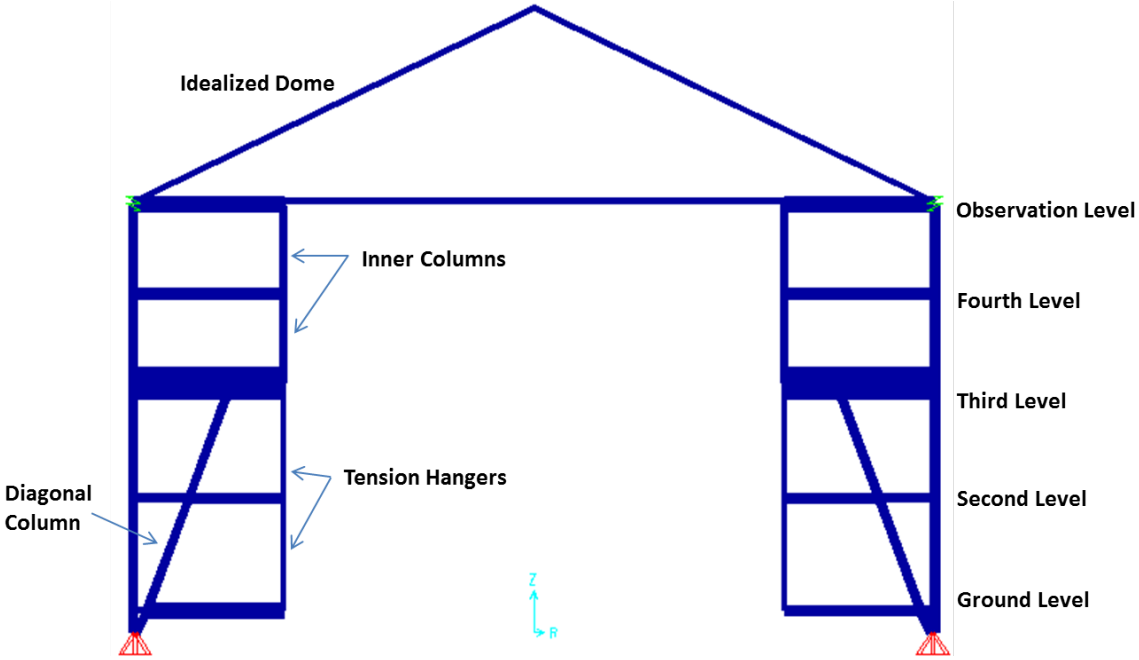

Figure 15: Typical radial view

The following figure presents the three-dimensional view of the structure.

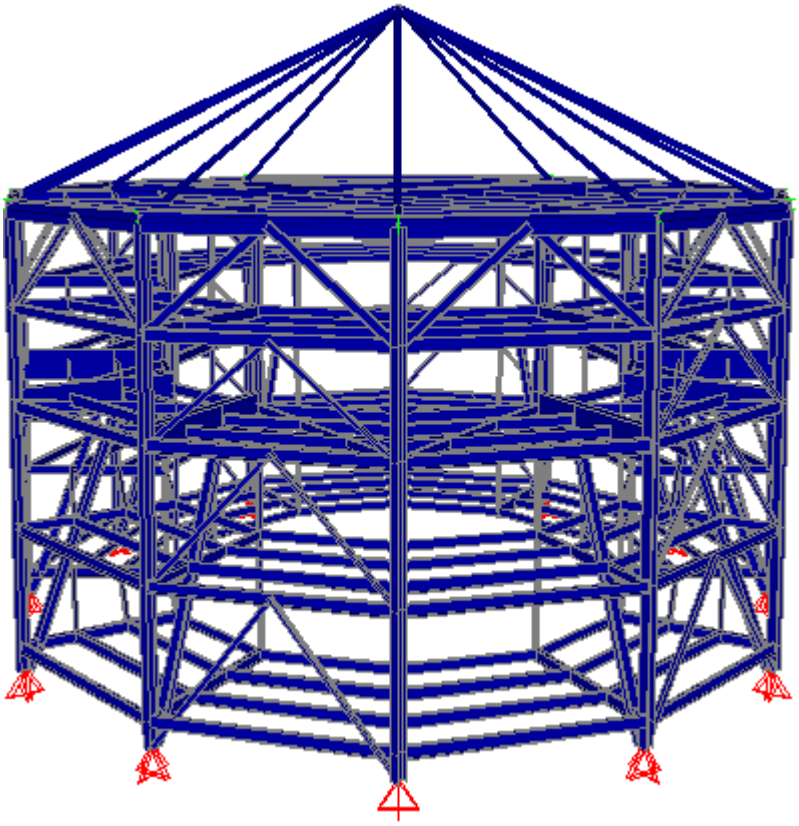

Figure 16: 3D view of the outer pier

2.1.1.2 Footing

The foundation is a ring footing of 4.267 m width and 1.828 m height. Longitudinal reinforcement bars are constituted of equally distributed 20 #8 bars on top and bottom faces. Radial reinforcement on the bottom is formed of #8 bars spaced at 203 mm. Two sets of #4 vertical shear reinforcement stirrups are provided. The stirrups are spaced at 203 mm at column locations and at 406 mm between the columns. Figure 17 below shows a cross section of the ring footing.

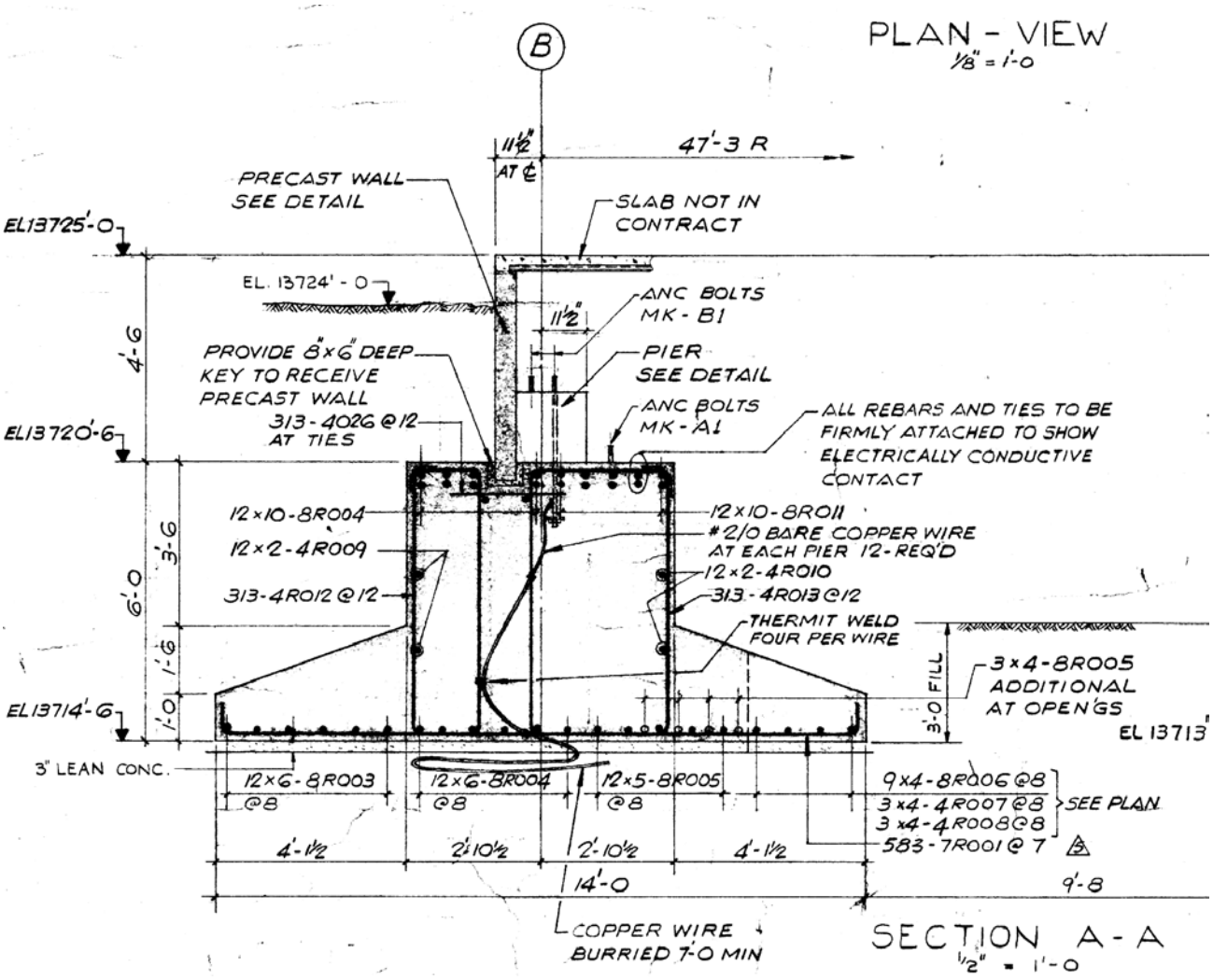

Figure 17: Ring footing cross section and reinforcement detailing

2.1.1.3 Dome

To evaluate the outer pier capacity, it is necessary to consider the forces produced by the dome on top of the structure. The dome is a complex structure and requires a considerable amount of time to be modeled in detail. Therefore, it is simplified as a pyramidal frame with the mass of the dome concentrated at its top. The frame is connected to the pier top on the external ring girder through spring elements. The spring elements have translational rigidity only; K_z is the vertical stiffness, K_r is the radial stiffness and K_t is the tangential stiffness. The pyramidal frame members are considered as rigid elements. The behavior and stiffness of the frame is controlled by the spring elements. To determine the stiffness of the spring, it is assumed that deflections due to the telescope dead load should be between 10 and 20 mm. Also the K_z and K_r are assumed to have the same stiffness and the tangential stiffness K_t to be 10% of the two other stiffnesses. The pyramidal frame nodes are interconnected with the rigid elements in the pattern presented in Figure 18. The pyramidal frame is connected at each exterior column top. This idealization of the dome is judged to be sufficient to represent the global behavior of the dome and to transmit the forces to the outer pier properly. It should be noted that the dome forces on the real structure will be transferred to the ring girder as point loads at the locations of the azimuth bogies.

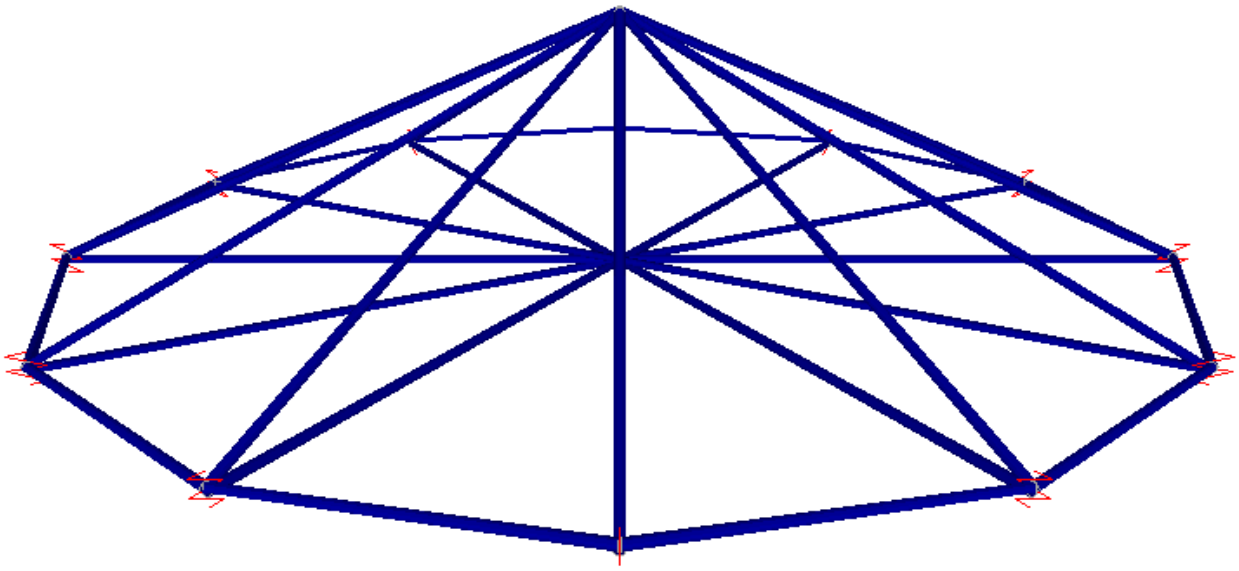

Figure 18: Dome configuration

The table below presents the spring stiffness in different directions that were assigned to the finite element model.

Table 2: Dome modeling parameters

Vertical stiffness - K_z (kN/mm)	27.777
Radial stiffness - K_r (kN/mm)	27.777
Tangential stiffness - K_t (kN/mm)	2.777
Center of gravity height over observation level (m)	11.929
Number of spring supports	12

2.1.2 Structural Weights

Table 3 below summarizes the weight of the structure with the existing and future dome systems. Replacing the existing dome with the new dome will increase the total weight of the structure by approximately 10%.

Table 3: Weight of the structure with the existing and the new telescope

	Existing structure	New dome
Dome weight (kN)	3783	5000
Outer pier weight without dome (kN)	8757	8825
Total weight (kN)	12539	13825

2.1.3 Materials

Steel sections material properties are defined according to CSA G40.12 - 1971 with a yield stress of 304 MPa, an ultimate stress of 448 MPa and a modulus of elasticity of 200 000 MPa. The reinforcing bars have a yield strength of 413 MPa, and a modulus of elasticity is 200,000 Mpa.

Concrete compressive strength is 20.7 MPa and the elasticity modulus is evaluated to be 21,525 MPa.

2.1.4 Soil

Soil data is taken from the Foundation Investigation Report prepared by Dames & Moore, (1973). The density of such soil varies from 700 kg/m^3 to 2300 kg/m^3, (Dames & Moore, 1973). In the calculation, an average of 1500 kg/m^3 is assumed for simplicity.

The Structural Design Brief for the Peripheral Building (SNC, 1974) for the outer pier uses a bearing capacity of 161 kPa, this value is lower and is used for the analysis.

2.2 Methodology and assumptions

A methodology was defined to evaluate the capacity of the structure. The following steps were pursued to successfully complete the assessment.

1. Building codes and design requirements to be used.
2. Load cases and load combinations definition.
3. Creation of a finite element model (FEM) of the structure.
4. Static and dynamic analysis of the structure.
5. Capacity checks
    a. Beams
    b. Columns
    c. Bracings
    d. Footing
    e. Foundation
    f. Deflections
6. Conclusions on the overall performance of the structure.

2.2.1 Building codes and design philosophy

The building was designed in 1974 conforming to the Uniform Building Code (1973). In the current study, the loads are defined by the American Society of Civil Engineers 7 - Minimum Design Loads of Buildings and Other Structures (ASCE 7) 2010. The design checks for the steel structure are based on the American Institute of Steel Construction (AISC) 2005 and the concrete capacity based on the Canadian concrete code CAN/CSA-A23.3-04.

Two design philosophies are used for design. The structural and footing designs are done using limit state design (LSD) and the soil foundation is evaluated using allowable stress design (ASD). For more details please refer to ASCE-7 (2010).

2.2.2 Load cases

This section of the report presents the load cases and combinations applied to the outer pier structure. The definition of load cases and combinations are provided in details in the ASCE-7 2010. The loads acting on the outer pier include dead, live, ice, snow, wind and earthquake loads. It should be noted that the center of gravity of the dome is located at a 1 m horizontal distance from the center of dome sphere due to the opening in the dome configurations. As a result, all the dome loads are applied as combination of point load and point moments on the center of sphere, which is located at a height of 11.929 m from the observation level.

2.2.2.1 Dead load

Dead load is the structural mass of the outer pier, which includes the total weight of the construction materials. Steel beam mass is intrinsic to each beam element. These loads are obtained from the Structural Design Brief for the Peripheral Building (SNC, 1974) as a pressure load on each floor. They are applied on

the beam in the model as vertical uniformly distributed forces. Table 4 presents the dead load applied on each floor.

Table 4: Dead loads per floor

Floor	Pressure (kPa)	Weight (kN)
Ground	2.873	1182.96
2	2.873	1182.96
3	2.873	1182.96
4	2.873	1182.96
Observatory- Peripheral	6.281	2586.35
Observatory- Center	6.281	1506.42
Outer pier total		8824.64

The current dome situated on the outer pier is wished to be replaced to accommodate the new telescope. The current dome weighs 3783 kN and it is approximated that the new dome will have a weight of approximately 5000 kN due to its overall bigger size. The dome dead load is applied as a point load and a point moment on the dome center.

Table 5: Dead load for the dome

Vertical reaction (kN)	Horizontal eccentricity (m)	Moment w.r.t. dome center (kN.m)
-5000	1.0	5000

The total dead weight of the structure including the dome is 13,825 kN or 1409 tonne.

2.2.2.2 Live load

Live load is the load due to the use and occupancy of the building. Similar to the previous section, the live loads are obtained from the original Structural Design Brief for the Peripheral Building (SNC, 1974). It is assumed that live loads have not changed significantly over the years, and they are applied as vertical uniformly distributed loads on each beam. Table 6 summarizes the live loads per floor. Note that based on building code requirements a portion of the live load may or may not need to be included in the seismic weight (to model inertial effects of the live load), depending on the nature of the occupancy. The live load requirements should be defined for final design.

Table 6: Live load per floor

Floor	Pressure (kPa)	Weight (kN)
Ground	7.182	2957.42
2	4.789	1971.614
3	4.789	1971.614
4	4.789	1971.614
Observatory – Peripheral	9.576	3943.23
Observatory - Center	4.788	1148.36

2.2.2.3 Ice load

Since the structure is located on Mauna Kea where freezing ice storms occur, it is necessary to take into account ice loads. It is approximated that the pressure applied by ice load is 68 kg/m^2. For the peripheral building, the vertical force per bay is 5.031 kN/m of height. The ice load is applied over half the circumference of the outer pier (approximately 45 tonnes) . The dome also has to resist ice loads on half of its surface. The dome loads are summarized in the following table.

Table 7: Ice load on the dome

Vertical Reaction (kN)	Horizontal Eccentricity (m)	Moment w.r.t. dome center (kN.m)
-851	9.1	7740

2.2.2.4 Snow load

The pressure applied by snow is approximated to be 150 kg/m^2 on the dome. It is assumed that snow loads can be neglected for the vertical walls of the outer pier. The snow load is applied as a combination of point load and point moment on the center of gravity of the dome.

Table 8: Snow load on the dome

Vertical Reaction (kN)	Horizontal Eccentricity (m)	Moment w.r.t. dome center (kN.m)
-334	0.0	0.0

2.2.2.5 Wind load

Effect of winds on the structure has also been considered in this study. The maximum wind speed that the structure resists is evaluated to be 78 m/s. The ASCE-7 2010 procedure for dome roofs is used to compute the forces induced on the structure by the wind. This procedure is used for the dome and the outer pier walls. It evaluates a force for each node of the dome. The lateral and vertical wind forces for the dome are summed and applied at a height of 6.865 m from the observation level (the center of pressure).

The wind loads applied to the exterior walls are concentrated at each intersection of column and a beam. This method gives a realistic assumption of the wind effects since it considers the positive and negative pressure effects over the whole perimeter of the outer pier. The forces are applied perpendicularly to the surface of the outer pier. The following table summarizes the wind loads. Two cases have to be considered according to the ASCE-7 2010, cases A and B.

Table 9: Lateral wind loads on outer pier

Bay	Lateral perpendicular force per vertical meter- Case A (kN/m)	Lateral perpendicular force per vertical meter- Case B (kN/m)
1	7.40	13.72
2	-5.23	2.05
3	-17.87	-15.43
4	-21.15	-21.15
5	-15.09	-15.09
6	-9.03	-9.03
7	-9.03	-9.03

8	-15.09	-15.09
9	-21.15	-21.15
10	-17.87	-15.43
11	-5.23	2.05
12	7.40	13.72

It should be noted that positive forces are compressive forces applied perpendicular to the surface of the outer pier and negative forces are tension forces. Table 10 presents the total lateral and vertical wind loads applied to the dome top.

Table 10: Wind loads on dome

Lateral reaction (kN)	Vertical uplift reaction (kN)	Center of lateral reaction (m)	Center of vertical reaction (m)	Moment w.r.t. dome center (kN.m)
1876	+1855	0.92 (height above dome center)	0	1718

2.2.2.6 Earthquake

The ASCE-7 2010 requires the structure to resist earthquake load for 2500 years return period. The structure is assumed to have a low ductility and energy dissipation capability. As a result, in order to have a conservative evaluation, ductility factor (R) is chosen to be equal to 2. The soil in place is evaluated to be a soil class C.

Equivalent static procedure is used to represent the effect of seismic forces on the building. It assumes the response of the structure under seismic excitation is mostly concentrated in the first lateral mode of vibration. The structure is pushed with a lateral force distribution representing the lateral deformation of the structure in its first vibration mode shape. To obtain theses forces it is first necessary to obtain the first natural period of the structure. The chosen fundamental period is 0.5 seconds. The period will be influenced by the final design of the enclosure including the compliance of the mechanical interfaces, so only an estimate is possible at this point. This period is used to get the spectral acceleration at the base of the structure. The spectral acceleration is obtained using the design spectrum which is function of the emplacement and the soil parameters. For a fundamental period of 0.5 seconds and the Mauna Kea site, the design spectral acceleration is 0.5g. The spectral acceleration is then multiplied by the seismic weight which is equal to the dead weight to acquire the base shear. The base shear is distributed over the height of the structure as a triangular distribution. The base shear is equal to 50% of the seismic weight (i.e. 0.5g times the seismic weight). The forces at each floor are presented inTable 11.

Table 11: Lateral seismic force at each level for the outer pier

Floor	Lateral force (kN)
Ground	28.05
2	169.71
3	315.02
4	427.24
Observatory	1866.40
Dome	4105.88
Total base shear	6912.32

2.2.3 Load combinations

Following the ASCE-7 requirements, the load cases are combined to represent the worst loading conditions to apply on the structure. It is important to note that no load factor is applied to the dome dead load since the mass will be known accurately, and the estimated 500 tonnes is felt to be reasonably. The capacity of the structure is compared to each of the load combination to ensure that the structure meets the requirements. The structural capacity is evaluated using limit state design and the foundations capacity is evaluated using allowable stress design. Each method uses different load combinations. The structural capacity of the beams, columns, bracings and footings are evaluated using limit state design. The following load combinations are used for the LSD, in which, D is the dead load of the outer pier, L the live load on the outer pier, S the snow load on the dome, I the ice load on the outer pier and dome, W the wind load on the outer pier and dome and E the overall earthquake load. Also, D_{Dome} is the dead load of the dome and W_A and W_B are wind load from case A and B, alternatively.

1. $1.4D + 1.0E + 0.2S + 1.2D_{Dome}$
2. $1.4D + D_{Dome}$
3. $1.2D + 1.6L + 0.5S + 0.2I + D_{Dome}$
4. $1.2D + 1.6S + 1.0L + D_{Dome}$
5. $1.2D + 1.6S + 0.5W_A + D_{Dome}$
6. $1.2D + 1.0W_A + 1.0\,L + 0.5S + 1.0I + D_{Dome}$
7. $0.9D + 1.0W_A + 1.0I + D_{Dome}$
8. $0.7D + E + 0.8D_{Dome}$
9. $1.2D + 1.6S + 0.5W_B + D_{Dome}$
10. $1.2D + 1.0W_B + L + 0.5S + 1.0I + D_{Dome}$
11. $0.9D + 1.0W_B + D_{Dome}$

The soils are evaluated using allowable stress design. The combinations used are listed below.

1. $1.0D + D_{Dome}$
2. $1.0D + 1.0L + 0.7I + D_{Dome}$
3. $1.0D + 1.0S + 0.7W_A + 0.7I + D_{Dome}$
4. $1.0D + 1.0S + 0.7W_B + 0.7I + D_{Dome}$
5. $1.0D + 0.75L + 0.75S + D_{Dome} + 0.525I + 0.525W_A$
6. $1.0D + 0.6W_A$
7. $1.0D + 0.6W_B$
8. $1.14D + 0.7E + 1.14D_{Dome}$
9. $1.0D + 0.45W_A + 0.75S + D_{Dome}$
10. $1.0D + 0.45W_B + 0.75S + D_{Dome}$
11. $1.1D + 0.75L + 0.525E + 0.75S$
12. $0.6D + 0.42W_A + 0.42I + 0.6D_{Dome}$
13. $0.6D + 0.42W_B + 0.42I + 0.6D_{Dome}$
14. $0.46D + 0.7E + 0.74D_{Dome}$
15. $1.0D + 0.75L + 0.75S + D_{Dome} + 0.525I + 0.525W_B$

The design checks are done for each of the combinations described to assess the structure and foundation performance.

2.3 Finite element modeling of the structure

Finite element assumptions are fundamental to get accurate results and need to be reflected carefully. Inaccurate assumptions can drastically change the distribution of forces, deflections and dynamic properties. An extensive analysis was performed to make sure the behavior of structure was well represented.

The structure is modeled in the structural analysis software SAP2000. SAP2000 permits to execute static and dynamic analysis. AISC sections are also available and the graphical interface permits to easily model and analyze its behavior. The steel sections are modeled using frame elements; wide flange sections are imported from AISC sections and built up sections defined in SAP2000.

Most of the beams are attached to other beams or columns through their webs only. This means that moments are not fully transmitted to the members it is attached to. For this reason the connections are designed as pinned connections, i.e. the moments are released at their extremities. Although, some of the connections do transfer moments, the design plans were carefully studied to assure the connections are properly modeled to obtain the most representative behavior of the real structure.

For simplicity, most floor framings are modeled using typical bay framing shown in the drawings. The structural model does not include the balcony on the observatory level. This was decided because the balcony does not induce significant forces and that it was over complicating the model.

External columns are drawn continuously and are pinned at the base. The connections between the ring girder members are clamped. The diagonal columns are also pinned at their base and clamped at their top at the connection with the 3rd floor radial beams. Tension hangers on the inner side support the second and third floor beams and are not supported on the ground. The bracings are also assumed to be pinned.

There are different ways of accounting for slabs in FEM. In simple structures, they can be ignored or rigid diaphragms can be applied. The CFHT outer pier is a complex 3D structure that requires realistic assumptions and accurate modeling to obtain reliable results. It was decided to model the slabs in the FEM. Different area elements exists to model them. Since there are no shear connectors joining the slabs and steel frame, membrane elements are chosen. Membrane elements are used to avoid having the slabs resisting the gravity loads because they only support in-plane forces and normal moments. Concrete slabs are modeled using membrane area element with a thickness of 63.5 mm for all levels expect for the observation level which has a thickness of 250 mm.

The slab on the center of the observation floor is connected with shear connectors to the beams in x direction. This means the slab participates in combination with the beams to resist loads. For simplification and conservatism, the composite action of the slab is ignored. Figure 19 presents the SAP2000 finite element model of the pier and dome structures including the membrane elements.

After the structural finite element model is completed the loads are applied to the different members and nodes. After the combinations are defined, the analysis can be run and the capacity checked.

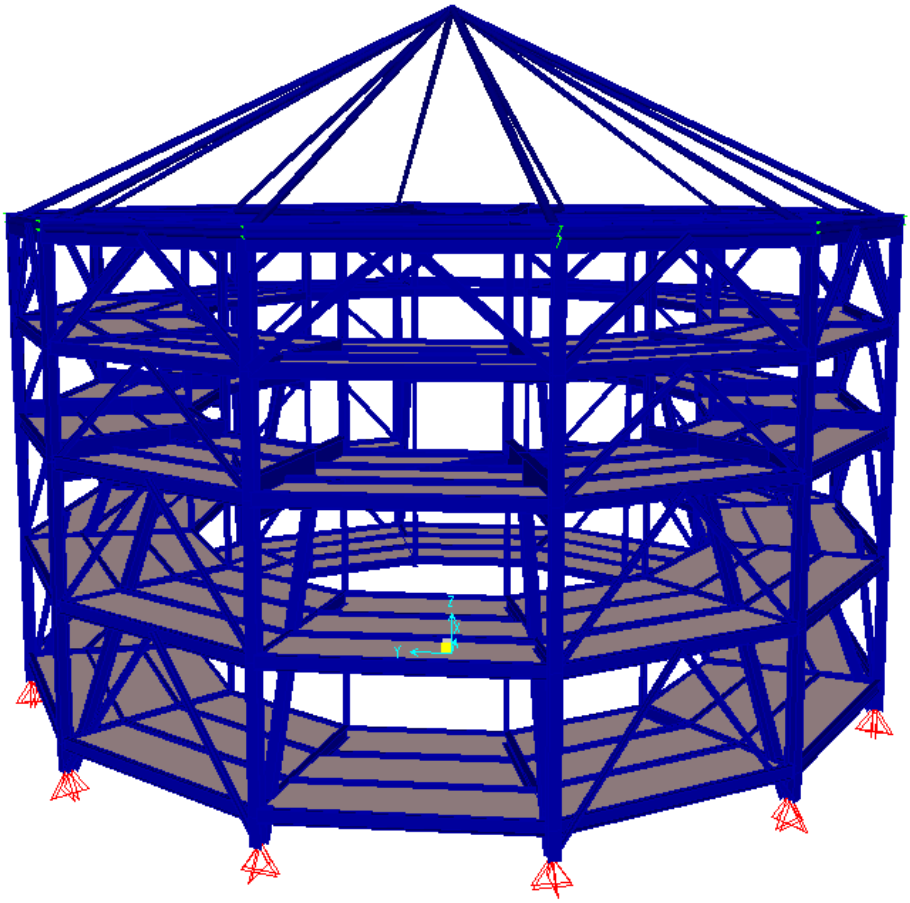

Figure 19: SAP2000 isometric 3-D view of outer pier steel frame and slabs

2.4 Analysis

For each of the load combinations described in the precedent section, the forces induced by these loads in the different structure's members have to be compared to the capacity of the members. Therefore, the beams, columns, hangers, bracings, footings and foundation have to be assessed. This chapter presents the design checks and results for each of the member types as well as the dynamic properties and the deflections under earthquake loads.

The capacity of the slabs of the structure is not verified because it is assumed the gravity loads on the floors of the outer pier are equal to the ones used for the initial design and that they do not participate in strengthening of the structure.

The following methodology is used to evaluate the strength performance of the structure's members. The axial forces, shear forces and moments at the extremities and center of each members for each load combination is exported from the SAP2000 model to EXCEL spreadsheets. These spreadsheets are set up according to the AISC requirements depending on the section type and the type of loads being resisted.

This section summarizes the design assumptions and results of the analyses that are performed to assess the performance and capacity of the outer pier. The first part presents the modal analysis of the outer pier and

dome idealization. The second part shows the design checks results that are done to assess the performance of the structure. The deflections of the structure are also assessed.

The earthquake and wind loads are applied parallel to the y-axis because of the smaller number of braced bays participating in resisting the loads in that direction.

2.4.1 Modal analysis

To study the dynamic behavior of the structure, modal analysis is performed using SAP2000. Modal analysis of the outer pier allows evaluating if the modeling of the structure has been done properly. Also, obtaining the fundamental period is necessary to determine the base shear and the earthquake loads described earlier in this document. In the load cases description, it was motioned that a period of 0.5 seconds is used. Modal analysis is highly dependent on modeling inacuracies and assumptions, the absence of non structural elements, etc. This leads to great variability in the natural periods of the structure. To make sure the structure is evaluated with conservatism a lower value for the first natural period should be chosen. This approach is in place building codes and they usually states that the period taken from a modal analysis should be limited to a certain value based on engineering judgement. It is determined to limit the first natural period to a value of 0.5 seconds to assure conservatism in the results. The results of the modal analysis and equivalent static force analysis obtained from the model are shown below.

Table 12: Natural periods and mode shape descriptions

Mode	Natural period from modal analysis (sec)	Mode shape description	Natural period for equivalent static force analysis (sec)
1	0.64	Translational mode in X direction	0.5
2	0.64	Translational mode in Y direction	0.5

The first two modes have a natural period of 0.64 seconds and their mode shape is a lateral translation of the whole structure. The mode shapes are plotted in the next figures.

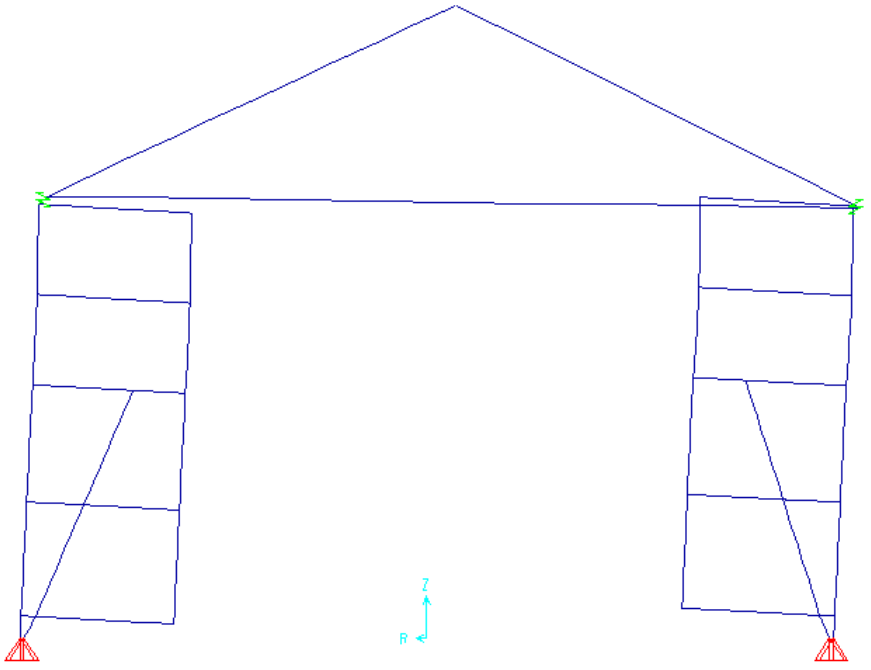

Figure 20: First translational mode of a radial segment

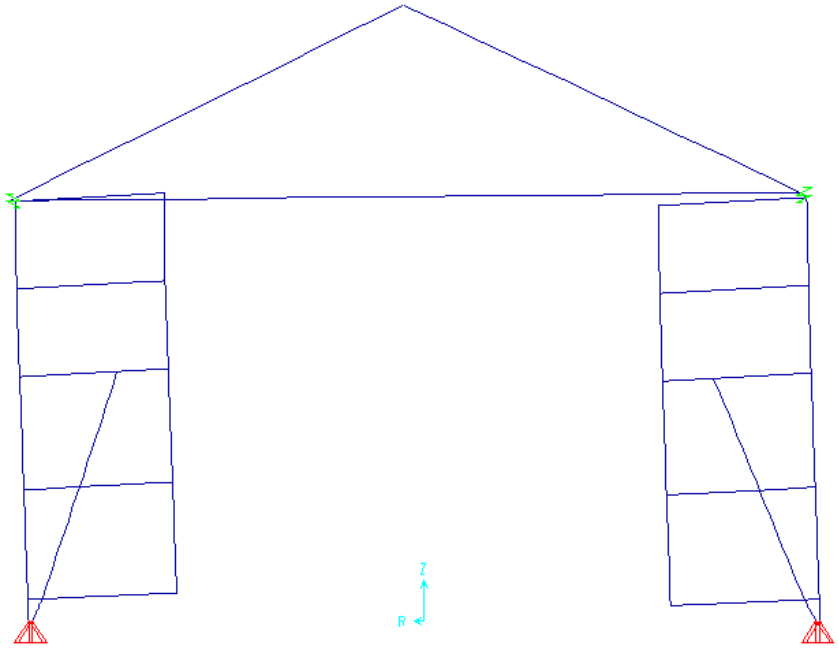

Figure 21: Second translational mode of a radial segment

2.4.2 Beams

The beams are referred as the elements of the structure with negligible axial loads. The beams in the outer pier are the horizontal steel members forming the framing of each floor. The gravity loads are applied perpendicularly to their longitudinal axis, so the axial load is negligible. The sections forming the floors are W sections, but for the external ring girder on the observatory floor which is a built up hollow structural section (HSS). According to the AISC, the following checks have to be done and the procedure is explained in details in the code.

Two limit states have to be verified for members being checked for flexure design. First, flexural lateral torsional buckling is evaluated, it verifies if the combination of flexural yield strength and the lateral torsional buckling strength is high enough. Finally, the shear strength has to be checked, it is defined as the capacity of the section to resist shear forces.

It was observed that all the beams have sufficient capacity to resist the loads applied on them. None of the beams present a demand higher than their capacity. These results were expected since the gravity loads on the floors of the outer pier have no changed compared to the original design. As a result, all the beams have a sufficient capacity.

2.4.3 Columns

The columns are members subjected to compression forces and bending moments. The columns in the proposed model are divided in three categories, the external columns, the internal columns present on the fourth and observation levels and the diagonal columns running from the footing to third floor. Each of these members is checked for the forces at their extremities and at mid span.

For each load combination and for each element, both the elastic buckling and the flexural lateral torsional buckling and the combination of those are checked.

The capacity of the columns is sufficient under every load combination. The results for each level for the worst internal, external and diagonal columns are given in the next tables.

2.4.3.1 Exterior columns

The exterior columns are W12x65 sections for each bay and level. The load combination inducing the greatest demand for each level is 1.4D + 1.0E + 0.2S + 1.2D_{Dome}. Only the column presenting the highest ratio of demand over capacity is given.

Table 13: Exterior columns performance under the worst load combination

Level	Ratio of demand to capacity for 1.4D + 1.0E + 0.2S + 1.2D_{Dome}
Ground	0.87
2	1.01
3	0.64
4	0.78
Observation	0.58

The column of the second level has a ratio of demand to capacity of 1.01. This result being really close to 1.0, it is judged that it has a sufficient capacity.

2.4.3.2 Interior columns

The steel sections for the interior columns are W12x65. Again, the interior columns are present on the inner perimeter of the outer pier on the third and fourth levels. The load combination governing the design check is 1.2D + 1.6L + 0.5S + 0.2I + 1.0D_{Dome}.

Table 14: Interior columns performance under the worst load combination

Level	Ratio of demand to capacity for 1.2D + 1.6L + 0.5S + 0.2I + 1.0D_{Dome}
4	0.47
Observation	0.36

The interior columns have sufficient capacity to resist the loads applied to them.

2.4.3.3 Diagonal columns

The sections are W12x96 for the ground level and W12x65 for the second and third level. The load combination inducing the highest demand is 1.2D + 1.6L + 0.5S + 0.2I + 1.0D_{Dome}.

Table 15: Diagonal columns performance under the worst load combination

Level	Demand vs. capacity ratio for 1.2D+1.6L+0.5S+0.2I+1.0Dome
Ground	0.54
2	0.84
3	0.96

The diagonal columns have adequate capacity to sustain the forces induced by the load combination 1.2D + 1.6L + 0.5S + 0.2I + 1.0D_{Dome}.

2.4.4 Hangers

Hangers are the vertical steel members at the interior of outer pier supporting the ground and the second floors. They are only subjected to axial tension forces.

Three ultimate limit states are checked for the hangers. The first limit state to be checked is yielding of the cross section in tension. Following that, the rupture of the section at the connection is assessed. Finally, the rupture of the bolts in shear is checked.

The hangers are tension members made of two back to back C6x10.5 sections. The capacity is controlled by the shear resistance of the bolts of the connections. The load combination that develops the most demand in the hangers is $1.2D + 1.6L + 0.5S + 0.2I + 1.0D_{Dome}$.

Table 16: Hangers performance under the worst load combination

Level	Ratio of demand to capacity for $1.2D + 1.6L + 0.5S + 0.2I + 1.0D_{Dome}$
Ground	0.52
2	0.77

The hangers present sufficient capacity and could even sustain higher loads.

2.4.5 Bracings

The bracings are the elements resisting the lateral loads induced by earthquakes and wind hazards. They are the diagonal elements on the external perimeter of the outer pier. For a load applied in one direction, in each bay, one bracing resists the load in tension and the other one resist it in compression. It is desirable to have both of these bracings staying in there elastic range. Only axial loads are developed in these members since they have pinned connections.

The tension bracings are checked for yielding of the cross section and rupture of the connection. The compression members are checked for axial compression capacity which is the elastic buckling strength and the rupture of the connection. The shear resistance of the bolts has the lowest resistance so it is assumed that the compression and tension capacity of the bracings is the one of the bolts in shear.

Between the observation and fourth levels bracings are incorporated at each bay and the bracings are composed of a built up section of 4 steel angles L5x3x1/2 forming and I-shaped section. Between the lower levels bracings are formed of double back to back angles L6x4x1/2 and only alternate bays are braced, see Figure 13.. The braces are attached at the base of the node points of the lower floor and at midspan of the beams of the higher level.

The load combination that induces the most demand in the bracing is $1.4D + 1.0E + 0.2S + 1.2D_{Dome.}$ The results are summarized in the next table.

Table 17: Bracing performance under the worst load combination

Level	Ratio of demand to capacity for $1.4D + 1.0E + 0.2S + 1.2D_{Dome}$
Ground and 2	4.19
3	3.73
4	2.95
Observation	1.57

It is observed that the braces at each of the floors do not have sufficient capacity to resist the forces the earthquake loads induces in them. It is mostly noticeable at the lower levels. The higher forces in the bracings

are expected. The outer pier was originally designed for a ratio of base shear over seismic weight (V_{base}/W) of 12%. The ratio of V_{base}/W the structure is assessed for in this study is of 50%. This original base shear is 4.16 times lower than the one used for the evaluation. This explains the demand to capacity ratio of 4.19.

To ensure the accuracy of the results obtained from the SAP2000 model, first principles approach is used to evaluate the forces in the bracings at the ground level. The following section presents the hand calculations.

2.4.5.1 First principles approach bracing forces calculations

It is wished to evaluate the force in the bracings at the ground level to compare to the values obtained in the finite element analysis. To do so, the number of bays participating in resisting the lateral forces is first calculated:

- Bays participating if a lateral earthquake load is applied in X direction: $2 + 4 \cos(60^o) = 4.0$

- Bays participating if a lateral earthquake load is applied in Y direction: $4 \cos(30^o) = 3.46$

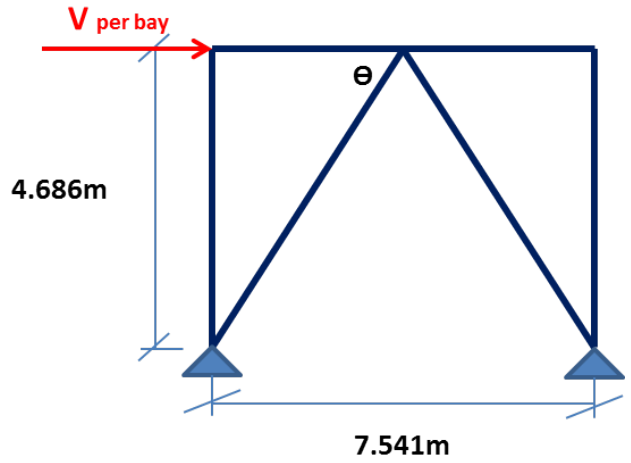

Figure 22: Braced bay representation

The shear per bay can then be obtained by dividing the total base shear by the smallest number of participating bays:

- V_{base} = 6912 kN (calculated from ASCE-7 2010)

- Lateral load applied to each bay: $V_{per\ bay} = V_{base} / 3.46 = 1995$ kN

The axial force in the bracings is calculated assuming both braces take the same amount of force and the angle of the brace:

- Angle between the horizontal beam and the bracing: $\theta = \tan^{-1}(h_1 / (b / 2)) = 51.19^o$

- Brace axial load: $P_{brace} = V_{per\ bay} / 2 \cos(\theta) = 1595$ kN

The brace load obtained from SAP2000 is 1681 kN. Therefore, there is 5% difference between the values obtained by the hand calculation and the one from the model. This difference is in part due to the moment applied on top of the dome and gravity loads.

It is concluded that SAP2000 provides accurate results.

2.4.6 Footing

The structural capacity of the concrete footing is also verified. It is assumed that only axial loads are transmitted to the footing and that the diagonal columns do not induces moments. The Structural Design Brief for the Peripheral Building (SNC, 1974) also made that assumption.

The bending and shear capacities in the tangential and radial directions have to be assessed as well as the tension in the hoops. The bending capacity of the section is evaluated using Response2000 and the shear capacity using CAN/CSA-A23.3-04 requirements.

The bending moment around the tangential axis of the footing is resisted by the reinforcement bars parallel to the width of the footing. The bending moment around the radial axis is resisted by the reinforcement parallel to the length of the footing. The shear for a radial section is resisted by the concrete and steel shear stirrups. The shear for a tangential section is resisted by concrete in the tangential direction in the bottom part of the footing. Finally, the longitudinal tension in the circular footing induced by the radial horizontal forces of the columns is resisted by the longitudinal steel reinforcement bars.

The following table presents the demand to capacity to ratio for each ultimate limit state.

Table 18: Structural performance of the footing

Ultimate state	Load combination	Demand to capacity ratio
Bending around tangential axis	$1.4D + 1.0E + 0.2S + 1.2D_{Dome}$	0.24
Bending around radial axis	$1.4D + 1.0E + 0.2S + 1.2\ D_{Dome}$	0.49
Shear for tangential section	$1.4D + 1.0E + 0.2S + 1.2\ D_{Dome}$	0.44
Shear for radial section	$1.4D + 1.0E + 0.2S + 1.2\ D_{Dome}$	0.33
Tension in hoops	$1.2D + 1.6L + 0.5S + 0.2I + 1.0\ D_{Dome}$	0.41

It is concluded that the footing has sufficient capacity since the ratio of demand vs. capacity are below 1.0.

2.4.7 Foundation

The foundations have to be evaluated using allowable stress design load combinations. The bearing capacity and the sliding of the footing are checked in this section.

2.4.7.1 Bearing capacity

It is also necessary to evaluate if the soils supporting the footings can resist the loads transmitted. The pressure induced by each column to the footing is assumed to be equally distributed to the soils via the footing over its tributary area, the total area of footing divided by 12 columns. The pressure applied on the soil has to be smaller than the bearing capacity of the foundation.

The bearing capacity from the Dames & Moore Soil Report evaluates the bearing capacity to 191 kPa. Although the Structural Design Brief for the Peripheral Building (SNC, 1974) uses a bearing capacity of 161 kPa. To obtain conservative results, the value of 161 kPa is used for the checks. The pressure includes the weight of the footing and of the soil in place over the footing. The bearing capacity results for the worst column for the earthquake load combination and gravity load combination are given in the next table.

Table 19: Bearing capacity performance for earthquake and gravity loads

Bearing capacity (kPa)	Demand to capacity ratio for $1.1D + 0.75L + 0.525E + 0.75S$	Demand to capacity ratio for $1.0D + 1.0L + 0.7I + 1.0\ D_{Dome}$
161	0.97	0.66

The bearing capacity for earthquake and gravity loads is not exceeded. The capacity is concluded to be sufficient.

2.4.7.2 Sliding of the footing

The sliding of the foundation is also verified. It consists of checking if the total lateral load is smaller than the sliding capacity. The sliding capacity is the summation of the friction between the footing and the foundation and of the passive pressure soil resistance placed around the footing.

The sliding of the footing calculations procedure was taken from Coduto (2001). It assumes the sliding resistance to be dependent on the allowable coefficient of friction of the soil, the area of the footing, the axial load applied on the foundation. The loads are also resisted by passive pressure which is dependent on the soil type and weight. The results are summarized in the next table.

Table 20: Sliding capacity performance for earthquake loads

Demand to capacity ratio for $0.46D + 0.7E + 0.74D_{Dome}$	Demand to capacity ratio for $1.14D + 0.7E + 1.14D_{Dome}$
0.74	0.60

The load combination $0.46D + 0.7E + 0.74D_{Dome}$ results in a lower ratio because of the lower axial loads compared to the load combination $1.14D + 0.7E + 1.14D_{Dome}$. The sliding capacity of the structure is sufficient to resist the loads applied.

2.4.8 Deflections

Deflections of the structure under earthquake loadings are needed to be evaluated to verify if the outer pier is interacting with the concrete inner pier and if the ASCE-7 2010 interstorey drifts limitations are respected. The distance at the fourth level between the outer and inner pier is 76.2 mm and the maximum interstorey drift is 2.5% according to the ASCE-7 2010. The displacements induced by the earthquake lateral forces applied are elastic deformation. To obtain the maximum inelastic displacements, the deformations need to be multiplied by the deflection amplification factor which is equal to 2 (since R=2). The deflections are checked for each level in X and Y directions in tables below.

Table 21: Outer pier deflections in Y direction summary

Level	Elastic displacements (mm)	Inelastic displacements (mm)	Demand to capacity ratio	Interstorey drifts
Ground	3.0	6.0	0.08	0.77%
2	18.0	35.9	0.47	0.77%
3	34.5	68.9	0.90	0.82%
4	47.0	94.0	1.23	0.81%
Observation	50.6	101.1	-	0.23%

Table 22: Outer pier deflections in X direction summary

Level	Elastic displacements (mm)	Inelastic displacements (mm)	Demand to capacity ratio	Interstorey drifts
Ground	2.4	4.9	0.06	0.63%
2	14.5	29.1	0.38	0.62%
3	27.9	55.7	0.73	0.66%

4	38.1	76.2	1.00	0.66%
Observation	41.8	83.5	-	0.24%

It is observed that the deflections in Y direction are higher than in X direction. The first principle approach of the bracings design taught us that more bracings are participating in X direction than in Y directions which permits us to expect higher deflections in Y direction. This confirms again that it was a good decision to perform the analysis in Y direction.

The interstorey drifts are all under 2.5% meaning the structure is stiff enough for the ASCE-7 requirements. The deflections in Y direction are higher than the space between the concrete internal pier and the outer steel pier which makes us conclude that interaction between both structures can be expected during major earthquake events. It should also be noted that the inner pier will also sustain deflections that are not necessary in the same direction as the outer pier because they have different vibration periods. The deflections in X direction are smaller than the allowable space between the two structures.

2.5 Conclusions from Existing Enclosure Pier Evaluation

The upgrade of the current Canada-France-Hawaii telescope and dome necessitated evaluating if the outer pier supporting the dome has enough capacity to accommodate the new design. The larger and heavier dome inducing higher forces to the outer pier and the new code requirements justify reassessing the capacity of the outer pier. The seismic requirements were analyzed with great care since the modern codes prescribes much higher demands than the ones from the original design. A methodology is developed to perform the assessment of the structure using finite element modeling and first principle approach. The load cases and combinations were defined using the ASCE-7 2010 requirements. The capacity of the beams, columns, bracings, footing and foundation were evaluated and the performance of these members assessed. The AISC requirements were used for the steel design. The following points were concluded:

- The beams forming the different level floors have sufficient capacity to resist the loads applied on them.
- The different columns transferring the loads to the footings have their capacities exceeding the demands induced by the different load combinations. The ratio of demand vs. capacity of the external columns is of 1.01 for the second level. There is no capacity left for the external columns.
- The bracings resisting the lateral loads have their demand exceeding their capacity by a ratio of 4.19. This outcome results from the fact that the earthquake forces are 416% higher than for the original design requirements. Different solutions exist to strengthen the bracings.
- The maximum interstorey drift requirement of 2.5% is met for all load combinations and the maximum deflection at the fourth floor is of 101 mm and exceeds the 76 mm space between the outer and inner pier. Interaction under high seismic hazard can be expected.
- The footings have sufficient bending, shear and tension structural capacity to resist the demands of every load combination. The ratios of demand to capacity are under 0.50.
- The maximum bearing pressure induced by the footing to the foundation is 97% of the 161 kPa bearing capacity. The sliding capacity is also sufficient since the demand to capacity ratio is of 0.74.

References

American Institute of Steel Construction, (2005). “Specification for Structural Steel Buildings (ANSI/AISC 360-05)” American National Standards Institute.

American Society of Civil Engineers, (2010). “Minimum Design Loads of Buildings and Other Structures – ASCE 7”. Reston Virginia, USA.

Bentz E. and Collins M.P. (2000), “Response-2000, Version 1.0.5, Reinforced Concrete Sectional Analysis using the Modified Compression Field Theory”. University of Toronto, Ontario, Canada.

CAN/CSA-A23.3-04, (2004) “Design of Concrete Structures”. Canadian Standard Association.

Coduto, D.P. (2001). “Foundation Design – Principles and Practices”. Prentice-Hall, Upper Saddle River, New Jersey, USA.

Dames and Moore, (1973). “Foundation Investigation Report”. Hawaii, USA.

IBC, (2003). “International Building Code”. International Code Council, Country Club Hills, Illinois, USA.

SNC, (1974). “Structural Design Brief for the Peripheral Building”, Canada-France-Hawaii Telescope.

SAP2000, Computers and Structures, Inc., Berkley. (2009). “Structural Analysis Program”. Version 14. Berkley. California, USA.

APPENDIX C. NGCFHT TELESCOPE OPTICAL DESIGN

NRC · CNRC
From Discovery to Innovation...

Herzberg Institute of Astrophysics
Institut Herzberg d'astrophysique

ngCFHT

Telescope Design

Optical Design

Paolo Spanò

REVISION 0.5

02 November 2012

National Research Council Canada
Conseil national de recherches Canada
Canada

CHANGE RECORD

Issue	**Date**	**Section/Page Affected**	**Reason/Initiation Documents/Remarks**
0.1	09-Lug-12	All	First draft
0.2	12-Lug-12	1.1	Integrate plot changed
0.3	08-Aug-12	3 1 5 6	Prime focus corrector case added Top level req. revised Primary segmentation revised Efficiency sections gathered together
0.4	16-Aug-12	All	Minor corrections
0.5	02-Nov-12	All	Add minor correction for self-consistency Section on Fiber entrance losses moved to Appendix Fiber throughput shifted into Tech. Report Glass selection moved to appendix Three-mirror telescope solution added.

Table of Contents

Executive Summary

The next generation Canada-French-Hawaii Telescope (ngCFHT) shall be mainly devoted to perform deep wide-field spectroscopic surveys at spectral resolutions from $\Re$~2'000 to ~20'000, at visible and near-infrared wavelengths.
Different telescope optical designs have been explored to find the best compromise matching scientific and top level technical requirements. While a scientific trade-off has been devoted to define a set of minimum requirements on system performances (telescope aperture, field of view, number of simultaneous objects, wavelengths, resolution), a provisional list of top level technical requirements have been defined here (Chapter 0) to drive the design and selection of the most promising one.
Three different classes of solution were analyzed here:

- One mirror design (Chapter 2)
- Two mirror design (Chapter 3)
- Three-mirror design (Chapter 4)

Primary mirror segmentation has been analyzed too (Chapter 5). Efficiency of the different solutions has been compared in Chapter 6.

1 Telescope top level requirements

We derived a list of requirements to be applied on the telescope optics.

- Telescope diameter: 10 m (segmented)
- Field of view diam.: 1.5 deg^2 (hexagonal)
- Vignetting: <15%
- Wavelength: 370 – 1300 nm
- Telescope image quality[1]: EE80D <0.45 arcsec (FWHM ~0.3)
- ADC: always installed
- Max. zenith angle: 60 deg
- Telecentricity: <3% pupil mismatch

The telescope focal plane will feed up to 3'200 fibers at low spectral resolution and 800 fibers at high resolution. Typical fiber diameters will be about 0.9 to 1.2 arcsec wide. A provisional scientific trade-off is reported in the main Technical Report, based onto overall system throughput, object size and SNR. To cope with different object sizes and different seeing conditions, the telescope image quality must always be a fraction of the fiber aperture, to guarantee small light losses at fiber entrance.
To perform deep spectroscopic surveys over such a wide bandwidth, an atmospheric dispersion corrector (ADC) must be incorporated along the telescope optics before the focal plane. Moreover, to efficiently feed fibers at the focal plane, telescope optics must be (almost) telecentric to avoid large vignetting losses.

[1] Image quality is defined as the telescope optical quality without atmospheric or dome/mirror seeing, as seen at fiber entrance, and including nominal image quality, residual atmospheric dispersion, manufacturing, alignment and control errors. This value can be convolved with the observed seeing profile to give the total PSF.

2 One mirror design

This design is based onto a single primary mirror equipped with wide field corrector optics at its primary focus. Design work is mainly devoted to optimize corrector lens design to deliver enough image quality over the required field of view, within a given wavelength region.
From top level requirements, it should include an atmospheric dispersion corrector, to cope with the very wide bandwidth of ngCFHT. Some works have been done in the past years to explore starting design of possible solutions. Some of them are reported in Appendix G of the main technical report. There, both 3- and 4-lens corrector designs were analyzed that barely provided enough image quality over the field of view. Here a new attempt to arrive to a better design was carried out. Three cases were firstly analyzed, based onto 4, 5, and 6 powered lenses (not including the ADC optics). Then, a full system including ADC optics, was optimized for improved image quality.

2.1 Hyper Suprime-Cam Wide Field Corrector

A quite important reference design is provided by the newly commissioned Hyper Suprime-Cam wide field corrector (WFC) installed on the Subaru telescope. This WFC will feed the planned Prime Focus Spectrograph (PFS), currently under final design stage.
HSC optics have been optimized for imaging purposes, with superb image quality (FWHM<0.1 arcsec) for *r*, *i*, *z* bands up to the zenith distance of 60 deg, with some degradation tolerated in *g*, and *Y* bands. Transmittance is optimized accordingly, with emphasis on the red wavelengths. Nominal optical throughput is ~90% at 600 nm, with a sharp cut-off below 370 nm and a much slower drop above 1000 nm. This is achieved through a "5+2" lens design, shown Figure 1, composed by 5 separate big aspherical lenses and a lateral-shift ADC, as successfully adopted on the previous Subary Prime Focus Corrector. HSC WFC maximum lens diameter is 850 mm, with an overall weight of 425 kg (optics only). Both image quality and lens diameter are kept within requirements at a cost of a significant 26% vignetting at the edge of the field. Moreover, HSC was not optimized to be telecentric, implying that PFS will suffer from additional entrance losses at the fiber input located at the edge of the field of view.

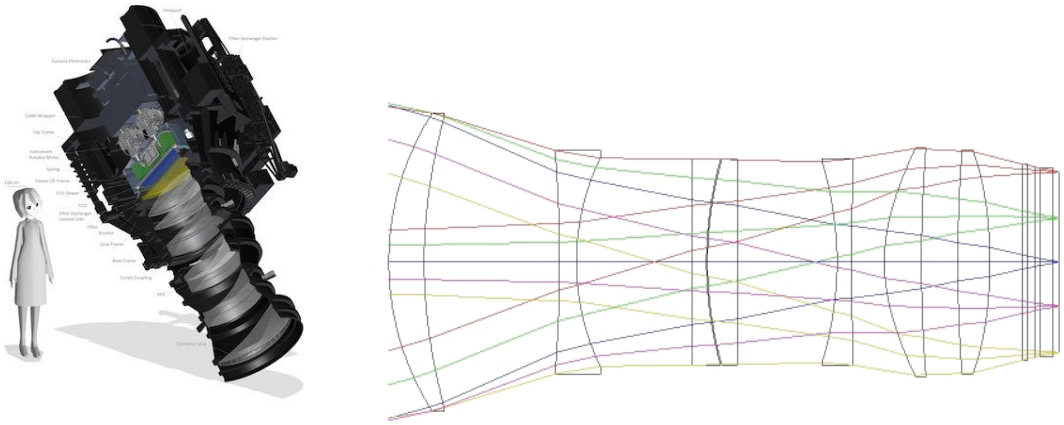

Figure 1. - Hyper Suprime-Cam (left) and its wide field corrector optics (right).

2.2 Lens design

While the 5-lens design provided the best overall image quality, we considered a 4-lens design a good compromise between complexity and performances. We refer to this design as the "4+2" lens design, where there are 4 powered lenses doing the field correction and other 2 lenses acting as lateral shift ADC.
Within the class of solutions based onto "4+2" lenses, a large number of runs have been generated, exploring the wide parameter space delivered by this large number of surfaces and aspherics. Different glass selections have been adopted, together with different (maximum) vignetting factors. To further increase the number of degrees of freedom, the central surfaces of the ADC have not been constrained to have the same curvature, as in the Subaru PFC and WFC designs. This should help to control ghosts, too.
To keep the overall telescope length within a given constraint, the primary mirror focal ratio has been fixed to F/1.83, barely fitting inside the expected dome (radius <19.5m). Also the primary mirror conic constant was allowed to vary, without constraining it to a parabolic shape (k = -1).
The optical design of the telescope is given in Figure 2, and the wide field corrector is shown in Figure 3. It is based onto 3 Fused Silica lenses (L1, L2, L4), available in large and homogeneous blanks up to 1.5-m diameters, and a large Schott F2HT (or equivalent Ohara PBM2Y) lens (L3). A flat window is placed near the focal plane to prevent dust contamination on top of fibers. Except for the largest 1.2-m diameter Fused Silica first element, all other lens diameters are below 1-m. If the overall size and cost of WFC optics should be descoped, a 1-m size optics will deliver almost identical performances, except for a larger vignetting (28% instead of 13%, see Section 2.3).

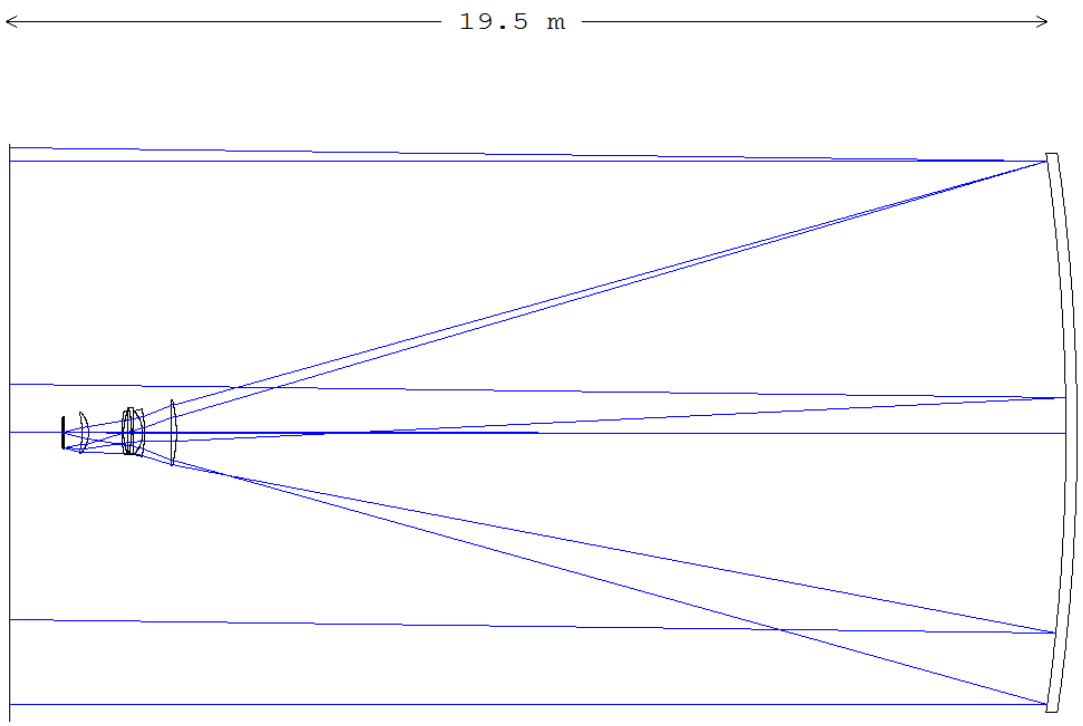

Figure 2. - Telescope one-mirror design.

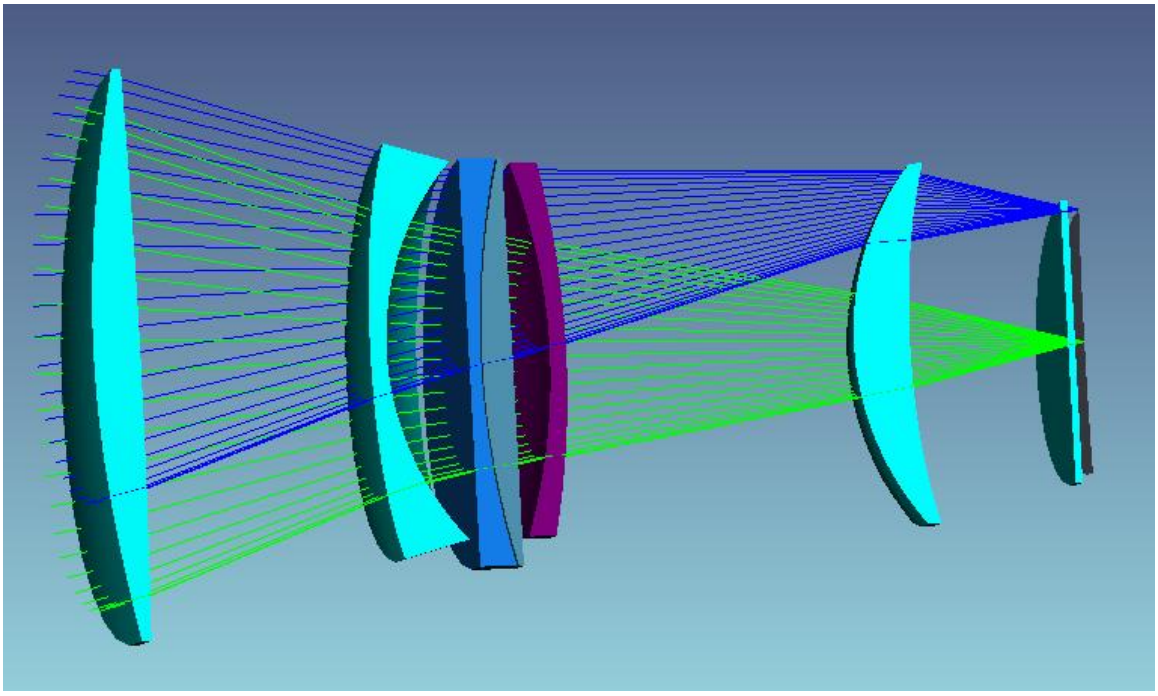

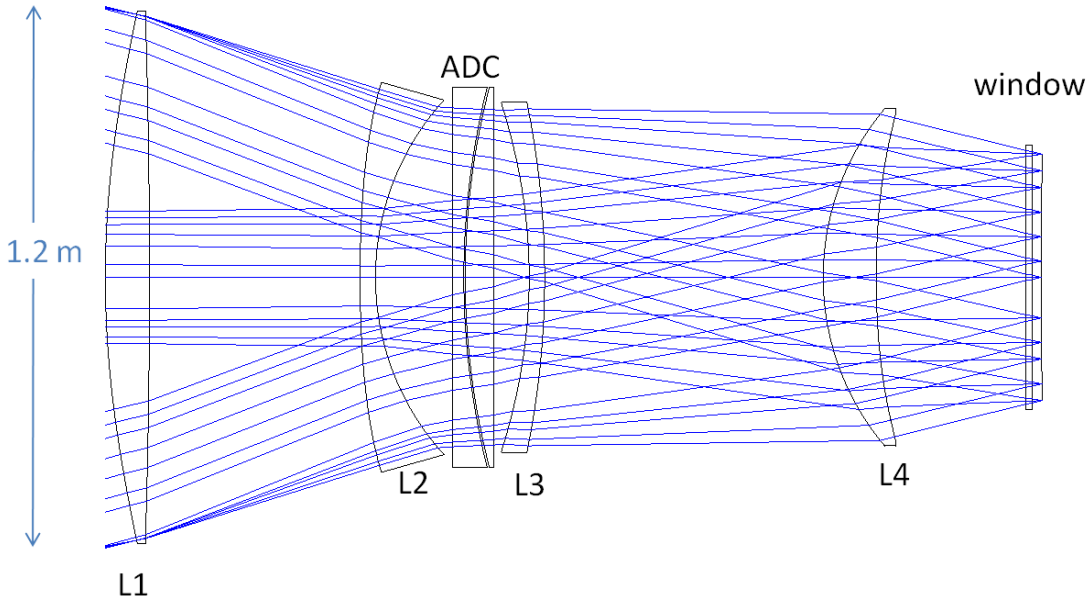

Figure 3. - Wide field corrector optics.

To improve overall throughput, the field corrector has been forced to be nearly telecentric (maximum incidence angle <0.8 deg) over a curved focal plane, because there is no need to have a flat focal plane for a spectrograph. Some vignetting will help to loose telecentricity tolerances, because it will reduce the size of the projected pupils for the fiber at the edge of the field (see Section 2.4).

All lenses are aspherical on one side, to evenly split required asphericity between elements, improving manufacturability without compromising image quality. Aspherical departure has been partially constrained. Very challenging aspherical lenses (~5 mm sag departure, ~100 millirad slope departure, *TBC*) have been manufactured for the Subaru WFC on smaller lenses.
The ADC is composed of Schott BK7/LLF1 glass pair (or the BSL7Y/PBL1Y Ohara equivalent). ADC lens diameter is about 860 mm. They will correct for atmospheric dispersion by a lateral shift of ~26 mm for a 60 deg zenith angle.

2.3 Performances

Here the main characteristics of this design:

- Primary mirror: 10-m diameter, F/1.83, hyperboloid (k= -1.17)
- Telescope f-ratio: F/2.1 (on-axis)
- Plate scale: 102 um/arcsec
- Field of view: 1.5 deg diameter
- Max. vignetting: 13%
- Wavelength: 370-1300 nm
- Focal plane curvature: 12-m (convex)
- Total mass: 590 kg (optics only)
- Image quality: EE80D <0.35" (average) at 0 zenith angle
  EE80D <0.45" (average) at 60 zenith angle
  including residual atmospheric dispersion
- Throughput: ~90% (average)

Encircled energy maps, as function of field position and zenith angle, are shown in Figure 4. Spot diagrams are given in Figure 5 and Figure 6. Very good nominal image quality is reached over most of the field of view and at different zenith angles, typically below 0.3 arcsec (EE80 diameters). Vignetting is shown in Figure 7 for our baseline solution, based on 1.2-m maximum lens diameter lenses. When maximum lens diameter is limited to 1-m only, vignetting will increase up to 30%, as shown in Figure 8.

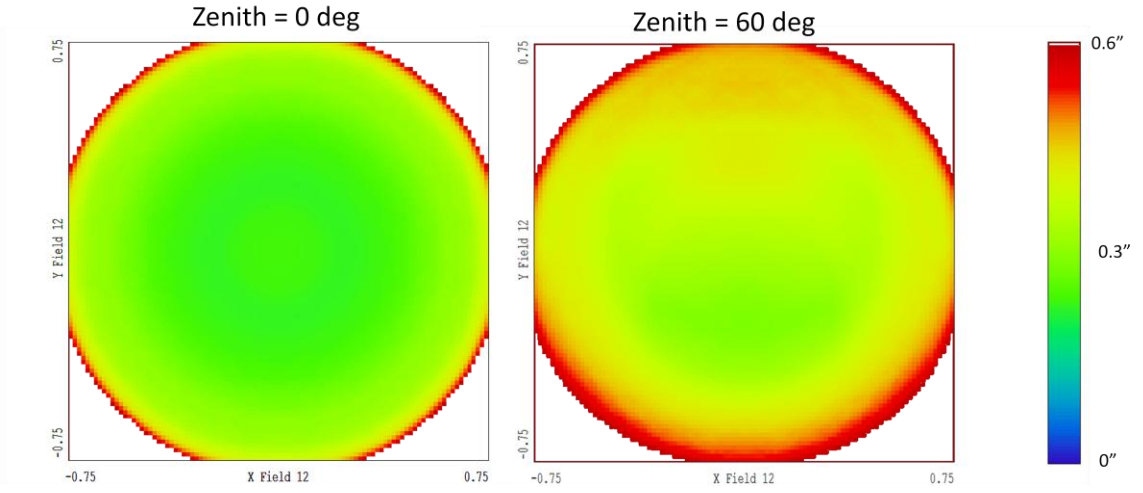

Figure 4. - EE80 diameter map across the field of view.

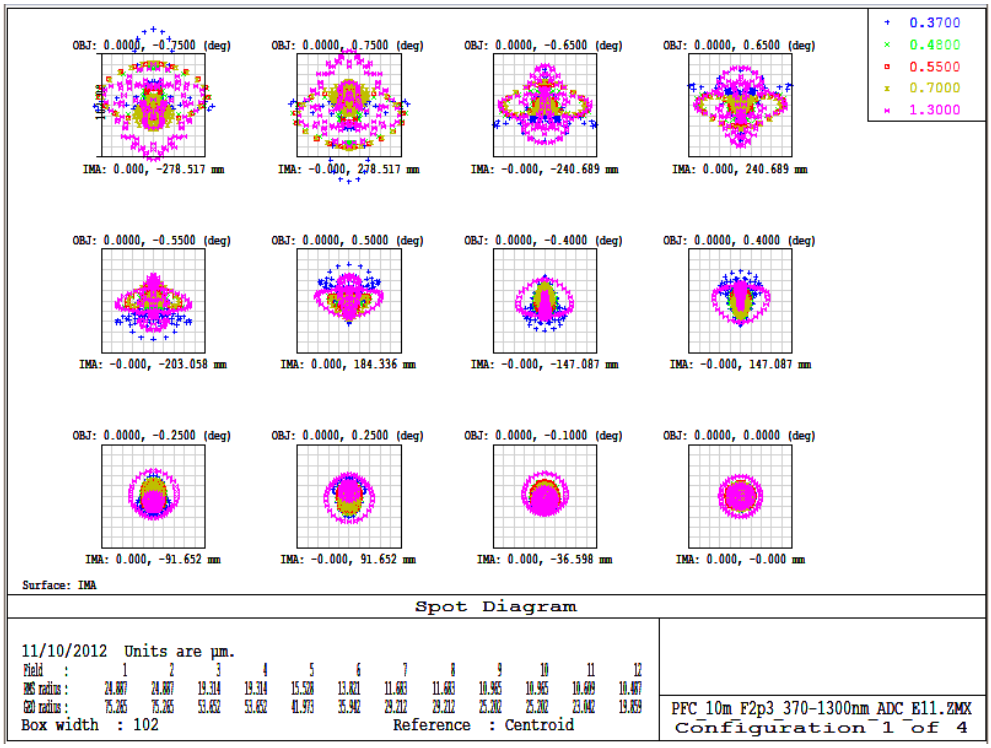

1x1 arcsec^2

Figure 5. - Spot diagrams at 0 degrees zenith angle.

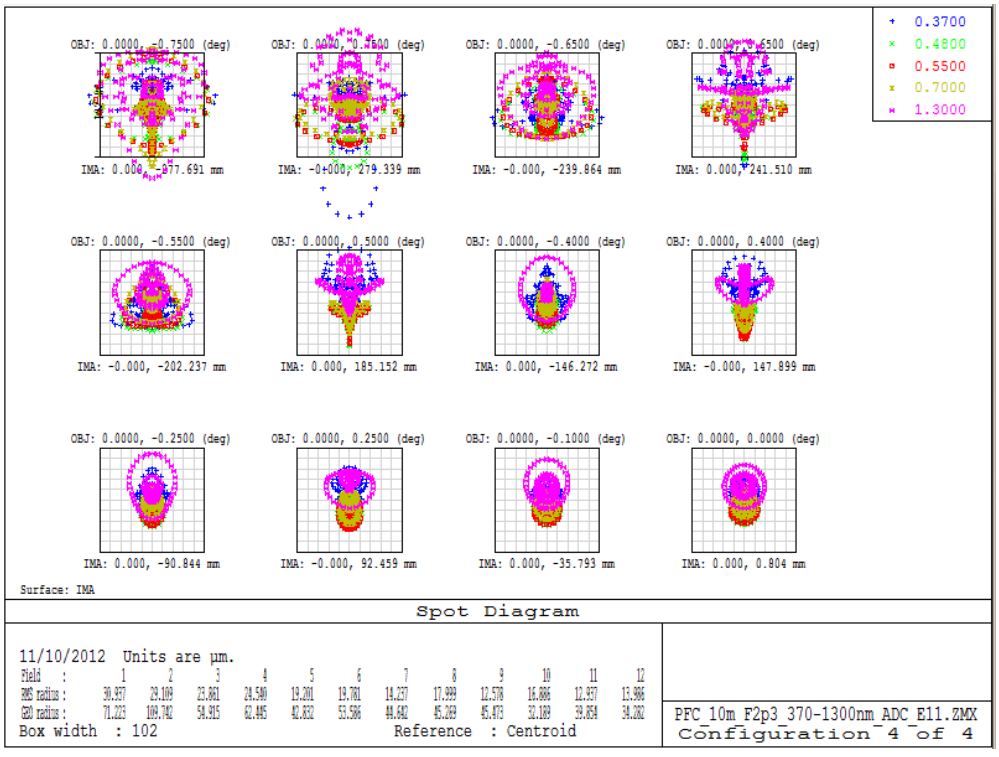

Figure 6. - Spot diagrams at 60 degrees zenith angle.

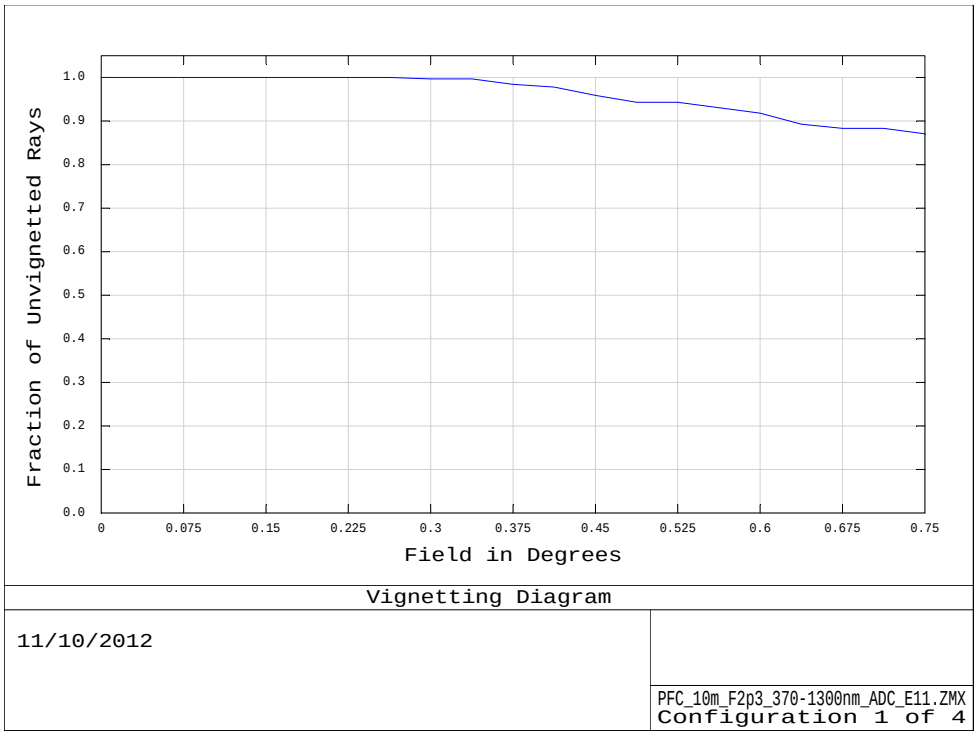

Figure 7. - Vignetting plot for the baseline solution (1.2-m max. lens size).

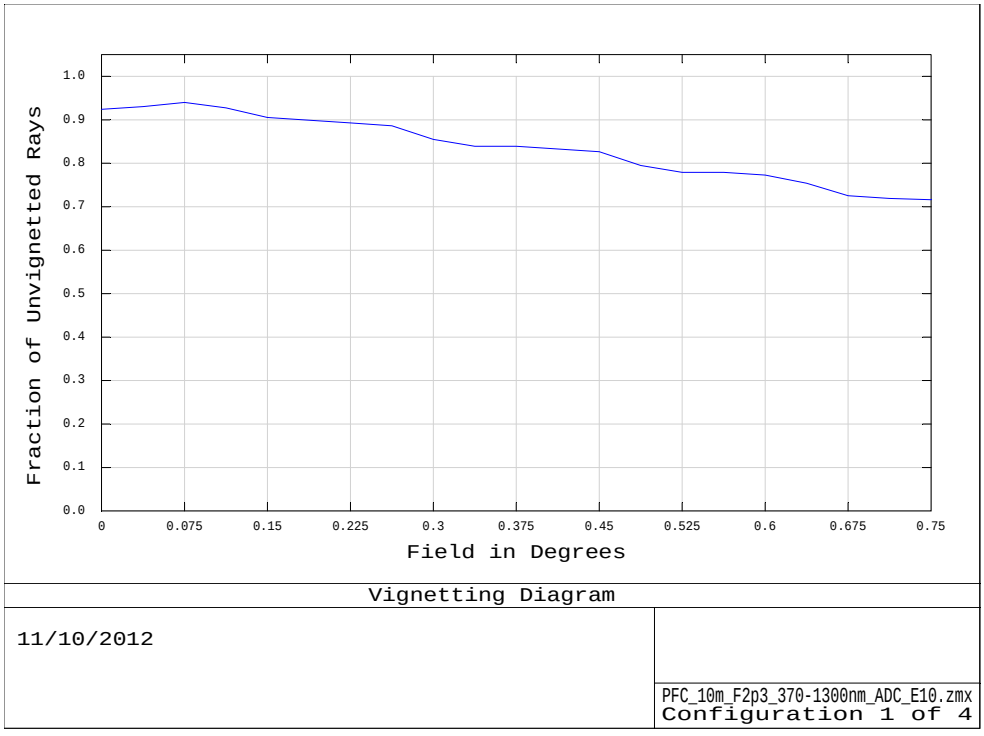

Figure 8. - Vignetting plot for a 1-m max. lens size.

2.4 Telecentricity

Telecentricity is not fully corrected, to loosen constraints during optimization, because the large vignetting factors will allow for small pupil misalignment without introducing further light losses at the fiber entrance, as shown in the plot above, where circles represent fiber cone aperture and ellipses are projected pupils.

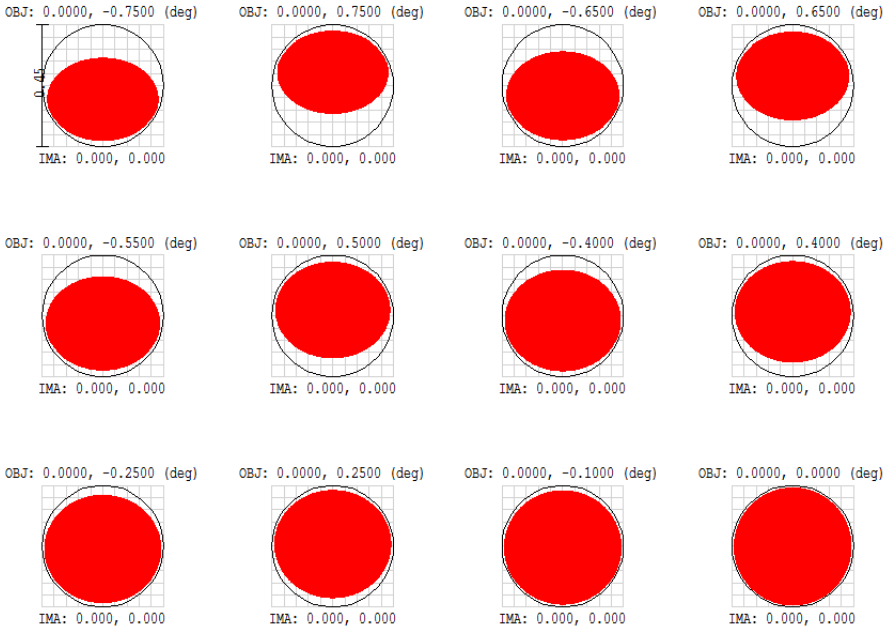

Figure 9. - Projected pupils across the field of view. Circle represent a F/2.2 beam.

2.5 Residual atmospheric correction

At different zenith angle, residual (uncorrected) atmospheric dispersion will vary from nearly zero (at the zenith, where prisms will cancel each other) to ±0.12 arcsec at zenith 60 deg.

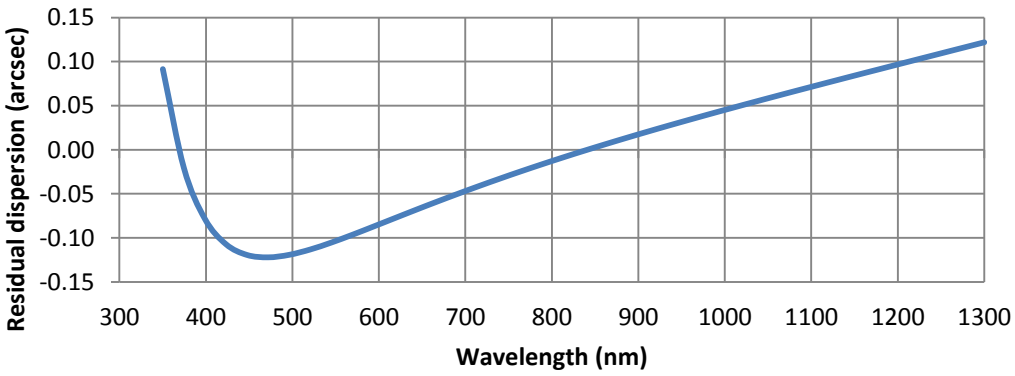

Figure 10. - Residual atmospheric dispersion for maximum zenith angles.

2.6 Transmission losses

Transmission optics will affect overall throughput. The major effect can be observed at both edges of the wavelength range, dominated by internal glass absorption. Average transmission is 90% from 370 to 1300. Some tuning can be done by proper optimization of the anti-reflection coatings.
This curve must be multiplied by the mirror reflectivity to provide the final telescope throughput (see Section 6.3 for a comparison between the one-mirror and the two-mirror solutions, based onto estimated throughput of reflective and refractive optics).

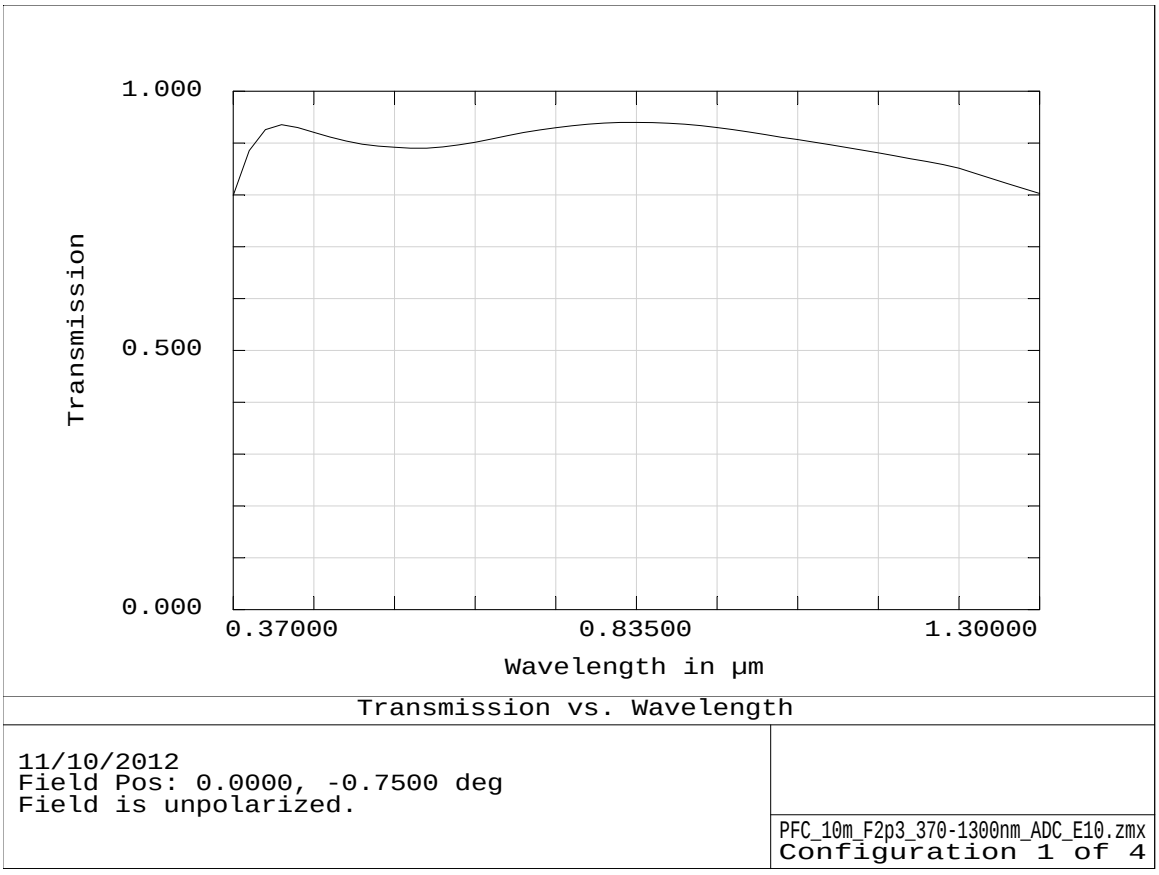

Figure 11. - Throughput of the wide field corrector optics. Mirror reflectivity is not included.

2.7 Optical alignment

During the alignment stage of the lenses some test setups should be developed to check system performances and optimize alignment. Two different interferometric setups can be implemented, similar to those ones used for the WFC on Subaru.

- The first will use a small plano window just in front of the nominal telescope focus to correct for spherical aberrations as those ones introduced by the flat window. To close the cavity a large spherical mirror can be used. This test can verify that WFE on the focal plane will be good enough as expected when combined with the primary mirror. However

this test is limited to one position over the focal plane (on-axis test), and many lenses will be only partially illuminated.

- A second test, called "total test", will illuminate a large fraction of all lenses and the whole focal plane. A null optics must be added to correct for out-of-focus aberrations. A state-of-the-art CGH, 100 mm in diameter, can be used for this purpose.

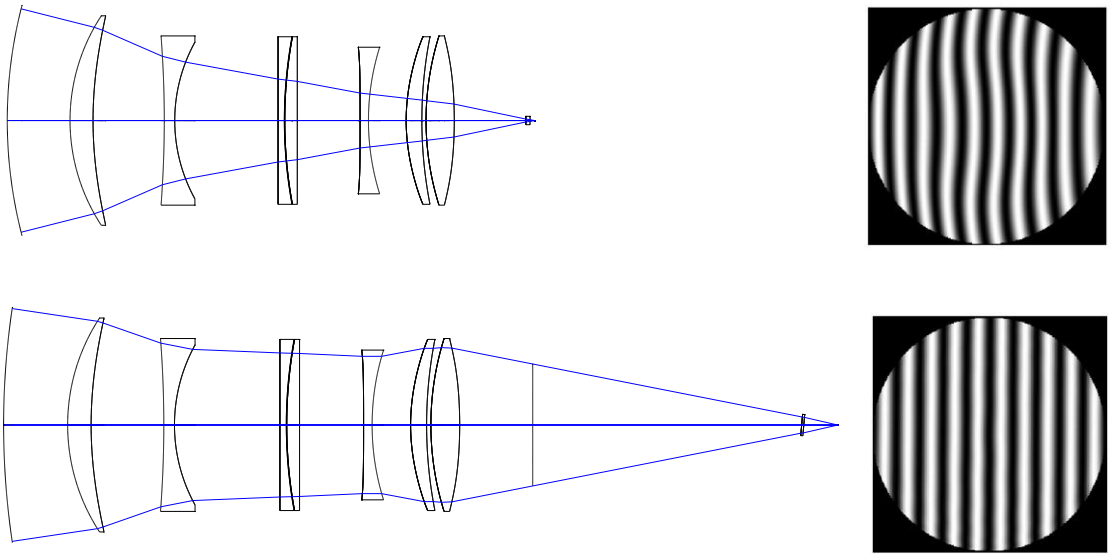

Figure 12. - Wide field corrector test setups (see text).

3 Two mirror design

3.1 Design philosophy

The large field of view cannot be achieved by any two-mirror telescope without a field corrector. By adding one or more lenses near the focal plane, corrected field of view can be increased to the required value. To keep the corrector lens diameter within current manufacturing capabilities, we should limit their size within 1.5 m (i.e, the largest Fused Silica blanks with good homogeneity), with a goal of ~1m size, to allow the possibility for cheaper blanks (e.g., BK7 or BSL7).
Another key aspect for a two-mirror configuration is to keep secondary mirror size and asphericity as small as possible. Existing secondary mirrors on 8-10m class telescopes range between 900 and 1450 mm (e.g., Keck telescope), for a much smaller field of view. We need to overcome this limit, if a two-mirror wide-field telescope must be built. We decided to keep the secondary diameter within ~2.5m, with a goal of ~2m maximum diameter. This seems feasible, comparing to the LSST secondary size (3.4m diameter).
A classical Cassegrain focal station is not required for ngCFHT, because fiber link can be easily routed even if nested inside the telescope optical train to the spectrograph. A two-mirror configuration offers the possibility to shorten the fiber length by a large amount, if the focal plane lies near the altitude axis of the telescope AltAz mount.
Finally, a two-mirror configuration allows to directly feed fibers at their "natural" best f-ratio, thus minimizing focal-ration degradation without further coupling losses due to imaging or pupil micro-optics, or any kind of focal reducer/elongator. Typical fiber entrance f-ratio is about F/3.6 (goal), but we can change it easily between F/4 to F/3.

3.2 Optical layout

The proposed solution is shown in the figure below. A very compact layout is obtained, for a total length of 10 m from secondary obscuration (including space for mechanics) to the vertex of the primary mirror (Figure 13).
Primary mirror is a hyperboloid with 10-m aperture. It will be a segmented one (see Chapter 5). Secondary mirror will be a hyperboloid mirror with a 2.4-m aperture. Then, a three-lens corrector is used to increase corrected field of view up to 1.4 deg (diameter). The ADC is nested within the second and third lens of the corrector and is composed of two counter-rotating coupled prisms (flat surfaces only). All refractive elements are smaller than 1.2-m diameter.
The focal ratio of the whole system if F/3.6, with a plate scale of 175 um/arcsec, well matching typical fiber diameters. The focal plane is slightly curved (radius 6.8m), and it is telecentric, thus simplifying the feeding of fibers.
Clearance between optical components is generous, to reserve space for mountings and baffles. The focal plane is located near the expected center of gravity of the telescope moving masses. Fiber can be routed or through the hole of the primary, or directly to two "Nasmyth-like platforms" on both side of the telescope fork mount, where spectrographs can be installed. Then, very short fibers can be foreseen, to achieve very high UV-throughput.

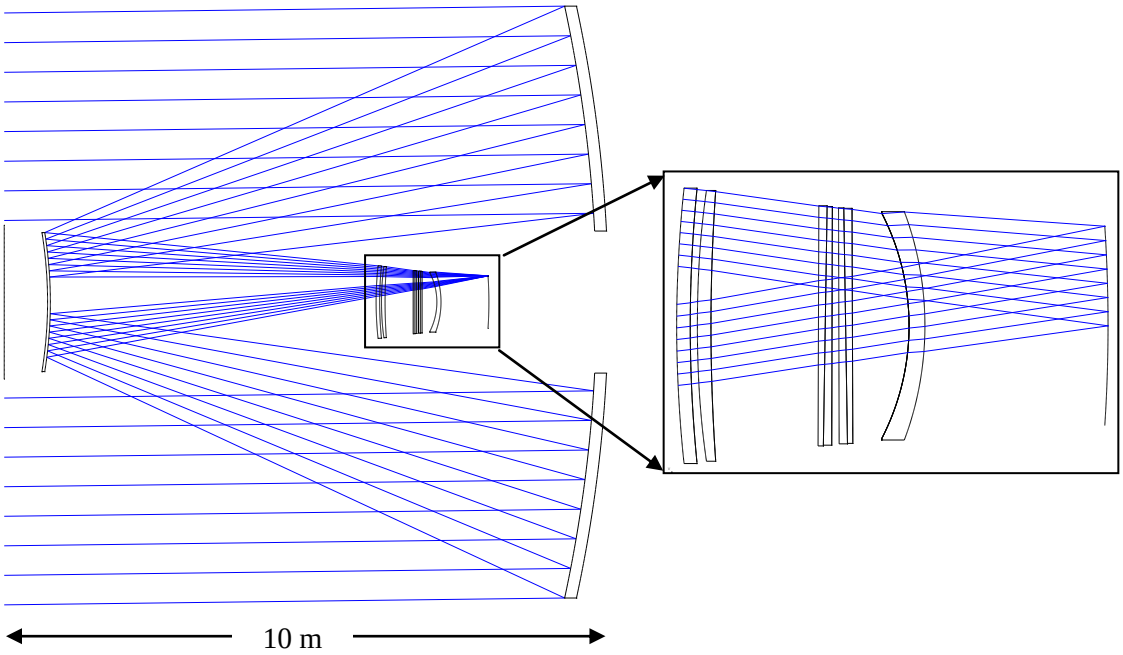

Figure 13. - Two mirror telescope design.

3.3 Secondary mirror

Secondary mirror is a hyperboloid with a unusual conic constant k = -5.10654, over a clear aperture of 2350 mm and a radius of curvature of 7.09 m. The total aspheric departure is 805 um, and the maximum slope deviation is 5.16 millirad. These parameters are considered feasible with current technologies, but further study will be devoted to address manufacturability aspects, and the test setup for such a mirror.

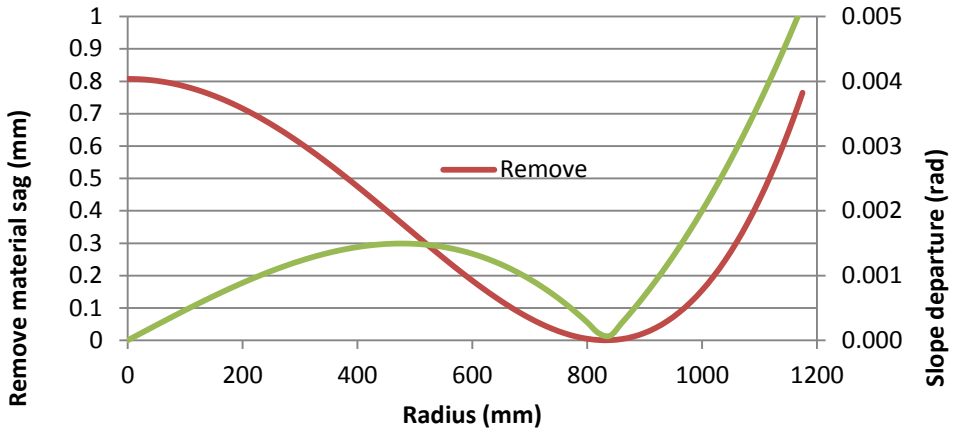

Figure 14. - Secondary mirror asphericity.

3.4 Corrector lens

The corrector lens has been optimized together with the telescope optics, in order to share aberrations between the whole optical train. Constraints over the maximum slope deviation have been fixed (5 millirad maximum). All three lenses are menisci, with aspherical convex surfaces.
Lens thickness-diameter ratio is about 1:20 for the first two elements, and about 1:13 for the last, most curved, meniscus.
Solutions based on both Fused Silica and BK7 exist, but to reduce internal transmission losses, Fused Silica (IR grade) should be preferred. All lenses can be AR coated with Solgel/MgF2 to improve efficiency and reduce ghost contamination.

3.5 ADC

The atmospheric dispersion correction is done through two identical double-prisms (Risley prisms), counter-rotating to vary chromatic corrections as function of telescope altitude. The size of prisms (1070 mm clear aperture) basically constrains the selection of available materials to a quite short list, further reduced by the large wavelength coverage and the differential CTE between the two materials, even if the two prisms will be coupled. Cementing such large parts could be very challenging, in order to carefully control the cement wedge.
Schott N-BK7HT and LLF1have been selected. Glass properties are summarized in Table 1.

3.6 Image quality

Polychromatic spot diagrams for different field of views are given Figure 15. Boxes are 1x1 arcsec^2 wide. Up to 1 deg, RMS spots diameters are <0.15". Maximum RMS spot diameter is 0.31". This compares well with required performances, even if they are specified in term of 50% encircled energy, more than RMS spot diameter. Spot diagrams in are given with no ADC in the telescope optics, substituting it with an equivalent thickness plano window. The effect of ADC over image quality is addressed separately, in the coming section.
Also encircled energy diagrams are given, as function of the field position, in Figure 16. For all field position, EE80 diameter is always less than 0.32", and 0.16" within 1degree field of view.
Delivered image quality is very good and uniform within the 1 deg FoV.

Glass	**N-BK7HT**	**LLF1**
Refraction index	1.517	1.548
Abbe number	64.2	45.8
Internal transmission (350 nm, 60 mm thickness)	92%	90%
Internal transmission (370 nm, 60 mm thickness)	97%	96%
Internal transmission (435-1075 nm, 60 mm thickness)	>99%	>99%
Internal transmission (1300 nm, 60 mm thickness)	98%	98%
Coefficient of thermal expansion (ppm/K)	7.1	8.1
Apex angle (deg)	0.747	0.707

Table 1. - Two mirror telescope ADC glasses.

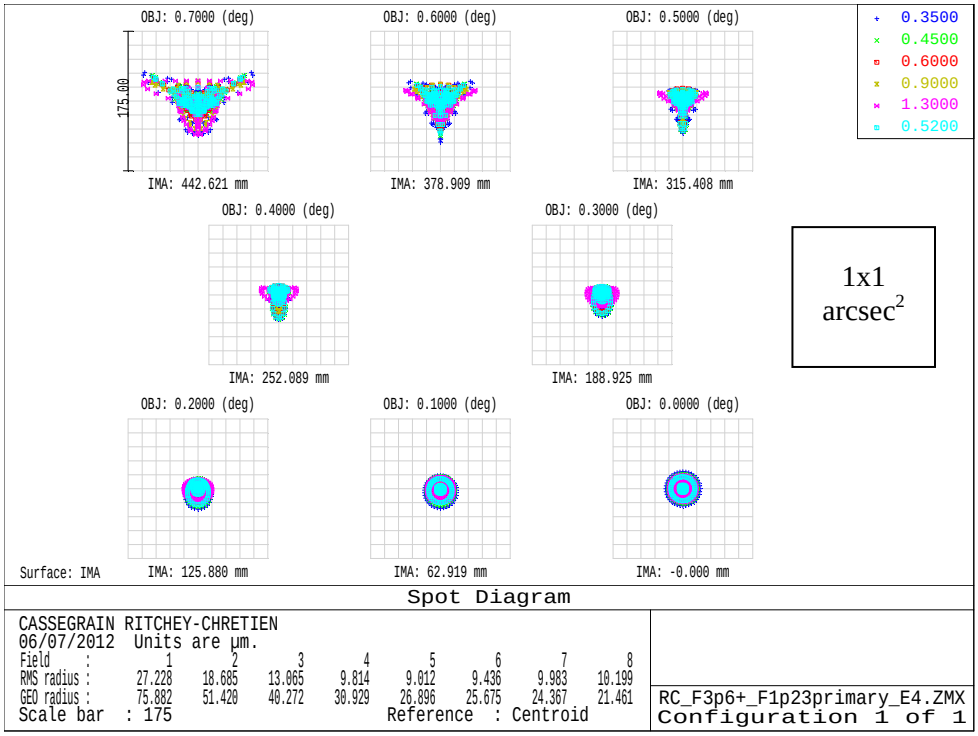

Figure 15. - Spot diagrams of the two mirror telescope optics (0 deg zenith).

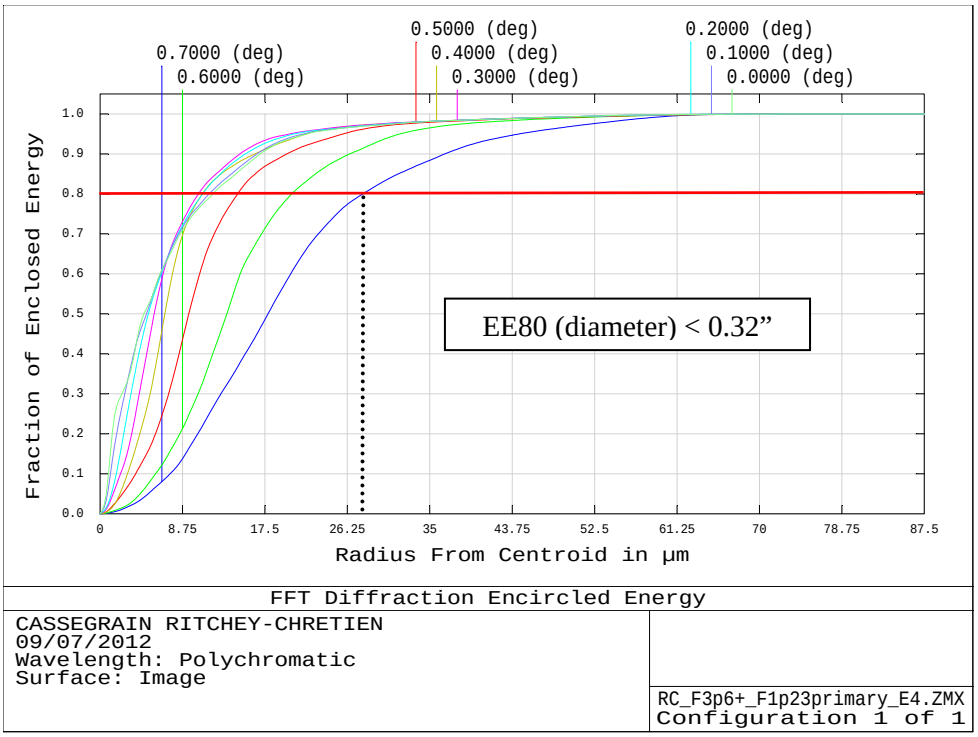

Figure 16. - Encircled energy diagram of the two mirror telescope.

3.7 Atmospheric dispersion correction

At different zenith angle, residual (uncorrected) atmospheric dispersion will vary from nearly zero (at the zenith, where prisms will cancel each other) to ±0.19 arcsec at zenith 60 deg. Figure 17 shows the correction residual. Spot diagrams at different zenith angles are given in Figure 18.

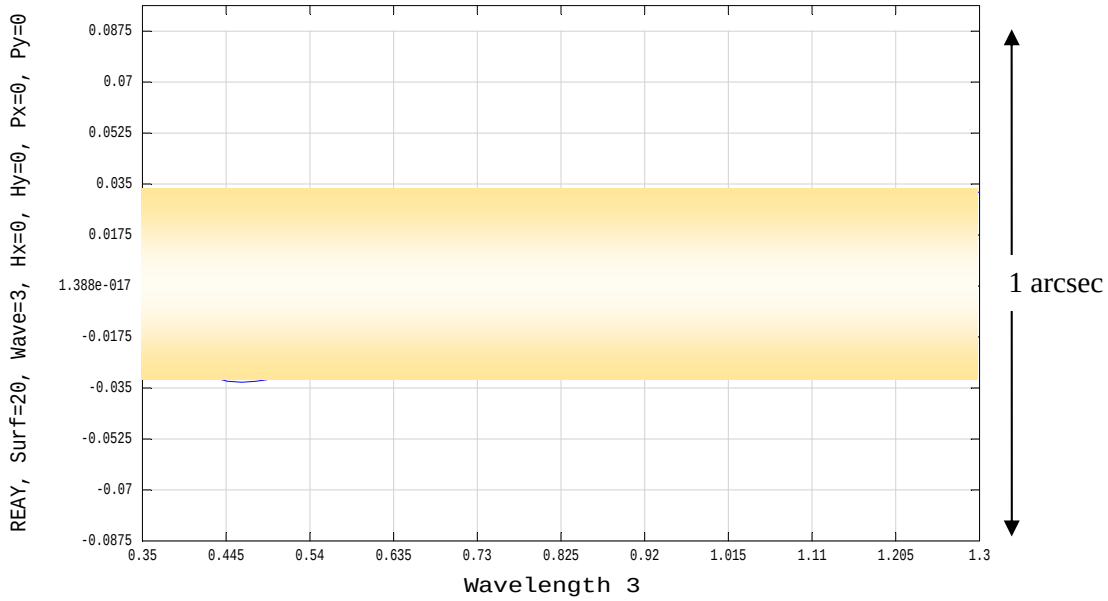

Figure 17. - Residual atmospheric correction at 60 deg zenith.

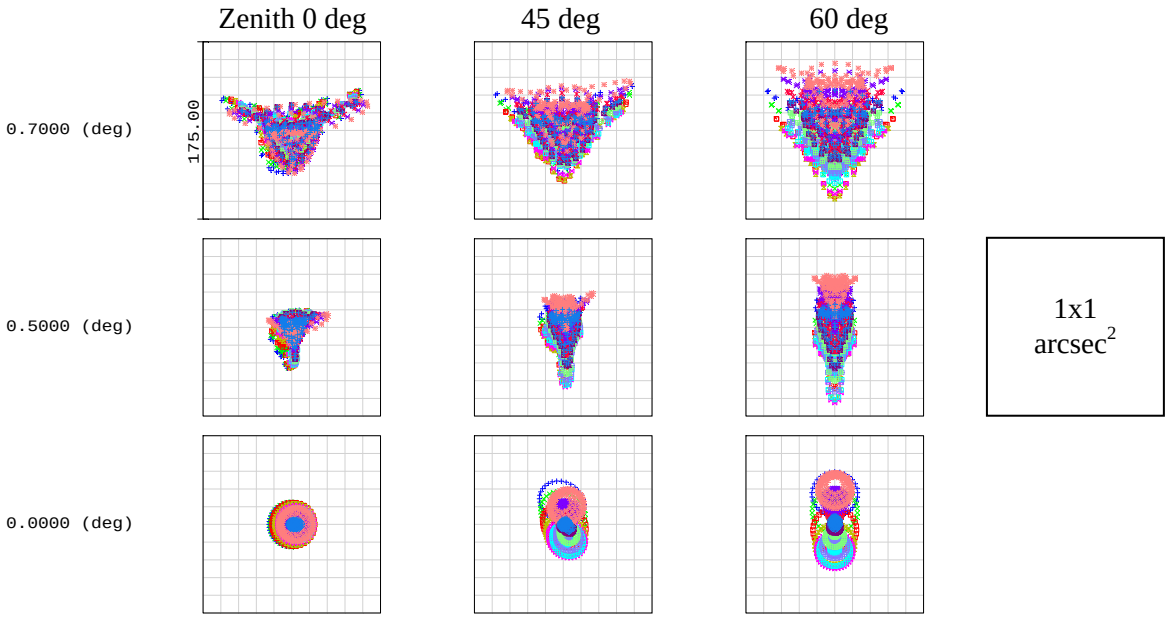

Figure 18. - Spot diagrams with ADC in place at different zenith angles.

3.8 Transmission losses and telescope baffles

Transmission optics will affect overall throughput by some percent, on average, because very small internal transmission losses can be achieved by proper selection glass material and lens/prism thicknesses. Moreover, very good anti-reflection coatings can be applied on them.
Average transmission is 91.6% from 350 to 1300 and 93.7% from 400 to 1000 nm. Some losses are expected at the real ends of the spectral range.
To compute the effective collecting area telescope vignetting must be evaluated, mainly due to secondary mirror optics and related mount. Secondary mirror 2.4-m diameter will ask for a ~3-m obscuration, to allow for proper mounting structures and telescope baffles, to prevent or minimize stray light (see Figure 20). The vignetting losses will amount to 10%, for a 3.2-m obscuration, and 13% for a 3.6-m one. Optimization of the final obscuration will depend on the stray light analysis. Here, as a conservative approach, we selected a 13% vignetting factor. The layout shows that such obscuration should be enough to prevent main direct stray light to reach the telescope focal plane.

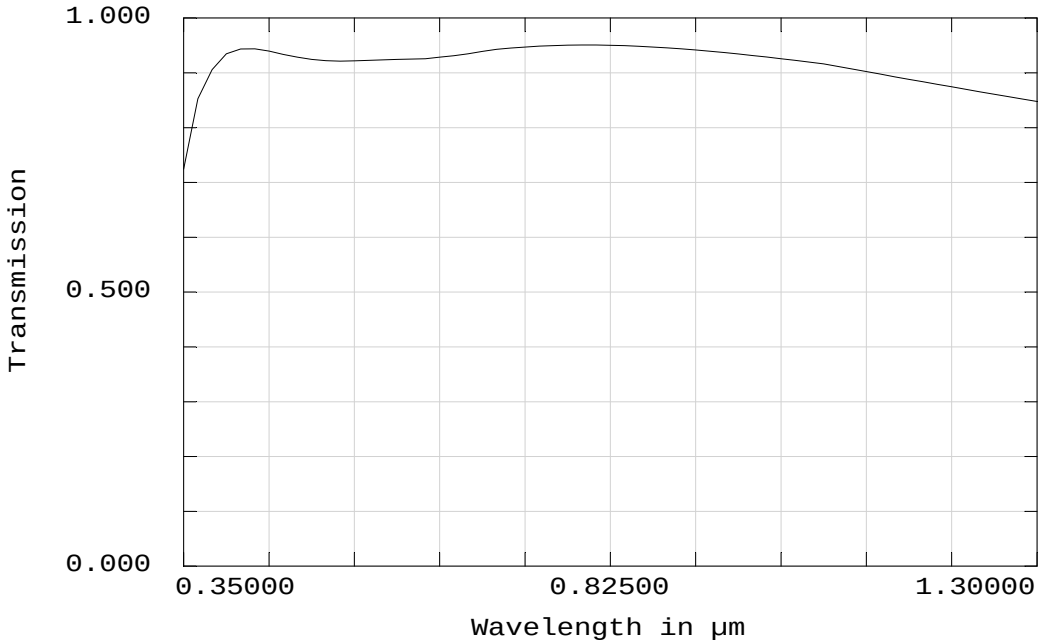

Figure 19. - Two mirror telescope throughput curve.

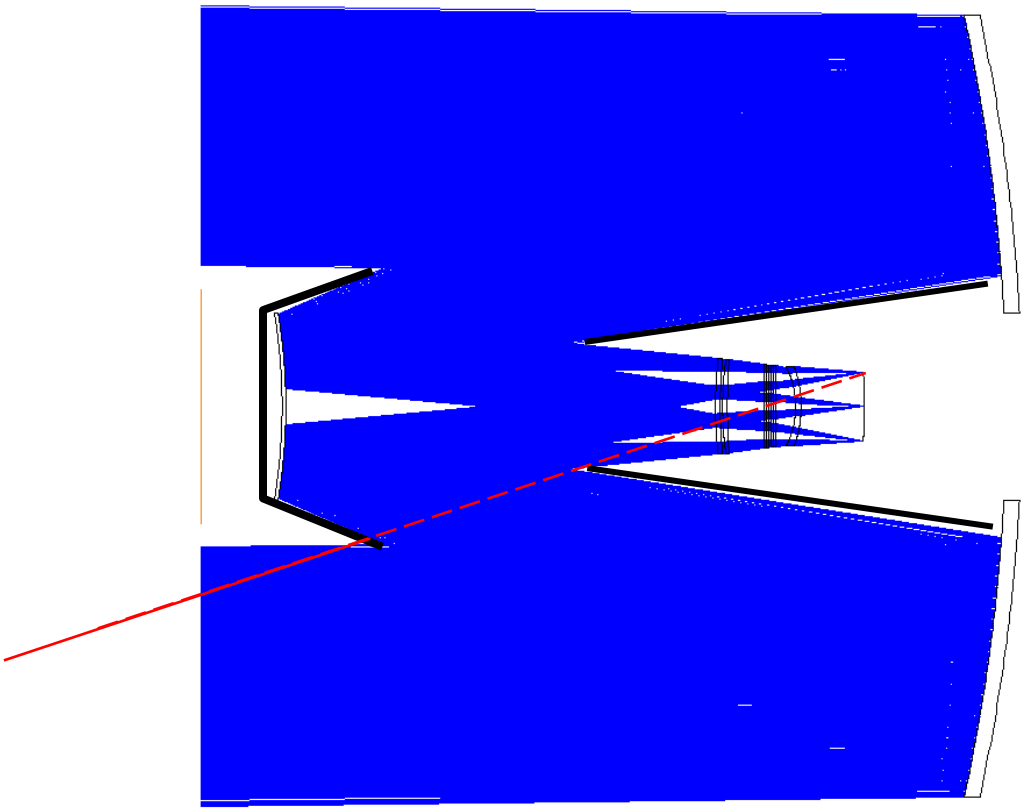

Figure 20. - Telescope layout with provisional baffle witha 3.6-m obscuration.

4 Three-mirror solutions

This class of solution is particularly suited for very large field of views. As examples, the LSST is a 8-m telescope with an extraordinary large 3.5 deg (diameter) field of view, optimized for imaging. The very fast focal ratio (f/1.2) has made any ADC unfeasible, so only single-band imaging is obtained. This makes a LSST-like design not suited for spectroscopy.

A slower f/2.5 telescope TMA has been designed in the past with partially compliant image quality (0.5-0.7 arcsec rms spot diameters). A ~25% vignetting is constant over the field of view. The LSST was used as the starting point and the refractive corrector was removed, the focal ratio targeted to f/2.5 (to use existing fibre technology) and the focal plane was placed so it was at the secondary mirror to make a convenient fibre location. As this concept was envisioned to be based on the LSST mirror polishing process of two curvatures on the same primary substrate the aperture was kept the same as LSST at 8.36m. The image quality is not quite to specification but it can be improved by lengthening the system with a slower primary or reducing the field of view.

Space for an ADC is very limited, unless to further increase vignetting, in order to host large refractive elements.

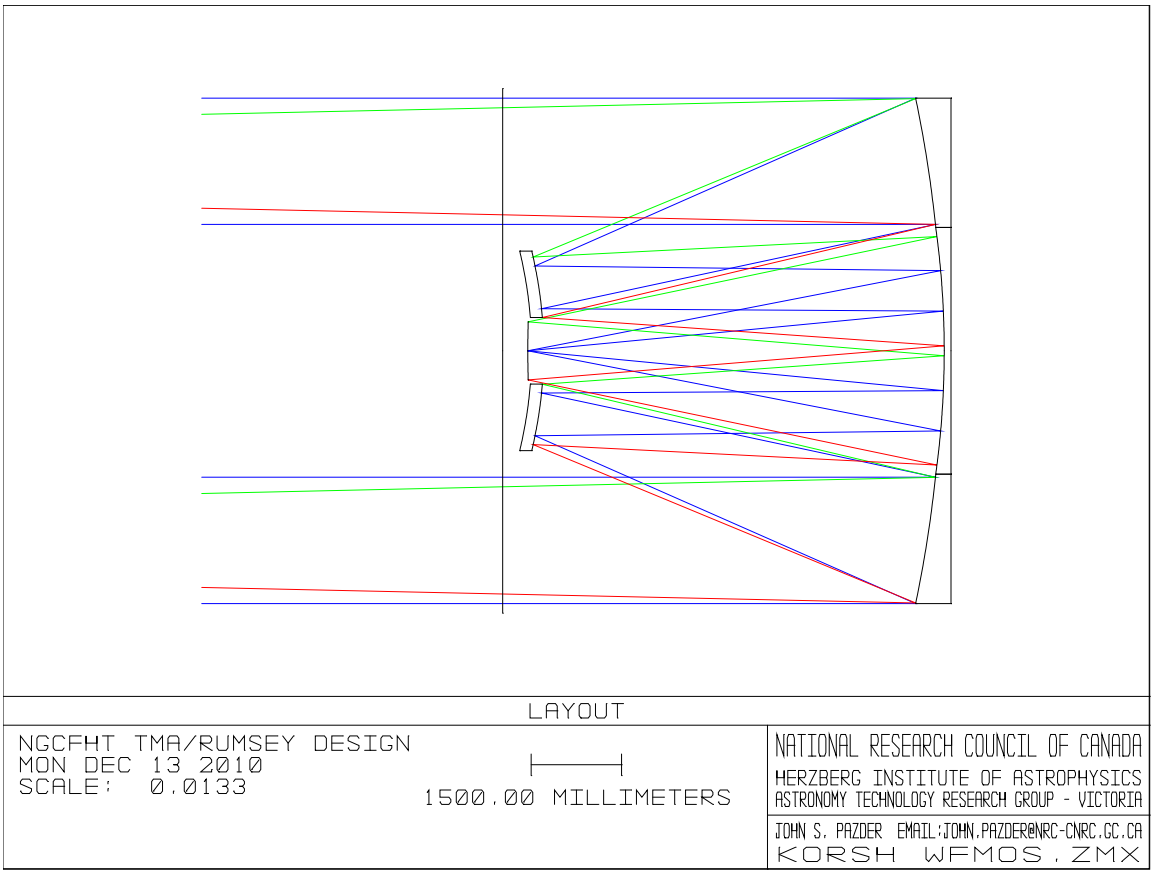

Figure 21. - Three-mirror LSST-like solution.

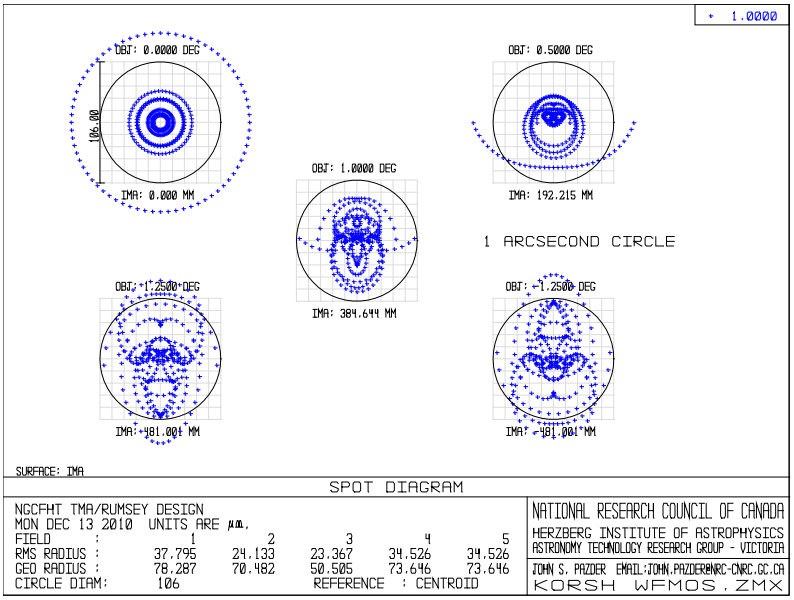

Figure 22. - Three-mirror image quality.

Another solution, again of the Paul-Baker type, with a tertiary mirror nested inside the primary, has been optimized to give better image quality over a smaller field of view, as shown in Figure 23. The diameter of the primary is now 11-m, while the other two mirrors have a 3.1-m and 4-m diameters. This F/2.2 telescope delivers very uniform monochromatic images (0.15” rms spot diameters) over the whole field view (Figure 24). Moreover, the focal plane is almost telecentric and it can be forced to be even more telecentric by adding a corrector lens in front of the focal plane. However, the quite fast focal ratio make the design of ADC very difficult, unless larger vignetting and more elements are introduced, making this solution not attractive anymore, and it is presented here only for reference.

Vignetting for such solution is very high, and constant over the field of view, as shown in Figure 25.

As a preliminary conclusion, all three-mirror solutions seems to be quite complex and will delivery very vignette field of view, making them less attractive in term of collecting area.

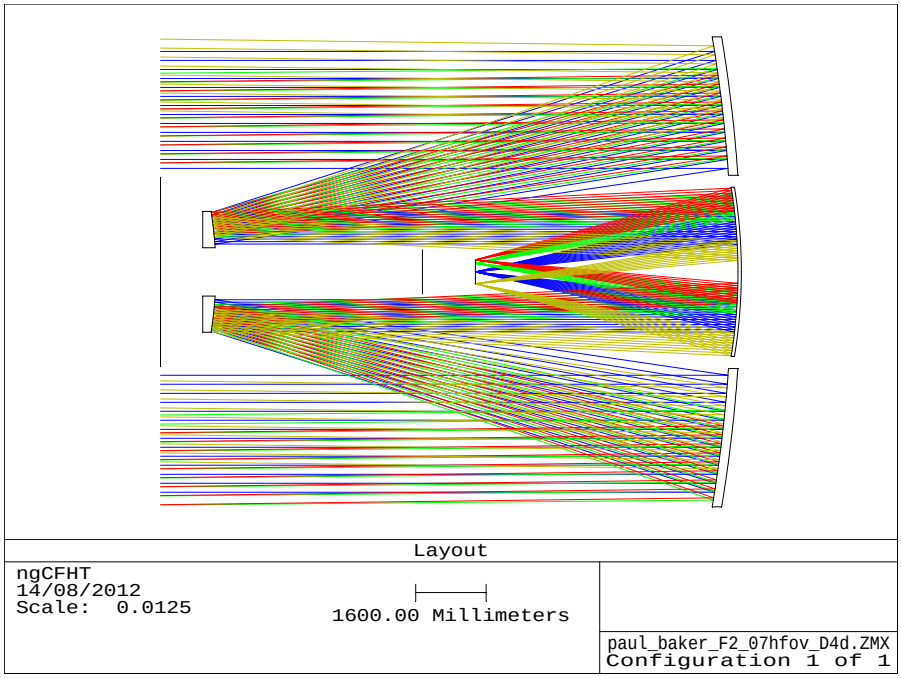

Figure 23. - Another three-mirror solution with smaller field.

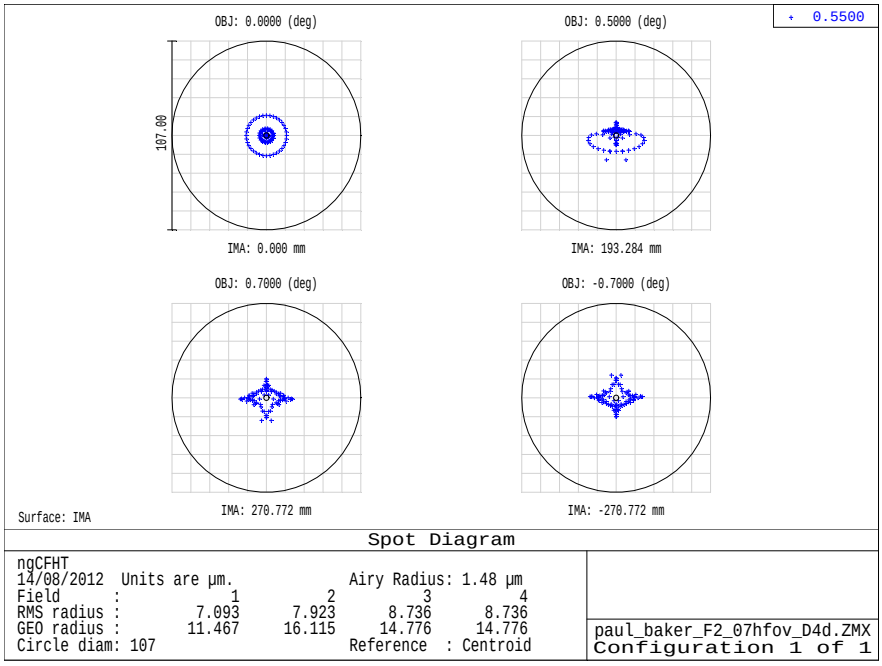

Figure 24. - Alternate three-mirror telescope image quality.

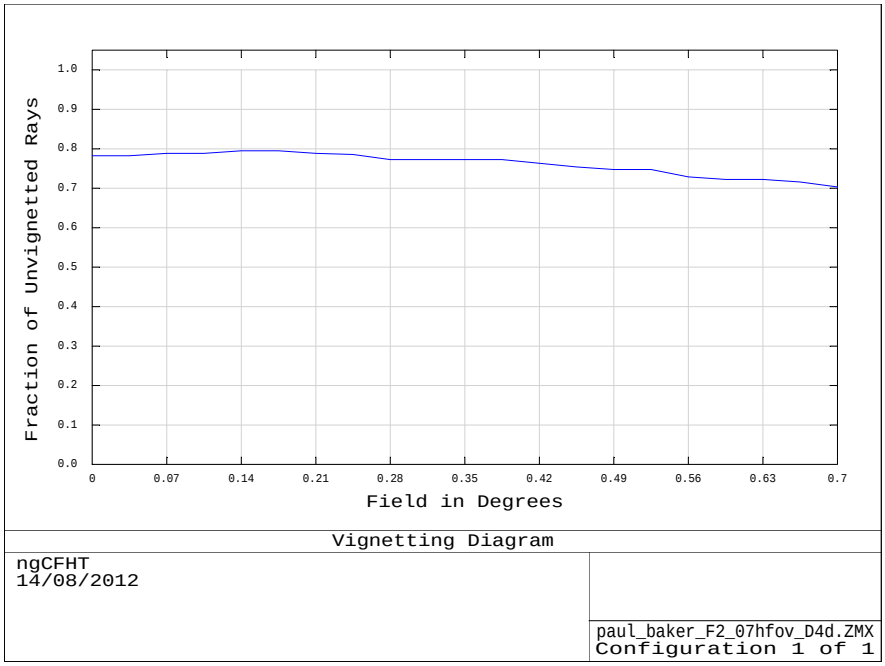

Figure 25. - Alternate three-mirror telescope vignetting.

5 Primary mirror segmentation

Different solutions can be foreseen for a segmented primary mirror. Monolithic mirror diameter up to 8-8.4 m have been produced (e.g., the 8.2-m thin shells of VLT, Gemini, Subaru, or the 8.4-m light-weighted LBT mirrors), however the 10-m seems to be above available capabilities, asking for a segmented version.
Taking leverage from past studies (VLOT, TMT, E-ELT), hexagonal segments up to 1.5-m largest size seems to be a good compromise, minimizing costs and the number of different elements to be polished and test during manufacturing, and aligned and controlled during operations.
Here we explored two limiting cases that can be applied on all above telescope options (one-mirror, two-mirror, or three-mirror designs) with minor variations. Figure 26 shows these two options.

5.1 Small segments

This solution can be best suited for the two-mirror solution, where the primary mirror is hyperboloidal, with a conic constant k = -1.0795 and a radius of 23.2 m, for an overall f-ratio of the primary of F/1.15.
While the asphericity over the full mirror area is quite large, each of the 1.2-m (corner-to-corner) hexagonal segments will take a small fraction of it, making their manufacturing much simpler. There are a total of 78 hexagonal mirrors, split in 13 different classes, as shown in the plot.
Phasing of the segments is not strictly required, because this telescope will never work near diffraction-limit conditions. However, to really gain from superb seeing conditions on top on Mauna Kea, an active control will be required. Differential piston between segments and differential segment shape and WFE will be optimized during this study.

5.2 Large segments

This solution adopts 1.45-m segments (corner to corner), to minimize the number of different mirrors, and is more applicable in the case of slower primary mirrors, like the one-mirror solution. This reduces the number of different segments from 13 to 9 (10, in case of a smaller inner ring).

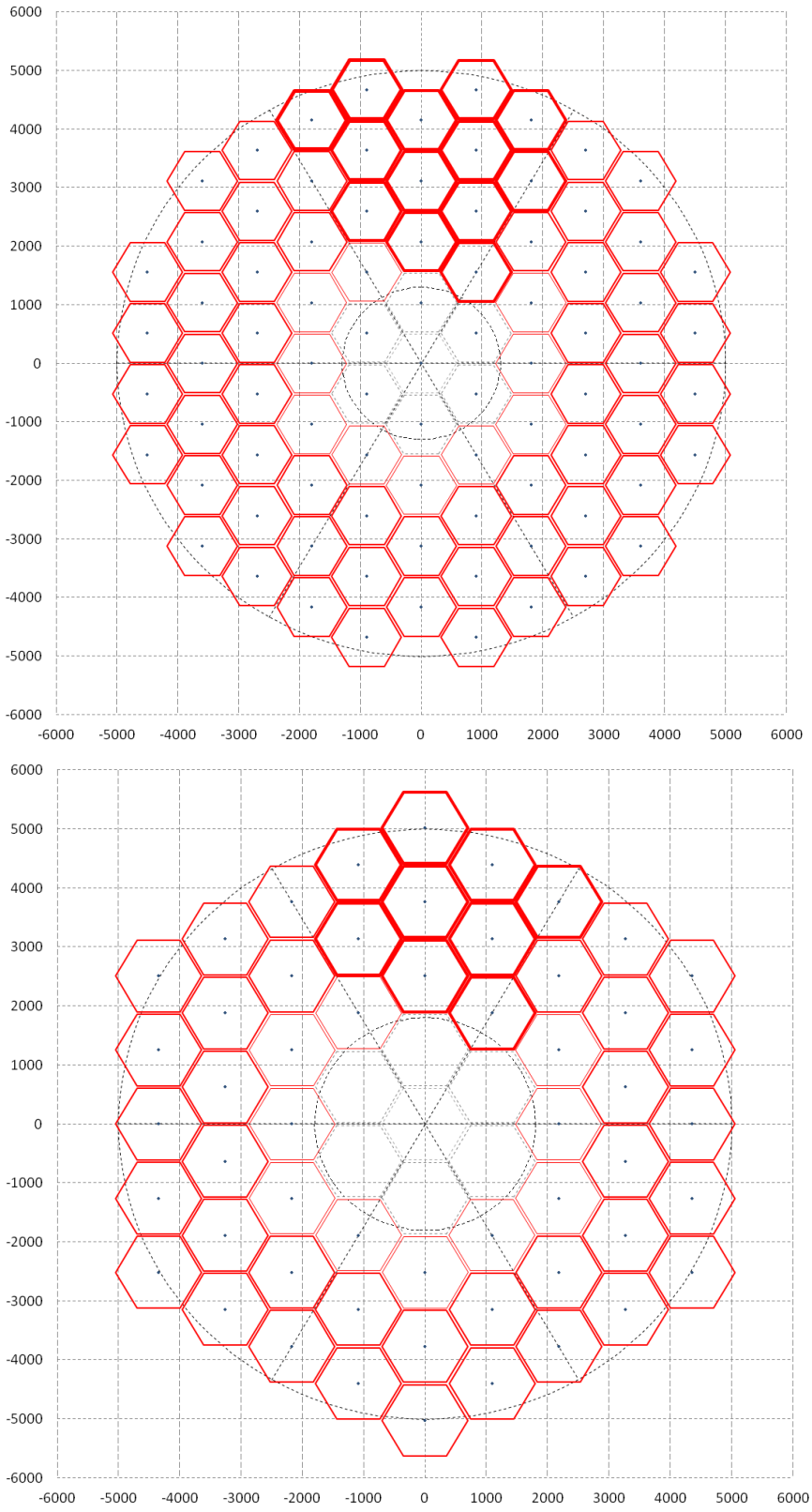

Figure 26. - Two segmentation options. Top: 1.2-m segments. Bottom: 1.45-m segments.

6 Efficiency

6.1 Mirror coating

Efficiency of mirror surfaces will depend on the coating selection, if Aluminium of protected Silver. These two different coatings will strongly differ below 450 nm, as seen in Figure 27. If UV coverage is really interesting, aluminium coatings should be preferred, even if average reflectivity will be smaller. Protected silver coatings have been used in the past (e.g., on Gemini), but a proper trade-off will be done later, depending on other factors (number of reflections, durability, NIR/UV weight factors).

6.2 Anti-reflection coatings

Figure Figure 28 show an optimized Solgel/MgF2 coating over n=1.46 substrates will deliver reflections <1% over most of the wavelength region (370-1150 nm), with a small increase at the two extremes. Similar performances can be obtained over n=1.52-1.55 materials.

6.3 Effective area

The overall effective telescope area, including transmission losses due to mirror reflections, lens and prism internal transmission and air-glass reflections, and telescope vignetting is summarized in for the one- and the two-mirrors telescope designs.

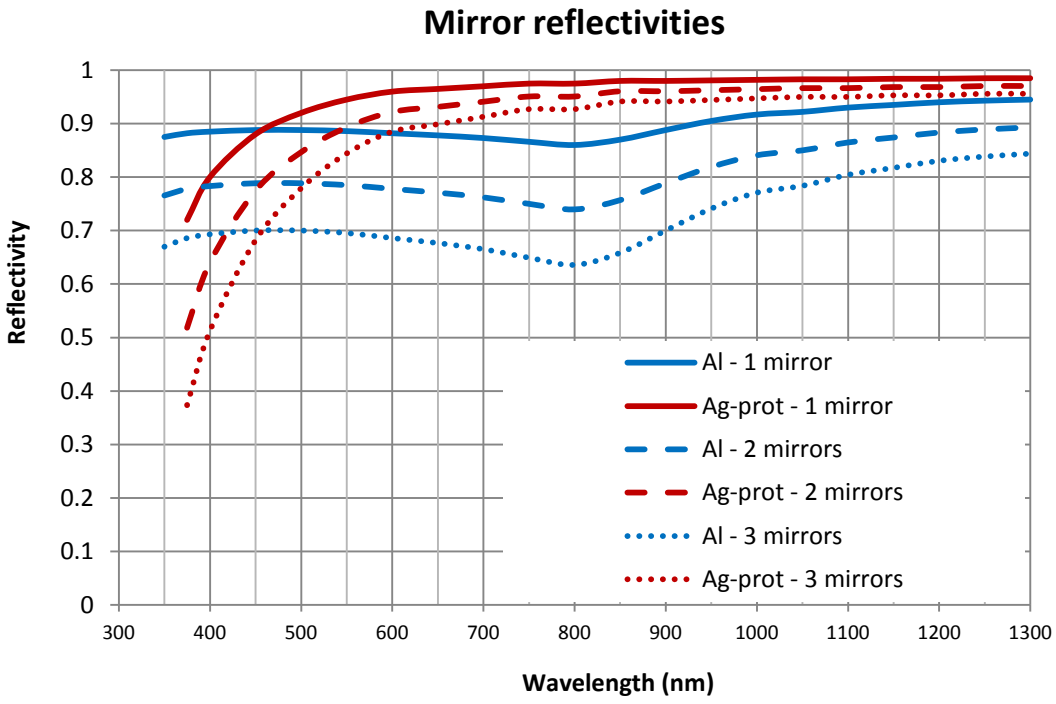

Figure 27. - Available mirror coatings, as function of number of reflections.

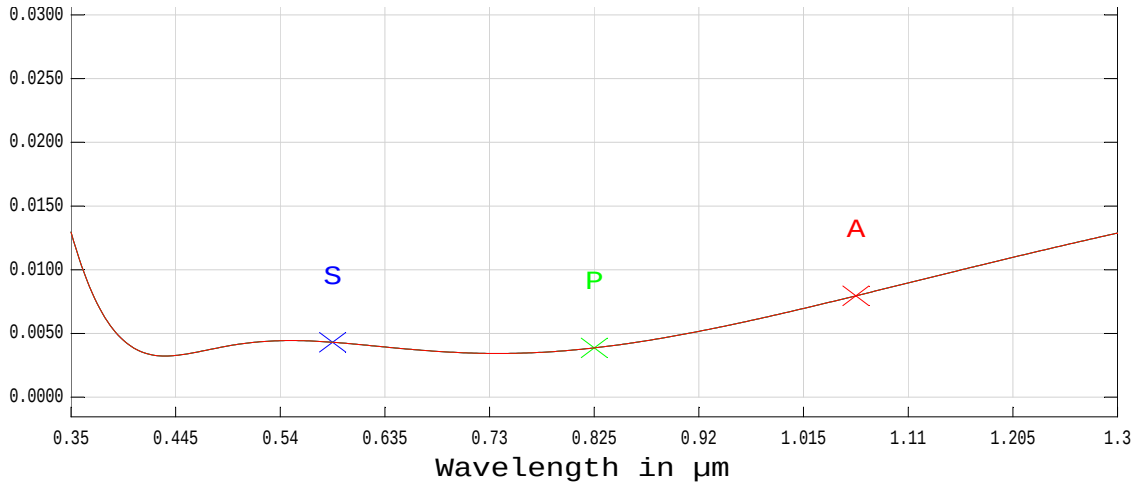

Figure 28. - Wide-band anti-reflection coating.

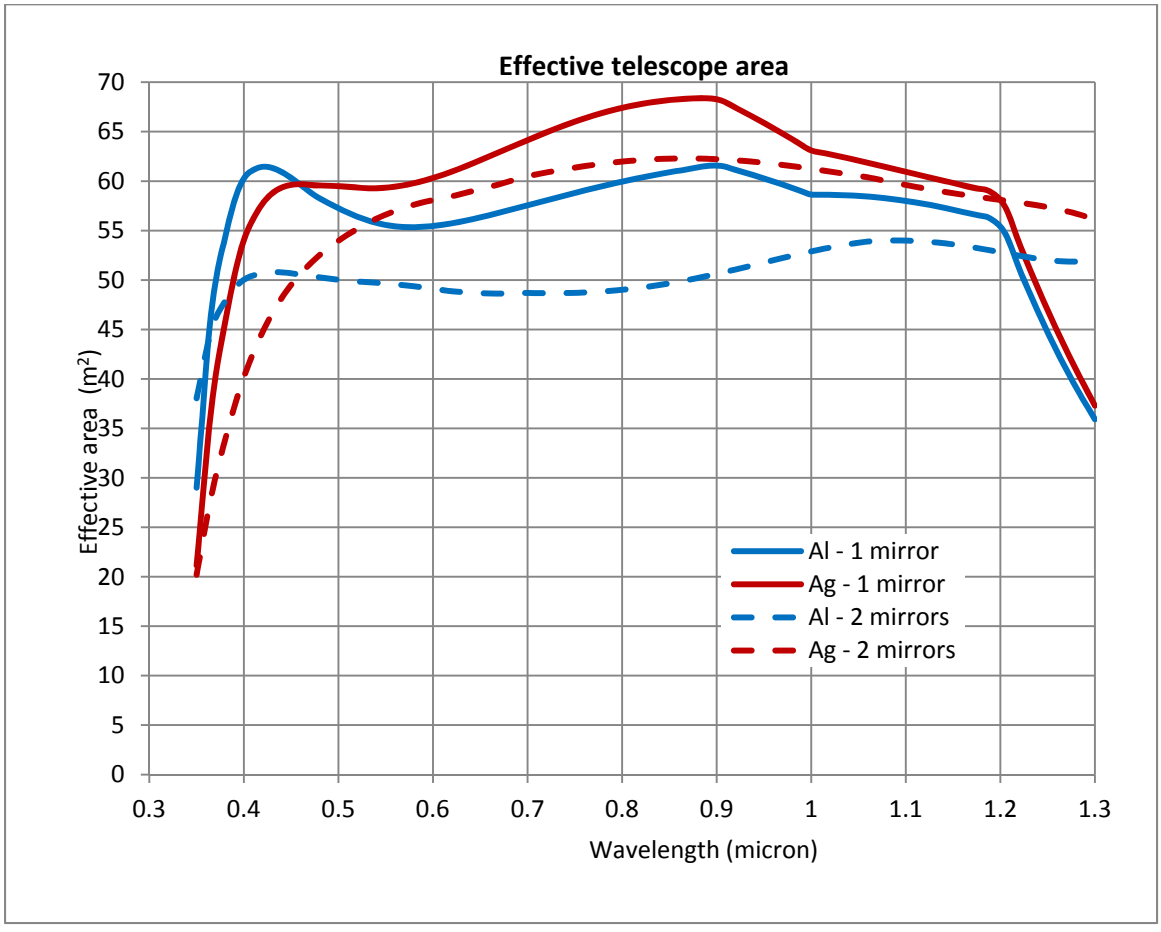

Figure 29. - Effective telescope area for the one- and two-mirror solutions.

APPENDIX A – Fiber Entrance Losses

When light is collected by a circular fiber, entrance losses are an important factor. Assuming a Moffat (β~2.3) profile[2] for the point spread function (atmosphere + telescope optics), integrated light within the fiber core can be computed.

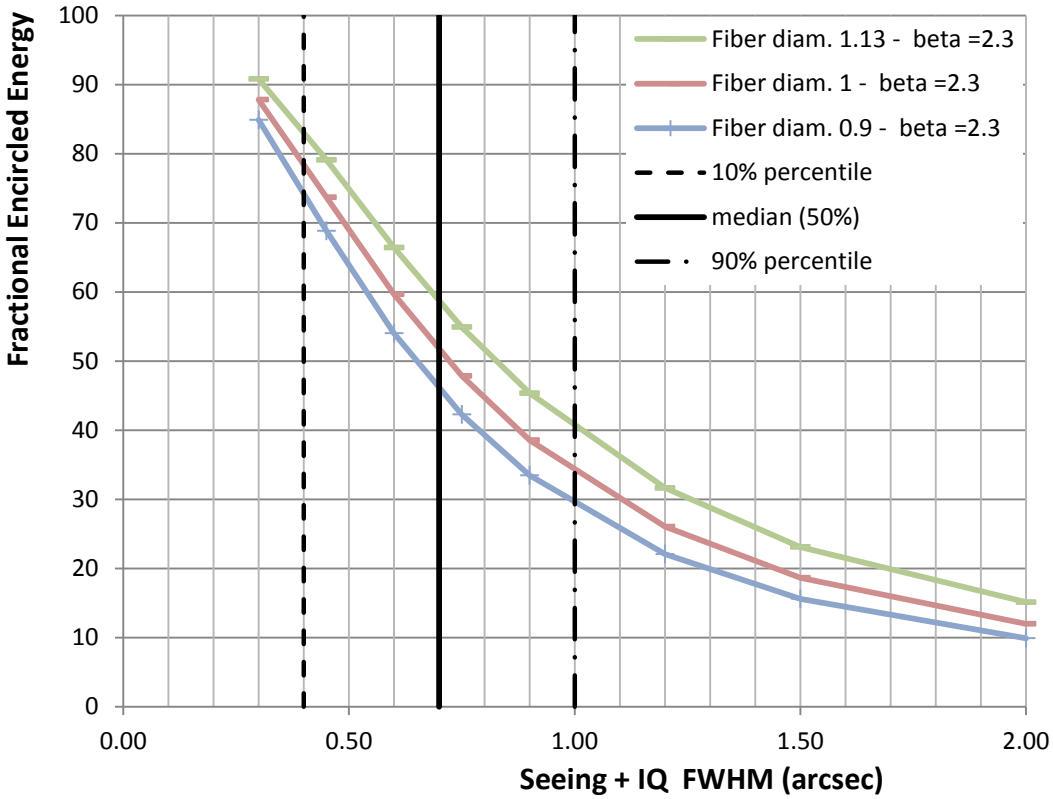

Figure 30. - Secondary mirror asphericity.

It is a strong function of atmospheric and telescope seeing + optical image quality, while it depends on fiber aperture at a lesser extent. Then, carefully minimization of telescope/dome seeing must be undertaken, more than increasing fiber diameter, or pushing telescope image quality too much.

[2] the β value of 2.3 was selected being a compromise between 2.0 and 2.6, used in the literature to fit PSF profiles on the WYIN telescope

APPENDIX B – Glass Selection

This chapter about glass selection is common to many different telescope designs, because both corrector lenses and ADC will ask for very large homogeneous blanks. Of course, within each design, glass choice was further optimized to maximize throughput and image quality.
Weight of the optics is a major limiting factor, and it is proportional to ~D^3. Current glass technologies at Schott are summarized in the Technical Information TIE-41, Table 2, reported here for convenience. Also Ohara can deliver very large blanks, up to 800 mm diameter, as done for the HyperSuprimeCam for the Subary telescope.
The other material of choice for very large optics is Fused Silica, available with diameters up to 1.5-m. This material is naturally very homogeneous, but its cost is much higher than optical glasses.
The list of glasses used for this study is given in Table 3. Different colors refer to glasses of the same color. Some of them are available from both Schott and Ohara catalogues, as equivalent glasses, and share very similar refractive index. However, internal transmission can be different. Enhanced UV transmittance , only *i*-line glasses should be considered.
There is a very restricted list of available glasses for 1-m size and good internal transmission down to 370 nm. Glass selection is quite important, when both UV and NIR wavelengths are considered. The following plot compares four different materials: Schott N-BK7, N-BK7HT, Ohara BSL7Y, and Fused Silica (e.g., Schott Lithosil-Q). As it can be seen, UV coverage can be partially compromised, and NIR wavelengts above 1.2 um, as well.
These materials do not match refraction indices very well, then the very impressive performance of a lateral-shift ADC (by Takeshi), as adopted on the Prime Focus Corrector at Subaru, will not be obtained. The best match has been considered the BK7-LLF1 couple, or the equivalent BSL7Y-PBL1Y. Their differential refraction index must be considered early in the lens design, because the typical "plano-powered-plano" design will introduce power.

Glass Type Family	Melting Tech-nology Min Prod*	Max Dim pre-sent capabili-ties	Max Dim with development	Restricted by	Preferred Glass Types
BK	Cont. Tank 5 tons	∅1000 x 300	∅1500 x 500 or equiv. Vol	CT, CS, ES	N-BK7
LLF, LF, F, SF	Cont. Tank 5 tons	∅1000 x 300	∅1500 x 500 or equiv. Vol	CT, CS, ES	LLF1, LF5, F2, SF6
FK, PK	Discont. Pot	∅360 x 60	∅460 x 100	Cryst, VS	N-FK51A
LAK, LAF, LASF	Discont. Pot	300 x 160 x 43 GD	360 x 280 x 80 GD	Cryst, VS	LAK8, LAK9
KZFS	Discont. Pot	300 x 160 x 43 GD	360 x 280 x 80 GD	Cryst, VS	KZFSN4

Table 2. - Typical large glass blanks from Schott.

Schott	Ohara	Other	Index n_d	Abbe ν_d	Internal transmission (25 mm thickness)	
					@365 nm	@1300 nm (*)
N-BK7	S-BSL7		1.52	64	97.7% / *96.8%*	99.3% / *97.2%*
N-BK7HT	BSL7Y		1.52	64	98.5% / *99.3%*	*99.3%* / *95.8%*
LLF1(HT)	PBL1Y		1.55	46	98.1% / *99.3%*	*99.3%* / *99.6%*
F2HT	PBM2Y		1.62	36	95.7% / *96.3%*	*99.6%* / *99.3%*
LF5(HHT)	-		1.58	41	95.4%	*99.5%*
-	PBL6Y		1.53	49	*99.3%*	*99.1%*
-	-	Fused Silica	1.46	68	99.9%	99.9%

(*) missing data are linearly interpolated from catalogue values and are given in Italics font.

Table 3. - Glass list used in this study.

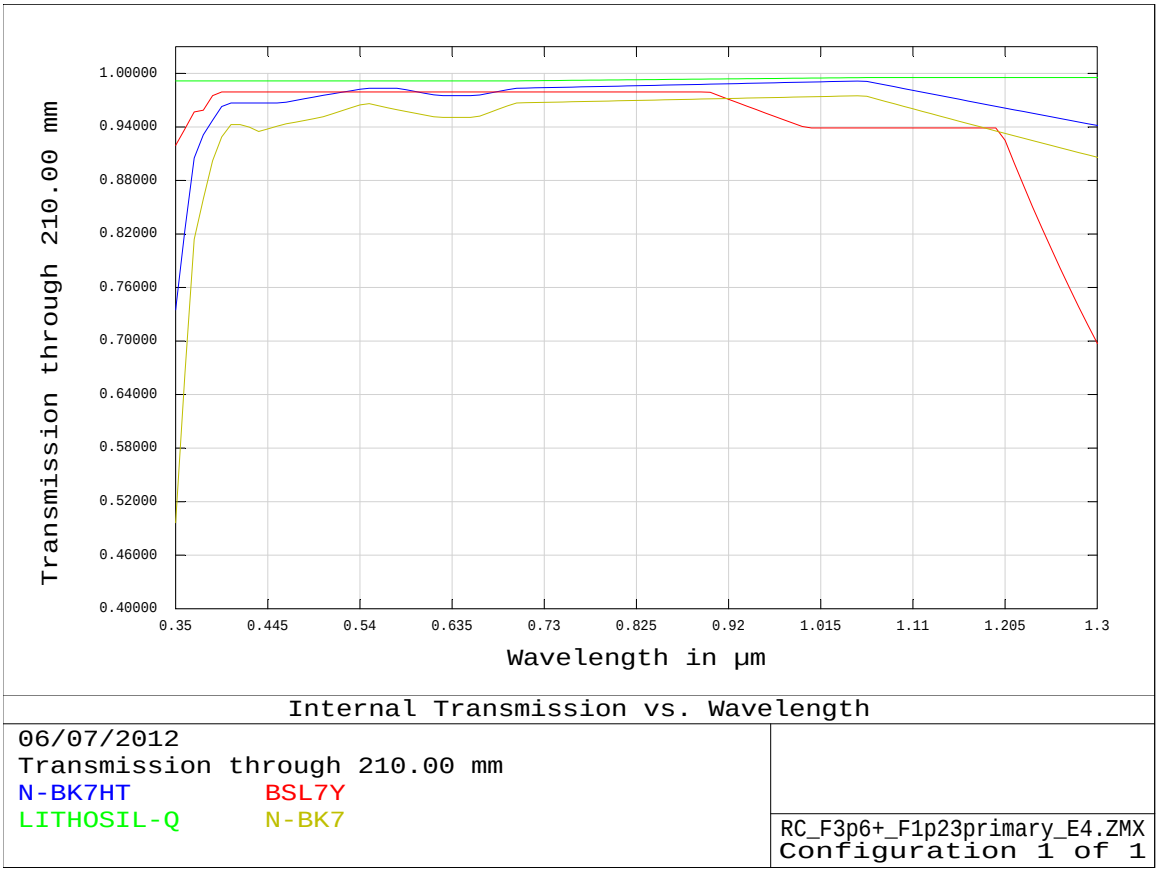

Figure 31. - Comparing internal transmission for different BK7 and Silica.

APPENDIX D. NGCFHT SPECTROGRAPH OPTICAL DESIGN

NRC · CNRC
From Discovery to Innovation...

Herzberg Institute of Astrophysics
Institut Herzberg d'astrophysique

ngCFHT

Spectrograph Design

Optical Design

Paolo Spanò

Revision 0.6

02 November 2012

National Research Council Canada
Conseil national de recherches Canada
Canada

CHANGE RECORD

Issue	Date	Section/Page Affected	Reason/Initiation Documents/Remarks
0.1	05-Sep-12	All 1-2	Table of Content defined First draft of the first two chapters
0.2	13-Sep-12	3	First draft of the third chapter
0.3	09-Oct-12	3	Filled sections.
0.4	25-Oct-12	2 4/5	Table 2, 6, 7 updated Performances and Feasibility sections filled.
0.5	29-Oct-12	2 Others	Fully revised after internal review Modified for self-consistency
0.6	02-Nov-12	4.1	EE80D vs FWHM conversion factor corrected

Table of Contents

List of Figures

List of Tables

1 Introduction

1.1 Scope of the Document

After comparison of different optical configurations for the spectrograph optics, an innovative solution is proposed that fulfils the scientific requirements.
In particular, a concept involving exchanging prisms and anamorphosers in the fore optics to enable both high-multiplex low- resolution modes as well as the high-resolution mode is discussed. This would permit all modes to be achieved using the same optics and detectors. Alternatively, the low resolution mode could be realized by the Subaru PFS design, for example, with a separate dedicated spectrograph for the higher resolution modes. Ultimately, factors like cost, schedule and partner interests will play a role in decisions regarding the precise designs for the instruments. Our goal here is to demonstrate that designs exist that will achieve the scientific goals, and are feasible with current technologies.

In this document we first outline the proposed new configuration and explain the design trade-off (**Chapter 2**). Then, a detailed description of the optical design of the different sub-systems is given (**Chapter 3**), together with main expected performances (**Chapter 4**). As a result of this study, we can anticipate that this concept appears to give highly competitive performances based onto existing state-of-the-art technologies.

1.2 Documents

Applicable documents

ID	Title	Doc. Nr.	Issue	Date
AD-1	ngCFHT Scientific Report	XXX-YYY-nnnn	4	01-Sep-12
AD-2	ngCFHT Technical Report		1	

Reference documents

ID	Title	Doc. Nr.	Authors	Year
RD-1	Volume Phase Holographic Gratings: Polarization Properties and Diffraction Efficiency	PASP, vol. 116, 403-414	Baldry, et al.	2004
RD-2	VPH gratings technology for the Thirty Meter Telescope instrumentation program	SPIE vol. 7018, 70184U	Pazder, Clemens	2008
RD-3	Development of a large mosaic volume phase holographic (VPH) grating for APOGEE	SPIE vol. 7739, 773913	Arns, et al.	2010
RD-4	Optically-athermalized construction optical design for the IMACS Short camera	SPIE vol. 4841, 612	Epps, Sutin	2003
RD-5	Performance of the Apache Point Observatory Galactig Evolution Experiment (APOGEE) high-resolution near-infrared multi-object spectrograph	SPIE vol. 8446, 84460H	Wilson et al.	2012

1.3 Acronyms and abbreviations

AD	Applicable Document
ADC	Atmospheric Dispersion Document
AIV	Assembly, Integration, and Verification
CCD	Charge Coupled Device
EExxD	Encircled Energy xx% Diameter
FEA	Finite Element Analysis
FDR	Final Design Review
FWHM	Full Width Half Maximum
I/F	Interface
LSF	Line Spread Function
NA	Not Available
PDR	Preliminary Design Review
PSD	Power Spectral Density
PSF	Point Spread Function
PTV	Peak To Valley
RD	Reference Document
RMS	Root Mean Square
RSS	Root Square Sum
TBC	To Be Confirmed
TBD	To Be Defined
TIR	Total Internal Refraction
VPH	Volume-Phase Holographic

2 Spectrograph overview

2.1 Design rationale

Many multi-object fiber-fed spectrographs have been designed, as reported also in the Scientific Report ([AD-1]). A summary of their main technical characteristics is given in Table 1 for reference.
As seen, most of them have been coupled to smaller telescopes, looking at smaller wavelength ranges, with smaller resolution ranges, and less objects. While we acknowledge that several ways exist to achieve requirements, especially for the low resolution mode, the design of a high-multiplexing, low-to-high resolution, high-efficiency, wide-band spectrograph as defined in the top-level design requirements (**Section 0**) is very challenging. This is due to existing constraints in the current manufacturing technologies, like the maximum size of efficient diffraction gratings. Scaling laws for spectrograph design together with some working examples are given (**Section 2.3)**. However, the requirements for the high resolution (R~20,000) mode, and our desire to be conservative regarding sizes of optical elements, led us to consider alternatives. Based onto a novel pupil slicing technique, a new high-resolution spectrograph is designed (**Section 2.4**). By this technique high-resolution is made feasible for a very large number of fibers with high throughput and extended spectral coverage. At the same time, spectrograph optics allows for low-resolution (R~2,000) to be available by an exchanging mechanism in the fore-optics and another set of gratings, delivering fully simultaneous spectral coverage over a larger set of fibers (**Section 0**). By virtue of this design, other two observing modes are obtained at a medium resolution (R~6,500), by proper combination of gratings and relay optics (**Section 2.6**). A proper trade-off analysis between competing technical constraints was carried out to tune first-order parameters for the different sub-components and optimize performances (**Section 0**).

Instr.	D_{tel} (m)	$\lambda\lambda$ (μm)	R_{max}	N_{MOS}	Fiber (")	Beam (mm)	Grating	ε_{max} (tot)
2dF	3.9	0.37-1.0	17,000	400	2.1	190	VPH	5%
FLAMES	8.2	0.37-0.95	25,000	130	1.2	180	Echelle	9%
Hectospec	6.5	0.36-0.92	40,000	240	1.5	260	Grating	10%
FMOS	8.2	0.9-1.8	2,200	400	1.2	150	Grat.,VPH	10%
HERMES	3.9	4 windows	28,000	400	2.0	195	VPH	10%
APOGEE	2.5	1.5-1.7	22,500	300	2.0	280	VPH	16%
PFS	8.2	0.37-1.3	4,500	2400	1.1	280	VPH	18%

Table 1. - Wide-field fiber-fed MOS facilities.

2.2 Top level design requirements

The next generation Canada-French-Hawaii Telescope (ngCFHT) shall be mainly devoted to perform deep, wide-field, spectroscopic surveys, at spectral resolutions from ~2'000 to ~20'000, at visible and near-infrared wavelengths.
The main baseline parameters for the system are:

- Telescope diameter: 10-m
- Field of view diameter: 1.5 deg^2 (hexagonal)
- Fiber diameter: 0.9 arcsec (goal: 1.2 arsec)
- Wavelengths: 370 – 1300 nm (goal: 350 – 1300 nm)
- Resolution: ~2'000 – 20'000 (goal: ~30'000)
- Simultaneous coverage: >λ/7 windows
- Number of objects: 800 – 3200 (3200 only for LR mode)
- Total throughput[1]: >20% (over 90% of all wavelengths)

At low resolution (R~2'000), simultaneous coverage should be complete at both visible and near-infrared wavelengths, while at high resolution (R~20'000), only some selected windows can be covered. At low resolution, the highest multiplexing should be reached, while at higher resolutions a decreased number of objects can be observed.
The ideal spectrograph should be able to switch between different resolutions by a small number of mechanisms, moving few elements in order to reduce failures and increase repeatability.
Efficiency should prevail over simultaneous coverage, thus favouring VPH first-order gratings over echelle gratings. High efficiency over very wide wavelength ranges can be achieved by splitting light into two or more arms by dichroic beamsplitters, and optimizing efficiency for each channel by proper selection of glass materials, coatings, and grating parameters.

2.3 Scaling laws for spectrograph design

Scaling laws for resolution and detector sampling are given below for reference, and have been used to define the key parameters of the spectrograph design. Resolving power for grating spectrographs scales as:

$$R = 206265 \frac{1}{s} \frac{d_{coll}}{D_{tel}} 2 \tan \delta_{Littrow} \qquad \text{(arcsec)}$$

where R is the resolving power $\lambda/\Delta\lambda$, s is the slit width (in arcsec), d_{coll} and D_{tel} are the diameter of the spectrograph collimated beam and the telescope diameter, and δ_{Littrow} is the grating Littrow angle (echelle grating Littrow angle is typical given as R-X, where X is tanδ). For a given telescope diameter, resolution can be increased by increasing collimated beam and grating size, or by pushing grating working angles to the maximum. Let's give few examples to gain some insight into typical resolutions.

Example A (UVES):
8-m telescope, 1" slit, 20-cm beam size, R4 echelle grating ⇨ *R~40'000*

Example B (HIRES):
10-m telescope, 1" slit, 30-cm beam size, R2.8 echelle grating ⇨ *R~40'000*

[1] it includes atmosphere, telescope mirrors, wide field corrector optics, ADC optics, fiber losses, spectrograph optics, and detector quantum efficiency. Entrance losses are not included, being strongly seeing dependent (see Telescope Optical Report).

Example C (FLAMES/GIRAFFE + Medusa fibers):
8-m telescope, 1.2" fiber, 18-cm beam size, R2 echelle grating ⇨ *R~25'000*

Example D (HECTOSPEC):
6.5-m telescope, 1.5" fiber, 26-cm beam size, R2 echelle grating ⇨ *R~35'000*

So far, high-resolution spectroscopy on 6-10 meter class telescopes has been achieved by echelle spectrographs only, with relatively low efficiencies. Moreover, increasing multiplexing by a large factor adds complexity to this task. VPH gratings offer higher efficiencies, but they work better on lower Littrow angles, thus delivering smaller resolutions. The only exception is provided by Dickson VPH gratings, where resolution and efficiency are maximized at expense of the spectral coverage (see APOGEE, [RD-5]), fighting against the requirement for large simultaneous spectral coverage.
The second scaling law is:

$$F_{cam} = \frac{N_{sampling}\Delta_{pixel}}{rD_{tel}s}$$

where F_{cam} is the camera focal ratio, $N_{sampling}$ is the spectral sampling, Δ_{pixel} is the detector pixel size, r is the anamorphic magnification of the grating (=cosα/cosβ, typically about 1). Larger telescopes need faster cameras, generally more difficult to be built.

2.4 A new pupil slicing technique for high resolution

To get the high-resolution for a large number of objects we propose a novel pupil slicing technique which offers good image quality and high throughput while keeping the size of dispersers within current technology constraints. The light is processed inside the spectrograph optics to reduce the effective size of the projected slit image, thus increasing resolution. To explain how this has been done, we can follow how images and pupils are modified along the optical path. This is shown in Figure 1.

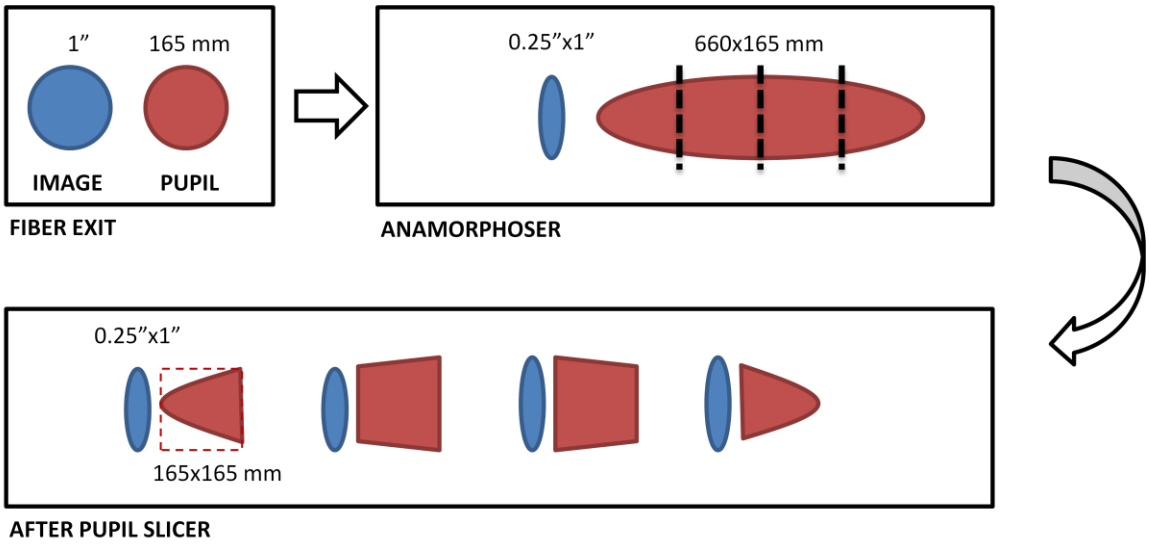

Figure 1. - High-resolution mode is achieved by slicing the pupil by a factor of 4X.

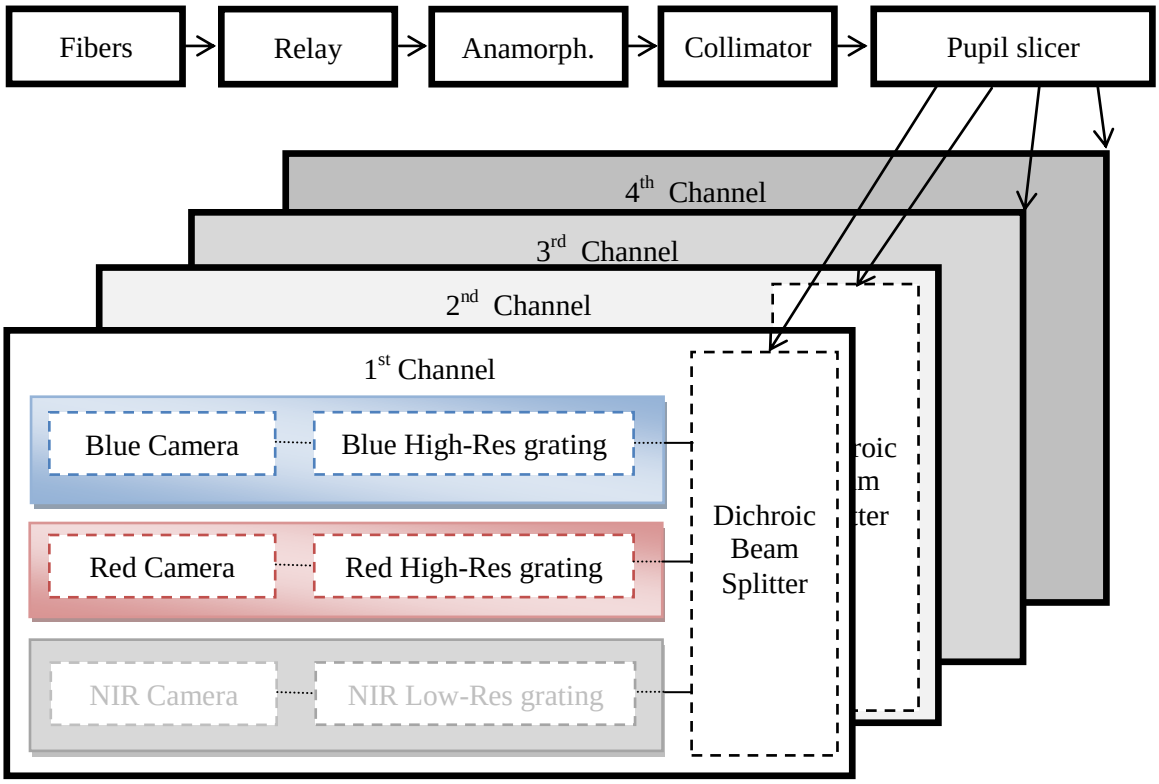

Figure 2. - Spectrograph conceptual scheme in HR mode.

At the entrance of the spectrograph, each fiber (1" diameter, in this example) will project a circular beam. After collimation, this beam will project a round pupil of 165 mm (this dimension can be different, of course, and it has been selected after the trade-off study, as described in Section 2.7). By mean of the anamorphoser, the collimated beam is effectively elongated by a 4X factor in one direction (165 x 660 mm). At the same time, the image is effectively reduced by the same factor 4X in the same direction (0.25" x 1"). Of course, different anamorphic ratios can be selected, but here we show the case that was selected as our best trade-off (see Section 2.7). By pupil slicing, each fiber will produce 4 identical images, each one illuminated by a different smaller sub-pupil. As a result, light collected by each fiber will be split into four channels, thus projecting four spectra onto different detectors. The spectrum of a single target needs to be recovered by adding together these four spectra by the data reduction software.
The implementation of this pupil slicing method is realized by the spectrograph conceptually described in Figure 2. Light from fiber arrays is reimaged onto the anamorphoser. The light is then collimated and split into four identical channels by a common pupil slicer placed near the exit pupil of the collimator. Each channel consists of a dichroic tree to separate wavelengths into arms (two visible arms, blue and red; a third near-infrared arm is not used in this mode, see Section 0). Finally optimized cameras will focus light onto detectors.

2.5 Low-resolution high-multiplexing mode

The required large collimation optics for the elongated pupil can accept the light distribution coming from four separate fiber arrays, as shown in Figure 3. Each fiber array will project its own circular pupil, as large as the not elongated pupil. Then, up to four circular pupils can be approximately fitted inside the same collimator exit pupil required for the high-resolution mode.

This is enabled by removing the anamorphoser and placing a prism-plate to direct the light from different fiber arrays inside the four channels. Each fiber of the array will see a "single-channel" spectrograph, producing a single spectrum. The effective slit width is larger than in the pupil-slicing mode, thus providing a lower resolution. At the same time more fibers can be simultaneous observer, gaining a factor 4X in multiplexing. The conceptual implementation of this mode is given in Figure 4, by switching some optical elements.

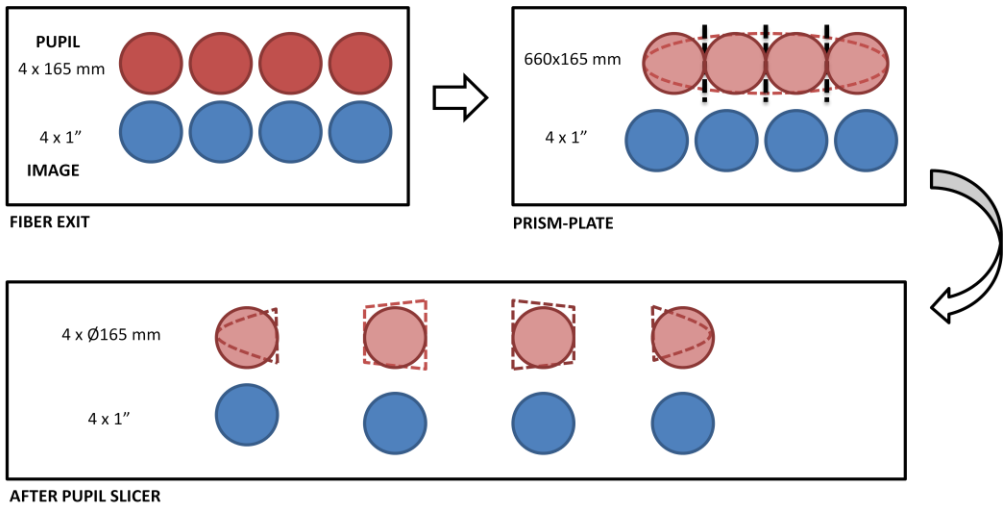

Figure 3. - Images and pupils in low-resolution, high-multiplexing mode.

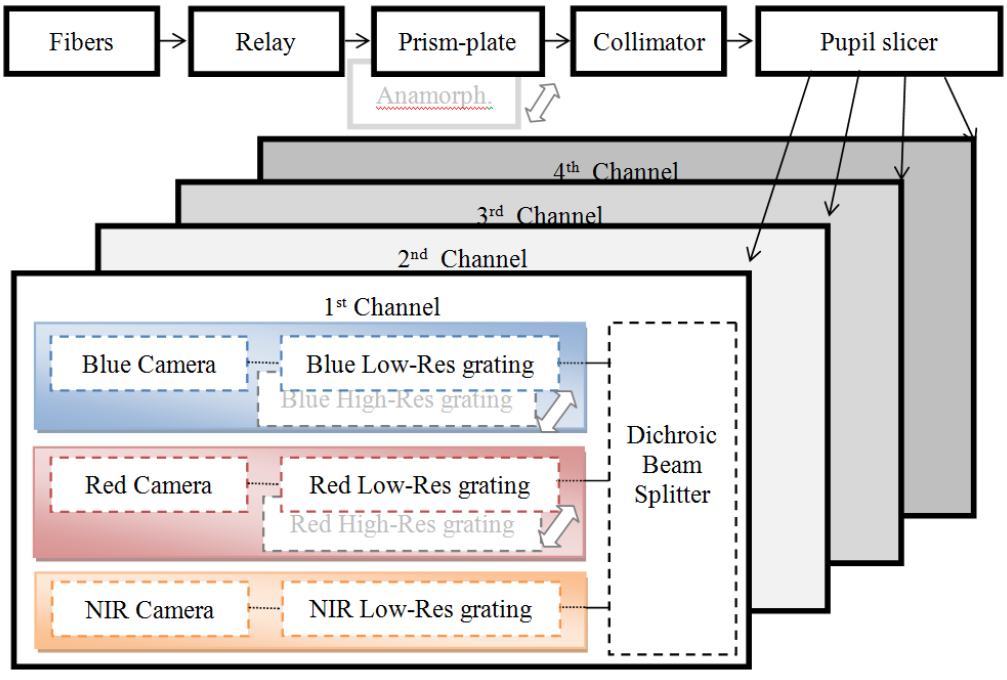

Figure 4. - Spectrograph conceptual scheme in LR mode.

2.6 Other observing modes

As a result of the exchange mechanisms between the anamorphoser/prism-plate and the HR/LR gratings, other observing modes can be defined, providing an intermediate resolution of about 6'500. This resolution can be achieved by two different combinations, i.e. by combining the anamorphoser with LR gratings, or the prism-plate with the HR ones.
Up to four different observing modes can be defined by virtue of these combinations. We assume that all HR gratings will be switched with the LR ones, and vice versa, to reduce the number of different observing modes. They are summarized in Table 2 and are described below:

- **Low-Resolution (LR)**: low-resolution gratings and prism-plate are selected. In this way up to 4xN fibers can be fed into the spectrograph, N per channel. Full spectral coverage is obtained at R~2'000, covering all visible and NIR wavelengths, simultaneously.

- **Medium-Resolution Full-Coverage (MR-FC)**: still keeping low-resolution gratings in place, the prism-plate is exchanged with the anamorphoser, thus selecting a subsample of N fibers to be observed at higher resolution (R~6'500). The spectral coverage is still complete in the visible, but NIR wavelengths are not measured, because fiber images are undersampled. Each fiber will produce four spectra, to be added by SW.

- **Medium-Resolution High-Multiplexing (MR-HM)**: another way to obtain an intermediate resolution (~6'500) for all 4xN fibers is to keep the prism-plate in place and insert the HR gratings. Spectral coverage is reduced to two wavelength ~λ/7 windows. Different gratings will be available to select the central wavelength of those two windows. Also near-infrared wavelengths can be observed, but at a lower resolution (the same of the LR mode).

- **High-Resolution (HR)**: when high-resolution is required, high-resolution gratings must be coupled to the anamorphoser, then delivering R~20'000 in the visible range. Due to limited detector size, only two ~λ/7 wavelength windows will be observed simultaneously, placed around two selectable central wavelengths. NIR wavelengths are not measured due to undersampling in the NIR arms. The multiplexing is reduced by a factor 4 with respect to LR mode.

Mode	Resolution VIS	Resolution NIR	Simultaneous Coverage	Fibers
LR	~2000	~2000	Full	4xN
MR-FC	~6500	*NA*	Full	N
MR-HM	~6500	~2000	2 windows λ/7 (in the visible)	4xN
HR	~20000	*NA*	2 windows λ/7 (in the visible)	N

Table 2. - Defined spectrograph observing modes.

2.7 First order parameter trade-off

In order to implement the two conceptual designs into a real optical design, many choices must be done about the main characteristics of the different sub-systems. For each of them we need to define the f-ratio, beam size, field size, wavelength range, and so on. Optical interfaces between sub-systems have been provisionally defined, to simplify the design stage. This modular approach allows to optimize or to change some of the sub-systems, if required, without the need to fully redesign the whole optical train.

Here we report about the main choices. The full list of first-order parameters are defined in the three tables at the end of the section.

One of the first choices to be made is the selection of the disperser type. Indeed, only two different types of gratings have been used for high-resolution astronomical spectrographs, namely echelle gratings, mostly used in reflection to enhance their throughput, and volume-phase holographic (VPH) gratings, used in transmission.
Echelle gratings can deliver very high-resolving power by mean of very steep blaze angles. The steepest angle used on existing astronomical spectrographs is 76 deg (or R-4, tan(76)=4). However, while providing very high resolving powers, these gratings are used at high diffraction orders, where the free spectral range is relatively small. Then, to recover larger wavelength ranges, many orders must be measured in different observations, or by cross-dispersing different orders in the spatial direction. In the former case higher multiplexing can be reached, at cost of a quite limited simultaneous spectral coverage. Then, many observations with different filter and/or gratings are required to retrieve the full spectrum. In the latter case, cross-dispersed echelle offer much larger simultaneous spectral coverage but for a much smaller amount of fibers, being the preferred choice for single object spectrograph.
VPH gratings behave very well in the first order providing very high peak efficiencies. The spectral coverage is a strong function of the Bragg angle that defines the working geometry to obtain the highest efficiency. Different authors (see RD-1, RD-2) have shown there is an optimal range of Bragg angles between ~15 and ~35 degrees for which efficiency peaks at ~90% and bandwidth is quite large. For higher angles, efficiency drops and then raise again for a smaller range of angles, defined as "Dickson" gratings (see RD-3 for a recent implementation). Those devices, while delivering high peak efficiency (~90%), exhibit relatively narrow bandwidths, making them less attractive for a wideband spectrograph as ngCFHT.
Our goal is to select two basic angles, one for the HR gratings and another one for the LR gratings, which simultaneously maximize resolving power, peak efficiency and bandwidth for both HR and LR modes. Our best trade-off is a HR grating angle of 37 deg (corresponding to a Bragg angle~24 deg for n=1.5 medium) with an estimated diffraction efficiency peak of 90%, and a LR grating angle of 14 deg, as it can be inferred from Figure 5.

Once telescope diameter, fiber aperture, grating angle, and resolution are fixed, the only free parameter is the collimated beam size, as derived from our scaling laws. This will give the size of our elongated pupil. Of course, without the pupil slicing technique, very large gratings and very fast camera optics should be required to design the spectrograph. Our goal, however, was to achieve the given resolution within current technologies, and there is where the pupil slicing helps a lot. Due to the fact that we required a ~65cm collimated beam (elongated direction), we selected a pupil slicing of 4X to reduce the beam size impinging on gratings to ~16 cm only. By combining together the 4X anamorphic factor with the 4X pupil slicing factor, each sub-pupil is almost squared, thus minimizing both grating and camera optics size.

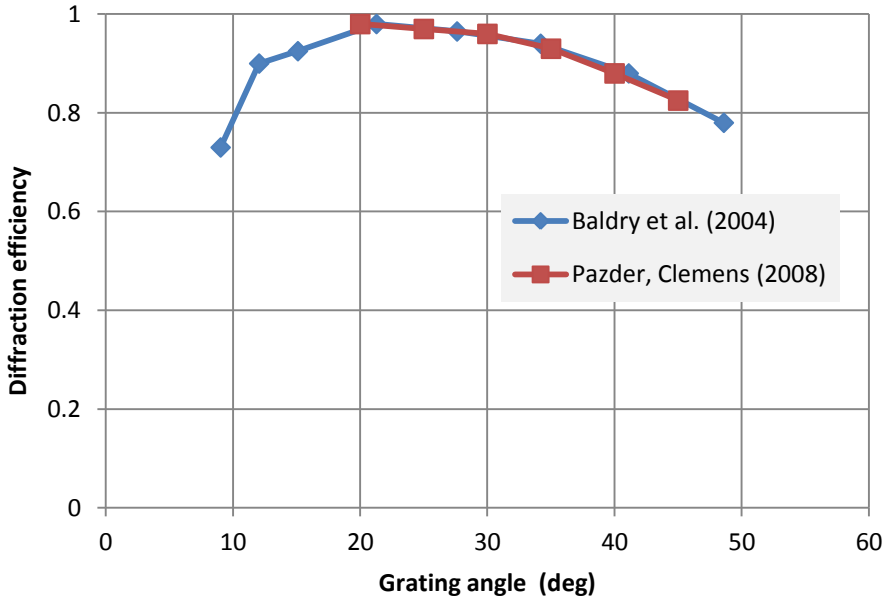

Figure 5. - First-order diffraction efficiency with unpolarized light (from RD-1, RD-2).

Once sub-pupil size is defined, camera optics parameters can be defined, too. Here is where the second of the two scaling laws enter. This new trade-off is between spectral sampling and simultaneous coverage. At the same time, also spatial sampling and multiplexing will be traded off. A reasonable sampling of spectra at both HR and LR modes must be defined. Multiplexing will be further controlled by the required minimum gap between adjacent spectra to allow proper data extraction, minimizing cross-contamination. The smaller the sampling, the higher the bandwidth and the multiplexing on a given detector area. There are manufacturing considerations to limit the camera f-ratio slower than F/1.5, in order to avoid very complex and expensive optics.

The final trade-off was done taking into account all these parameters together. There are some tables to define parameters for the High Resolution mode (Table 3), Medium-Resolution modes (Table 4, Table 5), and another one for the Low Resolution mode (Table 6). For the HR mode, three different cases were analyzed based on different number of slices (3 and 4) and different anamorphic factors: 3, 4, and 6. This last case, however, is done at the expenses of an efficiency loss, because the two more extreme sides of the pupil will be lost. Even if larger anamorphism will provide higher resolution, the projected slit width will be highly under-sampled, reducing final performances. As best compromise, we selected the "4 slices – 4 anamorphism" as baseline.

Finally, a summary of the main characteristic of the spectrograph are given in Table 7. Also numbers of the whole system, including the telescope, are given for reference. To fully match the required multiplexing, two twin spectrograph units must be built.

ngCFHT High-Resolution mode (VIS only)

		Case: 4 slices			Case: 3 slices			Case: 4 slices + larger anam.		
Sub-system	**Parameter**	**Input**	**Output**	**Units**	**Input**	**Output**	**Units**	**Input**	**Output**	**Units**
Telescope	Telescope diameter	10		m	10		m	10		m
	Focal ratio @ fiber entrance	3.5			3.5			3.5		
	Plate scale @ fiber entrance		170	um/arcsec		170	um/arcsec		170	um/arcsec
Fiber	Fiber core	155		um	155		um	155		um
	Fiber core @ sky		0.91	arcsec		0.91	arcsec		0.91	arcsec
	Fiber FWHM @ sky		0.79	arcsec		0.79	arcsec		0.79	arcsec
	Multiplexing (no gaps)		799	objects		991	objects		799	objects
Relay	Input f-number		3.5			3.5			3.5	
	Anamorphic magnification (spectral)	4			3			6		
	Output f-number (spectral)		16			12			16	
	Output f-number (spatial)		4.0			4			2.7	
	Output fiber size (spectral, FWHM)		153	um		153	um		102	um
	Output fiber size (spatial, geom.)		709	um		531	um		709	um
Collimator	Collimated beam diameter (spatial)	165		mm	200		mm	165		mm
	Collimated beam diameter (spectral)		660	mm		600	mm		990	mm
	Collimator f-number (spatial)	16			12			16		
	Collimator f-number (spectral)		4.0			4			2.7	
	Collimator focal length		2640	mm		2400	mm		2640	mm
	Collimator HFoV (spatial)		6.1	deg		6.3	deg		6.1	deg
	Slit height		566	mm		527	mm		566	mm
Pupil Slicer	Slices	4			3			4		
	Collimated beam size (spectral)		165	mm		200	mm		248	mm
	Collimated beam size (spatial)		165	mm		200	mm		165	mm
	Sub-pupil diameter		233	mm		283	mm		297	mm
Disperser	VPH Littrow angle	37		deg	37		deg	37		deg
	VPH size (spatial)		165	mm		200	mm		165	mm
	VPH size (spectral)		207	mm		250	mm		207	mm
Cameras	Camera focal length	430		mm	420		mm	430		mm
	Camera f-number (spectral)		2.6			2.1			1.7	
	Camera f-number (spatial)		2.6			2.1			2.6	
	Camera f-number (no vignetting, diagonal)		1.84			1.48			1.45	
	Camera HFoV (along diameter)		8.6	deg		8.8	deg		8.6	deg
	Fiber projection (spectral, FWHM)		25.0	um		26.8	um		16.7	um
	Fiber projection (spatial, geom.)		115.4	um		93.0	um		115.4	um
Detector	Detector size (square)	9		Kpixels	9		Kpixels	9		Kpixels
	Pixel size	10		um	10		um	10		um
	Detector length		92.16	mm		92.16	mm		92.16	mm
	Sampling (spectral, FWHM)		2.50	pixels		2.68	pixels		1.67	pixels
	Sampling (spatial, geom.)		11.54	pixels		9.30	pixels		11.54	pixels
	Interspectrum separation (spat., geom.)		6.67	pixels		5.38	pixels		6.67	pixels
	Flatness (PtV)	35		um	35		um	35		um
	Flatness defocus PSF		5.04	um		6.25	um		5.04	um
	Electro-optical PSF	10		um	10		um	10		um
	Sampling PSF (0.87X bin size)		8.70	um		8.70	um		8.70	um
SYSTEM	Spectral resolution (FWHM, no aberrations)		25936			23578			38904	
	Image quality PSF	15		um	15		um	15		um
	Detector PSF		14	um		15	um		14	um
	Overall PSF		21	um		21	um		21	um
	Spectral resolution (FWHM)		19996			18581			24433	
	Multiplexing (with gaps)		827			941			909	
	Spectal bandwidth (single channel)		7.0	lambda		6.9	lambda		7.0	lambda

Table 3. - First order parameters for three potential High Resolution modes.

ngCFHT Medium-Resolution Full-Coverage mode

		MR-FC - VIS			MR-FC - NIR		
Sub-system	**Parameter**	**Input**	**Output**	**Units**	**Input**	**Output**	**Units**
Telescope	Telescope diameter	10		m	10		m
	Focal ratio @ fiber entrance	3.5			3.5		
	Plate scale @ fiber entrance		170	um/arcsec		170	um/arcsec
Fiber	Fiber core	155		um	155		um
	Fiber core @ sky		0.91	arcsec			arcsec
	Fiber FWHM @ sky		0.79	arcsec			arcsec
	Multiplexing (no gaps)		799	objects			objects
Relay	Input f-number		3.5				
	Anamorphic magnification (spectral)	4			4		
	Output f-number (spectral)		16				
	Output f-number (spatial)		4.0				
	Output fiber size (spectral, FWHM)		153	um			um
	Output fiber size (spatial, geom.)		709	um			um
Collimator	Collimated beam diameter (spatial)	165		mm	165		mm
	Collimated beam diameter (spectral)		660	mm			mm
	Collimator f-number (spatial)	16			16		
	Collimator f-number (spectral)		4.0				
	Collimator focal length		2640	mm			mm
	Collimator HFoV (spatial)		6.1	deg			deg
	Slit height		566	mm			mm
Pupil Slicer	Slices	4			4		
	Collimated beam size (spectral)		165	mm			mm
	Collimated beam size (spatial)		165	mm			mm
	Sub-pupil diameter		233	mm			mm
Disperser	VPH Littrow angle	14		deg	15		deg
	VPH size (spatial)		165	mm			mm
	VPH size (spectral)		170	mm			mm
Cameras	Camera focal length	430		mm	290		mm
	Camera f-number (spectral)		2.6				
	Camera f-number (spatial)		2.6				
	Camera f-number (no vignetting, diagonal)		1.84				
	Camera HFoV (along diameter)		8.6	deg			deg
	Fiber projection (spectral, FWHM)		25.0	um			um
	Fiber projection (spatial, geom.)		115.4	um			um
Detector	Detector size (square)	9		Kpixels	4		Kpixels
	Pixel size	10		um	15		um
	Detector length		92.16	mm			mm
	Sampling (spectral, FWHM)		2.50	pixels			pixels
	Sampling (spatial, geom.)		11.54	pixels			pixels
	Interspectrum separation (spat., geom.)		6.67	pixels	3		pixels
	Flatness (PtV)	35		um	20		um
	Flatness defocus PSF		5.04	um		4.27	um
	Electro-optical PSF	10		um	10		um
	Sampling PSF (0.87X bin size)		8.70	um		13.05	um
SYSTEM	Spectral resolution (FWHM, no aberrations)		8582			9222	
	Image quality PSF	15		um	20		um
	Detector PSF		14	um		17	um
	Overall PSF		21	um		26	um
	Spectral resolution (FWHM)		6616			4984	
	Multiplexing (with gaps)		827			817	
	Spectal bandwidth (single channel)		2.3	lambda		2.5	lambda

NOT AVAILABLE

Table 4. - First order parameters for the Medium Resolution – Full Coverage mode.

ngCFHT Medium-Resolution High-Multiplex mode

		MR-HM - VIS			LR - NIR		
Sub-system	**Parameter**	**Input**	**Output**	**Units**	**Input**	**Output**	**Units**
Telescope	Telescope diameter	10		m	10		m
	Focal ratio @ fiber entrance	3.5			3.5		
	Plate scale @ fiber entrance		170	um/arcsec		170	um/arcsec
Fiber	Fiber core	155		um	155		um
	Fiber core @ sky		0.91	arcsec		0.91	arcsec
	Fiber FWHM @ sky		0.79	arcsec		0.79	arcsec
	Multiplexing (no gaps)		3194	objects		3157	objects
Relay	Input f-number		3.5			3.5	
	Anamorphic magnification (spectral)	1			1		
	Number of channels	4			4		
	Output f-number (spectral)		16			16	
	Output f-number (spatial)		16.0			16	
	Output fiber size (spectral, FWHM)		614	um		614	um
	Output fiber size (spatial, geom.)		709	um		709	um
Collimator	Collimated beam diameter (spatial)	165		mm	165		mm
	Collimated beam diameter (spectral)		165	mm		165	mm
	Collimator f-number (spatial)	16			16		
	Collimator f-number (spectral)		16.0			16	
	Collimator focal length		2640	mm		2640	mm
	Collimator HFoV (spatial)		6.1	deg		6.0	deg
	Slit height		566	mm		559	mm
Pupil Slicer	Slices	1			1		
	Collimated beam size (spectral)		165	mm		165	mm
	Collimated beam size (spatial)		165	mm		165	mm
	Sub-pupil diameter		233	mm		233	mm
Disperser	VPH Littrow angle	37		deg	15		deg
	VPH size (spatial)		165	mm		165	mm
	VPH size (spectral)		207	mm		171	mm
Cameras	Camera focal length	430		mm	290		mm
	Camera f-number (spectral)		2.6			1.8	
	Camera f-number (spatial)		2.6			1.8	
	Camera f-number (no vignetting, diagonal)		1.84			1.24	
	Camera HFoV (along diameter)		8.6	deg		8.5	deg
	Fiber projection (spectral, FWHM)		99.9	um		67.4	um
	Fiber projection (spatial, geom.)		115.4	um		77.8	um
Detector	Detector size (square)	9		Kpixels	4		Kpixels
	Pixel size	10		um	15		um
	Detector length		92.16	mm		61.44	mm
	Sampling (spectral, FWHM)		9.99	pixels		4.49	pixels
	Sampling (spatial, geom.)		11.54	pixels		5.19	pixels
	Interspectrum separation (spat., geom.)		6.67	pixels	3		pixels
	Flatness (PtV)	35		um	20		um
	Flatness defocus PSF		5.04	um		4.27	um
	Electro-optical PSF	10		um	10		um
	Sampling PSF (0.87X bin size)		8.70	um		13.05	um
SYSTEM	Spectral resolution (FWHM, no aberrations)		6484			2306	
	Image quality PSF	15		um	20		um
	Detector PSF		14	um		17	um
	Overall PSF		21	um		26	um
	Spectral resolution (FWHM)		6350			2149	
	Multiplexing (with gaps)		1820			1799	
	Spectal bandwidth (single channel)		7.0	lambda		2.5	lambda

Table 5. - First order parameters for the Medium Resolution – High Multiplexing mode.

ngCFHT Low-Resolution mode

		LR - VIS			LR - NIR		
Sub-system	**Parameter**	**Input**	**Output**	**Units**	**Input**	**Output**	**Units**
Telescope	Telescope diameter	10		m	10		m
	Focal ratio @ fiber entrance	3.5			3.5		
	Plate scale @ fiber entrance		170	um/arcsec		170	um/arcsec
Fiber	Fiber core	155		um	155		um
	Fiber core @ sky		0.91	arcsec		0.91	arcsec
	Fiber FWHM @ sky		0.79	arcsec		0.79	arcsec
	Multiplexing (no gaps)		3194	objects		3157	objects
Relay	Input f-number		3.5			3.5	
	Anamorphic magnification (spectral)	1			1		
	Number of channels	4			4		
	Output f-number (spectral)		16			16	
	Output f-number (spatial)		16			16	
	Output fiber size (spectral, FWHM)		614	um		614	um
	Output fiber size (spatial, geom.)		709	um		709	um
Collimator	Collimated beam diameter (spatial)	165		mm	165		mm
	Collimated beam diameter (spectral)		165	mm		165	mm
	Collimator f-number (spatial)	16			16		
	Collimator f-number (spectral)		16			16	
	Collimator focal length		2640	mm		2640	mm
	Collimator HFoV (spatial)		6.1	deg		6.0	deg
	Slit height		566	mm		559	mm
Pupil Slicer	Slices	1			1		
	Collimated beam size (spectral)		165	mm		165	mm
	Collimated beam size (spatial)		165	mm		165	mm
	Sub-pupil diameter		233	mm		233	mm
Disperser	VPH Littrow angle	14		deg	14		deg
	VPH size (spatial)		165	mm		165	mm
	VPH size (spectral)		170	mm		170	mm
Cameras	Camera focal length	430		mm	290		mm
	Camera f-number (spectral)		2.6			1.8	
	Camera f-number (spatial)		2.6			1.8	
	Camera f-number (no vignetting, diagonal)		1.84			1.24	
	Camera HFoV (along diameter)		8.6	deg		8.5	deg
	Fiber projection (spectral, FWHM)		99.9	um		67.4	um
	Fiber projection (spatial, geom.)		115.4	um		77.8	um
Detector	Detector size (square)	9		Kpixels	4		Kpixels
	Pixel size	10		um	15		um
	Detector length		92.16	mm		61.44	mm
	Sampling (spectral, FWHM)		9.99	pixels		4.49	pixels
	Sampling (spatial, geom.)		11.54	pixels		5.19	pixels
	Interspectrum separation (spat., geom.)		6.67	pixels	3		pixels
	Flatness (PtV)	35		um	20		um
	Flatness defocus PSF		5.04	um		4.27	um
	Electro-optical PSF	10		um	10		um
	Sampling PSF (0.87X bin size)		8.70	um		13.05	um
SYSTEM	Spectral resolution (FWHM, no aberrations)		2145			2145	
	Image quality PSF	15		um	15		um
	Detector PSF		14	um		17	um
	Overall PSF		21	um		23	um
	Spectral resolution (FWHM)		2101			2034	
	Multiplexing (with gaps)		1820			1799	
	Spectal bandwidth (single channel)		2.3	lambda		2.4	lambda

Table 6. - First order parameters for the Low Resolution mode.

Parameter	Value	Note
Telescope diameter	10-m	
Field of view	1.5 square degrees	
Fiber diameter	0.9 arcsec	*(155 um at F/3.5)*
Resolving power	2000 6500 20000	*LR mode* *MR-FC & MR-HM modes* *HR mode*
Spectral bandwidth	370 – 1300 nm	
Simultaneous coverage	Full (370 – 1300 nm) Full (370 – 850 nm) 2 selectable windows λ/7	*LR mode* *MR-FC mode* *HR & MR-HM modes*
Spectral Sampling	10 pixel 4.5 pixel 2.5 pixel	*Visible arms, LR & MR-HM modes* *NIR arm, LR & MR-HM modes* *Visible arms, HR & MR-FC modes*
Interspectra separation	7 pixel 3 pixel	*Visible arms* *NIR arms*
Number of fibers	1800 ± 10% 450 ± 10%	*LR & MR-HM modes* *HR & MR-FC modes*
Detectors	9kx9k, 10um CCD (8X) 4kx4k, 15um FPA (4X)	*Visible arms* *NIR arm*
Efficiency	50% ± 5% (at peak)	*Spectrograph optics + detectors*

Table 7. - Main spectrograph characteristics.

3 Spectrograph Optical Design

3.1 Overall spectrograph layout

Figure 6 shows the layout of the different components of the spectrograph unit. Fibers at the entrance will be processed by a set of identical relay optics. At the intermediate focal plane, anamorphosers or prism-plates can be inserted to switch between different observing modes. The light is then collimated by a mirror, and aberrations corrected by two lenses. The collimated beam is finally split into four identical channels by the pupil slicer. Each channel will consist of two dichroic beam-splitters, VPH gratings, and three optimized refractive cameras.

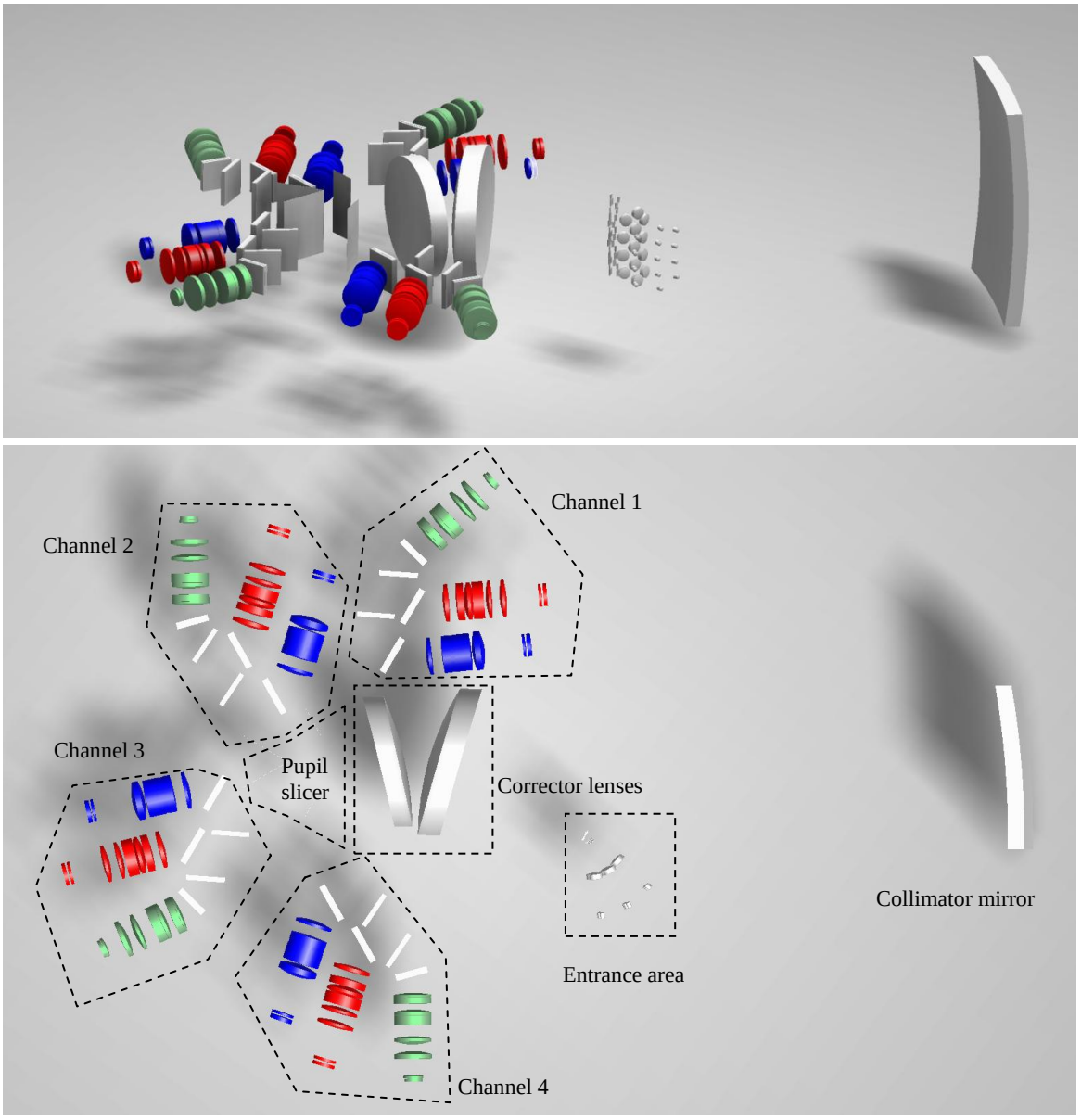

Figure 6. - Lateral (top) and top (bottom) views of the spectrograph optics.

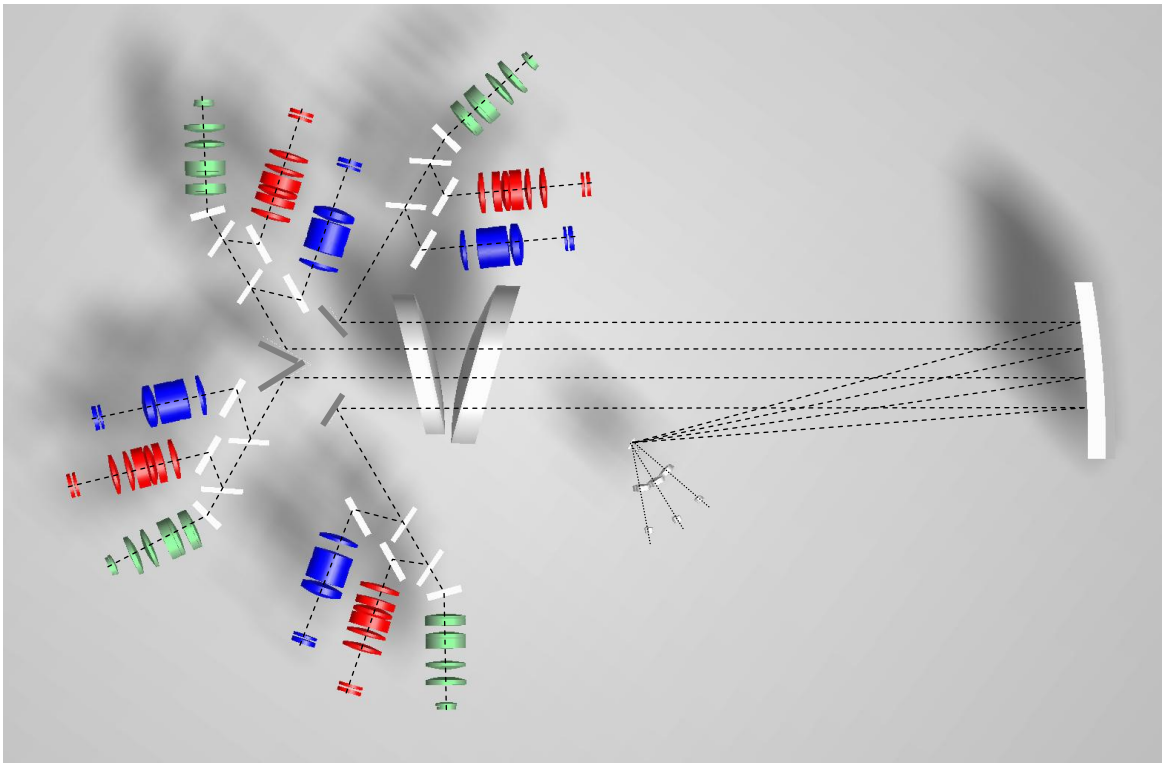

Figure 7. - Optical path of rays within the spectrograph

Light paths are drawn schematically in Figure 7. Many fiber bundles will populate the long entrance slit of the spectrograph collimator with different light patterns, according to the selected observing mode (see Section 0). In the HR and MR-FC case, the anamorphoser will enlarge the pupil in the main dispersion direction (lying in the plane of the figure), thus feeding the different channels with light coming from the same fiber array. Each fiber will project 12 different spectra: 4 in the blue detectors, 4 in the red ones, and 4 in the NIR ones (4 spatial split x 3 wavelength split). The same wavelength will be split into four detectors, and spectra will be reconstructed by SW. In the LR and MR-HM case, the prism-plate will send the light coming from four adjacent fiber arrays into the four channels (as like as feeding four separate spectrographs). Each fiber will project only 3 different spectra (wavelength split only). In this case, no reconstruction is required to recombine light with the same wavelength.
The modularity of this design allows replicating many sub-system components, for some engineering and cost savings.

3.2 Fiber interface

Fibers from the telescope focal plane will carry light at F/3.5, in order to minimize losses due to focal ratio degradation. They will be routed on bundles, each one containing 140 fibers, aligned into four different columns, as shown in the Figure 8. Different colours are used to identify different light paths along the spectrograph optical train.
The full set of fibers is split into 13 identical bundles (13x140 = 1820), each one coupled to relay optics. Then, smaller optics can be designed to feed the spectrograph, gaining in space, cost, and throughput performances.

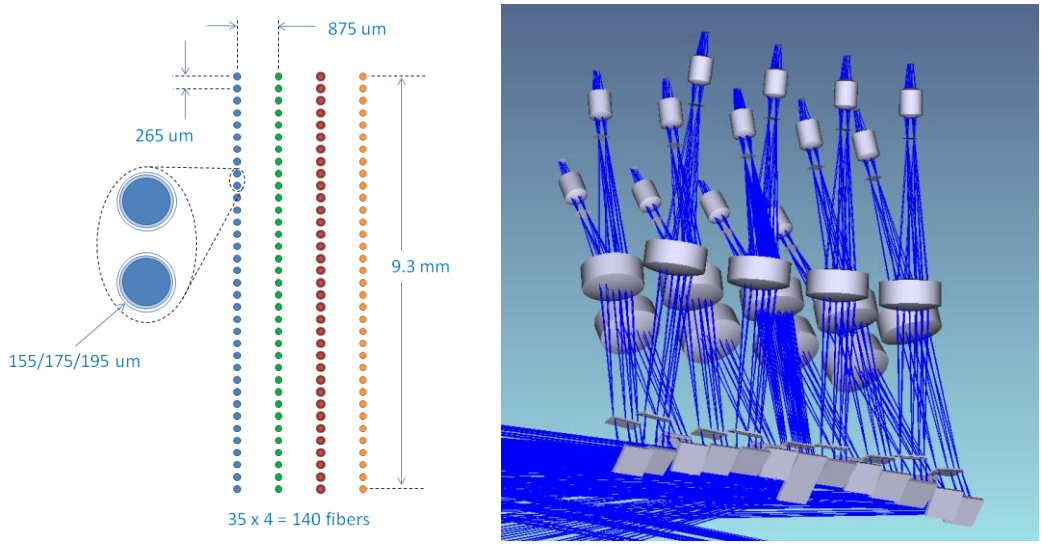

Figure 8. - Sketch of a fiber array at the exit of each bundle (left) and the full relay optics (right).

To keep the optical and mechanical interfaces as simple as possible, all fibers will be coaxial and perpendicular to a flat surface. This choice opens to both post polishing of the assembled bundle, or to assembly pre-polished fibers onto a laser machined micro-hole plate.
According to the selected focal ratio (F/3.5), fiber core diameter will be 155 um. Cladding and buffer diameters can be 175 and 195 um, respectively. These numbers are not far from typical core/cladding ratios or buffer size (e.g., Polymicro FBP Silica/Silica fibers) for which attenuation (Figure 9) and FRD properties have been thoroughly tested in the past.

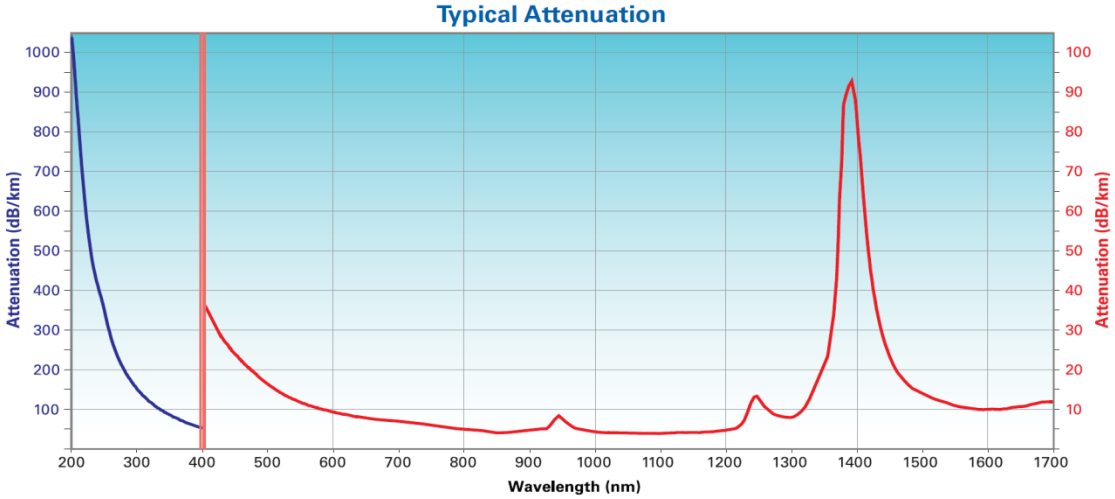

Figure 9. - Polymicro FPB low-OH fiber attenuation.

3.3 Optical relay

The relay optics will adapt the F/3.5 fiber output beam into the F/16 collimator input beam. It consists of 13 replicated optical trains, each one based onto two cemented triplets.
Triplets are done with CaF2and Schott N-BaK1/N-BaK2 glasses, with very small internal losses. Each triplet incorporates an aspherical surface (a pure conic constant, for easier test and manufacturing) to improve image quality (rms spot diam. < 0.15") and telecentric correction.
Lens diameters are 30 and 70 mm. Lenses will be anti-reflection coated. Due to the very wide bandwidth, the best candidate is a SolGel/MgF_2 coating, providing an average reflectivity of <1% between 365 to 1300 nm. The overall throughput is estimated >95% over the full band, and ~97% in the visible bands.
A pupil stop is placed between the two triplets, to control beam illumination patterns onto the spectrograph pupil.

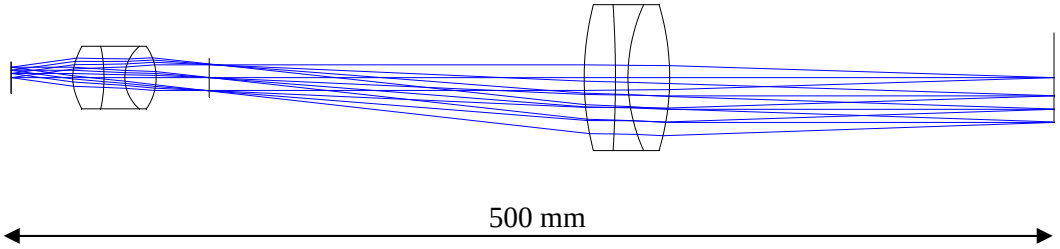

Figure 10. - Relay optics layout.

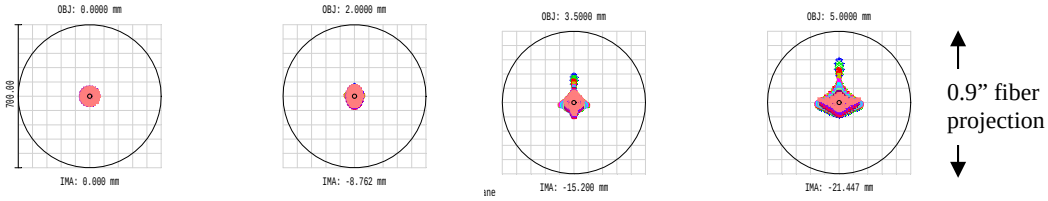

Figure 11. - Relay optics polychromatic spot diagrams.

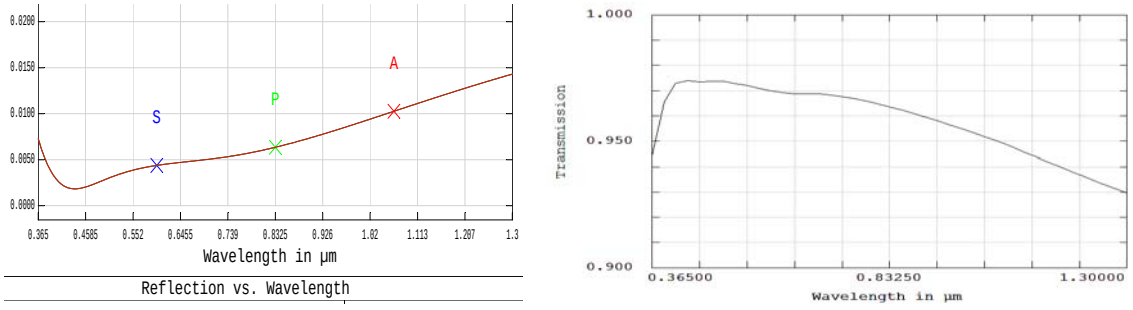

Figure 12. - Relay optics single surface reflectivity (left) and total throughput (right).

3.4 Anamorphoser

A cylindrical microlens is used to introduce a 4X anamorphic magnification. The entrance surface is an aspherical cylinder, and the exit surface is a toroidal, to correct for pupil position. The layout is shown in Figure 13. It can be manufactured by standard semiconductor technologies like photolithography, resist processing and reactive ion etching. These technologies allow a very accurate shaping of the lens profile and a precise positioning of the lenses.
Figure 14 shows the image of two adjacent circular fibers as projected onto the spectrograph detectors. The corresponding pupil image, before pupil slicing, shows some field and chromatic effects at the elongated edges. Light distribution in the four sub-pupils will vary according to wavelength, and between different fibers, but this will not affect line profile or instrumental stability, being a fixed pattern.
Figure 15 shows how light coming from a fiber will be modified by the anamorphoser in order to project an elongated pupil within the collimator optics. Each relay optics will host its own anamorphoser, mounted on a motorized linear stage. This allows to accurately position the microlens in front of the projected f/16 fiber image, and to exchange the anamorphoser with the prism-plate (see following section), to switch between observing modes.

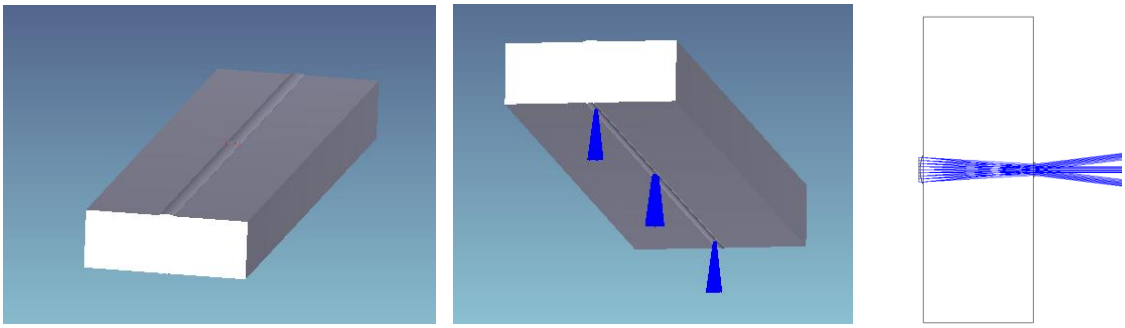

Figure 13. - Anamorphoser layout.

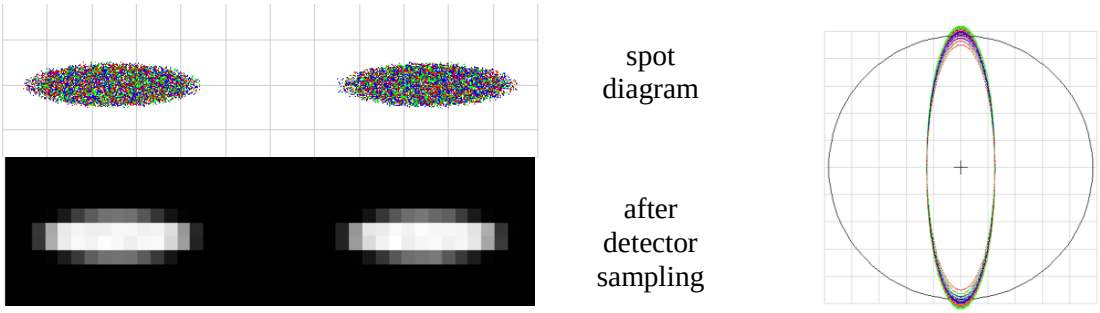

Figure 14. - Projected fiber images (left) and pupil (right).

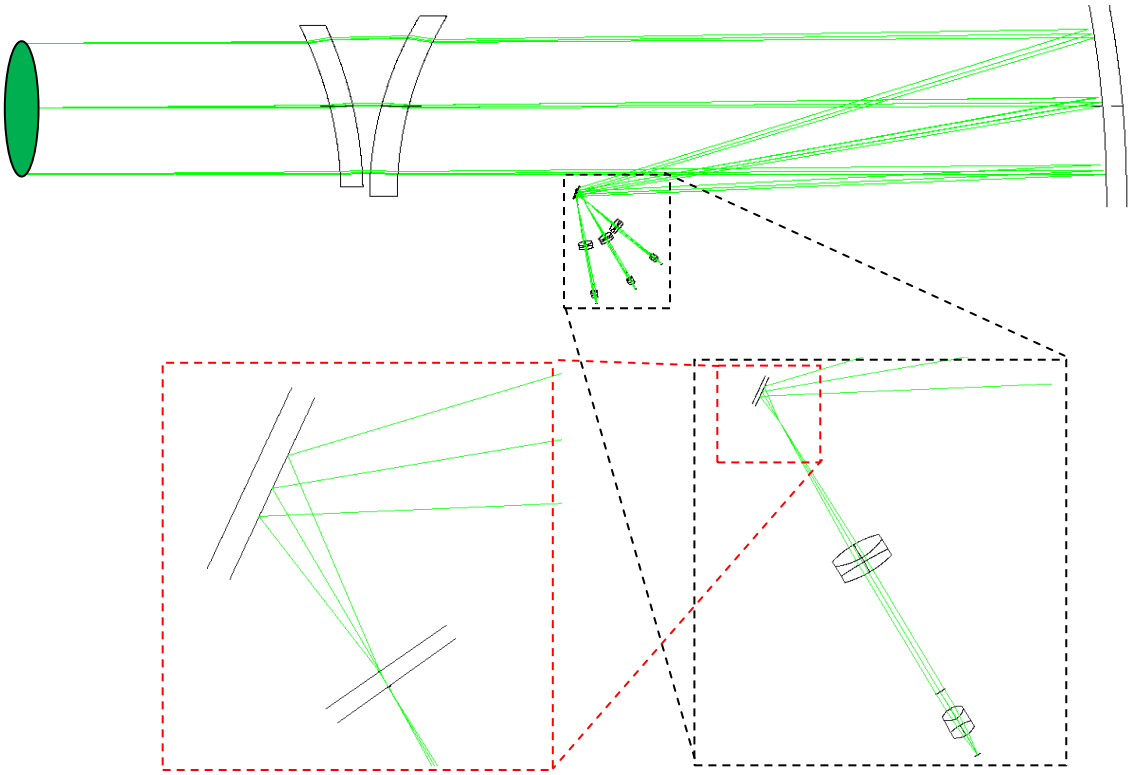

Figure 15. - Optical beams when the anamorphoser is inserted.

3.5 Prism plate

The optics will project each one of the four columns of the fiber array onto the four channels of the spectrograph. This is done by tilting the chief ray of each column into the proper sub-pupil position, by mean of TIR prisms (Figure 17).
Light beams across the collimator optics are shown in Figure 18, where light belonging to different fiber columns are shown with different colours.
To prevent cross-contamination between adjacent channels, a rectangular diaphragm is inserted into the relay optics, providing room for clean beam separation, as shown in the projected pupil (Figure 19). This small vignetting will be enough to increase the physical separation between projected pupils, while introducing a marginal 1.3% light loss.
By using wideband anti-reflection coatings (Figure 16), overall throughput for this system, including the small vignetting factor above, amount to about 3%.

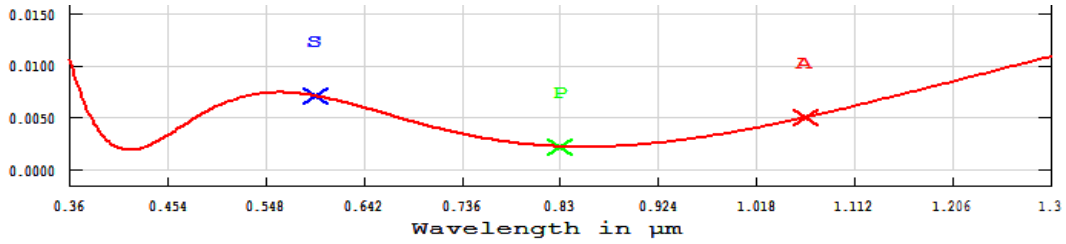

Figure 16. - Optimized anti-reflection coating for the prism plate.

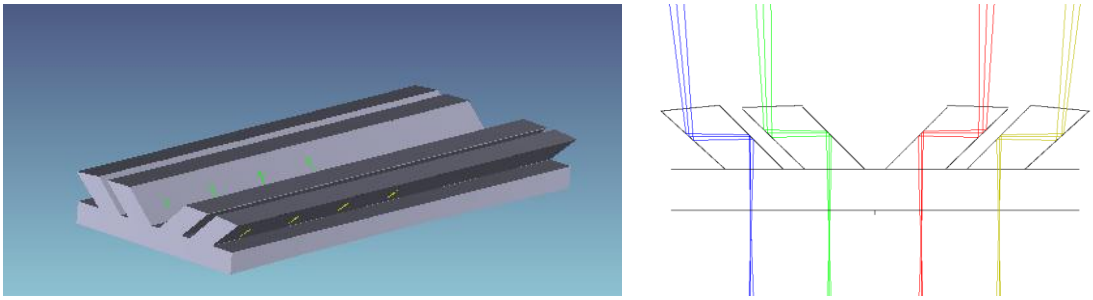

Figure 17. - Optical layout of the prism plate.

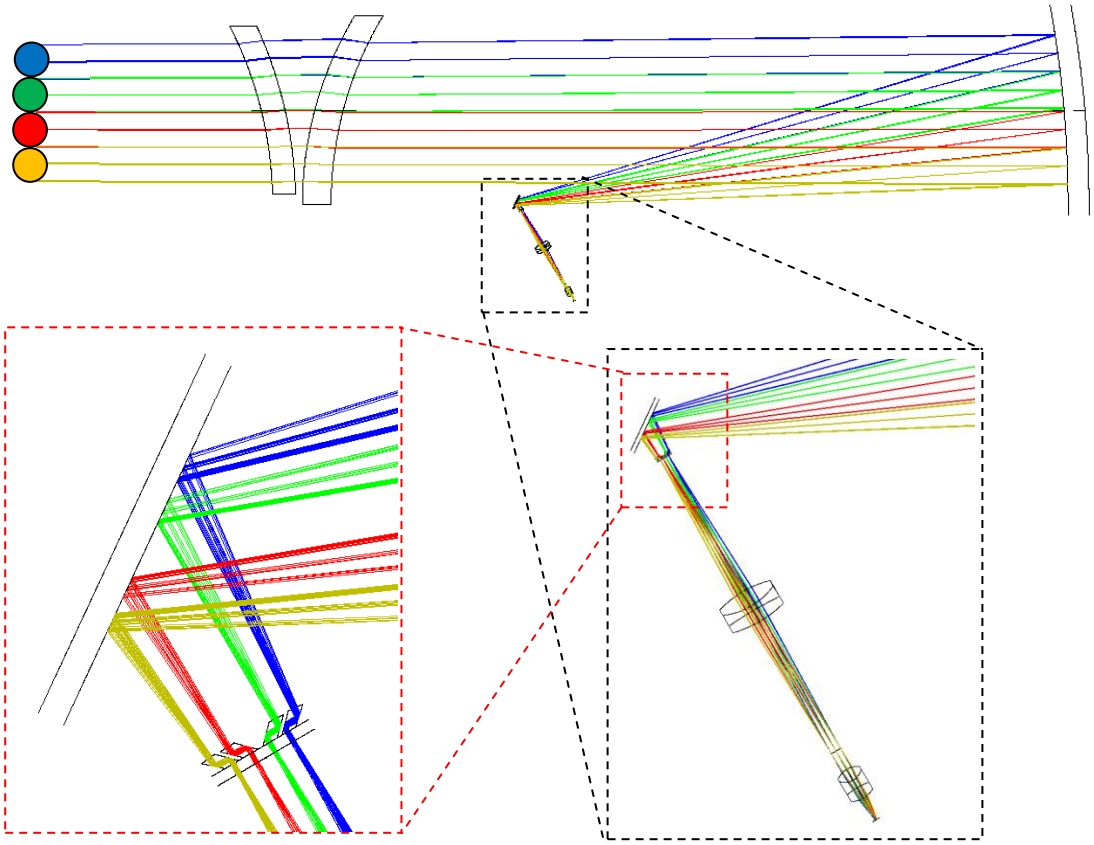

Figure 18. - Optical beams when the prism-plate is inserted. Different fibers will feed different pupils.

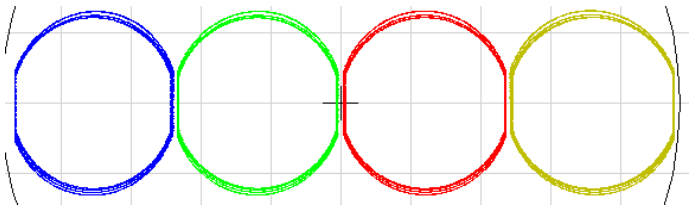

Figure 19. - Pupils projected by the different fiber columns passing through the prism plate.

3.6 Collimator

The largest component of the optical train is the collimator, based onto a spherical mirror and two corrector lenses. Parameters of the collimator are given in Table 8. The layout of the collimator optics is given in Figure 20.
The spherical mirror aperture is 1.5 x 1.0 m, while the two corrector lenses are off-axis portion of meniscus shaped lenses. Their clear aperture is 90-cm. One corrector lens is spherical, while the other contains an aspherical surface (~350 um departure, <4mrad slope deviation), to correct for aberrations. Both corrector lenses are done in NIR-grade fused silica (high-transmission over the whole band, high-homogeneity, available in large sizes).
Image quality of the collimator is much better than typical image sizes. The most stringent case is for the HR mode, where elongated images will be projected (0.22" x 0.9"). Typical rms spot diameters are <0.05", as shown in Figure 21.
One of the main issues is the coating of the mirror and the two lenses, to maximize throughput over the whole bandwidth. SolGel/MgF_2 coatings are foreseen for the lenses. On the spherical mirror, enhanced Silver has been successfully applied in the past for large mirrors (Figure 22), but some tests should be performed to check performance over the whole bandwidth.

Parameter	Value	Note
Focal length	2640 mm	
F/number	F/4 x F/16	*Elliptical pupil*
Entrance pupil diameter	660 x 165 mm (1650 mm in front of the corrector)	*It can accept also 4 circular pupils (165mm diameter)*
Field of view	0.5° x 6°	
Slit height	560 mm	*It can be populated by ~1800 fiber images*
Spectral bandwidth	370 – 1300 nm	

Table 8. - Collimator optics parameter.

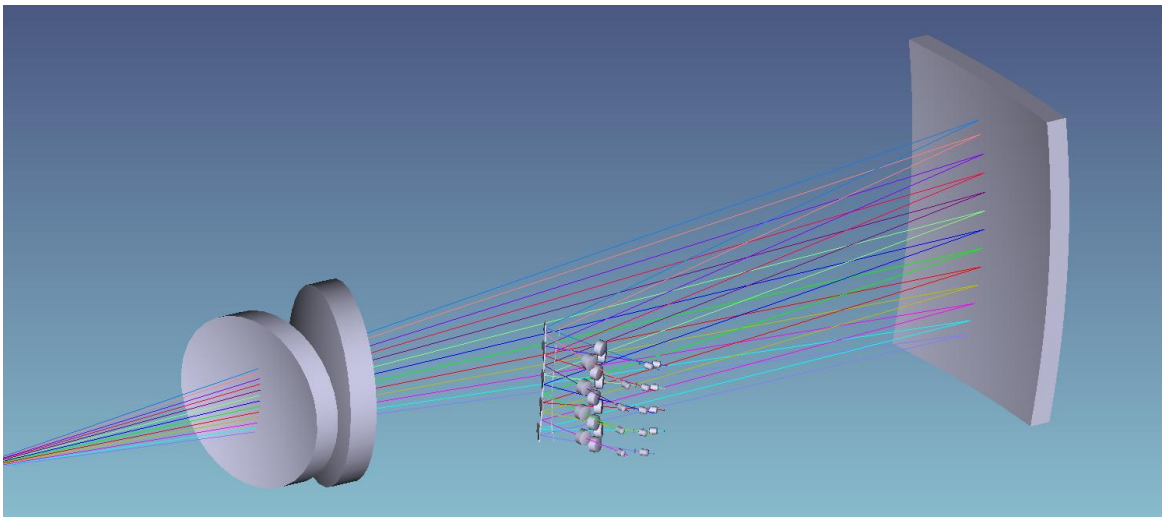

Figure 20. - Collimator optical layout.

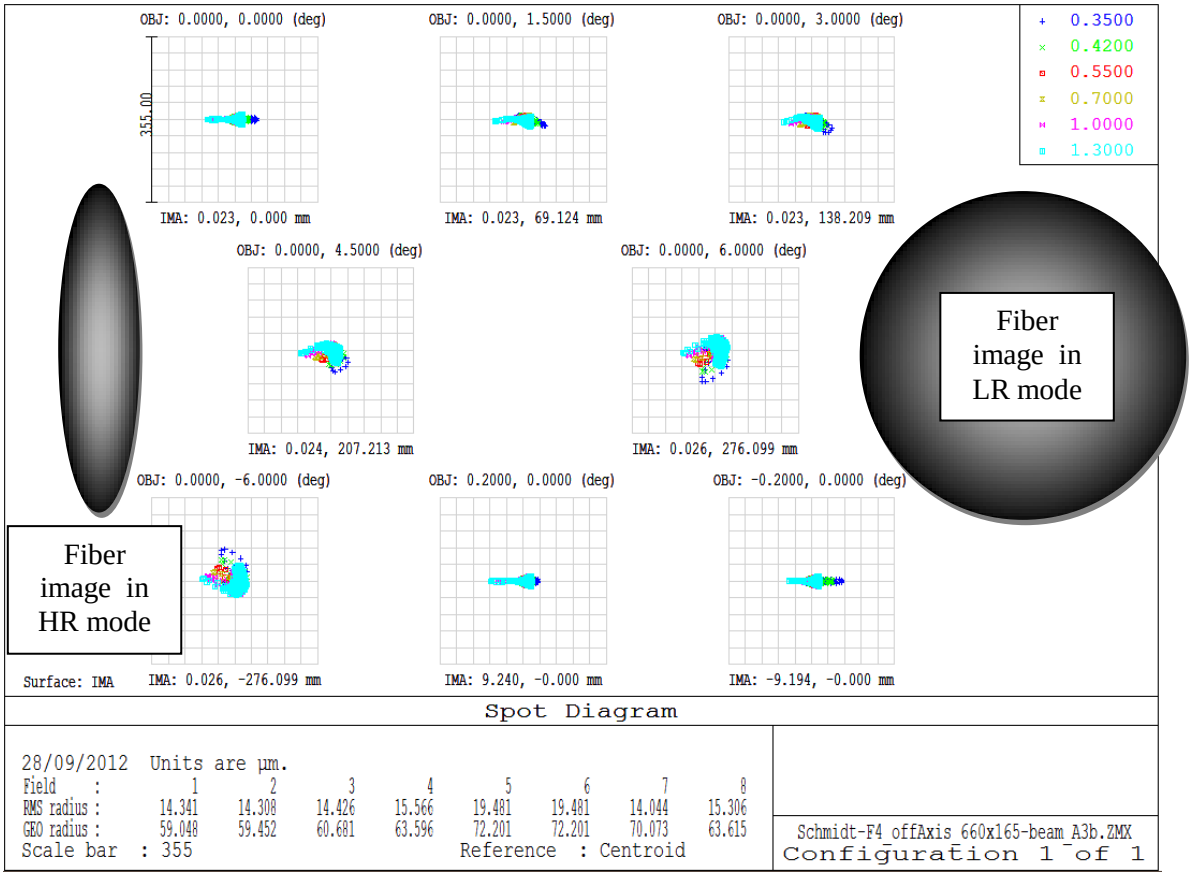

Figure 21. - Collimator spot diagrams.

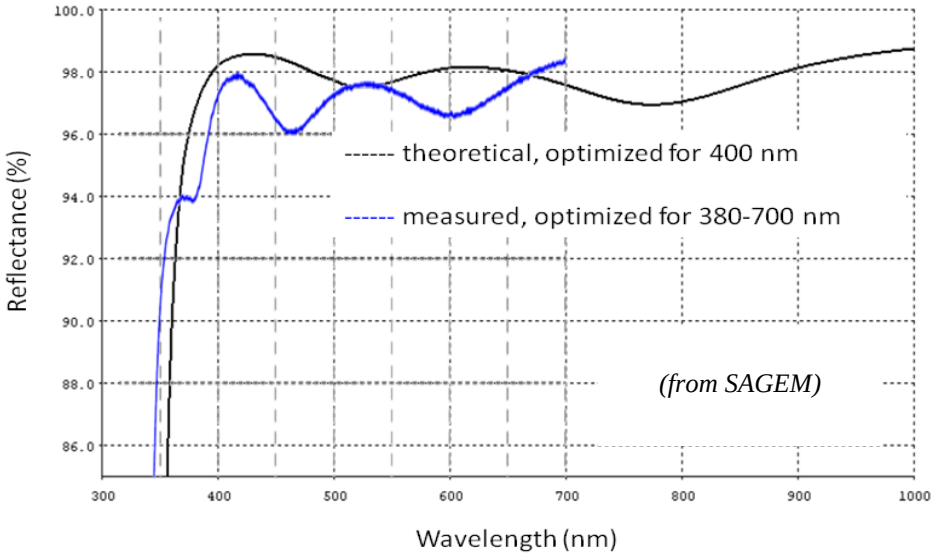

Figure 22. - State-of-the-art mirror reflectivity (theoretical and measured curves).

3.7 Pupil slicer

In order to slice the elongated pupil, four rectangular shape flat mirrors have been used. They are shown in Figure 23. Those mirrors are displaced from the pupil plane, but the beams belonging to different fibers are almost aligned in one direction only, making it possible to slice the pupil far from the pupil plane.
Each mirror will have a sharp edge to slice the beam, but being a large beam, small errors will not affect performances.
These mirrors can share the same reflective coating of the primary, but even better performances could be obtained with all-dielectric coatings, because of the much smaller size. Up to 99% flat reflectivity has been produced on small mirrors (Qioptiq). Figure 24 shows an example of such a coating, even if over a different wavelength range. This design is adaptable in our spectral range and incidence angles, to improve NIR reflectance.

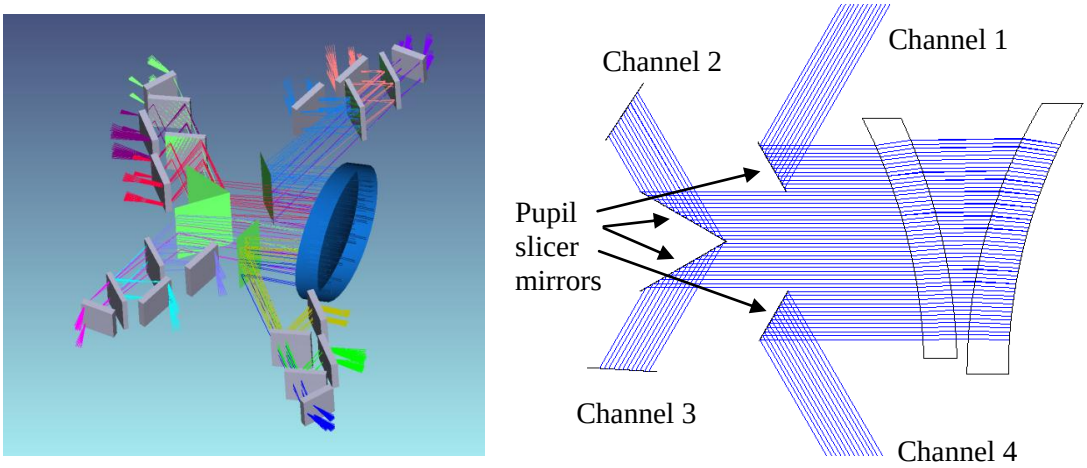

Figure 23. - Pupil slicer mirror layout.

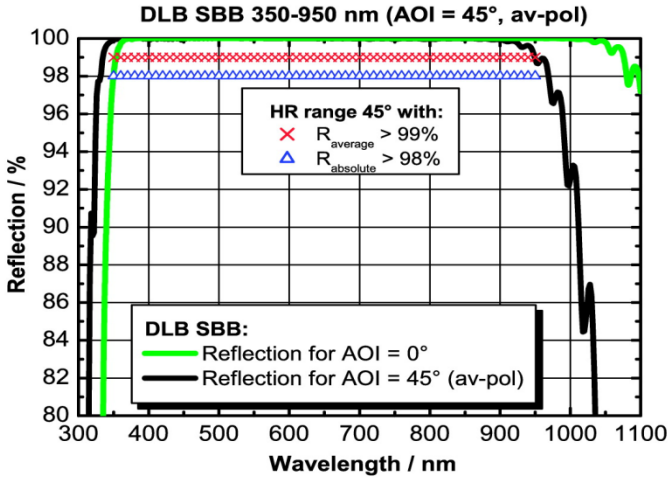

Figure 24. - All-dielectric high-reflectivity coatings.

3.8 Beamsplitters

Different wavelengths will be separated through two dichroic beam splitters in series. The first one will reflect the "blue" wavelengths and transmit the "red" and "nir" wavebands, the second will reflect the "red" and transmit the "nir" ones, as seen in Figure 25.
They work at a relatively small angle of incidence (~25 deg), to make the transition region sharper, with smaller variations for different fibers. Maximum clear aperture is about 22x28 cm, well within current manufacturing technologies.
To improve performances, an exchange mechanism can be implemented, to select the best transition region for the given observing mode. Moreover, when observed wavelengths fall in a single arm, its efficiency can be maximized dichroics can be replaced by mirrors and/or a dummy window (with enhanced anti-reflection coatings). Due to the crowded area, a linear stage should be implemented, out of the plane of the layout.

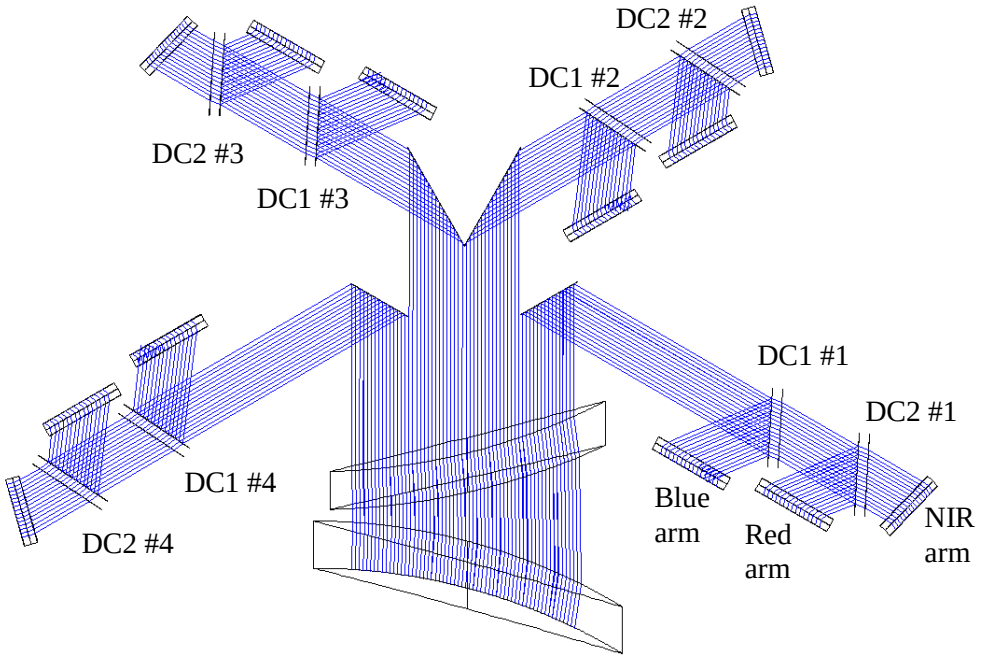

Figure 25. - Dichroic tree layout. Each dichroic mirror is replicated four times.

3.9 Gratings

As previously discussed in Section 2.7, volume-phase holographic (VPH) gratings have been selected to provide wavelength separation at very high efficiency.
Grating parameters have been defined to cover the whole bandwidth of the spectrograph. HR mode gratings are summarized in Table 9, LR ones in Table 10. Two angles, 37 and 14 degrees, have been defined for high- and low-resolution modes, respectively. Maximum substrate size is 20x20 cm, well within current state-of-the-art technologies for VPH gratings.
HR gratings share an incidence angle of 37 degrees, and a bandwidth of 1/7 of the central wavelength. A 10% overlap between adjacent VPH has been added, to provide some room for merging spectra during the data reduction. Blaze curve bandwidth (as defined by its FWHM, given in the last column of following tables) has been derived according to [RD-1]. Three HR

gratings will be installed in the Blue arms, while the Red arms will host up to 4 different HR gratings.
LR gratings shall have a 14 degree incidence angle, even if some tuning of this angle can be done to optimize the placement of the transition region, the resolving power on the different wavelengths, and/or the width of the overlapping region. The LR gratings will allow simultaneous full coverage of the spectrograph bandwidth.
To switch between the HR and LR modes, an exchange mechanism has been foreseen (see Section 3.13 for details) that preserve the total beam deviation between the two modes, making the camera optics fixed.
Some diffraction efficiency curves for quite similar VPH parameters are shown in Figure 26, where smaller incidence angles have been simulated, at two different wavelength regions, one in the bluest end of ngCFHT and one in the red. A thoroughly study should be performed to validate these first efficiency estimates, since the disperser efficiency is a bottle-neck for the overall instrument performances.

VPH #	Central wavelength (nm)	Bandwidth (nm)	Line density (l/mm)	FWHM (nm)
HR BLUE 1	398	368-425	3025	60
HR BLUE 2	455	421-486	2650	80
HR BLUE 3	520	482-555	2315	103
HR RED 1	594	550-634	2025	135
HR RED 2	679	630-725	1775	175
HR RED 3	776	720-828	1550	230
HR RED 4	887	823-947	1355	300

Table 9. - HR VPH grating parameters (37 deg incidence angle).

VPH #	Central wavelength (nm)	Bandwidth (nm)	Line density (l/mm)
LR BLUE	465	370-560	1040
LR RED	696	552-844	695
LR NIR	1048	836-1260	462

Table 10. - LR VPH grating parameters (14 deg incidence angle).

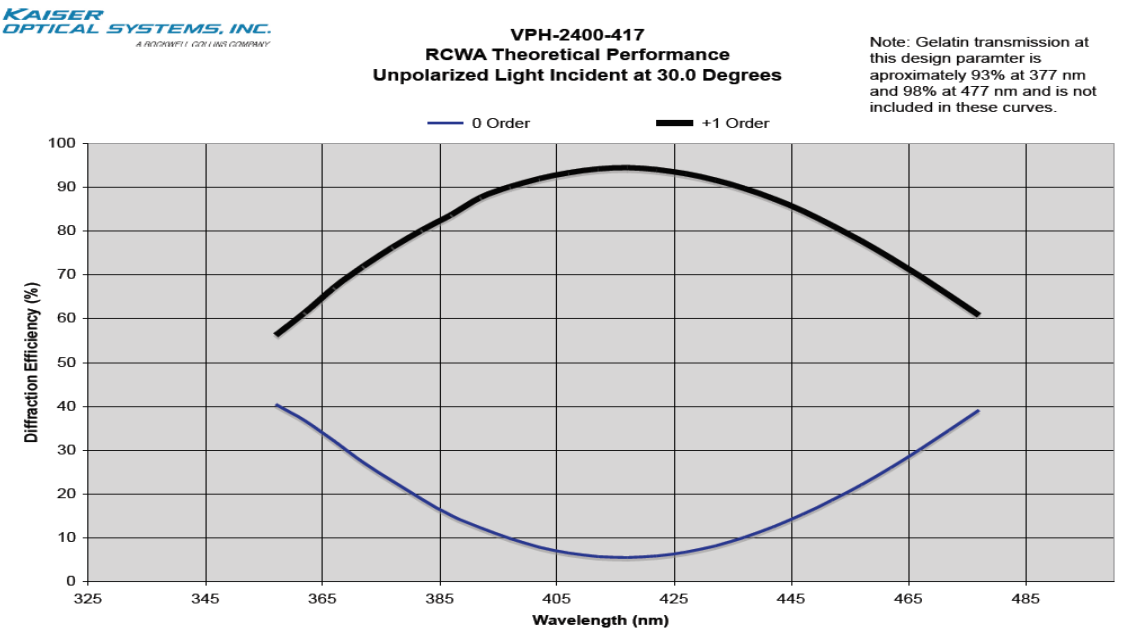

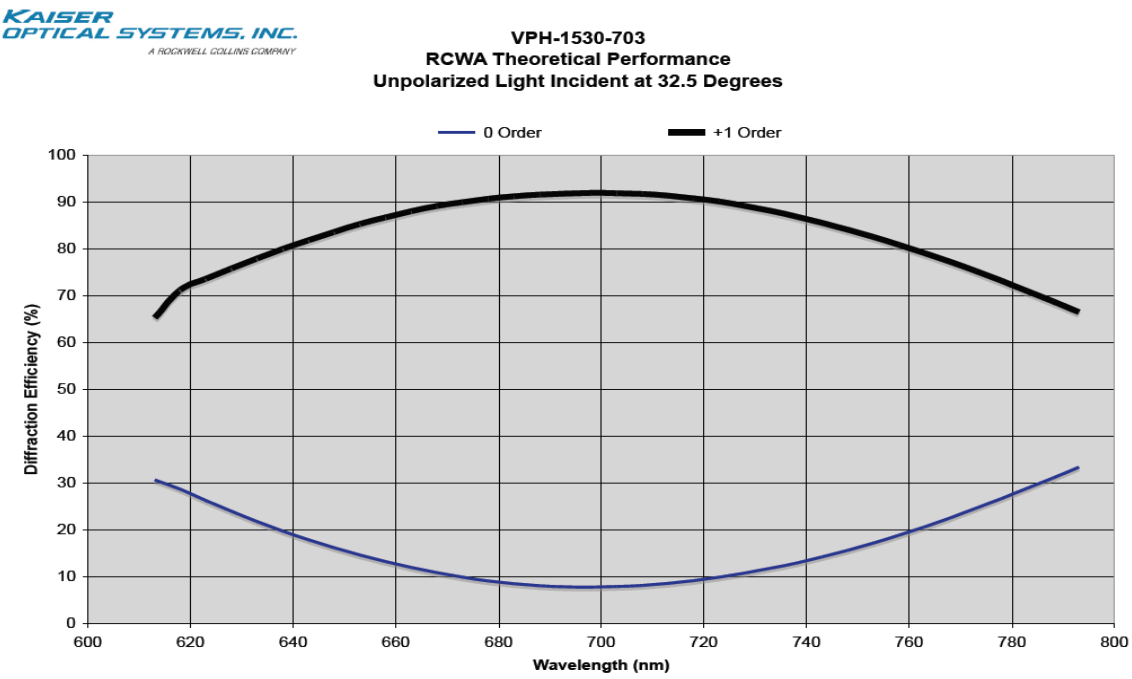

Figure 26. - Simulated VPH grating efficiency for two cases.

3.10 Cameras

Three different optimized cameras will be coupled to each different arm. The wavelength splitting allow performance improvements, both in term of image quality and efficiency, because smaller chromatic corrections are required, together with enhanced anti-reflection coatings and very low internal transmission losses.
Main properties of the cameras are given in Table 11. Real entrance pupils will be different at each channel in HR mode, because of the pupil slicing, and of the geometrical distortion introduced by the gratings. For some wavelength and fiber positions, some small vignetting has been introduced to save lens diameter, making easier to reach image quality performances.
Optimization of the camera optics has been preliminary done without the spectrograph optics in front of its entrance pupil - referred as *"stand-alone"* optimization - making it easier to control optical interfaces between the two sub-systems. Anyway, better image quality can be obtained by reoptimizing lens design within the overall spectrograph design – hereafter referred as *"built-in"* optimization - because some chromatism can be left uncorrected without introducing further aberrations. While final decision will be done during the next study phases, in this study phase we preliminary explored both optimization paths. Both are quite successful, so we prefer to follow the "stand-alone" optimization, being simpler, faster, and allowing for a clear interface between optical sub-systems.
Figure 27 shows the layout of some of the many camera layouts generated. Numbers of lenses, glass selection, design configuration, anti-reflection coatings, and placement of aspherical surfaces have been optimized according to the initial camera parameters.
In the Blue camera, preferred lens materials are Fused Silica, CaF_2, and i-line glasses, to provide very high internal transmission. In the other two cameras, more standard materials can be used. An interesting option to improve both image quality and efficiency performances is to use some coupling fluids between some lenses, to reduce the number of air-glass interfaces. Moreover, refraction index of those coupling compounds can be tuned easily to match properties of the glass, and thus reduce internal Fresnel losses, together with opening the possibility to "athermalize" the camera layout, as successfully done in BINOSPEC and IMACS (see [RD-4]). This "athermalized" option seems to be even more important for the NIR camera, being a faster camera, where thermal defocus constraint is tighter.

	BLUE camera	RED camera	NIR camera
Focal length (mm)	420	420	290
Entrance pupil (mm)	220	220	200
F/number	1.9	1.9	1.45
Field of view (deg)	17	17	17
Wavelength range (nm)	365-550	500-1000	800-1300

Table 11. - Camera parameters.

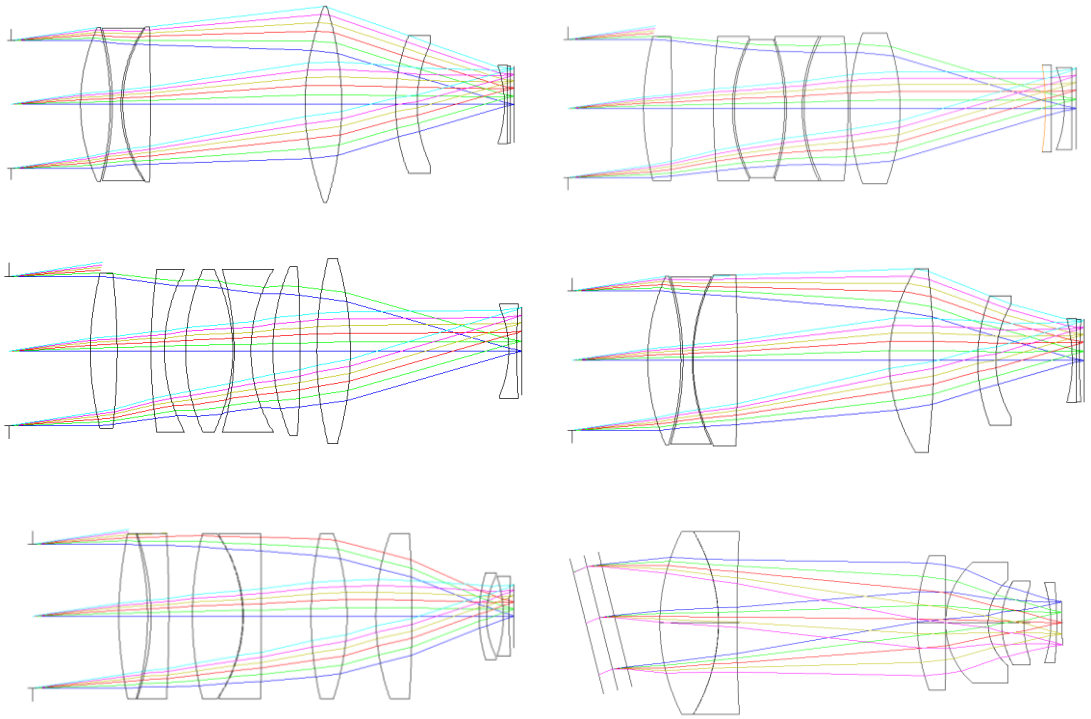

Figure 27. - Camera layouts. Top: blue - middle: red – bottom: near-infrared (not in scale).

3.11 Detectors

CCDs and NIR focal plane arrays will be adopted for the Blue/Red and Nir arms.
Both Blue and Red cameras will share the same f-number and field of view, so then an identical opto-mechanical interface can be adopted, except that two different coatings should be applied on CCD detectors, in order to maximize throughput. In order to maximize the simultaneous spectral coverage at high-resolution modes, still keeping a reasonable good spectral sampling (smallest line spread function > 2.5 pixels), the best candidates are CCDs with the highest number of pixels, at least across the dispersion direction. There are some available devices, others ones are currently under development from different suppliers. Here we give just some examples of state-of-the-art devices, for reference. Figure 28 and Figure 29 show two typical devices. Their technical characteristics are given in Table 12 and Table 13, respectively.

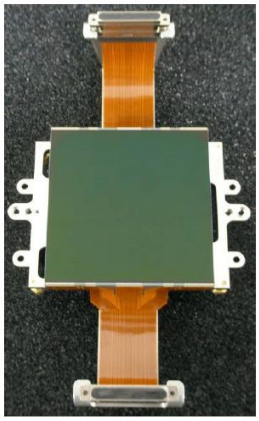

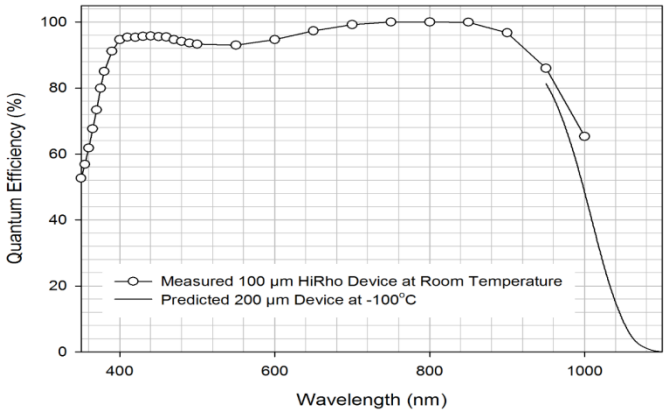

Figure 28. - e2V CCD290-99 (left) and its quantum efficiency (right).

Parameter	Value	Note
Pixel area	9216x9126 10 um pixels	92x92 mm active area
Outputs	16	*18 sec readout at 500 kHz*
Readout noise	<3 e- rms	*at <300 kHz*
Quantum efficiency	>90% @400-900 nm	*See Figure 28*

Table 12. - CCD290-99 technical characteristics.

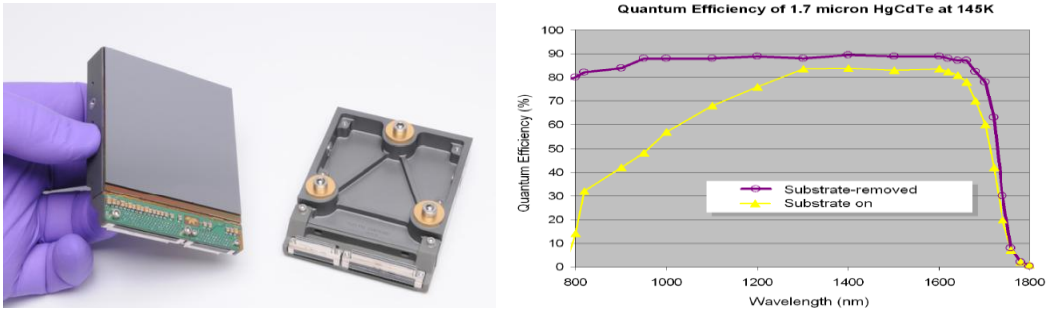

Figure 29. - H4RG™ from Teledyne (left) and its measured quantum efficiency (right).

Parameter	Value	Note
Pixel area	4088x4088 15 um pixels	
Outputs	up to 64 programmable	
Cut-off wavelength	1.7 um	*at 120 K*
Readout noise	<30 e- (goal 15)	*corr. double sampling, 100 kHz*
Quantum efficiency	>50% (goal 70%) @800-1000 nm >70% (goal 80%) @1230 nm	*See Figure 28*

Table 13. - Hawaii H4RG technical characteristics.

By comparing the two quantum efficiencies of these devices, it can be easily seen that the best transition region between the Red and Nir arms should lie between 800 and 900 nm, where both devices are still very sensitive. This allows some degree of freedom for the optimization of the parameters of each arm, especially for the LR observing mode. When in HR mode, however, transition region should be put well above all the interesting spectral lines covered by the Red arm, because HR mode will not be available in the Nir arm. Placing a mirror instead of a dichroic beam-splitter seems the best choice.

3.12 Wavelength calibration

Different spectral calibration lamps shall be available. Mercury-Argon and Thorium-Argon lamps shall be put in front of all fiber, to calibrate the dispersion law of each fiber. This should require quite complex and large calibration optics, to fully illuminate the overall field of view. Some retractable pick-up mirror should simplify this system, while illuminating only a small fraction of

the field. In this case, the calibration time could be quite long and should be done in daytime, provided that some dark cover can be put in front of the focal plane.
By dedicating some fiber for simultaneous calibration, it is possible to enhance calibration, by tracking any potential drift inside the spectrograph. This is particularly important for high-resolution observations. In this case, one fiber per bundle (see Figure 8) can be fed by a Th(Ar) lamp.

3.13 Exchange mechanisms

In order to exchange from the LR to the HR gratings, by keeping fixed the total beam deviation, some additional optics must be added, in order to recover for the different beam deviation introduced by different VPH Bragg angles.
In the past most of the proposed solutions were based onto prisms. However, in our design those prisms should be very large, with steep incidence angles, thus reducing the width of the grating blaze function, because the entrance prism should disperse incoming light.
Here we propose the addition of a single flat mirror, as shown in Figure 30. The exchange mechanism should switch between the HR grating and the LR grating + mirror. This solution implies a shift of the pupil at the camera entrance, but this will not degrade performances, because the layout shall be optimized for the HR mode, and the LR mode will tolerate a smaller larger (aberrated) image size, where best image quality is not strictly required.

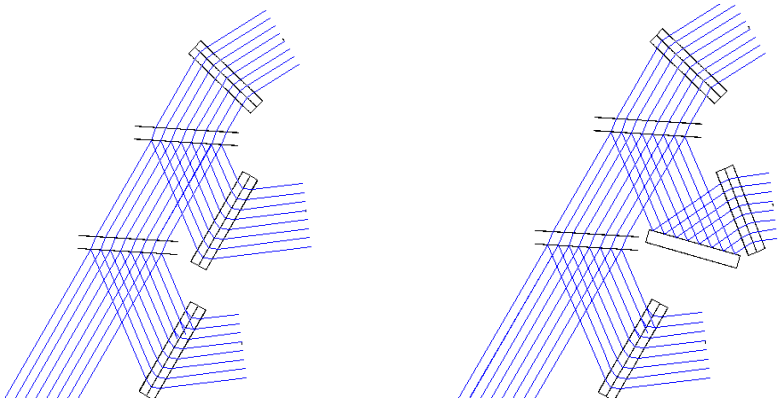

Figure 30. – HR grating (left) and LR grating (right) layouts.

4 Spectrograph performances

4.1 Image quality

Spectrograph image quality has been optimized in order to deliver the highest resolving power when in HR more. In that case the anamorphoser is in delivering the smallest fiber images (in the dispersion direction). For other observing modes, like LR, fiber images are much larger, allowing for larger aberrations.
A provisional image quality budget has been derived as guideline during the design process of the different optical subsystems. As metrics, EE80 diameter as projected on the detector focal plane has been selected. This is summarized in Table 14. HR and LR observing modes shall have different budgets. This led to simpler camera solution for the NIR arms, where only larger fiber images will be projected.

Sub-system	HR	LR
Fiber input defocus	4	4
Relay optics	4	4
Anamorphoser/Prism-plate	8	5
Collimator	10	10
Pupil slicer	2	2
Gratings	2	2
Cameras	18	27
OVERALL	**23**	**30**

Table 14. - Image quality budget. Units are EE80 diameter at the detector focal plane.

In the following pages spot diagrams and EE80 maps are shown. Figure 31 refers to Blue and Red cameras stand-along spot diagrams. Camera optics shall control most of the total image quality budget. It should be noted the almost uniform image quality across the whole detector area.
Figure 32, Figure 33, and Figure 34 show the overall spectrograph spot diagrams for different wavelengths and channels (the two columns refer to two different channels), belonging to the Blue, Red, and NIR arms, respectively. Nominal RMS spot diameters are always in the 10-20 micron range, or even better.
Then, EE80 diameter maps for the Blue, Red and NIR arms are given in Figure 35, Figure 36, and Figure 37 respectively, for both LR and HR observing modes.

All these plots show that nominal image quality requirement was matched by a large fraction, on average, leaving space for tolerances, manufacturing and alignment errors.

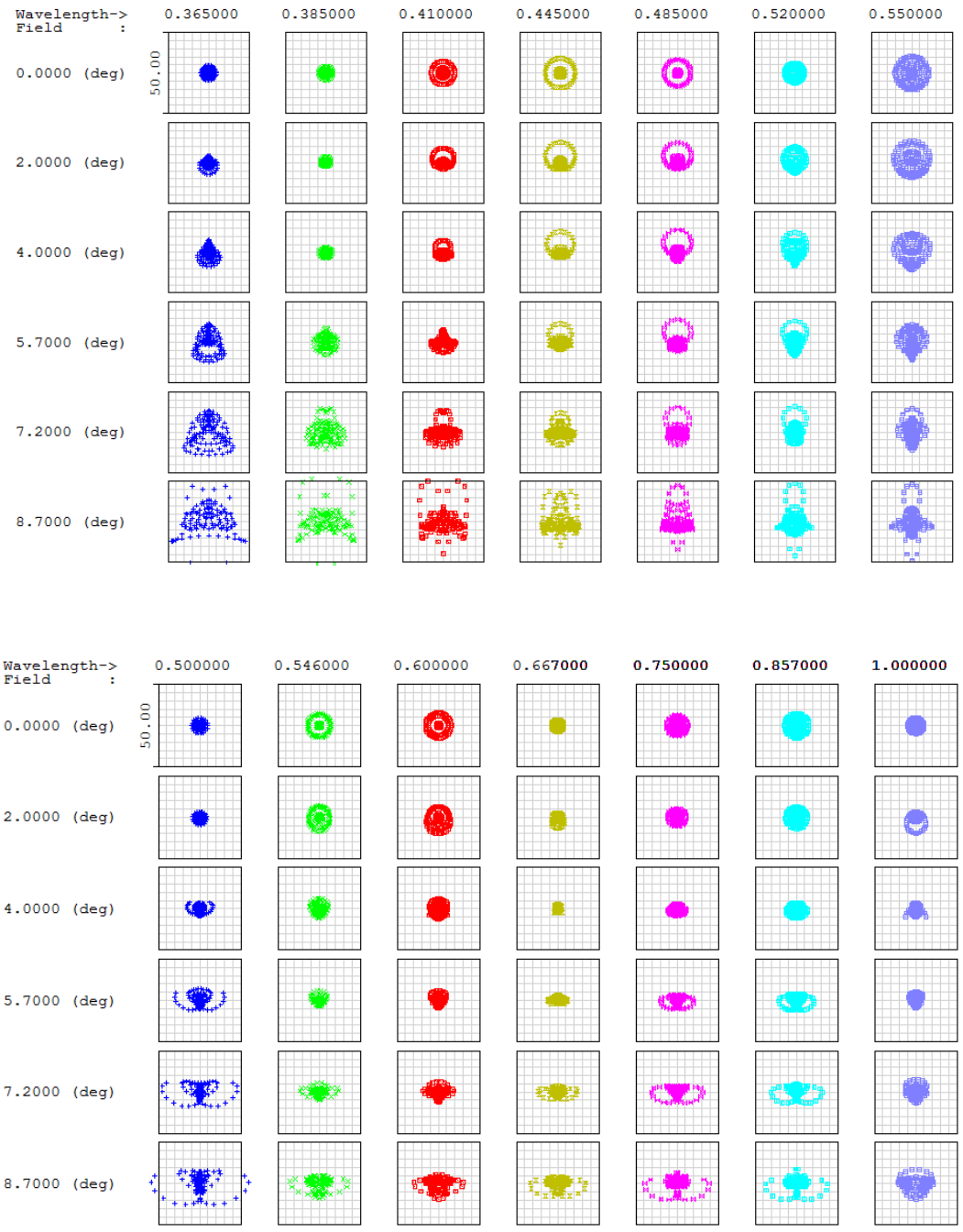

Figure 31. – Blue (top) and Red (top) camera spot diagrams as stand-along sub-systems.

Figure 32. – Spectrograph blue arm, HR mode, spot diagrams for different wavelengths and gratings.

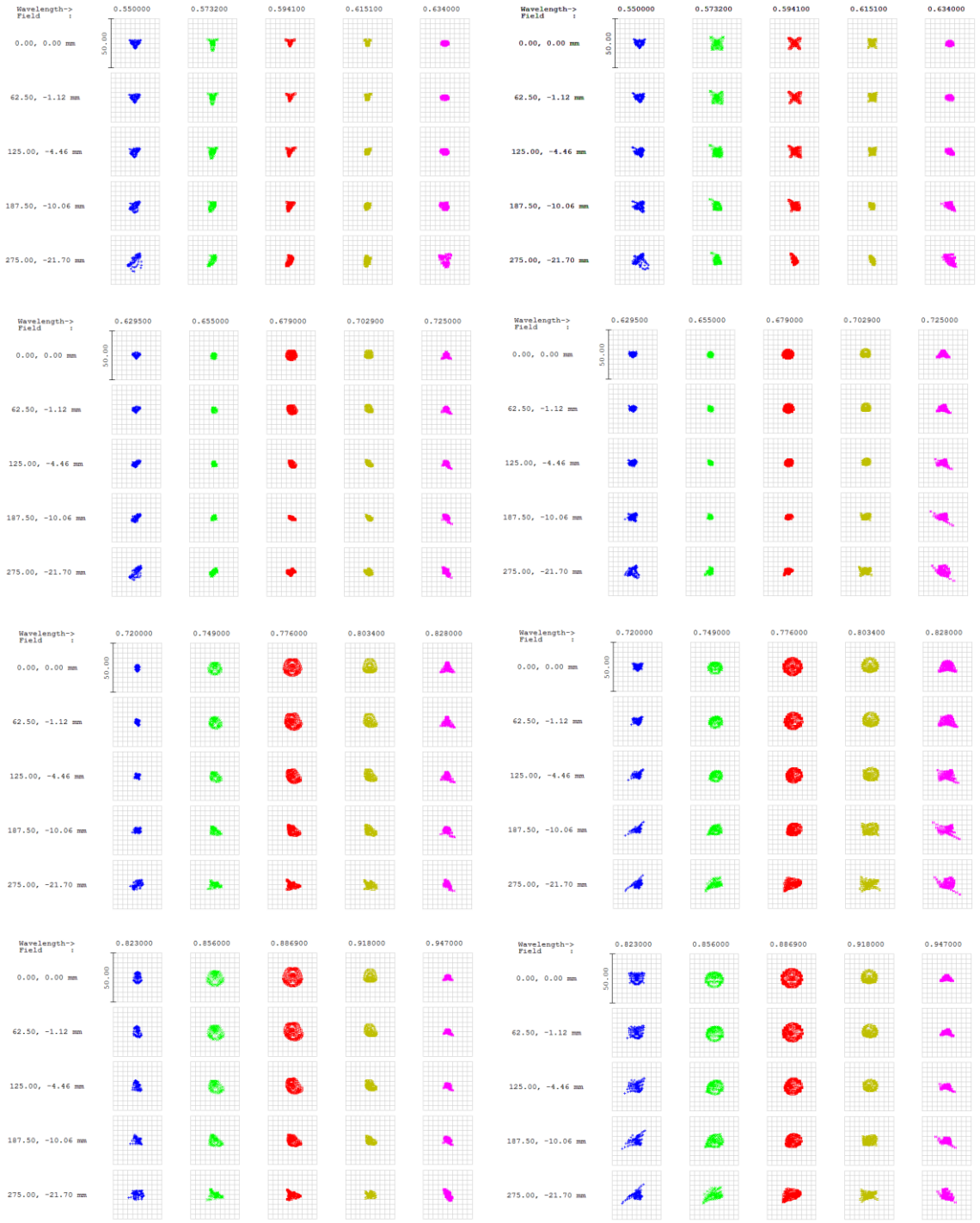

Figure 33. – Spectrograph red arm, HR mode, spot diagrams for different wavelengths and gratings.

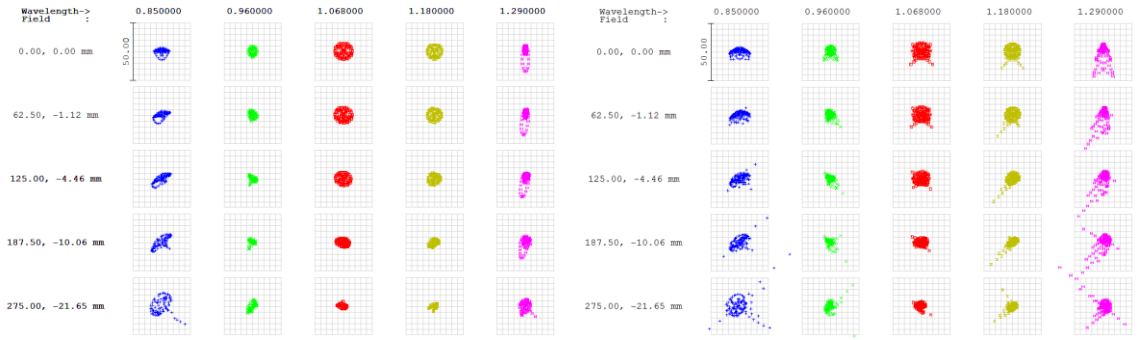

Figure 34. – Spectrograph NIR arm, LR mode, spot diagrams for different wavelengths.

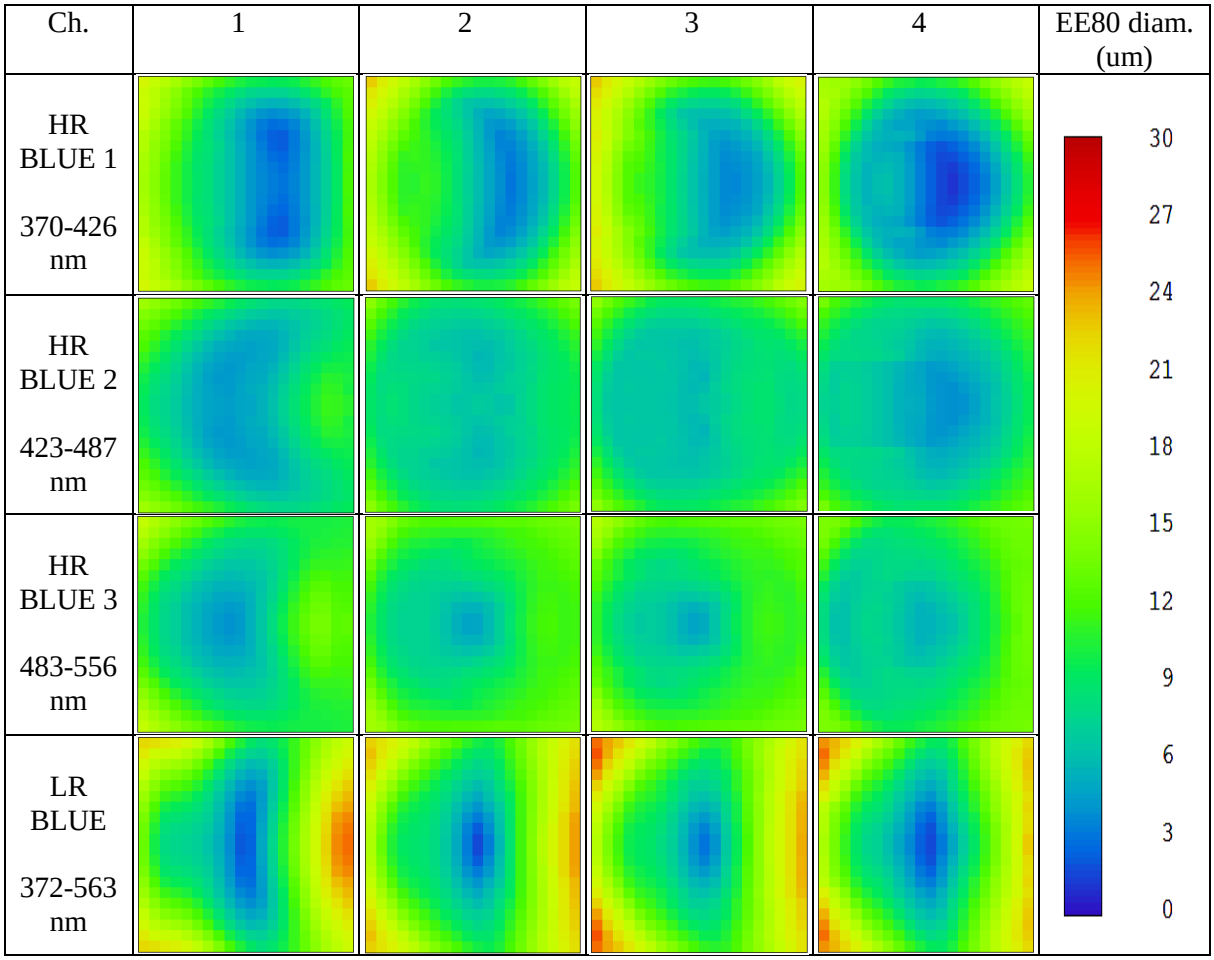

Figure 35. – Spectrograph blue arm EE80 diameter maps.

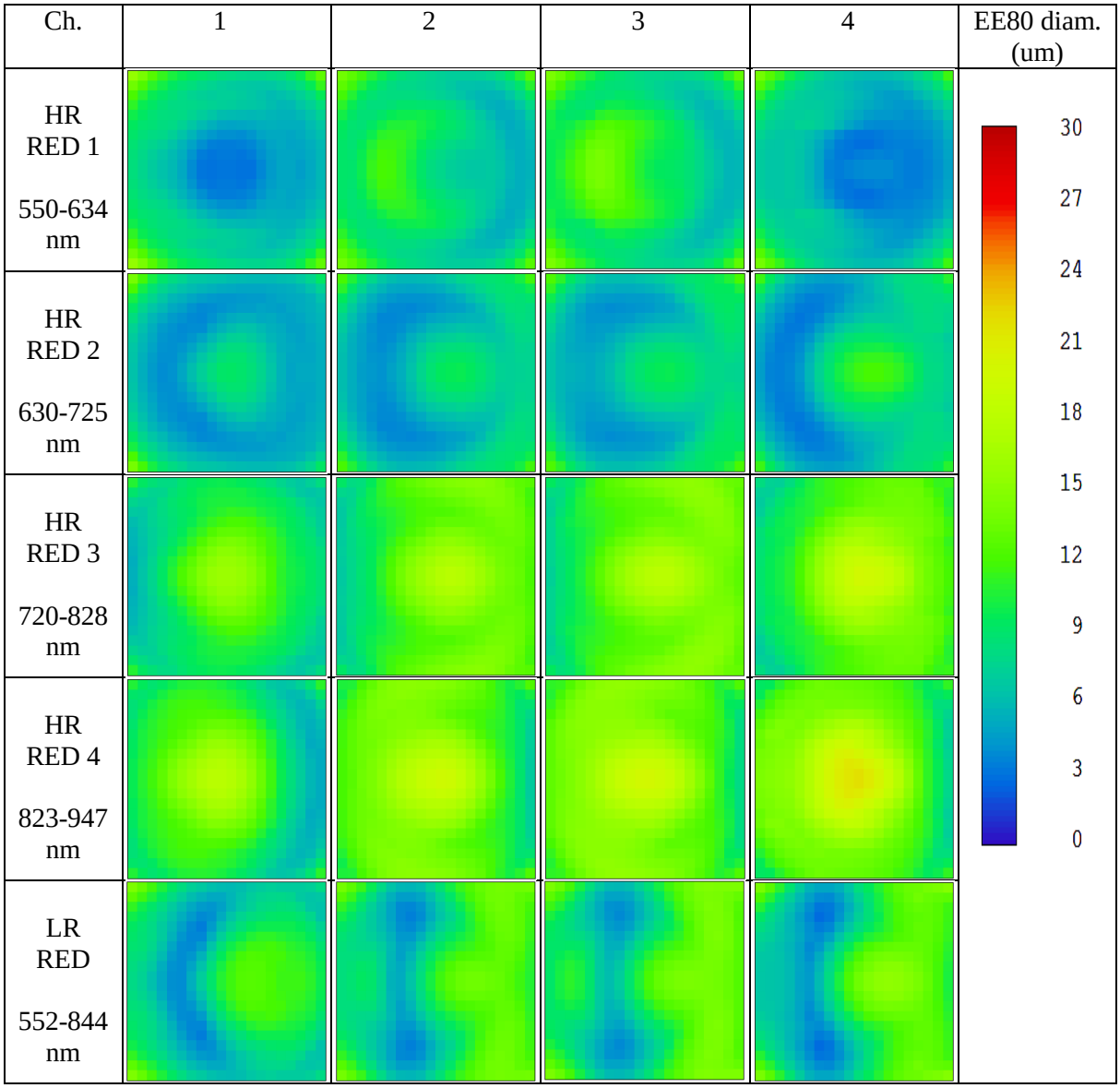

Figure 36. – Spectrograph red arm EE80 diameter maps.

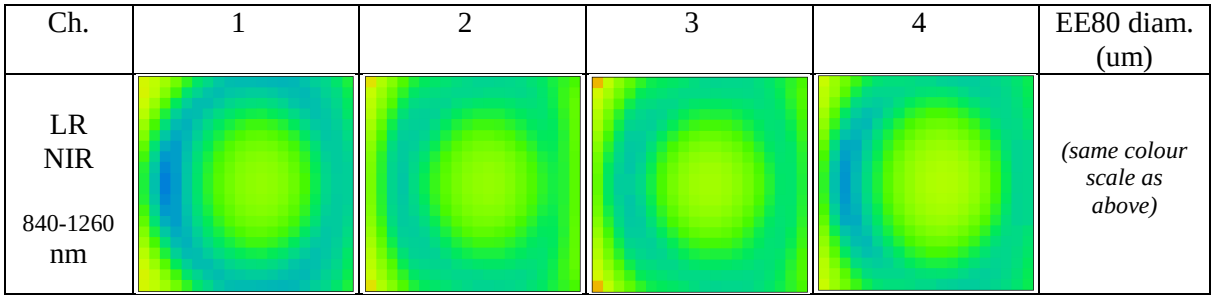

Figure 37. – Spectrograph NIR arm EE80 diameter maps.

4.2 Spectral resolution

Resolution is defined as $\lambda/\Delta\lambda$ where $\Delta\lambda$ is the Full Width Half Maximum (FWHM) of a spectral line at a given wavelength λ. For a Gaussian shape line spread function (LSF), with standard deviation σ, we can easily convert from EE80 diameter to FWHM, according to the following scaling laws:

$$FWHM = 2.35\,\sigma$$

$$EE80D = 3.57\,\sigma$$

$$FWHM = 0.66\ \text{EE80D}$$

Overall resolving power can be computed by summing up together, via RSS, the projected fiber image size, spectrograph image quality, and detector effects (flatness error, sampling, electro-optical response).

Item	Description	HR	LR-VIS	LR-NIR
Fiber image	Projected image fiber defined as the FWHM in the dispersion direction	25	100	67
Image quality	Spectrograph overall image quality (FWHM)	15	15	20
Detector flatness	Deviation from flatness	5	5	4
Detector electro-optical PSF	It is equivalent to the MTF, it includes diffusion in the detector, interpixel capacitance, intrapixel response	10	10	10
Detector sampling	Given by 0.866x bin size	9	9	13
OVERALL		**32**	**102**	**72**
RESOLVING POWER		**20000**	**2100**	**2000**

Table 15. - Spectral resolution budget. Units are micron on detector plane.

Similar computation can be done for the MR modes.

4.3 Wavelength coverage

All wavelengths from 370 to 1260 nm will be simultaneously observed in the LR and MR-FC modes, split into three arms. Some small overlap between wavelength ranges allow for SW reconstruction of the overall spectrum.
In HR and MR-HM modes, only two wavelength regions per exposure can be taken, selected among those available, as defined in Table 9 (see page 32).

4.4 Sampling

In LR and MR-HM modes each fiber will project an (almost) circular shape image. Due to varying anamorphism at grating level, sampling will vary along the spectrum, slightly changing the spectral sampling. Spatial sampling will be not affected by this anamorphism.
Due to the relatively large number of pixels covered by such an image, rebinning (in the Blue and Red detectors) should be preferred, to decrease detector readout noise. Without rebinning the sampling (both spectral and spatial) will be about 10 pixel in the Blue and Red arms, and about 4.5 pixel in the NIR arm, as measured across the spectral line FWHM.
In HR and MR-FC modes, due to the additional anamorphism introduced by the anamorphoser, the spectral sampling will be decreased by a factor 4, obtaining a value of 2.5 pixel, considered well above the Nyquist limit.

4.5 Spectral format

All spectra will be parallel each other as projected on the detectors, almost evenly spaced. Some large gaps will be found between fiber images belonging to different fiber bundles. This empty space can be useful to add additional simultaneous calibration fibers, if any.
Due to varying incidence angles on the VPH gratings, some wavelength shift between adjacent fibers can be observed, like in long-slit spectrographs. To maximize simultaneous spectral coverage in HR mode, this effective "slit curvature" has been nulled by curving the entrance slit. Of course, this correction will work for one VPH incidence angle only. Then, in LR mode, a residual slit curvature can be seen. This has been taken into account to properly define the coverage of each LR arm.
Figure 38 shows the two cases.

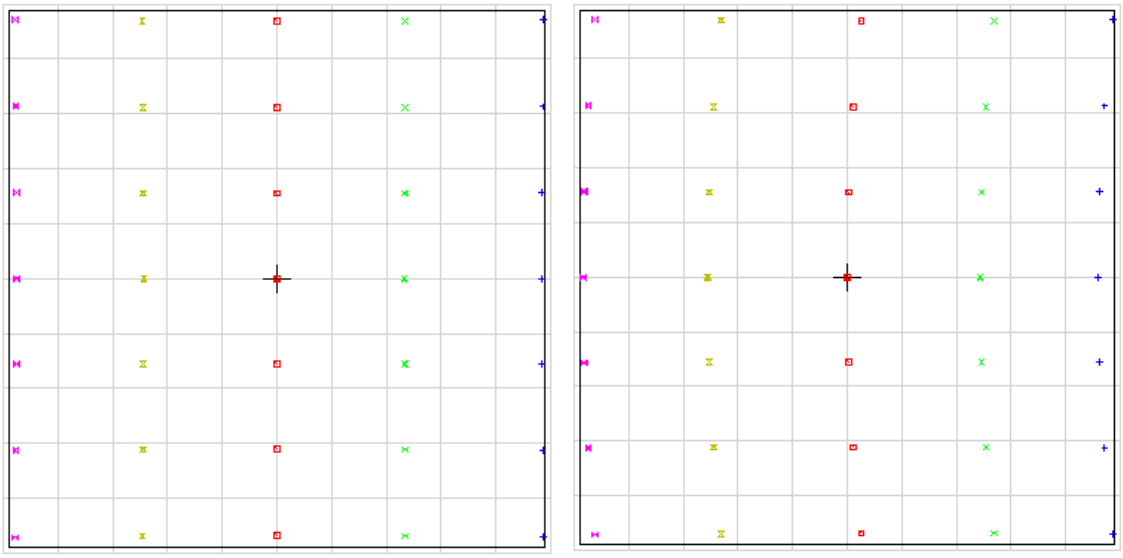

Figure 38. – Spectral formats. HR (left) and LR (right). Same colours refer to the same wavelength.

4.6 Throughput

An overall throughput budget has been built for the system, including telescope optics, wide field corrector, ADC, fiber train, and spectrograph optics, as shown in Figure 39 and Table 16. Also the spectrograph optics budget, including detectors, is given.
These numbers are in line with requirements.

Wavelength (nm)		**360**	**400**	**500**	**700**	**900**	**1100**	**1300**
Telescope (1 mirror, Al-coated)		88%	88%	89%	87%	89%	93%	95%
Prime Focus Corrector + ADC		69%	91%	89%	91%	93%	88%	79%
Fiber train (35-m)		52%	65%	77%	83%	84%	85%	82%
	Fiber internal transmission	*59%*	*74%*	*88%*	*95%*	*96%*	*97%*	*94%*
	FRD	*95%*	*95%*	*95%*	*95%*	*95%*	*95%*	*95%*
	Fresnel losses	*94%*	*94%*	*94%*	*94%*	*94%*	*94%*	*94%*
	Alignment losses	*98%*	*98%*	*98%*	*98%*	*98%*	*98%*	*98%*
Spectrograph optics (HR)		45%	51%	55%	54%	54%	55%	50%
	Relay optics	*94%*	*96%*	*96%*	*96%*	*95%*	*93%*	*90%*
	Anamorphoser / Prism plate	*96%*	*96%*	*96%*	*96%*	*96%*	*96%*	*96%*
	Collimator optics	*85%*	*86%*	*86%*	*84%*	*85%*	*89%*	*91%*
	Pupil slicer	*97%*	*98%*	*98%*	*99%*	*99%*	*99%*	*98%*
	Dichroic beam-splitter	*95%*	*95%*	*95%*	*95%*	*95%*	*95%*	*95%*
	VPH gratings	*75%*	*80%*	*85%*	*85%*	*85%*	*85%*	*80%*
	Camera optics	*85%*	*87%*	*87%*	*87%*	*87%*	*87%*	*85%*
Detector		70%	92%	90%	95%	87%	90%	90%
Spectrograph + Detectors		*32%*	*47%*	*49%*	*51%*	*47%*	*50%*	*45%*
OVERALL		**10%**	**25%**	**30%**	**34%**	**33%**	**35%**	**28%**

Table 16. - Overall throughput budget.

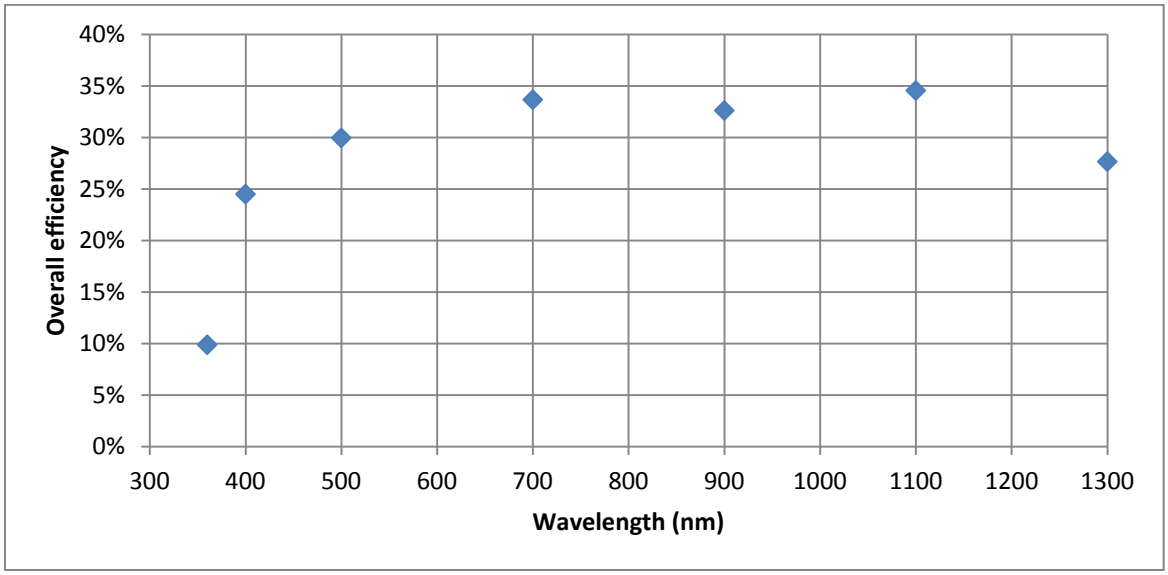

Figure 39. –Throughput curve.

5 Feasibility of Optical Components

5.1 Large optical blanks

All optical spectrograph components (lenses, mirrors, beam splitters, gratings) has been selected and designed around existing state-of-the-art manufacturing capabilities.
One of the main concerns refer to the availability of large glass blanks for lenses and mirrors substrates.
The largest components are in the collimator optics. A 1.5-m spherical mirror can be easily done on Zerodur substrate, the same size of the telescope primary mirror segments. Moreover, its spherical shape will make it quite fast to be realized and tested with the greatest accuracy.
The two corrector lenses will be done un Fused Silica substrates, available on meter size with good homogeneity.
All other plano optics (beam splitters, VPH gratings, pupil slicer mirrors) are in the 30-40cm range, making them easily available from different suppliers.
Camera lenses, with a maximum diameter in the 20-30 cm range, will be done on preferred glass materials, available as equivalent glasses from different glass suppliers, as Schott, Ohara, Corning. However, some glasses are more easily available in large homogeneous blanks than others, as inferred from Table 17. Other optical glasses available for that size are the i-line glasses, used for photolithography, where very stringent requirements on homogeneity are put. A list of those glasses are given in Table 18 for Ohara, available up to 300 mm diameters. Schott states that i-line glasses are available with diameters up to 300 mm and thicknesses up to 100 mm. They are labelled with the suffix "HT" onto the glass name.
Other materials available in large size, and commonly used to control chromatic aberrations are Calcium Fluoride (CaF2), Barium Fluoride (BaF2), and Fused Silica. They are available from many suppliers, too. We have inquired about maximum blank dimensions, and we report them in Table 19.

Glass Type Family	Melting Technology Min Prod*	Max Dim present capabilities	Max Dim with development	Restricted by	Preferred Glass Types
BK	Cont. Tank 5 tons	∅1000 x 300	∅1500 x 500 or equiv. Vol	CT, CS, ES	N-BK7
LLF, LF, F, SF	Cont. Tank 5 tons	∅1000 x 300	∅1500 x 500 or equiv. Vol	CT, CS, ES	LLF1, LF5, F2, SF6
FK, PK	Discont. Pot	∅360 x 60	∅460 x 100	Cryst, VS	N-FK51A
LAK, LAF, LASF	Discont. Pot	300 x 160 x 43 GD	360 x 280 x 80 GD	Cryst, VS	LAK8, LAK9
KZFS	Discont. Pot	300 x 160 x 43 GD	360 x 280 x 80 GD	Cryst, VS	KZFSN4

Min Prod*	Minimum production amount needed for high quality
CT:	Casting Time
CS:	Center-
ES:	Edge-
VS:	Volume Striae
Cryst:	Crystallization
GD:	Gross diameter

Table 17. - Schott glass blank typical and maximum sizes (from TIE-41).

Glass Type	Internal Transm-ittance 10mm thick (365nm)	Solari-zation Resista-nce	Optical Homogeneity Capability ($x10^{-6}$)			Deviation of n_i within a single lot ($x10^{-5}$)	Tolerance of Refractive Index ($x10^{-5}$)
			Dia160 or less	Dia210 or less	Dia260 or less		
S-FPL51Y	0.997	Good	±1.0	-	-	±2	+20±20
S-FSL5Y	0.999	Good	±0.5	±0.8	±1.0	±2	+15±20
BSL7Y	0.998	Good	±0.5	±0.8	±1.0	±1	+20±20
BAL15Y	0.994	Good	±0.5	±0.8	±1.0	±2	+10±20
BAL35Y	0.996	Good	±0.5	±0.8	±1.0	±2	+20±20
BSM51Y	0.995	Good	±0.5	±0.8	±1.0	±2	+30±20
PBL1Y	0.997	Good	±0.5	±0.8	±1.0	±2	+10±20
PBL6Y	0.998	Good	±0.5	±0.8	±1.0	±2	+10±20
PBL25Y	0.995	Good	±0.5	±0.8	±1.0	±2	+10±20
PBL26Y	0.996	Good	±0.5	±0.8	±1.0	±2	+10±20
PBM2Y	0.986	Good	±0.5	±0.8	±1.0	±2	+10±20
PBM8Y	0.991	Good	±0.5	±0.8	±1.0	±2	+10±20
PBM18Y	0.993	Good	±0.5	±0.8	±1.0	±2	+10±20

Table 18. - Ohara i-line glasses.

Supplier	Material	Max. dimension typical (diam. X thick., mm)	Max. dimension with development (diam. X thick., mm)
Hellma Materials GmbH (D)	CaF2	Ø350 x 80	Ø440 x 250
	BaF2	Ø360 x 100	
Nikon Corp. Glass Division (JP)	CaF2	Ø300 x 50	
Ohara (JP)	CaF2	Ø350	
	Silica	Ø500	Ø1000
Corning (US)	Silica	Ø1000	Ø1500
Heraeus Quarzglas GmbH (D)	Silica	Ø650	

Table 19. - CaF2, BaF2, and Fused Silica maximum dimensions.

5.2 Camera optics

Camera lenses will have both spherical and aspherical shapes. Current grinding, polishing, and testing technologies have been improved in the last years making aspherical lenses with very large aspherical departure from the best fit sphere feasible.
All steps to make aspherical lenses have now been addressed by many suppliers, with different technologies. Here we give some examples of suppliers and available technologies.

Supplier	Processing steps	Available technologies	Characteristics
QED	Polishing, Testing	MRF, SSI	generating aspheric departure up to hundreds of micron up to 400 mm diam., testing >650 micron departure on 200 mm (and above)
Zygo	Generating, Polishing, Testing	CCS, MRF, IBF, INL, CGH	<500 mm
Zeeko	Generating, Polishing, Testing	CCS, CCP, PRO	>400 mm diameter, swing arm profiler
Satisloh	Generating	CCS	<500 mm diameter by 5/6-axis machine
SAGEM	Generating, Polishing, Testing	CCS, CCP, IBF, PRO, INL	<1.5-m
Thales-SESO	Generating, Polishing, Testing	CCS, CCP, MRF, INL	

Legend: CCS – Computer controlled surfacing
CCP –Computer controlled polishing
MRF – Magnetorheological Finishing
IBF – Ion Beam Figuring
PRO – Profilometry
INL – Interferometry with classical null-lenses
SSI – Sub-aperture Stitching Interferometry
CMM – Computer metrology machine
CGH – Computer Generated Holograms

Table 20. – Aspherical manufacturing companies and available techologies.

5.3 Micro-optics

The anamorphoser will be an aspherical cylindrical optics. They can be done via photolithography on Silica plates, and then anti-reflection coated. Current design foresees a two-side design, then the two profiles must be co-aligned together. This is currently done by more than one manufacturer. Just as an example, both SUSS MicroOptics (see Figure 40) and Jenoptik provide similar cylindrical aspherized micro-optics array off-the-shelf.

SÜSS MicroOptics

4.6. Cylindrical Microlenses

General specifications	
Substrate Material	Fused Silica (Quartz)
Array Type	Cylindrical lenses
Lens Type	Refractive, Plano-Convex
Lens Profile	Parabolic
Pitch Accuracy	± 0.25 µm
Tolerance on ROC	± 5%
Array clear aperture	1mm smaller than outer tolerances
Far-Field	Flat-Top
Application	Beam Homogenizing & Shaping, Slow Axis Collimation

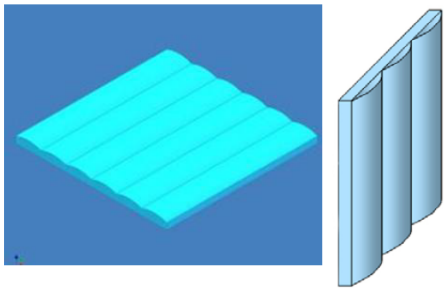

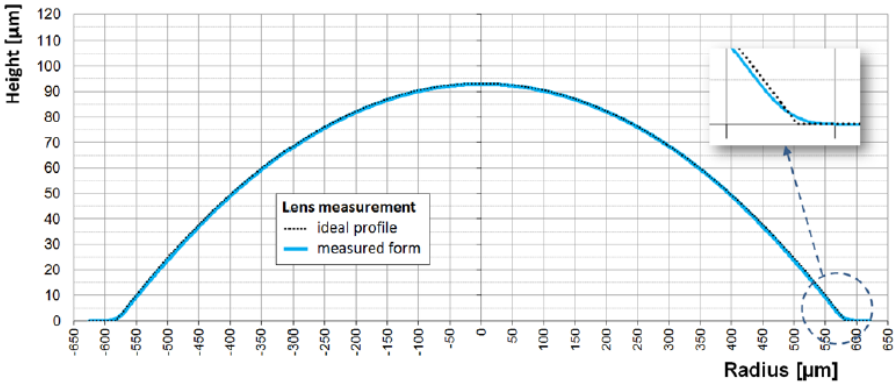

Figure 40. –Example of an existing cylindrical aspherical micro-array.

5.4 Beamsplitters

One of the key aspects of a high-efficiency, multi-arm, spectrograph is the availability of large dichroic beam-splitters. Their performances are strongly dependent on the selection of the wavelength regions (both in reflection and transmission), the incidence angle and its aperture, steepness of the transition region, and size.

Size is one of the biggest concerns, because it makes dichroic multi-layer design very challenging. We made a preliminary worldwide inquiry among coating suppliers, to check what is the maximum size and general performances. Some feedbacks where received about potential or critical areas.

Table 21 gives a list of potential suppliers giving us positive feedbacks about manufacturing of large size dichroics. Some of them provided also simulated performances. An example is shown in Figure 41.

Supplier	Max. diameter (mm)
Vaculayer Corp	580 mm
Spectral Products	330 mm
Asahi Spectra	175 mm
Laser Components	200 mm
Abrisa / ZC&R	600 mm
Spectrum Coatings	600 mm
BMV Optical	250 mm
Optics Balzers	350 mm square

Table 21. – List of potential suppliers for dichroic beam-splitters.

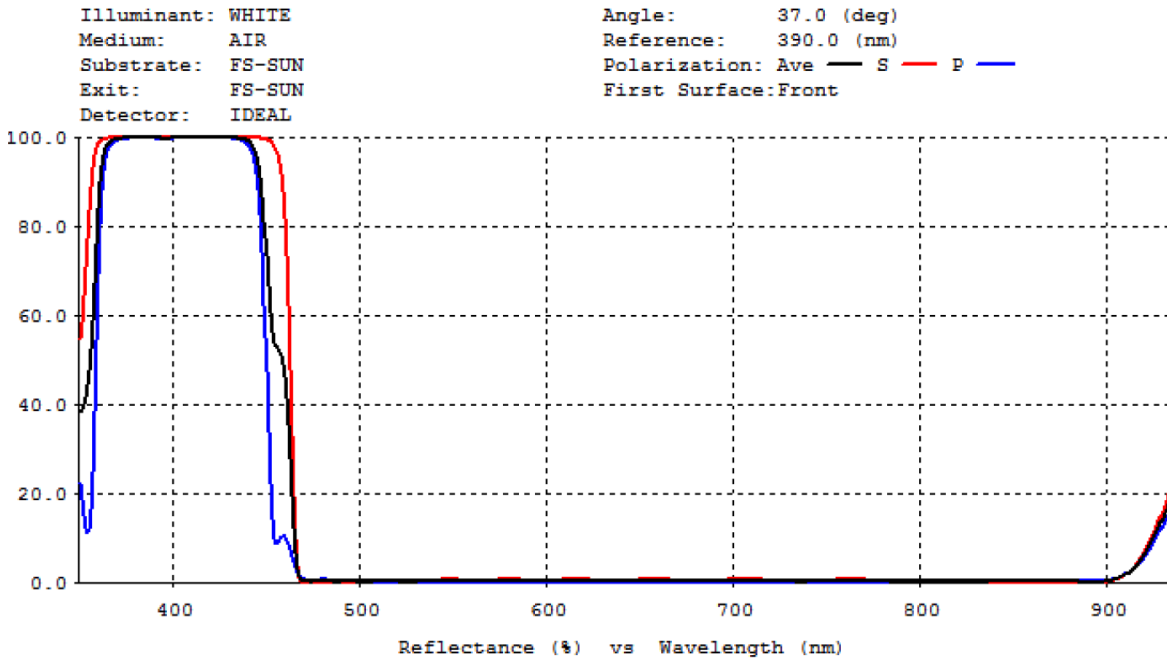

Figure 41. –Example of a dichroic beam splitter reflectivity.

APPENDIX E. NGCFHT VENT SYSTEM CFD STUDY STATEMENT OF WORK

Appendix E. NGCFHT Vent System CFD Study Statement of Work

Objectives:

- To compare the performance of the passive venting system with vent doors against the active venting system using floor mounted exhaust system
- To find the air exchange time and flow profiles in the optical path
- To check that minimum turbulence is generated, turbulent kinetic energy is low close to the secondary mirror (M2) and temperature does not vary significantly inside the enclosure

Numerical details:

- Domain and Mesh
  - → Domain to be determine based on the enclosure "characteristic" diameter D, (typically 3-4 D in front, 7-8 D behind and 3-4 D on each side); domain will be created according to the CFD guidelines and previous study experience
  - → Number of grid cells can be estimated once the CFD version of the CAD model is provided. However, the target number of grid cells for the enclosure study is approximately 2.5 million to save computational time while maintaining reasonable accuracy
  - → Three different grids will be generated for three different azimuthal; will explore alternate technique with using one grid for three azimuth angles
- Boundary conditions
  - → Baseline wind speed at the inlet of the domain is 5 m/s, direction from the east
  - → Adiabatic lapse rate will be imposed based on the typical humidity of the site
  - → Enclosure surface temperature will be provided
  - → For the active venting system, three fan flow rates will be required
  - → The sides and top of the domain will be treated as slip walls with zero normal velocity component
  - → An outflow type boundary will be employed at the outlet
- Numerical schemes
  - → 3D Unsteady Reynolds Averaged Navier-Stokes (URANS) simulations will be performed; will also consider the Detached Eddies Simulation (DES) as alternative with final simulation to be determined.
  - → Shear Stress Transport (SST) k-ω turbulence model will be employed.

→ Second order discretization schemes for gradient, divergence and Laplacian terms in the governing equations will be used

→ PISO (Pressure Implicit with Splitting of Operators) algorithm will be employed for the pressure-velocity coupling

→ Flow time and time step: Flow time for which the simulation will have to run is dependent on the air flush time of the enclosure volume. A simplified enclosure test case with no telescope will be studied in order to obtain typical flush time required. Total flow-time will be set to at least three times of the flush time. Time step size is dependent on the grid and will be adjusted to satisfy the CC.F.L condition.

- Solver
  → Segregated
  → Software: ANSYS FLUENT 13.0

Study Cases:

- Proposed cases with one fixed zenith angle of 30°:

Study Case	Wind Speed	Azimuth Angle	Venting System	Fan Flow Rate*	Vent Door Opening**
1	5 m/s	90°	Active	f2	
2	5 m/s	90°	Passive		Half, TBC
3	5 m/s	90°	Active	f1	
4	5 m/s	90°	Active	f3	
5	5 m/s	0°	Active	f2'***	
6	5 m/s	0°	Passive		Half, TBC
7	5 m/s	180°	Active	f2'	
8	5 m/s	180°	Passive		Half, TBC
9	2.5 m/s	90°	Active	f2'	
10	2.5 m/s	90°	Passive		Full
11	10 m/s	0°	Passive		Closed
12	10 m/s	0°	Active	f2'	

*f2 = fan rate estimate (TBD, assumed optimum), f1 = lower rate and f3 = higher rate
**Opening is assumed to be defined by porosity in the CFD model
***f2' = modified optimum fan rate

Deliverables:

The results of the Study will be reported by the WindEEE Research Institute at the University of Western Ontario.

For each case the following results will be provided:

- Contour plots of mean velocity inside the enclosure
- Contour plots of turbulence characteristics (e.g. T.K. E, r.m.s) inside the enclosure
- Temperature contour plots inside the enclosure
- Plot of spatial RMS of temperature through a predetermined cylindrical optical volume at every time step subtracted from the mean temperature of the volume
- Complete air exchanges inside the enclosure
- Velocity and turbulence profiles inside the enclosure along the optical axis, i.e. the telescope centerline
- For first four cases (1-4), one Advanced Report will be provided after 10 weeks of the start of the project. Following review a Final Report will be issued
- For Additional Case which involves changing in boundary conditions (but no re-meshing), running and post-processing, one Advanced Report will be provided after 2 weeks. After review, the report will be included in the Final Report
- For Additional Case which involves changing in changes in meshing, running and post-processing, one Advanced Report will be provided after 3 weeks. After review, the report will be included in the Final Report

Timing and Pricing:

The starting date for the project is considered to be when all pertinent information has been received including solid works files for all enclosure and telescope geometries and topographic features as well as fan flow rates, wind and temperature conditions.

The first 4 Base Cases (Case 1 to 4) are estimated to be completed in maximum 10 weeks, time at which an Advanced Report will be issued. The effort related to these Base Cases, including manpower and capacity utilization for creating meshes, setting up the case, post processing and reporting is estimated at $18,640.

Every Additional Remeshing Case (Case 5 and 7) which involves changes in meshing with running, post-processing and reporting was estimated to take 3 weeks to complete at $4,985/case. These cases are limited to the cases for which a change in azimuth angle is needed (only two cases, 0° and 180°).

Every Additional Non-Remeshing Case (Case 6 and 8 to 12) which involves changing in boundary conditions only with running, post-processing and reporting was estimated to take 2 weeks to complete at $3,545/case.

APPENDIX F. PROGRAMMATIC STUDY FOR UPGRADE OF TELESCOPE STRUCTURE AND ENCLOSURE

Next Generation CFHT

DSL Phase II Report:

Programmatic Study for Upgrade of Telescope Structure and Enclosure

Dynamic Structures Ltd. &

University of British Columbia

October 2012

Revision History

Version	Date	Comments
DRAFT1	Sep 20, 2012	Interim report including deconstruction plan and cost estimate
REV 1	Oct 31, 2012	Added manufacturing & construction plan and cost estimate; updated deconstruction plan based on Sept 27, 2012 telecon with K.Szeto & CFHT staff
REV 2	Nov 8, 2012	Implemented comments from Kei Szeto

Table of Contents

List of Tables

List of Figures

1. Introduction

This report is a summary of the results of a study on the Next Generation Canada-France-Hawaii Telescope (ngCFHT). The work was carried out by Dynamic Structures Ltd. (DSL) in conjunction with the University of British Columbia (UBC) in September and October 2012. The objectives of the study are to develop and outline the programmatic requirements including the sequence, cost, schedule and construction equipment required to upgrade the current CFHT to the ngCFHT facility.

The work builds on previous studies carried out by DSL and UBC in 2011, which included an assessment of existing CFHT telescope and enclosure pier capacity, and the development of the ngCFHT telescope and enclosure configuration.

Deliverables for this phase of work include the following:

1. Provide cost and schedule estimates for deconstruction of the current CFHT facility including removal of the existing enclosure and telescope structure and the associated services
2. Provide cost and schedule estimates to upgrade the load capacities of the existing enclosure and telescope piers to meet current structural code requirements based on findings from the Phase I studies
3. Provide cost and schedule estimates for construction of the new ngCFHT facility including the new enclosure and telescope structure systems based on the baseline enclosure and telescope configuration developed in Phase I
4. Provide CAD model support for the ngCFHT CFD aero-thermal study which will consist of reviewing the model provided by the client for geometrical correctness and proposing ventilation schemes that are consistent with the structural/mechanical design concept
5. Provide photo-realistic rendering of telescope and enclosure using summit topology provided by the client

The information used for this study is based on:

1. Historical data of the current CFHT dome and telescope available at DSL and CFHT
2. Findings from the previous pier load capacity studies and ngCFHT enclosure and telescope configuration study
3. Where information is insufficient, best engineering estimates are used and the assumptions are documented in the study report.
4. It is noted that the designs of the ngCFHT enclosure and telescope structures are presently at an early conceptual level, and the cost estimating methodology and associated contingencies used during this phase reflect this. The cost estimating uses a combination of top-down cost scaling from other observatories as well as bottom-up cost estimating.

2. Deconstruction Plan

2.1 Introduction/Methodology

DSL worked with Jim Waldbauer, who was one of the foremen who worked on the construction of the dome and telescope for the original CFHT, to develop the deconstruction plan and cost estimate outlined below. The original construction drawings for the telescope structure were used to determine component sizes and weights.

2.2 Deconstruction Assumptions

The following outlines the assumptions made by DSL in the development of the deconstruction plan and cost estimate:

- General assumptions on pre-deconstruction conditions:
  - All instruments removed before deconstruction
  - All control room and computer equipment removed before deconstruction
  - All lab and instrument equipment removed before deconstruction
  - All furniture and office equipment removed before deconstruction
  - All telescope optics removed before deconstruction
- Scope of enclosure deconstruction:
  - All steel work to be removed, including azimuth ring girder, bogies, and drive system
  - Components do not need to be preserved for future use
- Scope of telescope deconstruction:
  - All steel work to be removed
  - Removal of observation floor around telescope structure and glycol lines
    - It is assumed that the existing observation floor (5^{th} floor) will remain as the observation floor for the new observatory. It will be required that the center portion of the observation floor around the existing telescope will be removed in order to allow deconstruction of the existing telescope and to allow clearance for construction and operation of the new telescope.
  - Components do not need to be preserved for future use
- The following items have **not** been included in the scope of deconstruction estimated by DSL
  - Removal of coating chamber/aluminizing tank
  - Remove the glycol chiller and distribution facility
  - Remove hydraulic lines, pump and distribution equipment
  - Removal of electrical distribution equipment
  - Removal of air handling units

2.3 Site Set-up for Deconstruction

A mobile crane will be set-up on the south side of the building where there is good access for the crane. The telescope will be disassembled prior to the dome using a combination of the existing dome crane (12 ton capacity) and a temporary 40 ton capacity crane system mounted to the dome arch girders. These cranes will be used in conjunction with the dome rotation to disassemble the telescope and place the disassembled

components on the south side of the observatory floor. From this point the mobile crane can reach through the dome slit and lift the components from the observatory floor and remove them from the dome. After the telescope deconstruction is complete the dome will be deconstructed using the mobile crane. The figures below show the site set-up for deconstruction, and further details of the deconstruction sequence are provided below.

Figure 1: CFHT observatory from the south

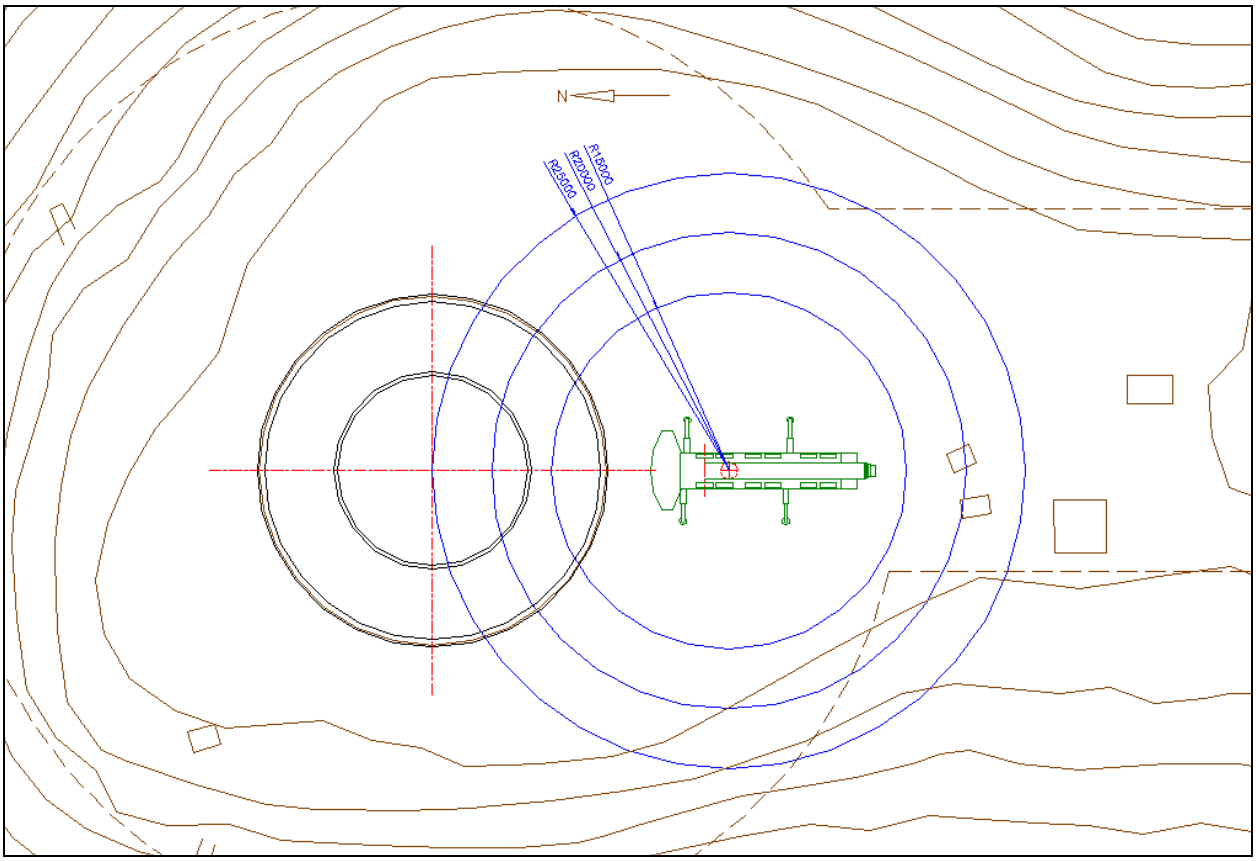

Figure 2: Plan view showing mobile crane set-up for deconstruction

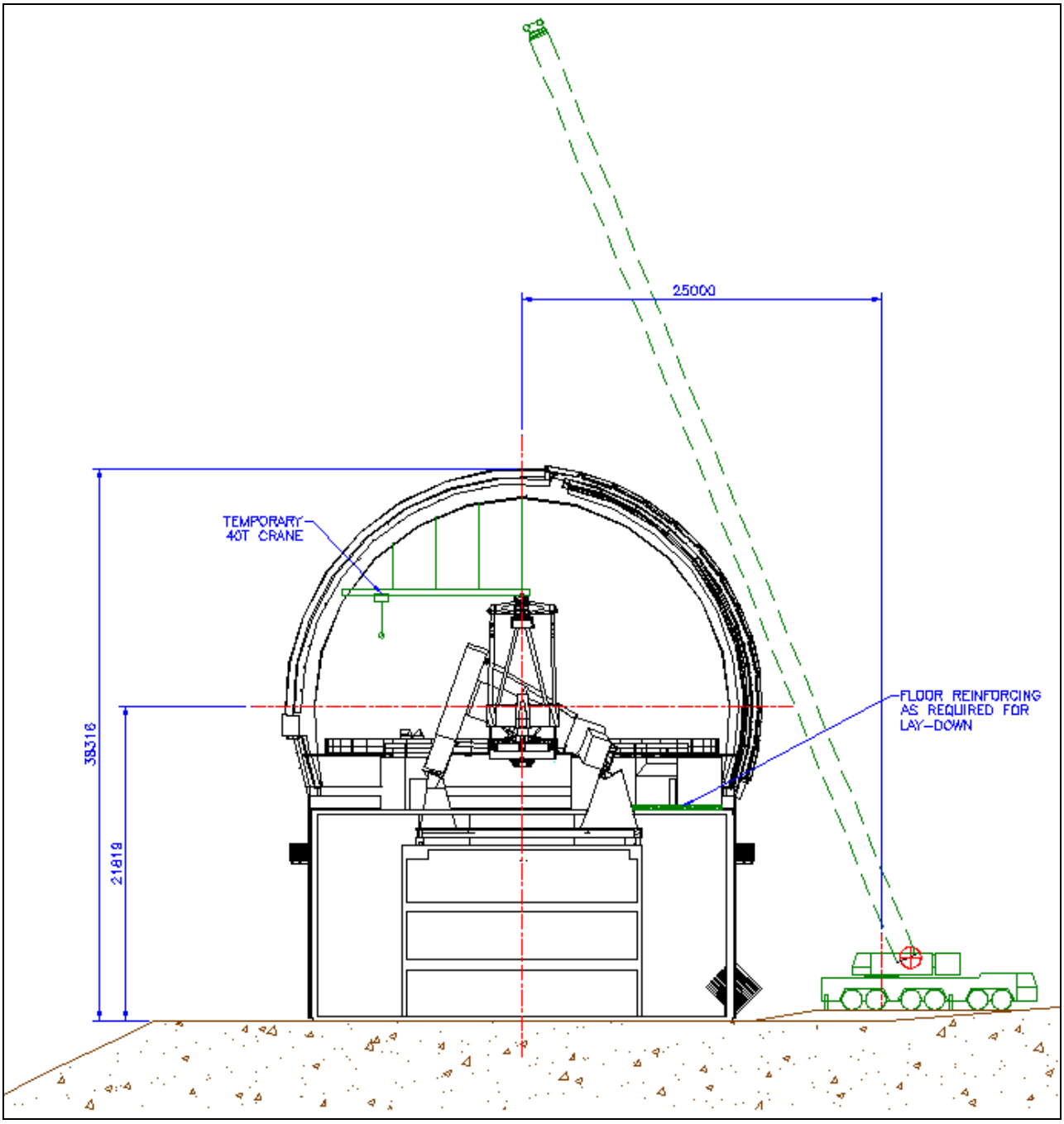

Figure 3: West elevation of site set-up for deconstruction

A 250 tonne hydraulic crane is assumed for the preliminary mobile crane selection. The crane has sufficient capacity to reach into the dome between the arch girders and remove the telescope components from the south side of the observatory floor. Furthermore, it is hoped that this crane has sufficient capacity that it can also be used to erect the new telescope and enclosure in order to save costs on freight and mobilization.

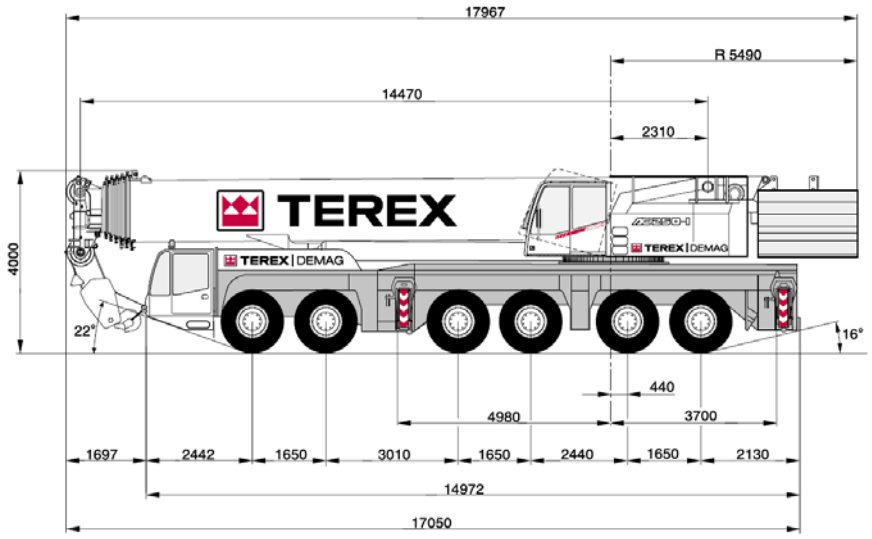

Figure 4: Terex 250 tonne hydraulic crane

2.4 Telescope Deconstruction Sequence

The major components of the telescope structure are labelled in the figure below and are referenced in the deconstruction sequence.

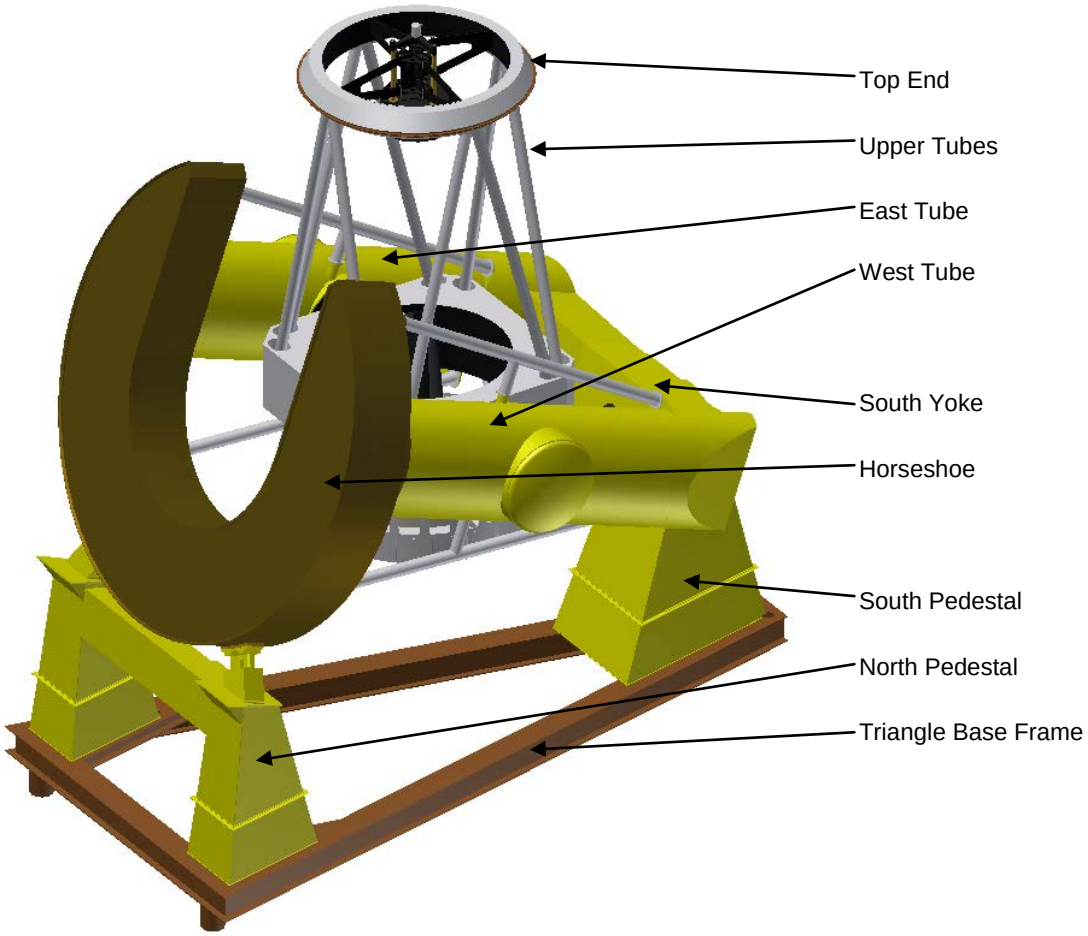

Figure 5: Existing telescope main components

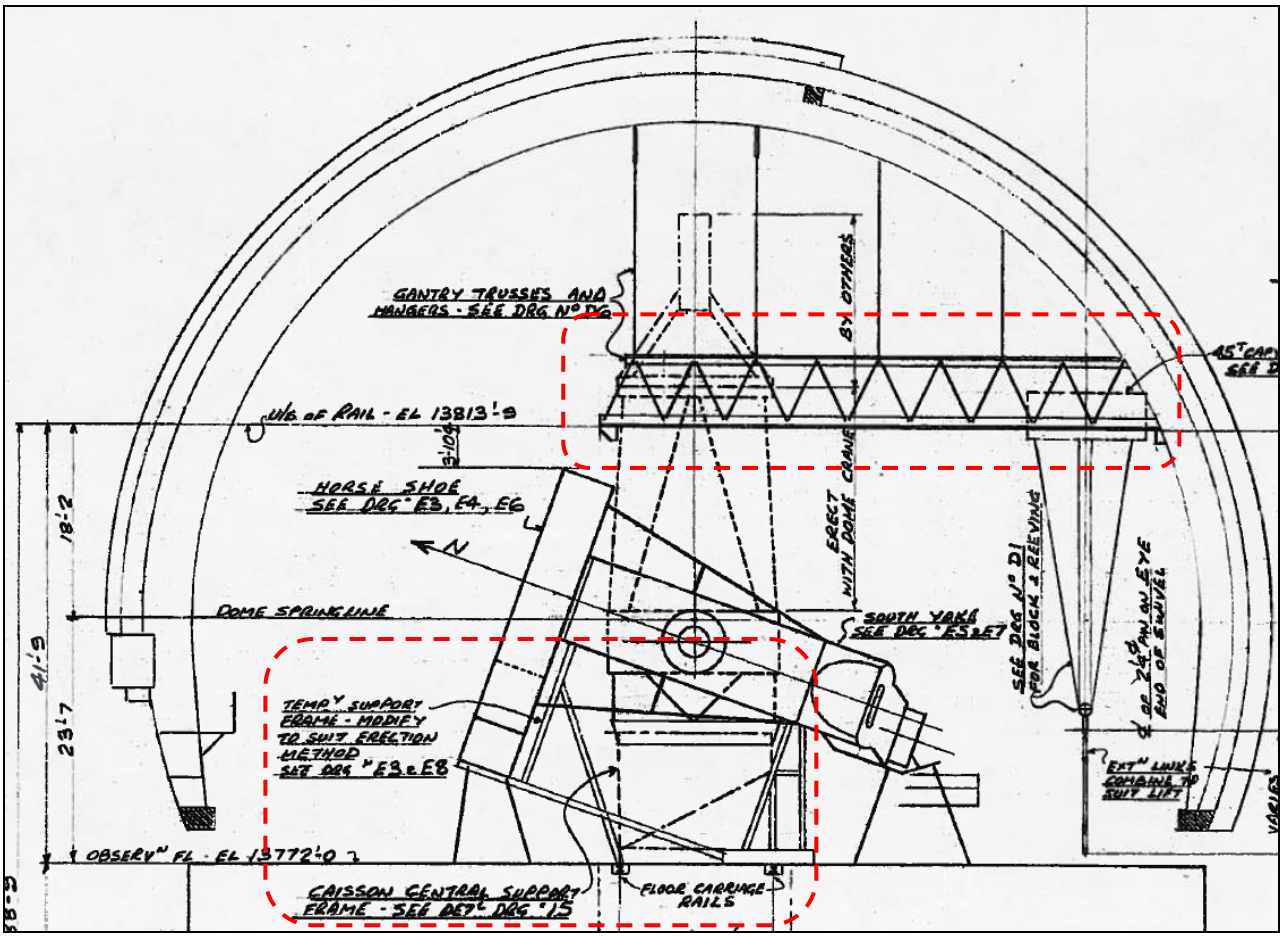

Figure 6: Original CFHT telescope erection drawings with location of falsework and temporary construction gantry highlighted

The telescope deconstruction sequence is as follows:

1. Remove top end & upper tubes with top-end crane
2. Attach rigging and temporary crane to dome arch girders
3. Erect center section of false work
4. Erect temporary support for east and west tube
5. Erect temporary supports for horseshoe
6. Prep horseshoe, east and west tubes
7. Remove horseshoe horns (28.6 tons each)
8. Remove horseshoe center section (28.6 tons)
9. Remove east and west tubes (9.9 tons each)
10. Remove south yoke (26.7 tons including bearing)
11. Remove center ("caisson central") section (27.6 tons)
12. Prep telescope floor and glycol lines
13. Remove telescope floor and glycol lines

14. Remove south pedestal
15. Remove north pedestal
16. Remove triangular base frame
17. Clean-up observatory floor
18. Provide weather protection over floor and floor opening
19. Load trucks
20. Remove rigging and temporary crane from dome

2.5 Dome Deconstruction Sequence

The major components of the dome are labelled in the figure below and are referenced in the deconstruction sequence.

Figure 7: Existing dome main components

The dome deconstruction sequence is as follows:

1. Remove dome insulation
2. Remove mezzanine, catwalks and air handling units on observation floor
3. Remove catwalks and bus-bar
4. Remove shutters
5. Remove wind screen & drive system
6. Erect exterior work platform on arch girders
7. Remove vent platforms

8. Prep intermediate infill shell plates
9. Remove intermediate infill shell plates
10. Install temporary pipe struts on arch
11. Remove rack at arch splices
12. Prep shell modules, including vents (if required)
13. Remove shell modules, including vents (if required)
14. Remove outer skirts
15. Adjust bogie loads as required to distribute even loads as dome elements are removed
16. Prep arch falsework
17. Erect arch falsework
18. Connect arch girders and tower
19. Gouge arch girders splices
20. Gouge tie beam
21. Prep back shell
22. Remove back shell and tie beam
23. Remove top-end crane
24. Remove two arch center sections
25. Remove four arch internal sections
26. Remove four arch horn sections
27. Dismantle erection falsework tower
28. Gouge ring girder sections
29. Erect temporary bogie supports
30. Remove ring girder sections, including bus bar
31. Remove bogies
32. Load & transport dome parts

2.6 Deconstruction Cost Estimate & Schedule

A preliminary cost estimate was developed for the deconstruction activities and scope assumptions described above. The following outlines the estimate methodology and exclusions.

- Deconstruction labour:
    - Supervision & crane operators: includes import DSL supervision (superintendent + site engineer), local foreman, mobile crane operator, and oiler
    - Telescope & enclosure labour assumes local (Hawaiian) labour is used for deconstruction tasks described above. Labour rates are based on local union rates and a 54hr working week (6 days x 9hrs/day) with overtime and travel time applied per union agreements
    - Live-out and travel: includes daily live-out allowance, air travel, and travel time for shift turn-around for both import and local workers
    - Workers compensation insurance is included in the estimate
    - Labor hours include an efficiency factor of 1.6 to account for working at high altitude.
- Deconstruction equipment:
    - Large equipment: includes rental of 250t mobile crane, 25t rough-terrain crane, 2 x aerial boom lifts, and tractor trailer unit. Freight, fuel, mobilization and de-mobilization costs are included for all equipment. Includes temporary 40 ton dome crane.

  - Misc. equipment, tools & falsework: includes small equipment such as tools, compressors, welding equipment, consumables, temporary power distribution, and scaffolding. Includes 50 tonnes of falsework, including material, labour, and shipping costs.
  - Ground transport & trucking: includes purchase of 1 x SUV and 1 x pickup truck for worker transport and fuel. Includes trucking of deconstructed components from summit to Hilo.
- Contingency: a suggested overall contingency of 20% is applied
- Exclusions:
  - Scrapping: no costs have been including for scrapping of the structure other than trucking of the components from the summit to Hilo
  - Hazardous material disposal: costs have not been included for proper disposable of any hazardous materials (such as glycol or hydraulic fluid)
  - Crane access ways (compacted, level roadways suitable for moving large cranes)
  - Water supply, toilets, and first aid facilities
  - See also scope assumptions and exclusions in section 2.2 Deconstruction Assumptions above.

The cost estimate summary is given in the table below. Costs are given in 2012 US dollars.

Table 1: Deconstruction cost estimate

Deconstruction Labour		
	Supervision & crane operators	$871,992
	Telescope labour	$380,289
	Enclosure labour	$766,561
	Live-out & travel	$304,741
	Workers comp insurance	$521,565
	Total labour	**$2,845,148**
Deconstruction Equipment		
	Large equipment	$1,343,821
	Misc. equipment, tools & falsework	$396,951
	Ground transport & trucking	$198,638
	Total equipment	**$1,939,410**
Subtotal		**$4,784,558**
	Mark-Up (15%)	$717,684
	Contingency (20%)	$1,100,448
TOTAL		**$6,602,690**

A preliminary schedule for the deconstruction is shown below, assuming a nominal start date of Jan 1, 2014.

ID	Task Name	Predecessors	Duration
1	**CFHT Deconstruction**		**231 days**
2	Facility & site ready for telescope & enclosure deconstruction		0 days
3	**Telescope Deconstruction**		**95 days**
4	Remove top end and upper tubes with top end crane	2	4 days
5	Attach rigging/beams to arch girders	4	14 days
6	Erect center section of falsework	5	2 days
7	Install temporary support for east and west tube	6	3 days
8	Install temporary support for horse shoe	7	2 days
9	Prep horseshoe and east and west tubes	8	5 days
10	Remove horse shoe horn	9	3 days
11	Remove horse shoe center section	10	1 day
12	Remove east and west tubes	11	3 days
13	Remove south yok	12	2 days
14	Remove center section	13	3 days
15	Prep telescope floor and glycol lines	9	26 days
16	Remove telescope floor and glycol lines	14,15	13 days
17	Remove south pedestal	16	4 days
18	Remove north pedestal	17	4 days
19	Remove triangular base frame	18	4 days
20	Observatory floor clean up	19	7 days
21	Load truck	20	4 days
22	Remove rigging	21	3 days
23	**Enclosure Deconstruction**		**136 days**
24	Remove dome insulation	22	28 days
25	Remove shutter	22	7 days
26	Remove wind screen and drive system	25	4 days
27	Erect exterior work platforms on arch girders	26	2 days
28	Remove vent platform	27	4 days
29	Prep intermediate infill shell plates	28	28 days
30	Remove intermediate infill shell plates	29	4 days
31	Install temporary struts on arch	30	1 day
32	Remove rack at arch splices	31	1 day
33	Prep shell modules	32,24	5 days
34	Remove shell modules	33	11 days
35	Remove outer skirt	34	4 days
36	Adjust bogies	35	4 days
37	Prep arch falsework	36	3 days
38	Erect arch falsework	37	8 days
39	Connect arch girders to falsework tower	38	2 days
40	Gouge arch girder splices	39	3 days
41	Gouge tie beam	40	1 day
42	Prep back shell	41	2 days
43	Remove back shell and tie beam	42	4 days
44	Remove top end crane	43	3 days
45	Remove both arch center sections	44	1 day
46	Remove arch girder 4 interior sections	45	4 days
47	Remove arch girder 4 horn sections	46	2 days
48	Dismantle erection tower	47	6 days
49	Gouge ring girder sections	48	6 days
50	Erect temporary bogie supports	49	3 days
51	Remove ring girder	50	4 days
52	Remove bogies	51	3 days
53	Load and transport dome parts to port	52FF+6 days	23 days
54	Telescope & enclosure deconstruction complete	53	0 days

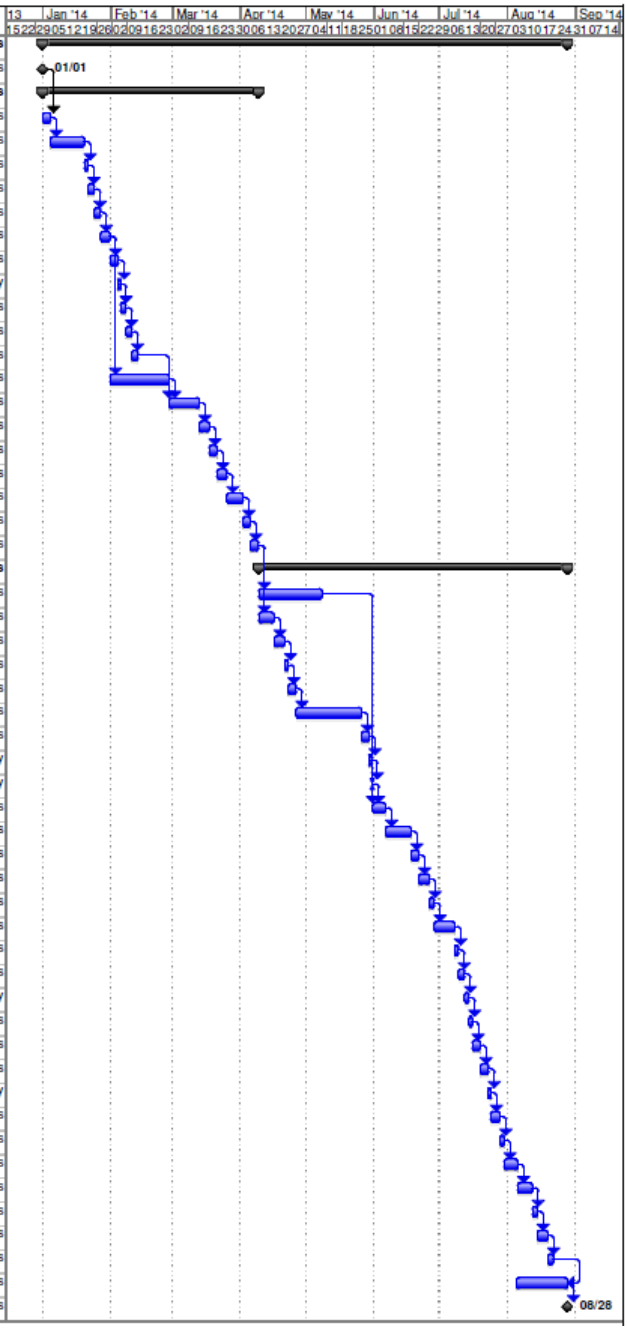

Figure 8: Preliminary deconstruction schedule

3. Outer Pier Structure Upgrade

The study done by DSL and UBC titled *"ngCFHT Telescope and Enclosure Configuration and Outer Pier Capacity Study"* in January 2012 revealed that diagonal braces along the outer steel pier need to be upgraded in order to meet the current design standards. The pier was designed and built in the mid-70s. The existing pier was analyzed under various combinations of loads, including wind, snow and seismic. The study determined that the diagonal braces on the outer pier do not meet the load requirements for seismic strength. Figure 9 below shows the pier under construction.

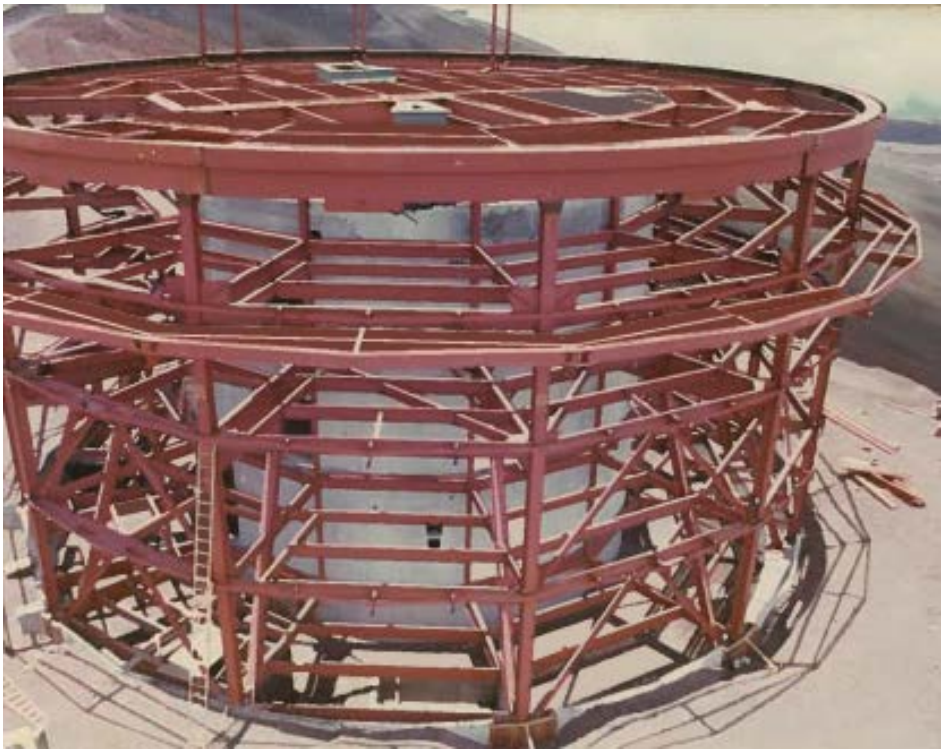

Figure 9: Existing CFHT Pier Structure

The previous report was reviewed and an estimate was developed for the cost and hours involving the upgrade. In addition, old drawings of the existing CFHT pier were reviewed to determine access and existing conditions.

3.1 Upgrade Assumptions

The following assumptions have been taken in order to estimate the hours:

1. The brace upgrade works will happen at the same time as enclosure deconstruction.
2. There are a total of 29 panels with braces, resulting in 58 individual braces in total.
3. The 25 ton RT crane used during the deconstruction phase will be utilized during brace upgrade works.
4. All access to braces inside the outer pier will be from outside. This work should be done under a tent that locally protects each opening from weather conditions.
5. The 4th floor cantilevered deck will be utilized for access to braces on the 4th floor. Access to remainder of floors will be via movable scaffolding.

6. New braces would be HSS 8x8x5/8 welded to new gussets plates on 1st, 2nd and 3rd floors.
7. New braces would be HSS 10x10x1/2 welded to new gusset plates on 4th floor.
8. The braces would be standard slotted HSS with reinforcing plates field welded to new gussets framed into existing beams and columns.

3.2 Brace Replacement Procedure

The following is a rough procedure outlining the main steps for removal and replacement of existing braces:

1. Setup scaffolding.
2. Cut exterior siding and remove along with insulation.
3. Setup and connect temporary strut underside of main ring beam on 4th floor only. This only applies to braces on 4th floor. A temporary strut is used to take the weight of outer ring beam, if required for safety. This step is omitted on other floors.
4. Gouge off gussets and braces.
5. Prep and clean up beam for fitting new gussets.
6. Fit and tack new gussets.
7. Hoist and install new braces.
8. Weld gussets and braces.
9. Apply fire retardant to new braces and gussets.
10. Re-install insulation and exterior siding and seal.
11. Move scaffolding to next panel.

3.2.1 Brace Upgrade Construction Schedule & Cost Estimate

A preliminary cost estimate was developed for the brace upgrade activities and scope assumptions described above. The following outlines the estimate methodology and exclusions.

- Construction labour:
    - Supervision & crane operators: includes import DSL supervision (superintendent shared from deconstruction phase), local foreman, mobile crane operator, and oiler also shared from the deconstruction phase.
    - Brace replacement labour assumes local (Hawaiian) labour is used for all tasks described above. Labour rates are based on local union rates and a 54hr working week (6 days x 9hrs/day) with overtime and travel time applied per union agreements
    - Live-out and travel: includes daily live-out allowance, air travel, and travel time for shift turn-around for both import and local workers
    - Worker's compensation insurance is included in the estimate
    - A labor efficiency factor of 1.6 has been applied to the estimated hours to account for effects of working at high altitude.
- Construction equipment:
    - Large equipment: includes rental of the 25t rough-terrain crane (shared during the deconstruction phase), and 2 x aerial boom lifts. Freight, fuel, mobilization and de-mobilization costs were included in the deconstruction phase. Therefore, these were not included in the costs for brace upgrade.
    - Misc. equipment, tools such as: compressors, welding equipment, consumables, temporary power distribution, and movable scaffolding included.

  - Ground transport & trucking: The cost of 2 pickups has been included along with fuel and maintenance for the additional crew responsible for brace replacement works.
- Contingency: a suggested overall contingency of 30% is applied. A higher rate is suggested due to some of the risk involved in such remediation project, where there is always some element of risk until the walls are actually opened to see actual conditions.
- **Exclusions**
  - Crane access ways (compacted, level roadways suitable for moving large cranes)
  - Water supply, toilets, and first aid facilities
  - See also scope assumptions and exclusions in sections 2.6 and above.
  - Permits

The cost estimate summary is given in the table below. Costs are given in 2012 US dollars.

Table 2: Outer Pier Upgrade Cost Estimate

Labour & Material		
	Supervision & crane operators	$131,131
	Live-out & travel	$104,945
	Brace Replacement Labor	$667,450
	Materials	$303,050
	Shipping	$58,870
	Insurance	$239,574
	Total labour	**$1,505,020**
Construction Equipment		
	Large equipment	$22,605
	Misc. equipment, tools & falsework	$180,528
	Ground transport & trucking	$90,212
	Total equipment	**$293,345**
Subtotal		**$1,798,365**
	Mark-Up (15%)	$269,755
	Contingency (30%)	$620,436
TOTAL		**$2,688,556**

The duration of this work is expected to take approximately 7 months with two crews of 2 welders, one helper and one foreman. The two crews would work in parallel as shown next page. A preliminary schedule for the brace upgrade works is shown below, assuming a nominal start date of Jan 1, 2014 (same start date as deconstruction phase). Note, the "lines" in tasks in schedule below refer to bay lines as depicted on the original CFHT architectural drawings.

ID	Task Name	Duration
1	**ngCFHT Brace Upgrade Works**	**192 days**
2	**Facility & site ready for brace upgrade work**	**192 days**
3	**Crew #1**	**192 days**
4	**Brace Replacement on 4th Floor**	**84 days**
5	Replace braces on panel between lines 1 & 2 on 4th floor	14 days
6	Replace braces on panel between lines 2 & 3 on 4th floor	14 days
7	Replace braces on panel between lines 3 & 4 on 4th floor	14 days
8	Replace braces on panel between lines 4 & 5 on 4th floor	14 days
9	Replace braces on panel between lines 5 & 6 on 4th floor	14 days
10	Replace braces on panel between lines 6 & 7 on 4th floor	14 days
11	**Brace Replacement on 3rd Floor**	**36 days**
12	Replace braces on panel between lines 1 & 2 on 3rd floor	12 days
13	Replace braces on panel between lines 3 & 4 on 3rd floor	12 days
14	Replace braces on panel between lines 5 & 6 on 3rd floor	12 days
15	**Brace Replacement on 2nd Floor**	**36 days**
16	Replace braces on panel between lines 1 & 2 on 2nd floor	12 days
17	Replace braces on panel between lines 3 & 4 on 2nd floor	12 days
18	Replace braces on panel between lines 5 & 6 on 2nd floor	12 days
19	**Brace Replacement on Ground Floor**	**36 days**
20	Replace braces on panel between lines 1 & 2 on Ground floor	12 days
21	Replace braces on panel between lines 3 & 4 on Ground floor	12 days
22	Replace braces on panel between lines 5 & 6 on Ground floor	12 days
23	**Crew #2**	**192 days**
24	**Brace Replacement on 4th Floor**	**84 days**
25	Replace braces on panel between lines 1 & 2 on 4th floor	14 days
26	Replace braces on panel between lines 2 & 3 on 4th floor	14 days
27	Replace braces on panel between lines 3 & 4 on 4th floor	14 days
28	Replace braces on panel between lines 4 & 5 on 4th floor	14 days
29	Replace braces on panel between lines 5 & 6 on 4th floor	14 days
30	Replace braces on panel between lines 6 & 7 on 4th floor	14 days
31	**Brace Replacement on 3rd Floor**	**36 days**
32	Replace braces on panel between lines 1 & 2 on 3rd floor	12 days
33	Replace braces on panel between lines 3 & 4 on 3rd floor	12 days
34	Replace braces on panel between lines 5 & 6 on 3rd floor	12 days
35	**Brace Replacement on 2nd Floor**	**36 days**
36	Replace braces on panel between lines 1 & 2 on 2nd floor	12 days
37	Replace braces on panel between lines 3 & 4 on 2nd floor	12 days
38	Replace braces on panel between lines 5 & 6 on 2nd floor	12 days
39	**Brace Replacement on Ground Floor**	**36 days**
40	Replace braces on panel between lines 1 & 2 on Ground floor	12 days
41	Replace braces on panel between lines 3 & 4 on Ground floor	12 days
42	Replace braces on panel between lines 5 & 6 on Ground floor	12 days
43	Brace Upgrade Works Complete	0 days

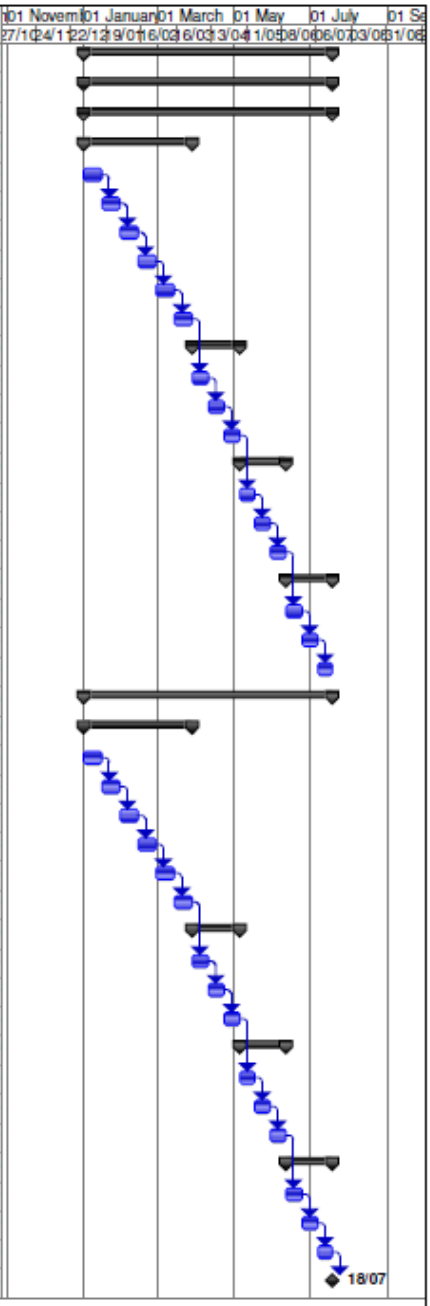

Page 1

Figure 10: Brace Upgrade Schedule

4. Foundations Assessment

The reappraisal of the footing and foundation of the ngCFHT Phase II work was performed by the UBC team. The objective of this work was to determine the capacity of the footing and foundation of the ngCFHT pier and enclosure by using recent design codes. This analysis was performed based on the ngCFHT Phase I work, the information, plans and reports from the original design. In conclusion it was found that no changes to the pier and enclosure footing and foundations are necessary. Please refer to **Appendix A - ngCFHT Foundation Capacity Study** for further details.

5. Manufacturing & Construction Plan

The proposed ngCFHT telescope and enclosure concept was presented by DSL and UBC in a previous study report titled "*ngCFHT Telescope and Enclosure Configuration and Outer Pier Capacity Study*" in January 2012. The proposed enclosure will have a calotte dome configuration, similar to TMT. Figure 11 shows views of the proposed enclosure on top of the existing enclosure pier along with names of the main enclosure components. The red line in Figure 11 represents the approximate division between vent and base structures. Figure 12 shows a cross-section view of the proposed enclosure and telescope inside.

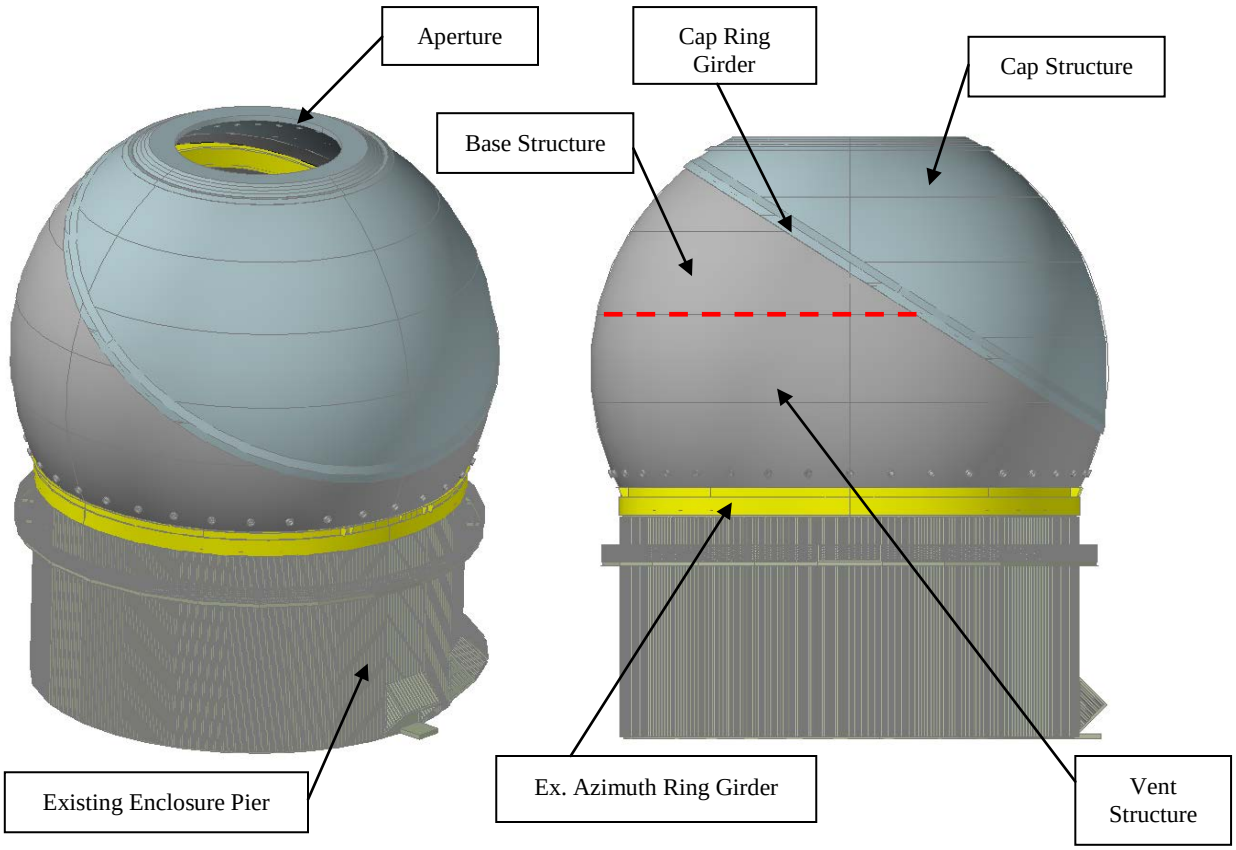

Figure 11: Proposed ngCFHT Enclosure Components

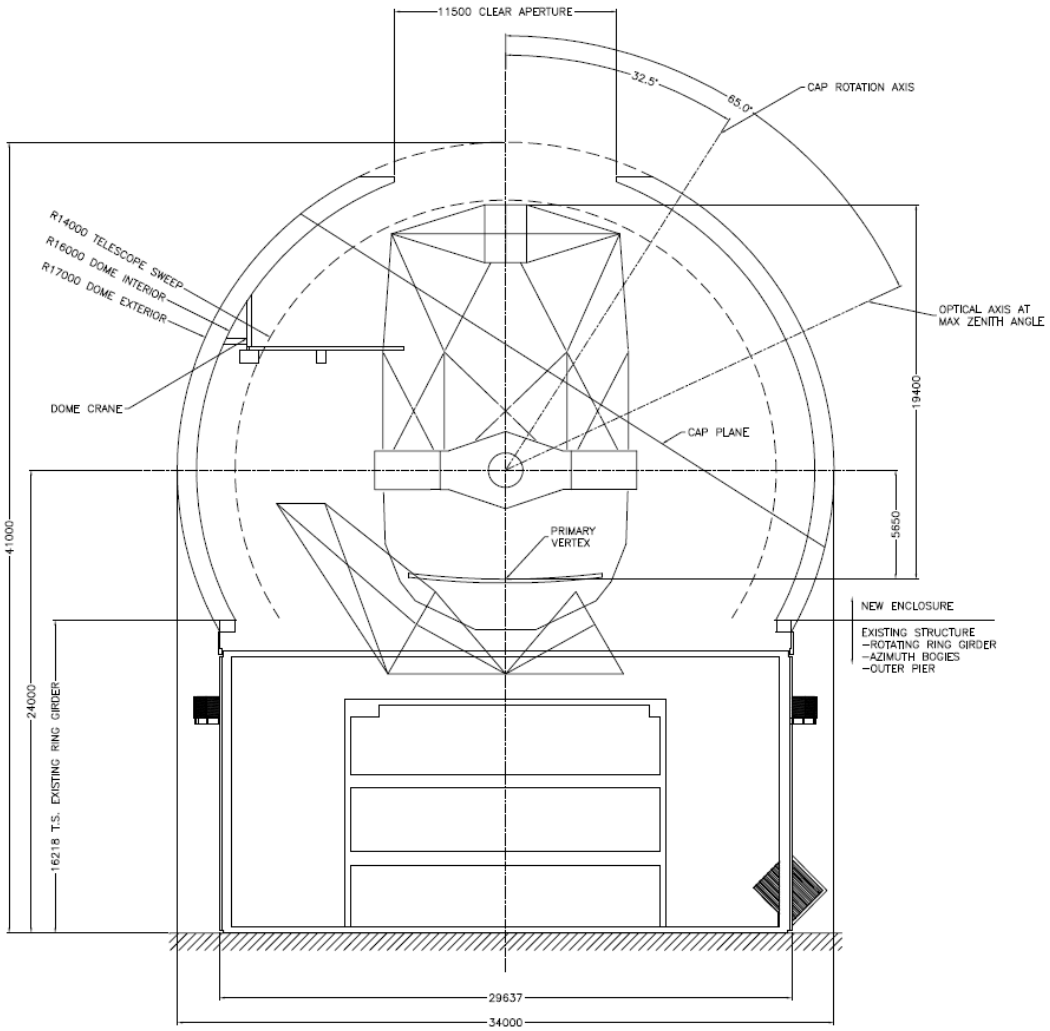

Figure 12: Cross-section of Proposed Telescope & Enclosure

The proposed telescope design is similar to Keck II. Figure 13 shows side and isometric views of the proposed telescope in a rough 3D model. Various telescope components referred to in the installation sequence are labeled in the following figure.

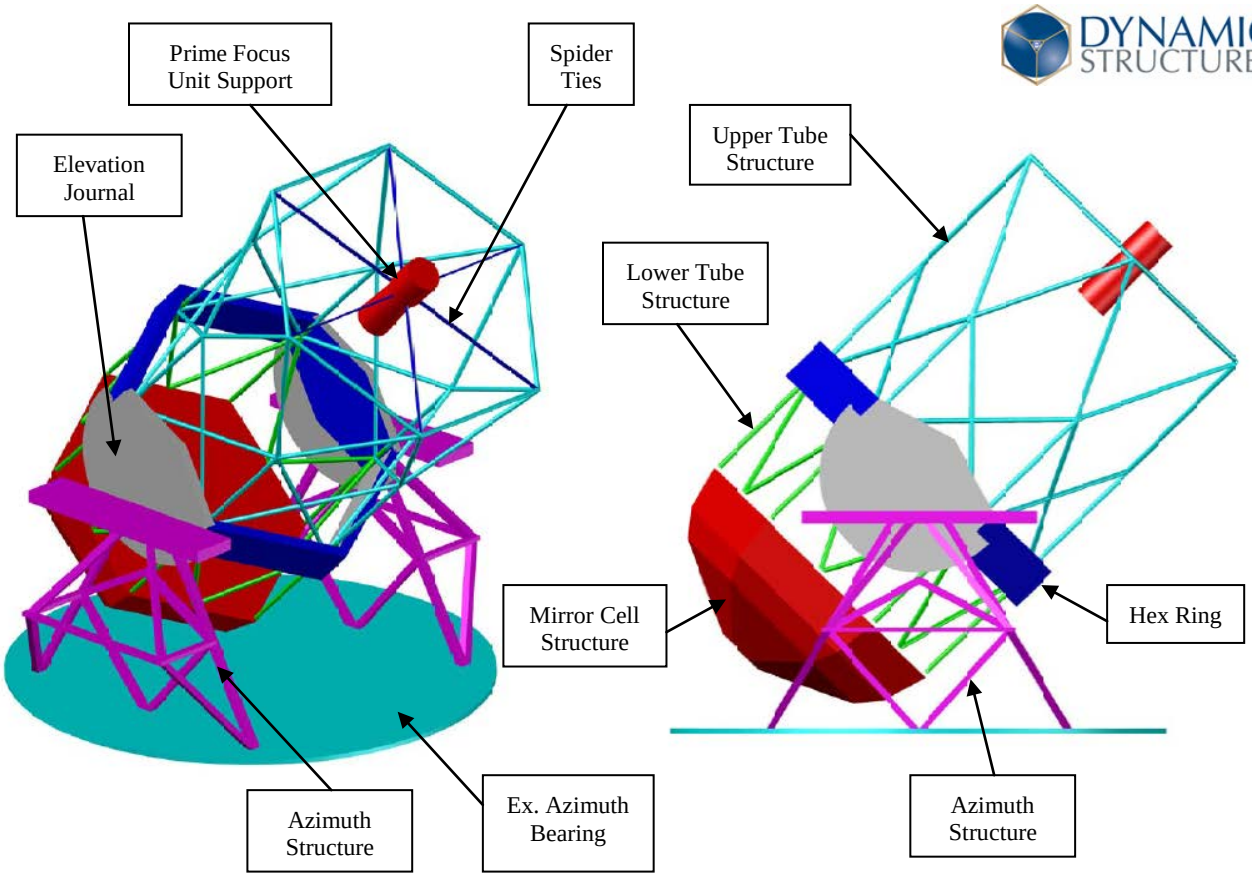

Figure 13: ngCFHT Telescope Components

5.1 Manufacturing Cost Estimate

Since the enclosure and telescope are at a very early conceptual level, the cost estimate is based largely on scaling from existing information, primarily the DSL estimate for TMT which provides the most recent estimating data for manufacturing costs for large optical telescopes. The TMT estimate itself utilizes data from previous DSL projects including the Gemini enclosures and the Keck enclosure and mount. Based on the cost estimating methodology the estimates are rough-order-of-magnitude at this point. The cost estimate below is based on Canadian Ironworkers Union manufacturing rates. For the telescope, trial assembly is assumed to include a factory trial assembly of the structural components, and does not include the dummy masses.

Table 3: ngCFHT enclosure manufacturing estimate

Enclosure Manufacturing		
	PM, Engineering, DO, Travel	$1,317,967
	Superstructure	$1,457,046
	Cladding	$317,379
	Insulation	$334,070
	Azimuth mechanical	$947,536
	Cap/base interface mechanical	$495,766
	Shutter structural/mechanical	$415,941
	Ventilation doors	$507,564
	Walkways, cranes	$765,674
	Electrical & control	$1,375,039
	Shipping	$747,089
Subtotal		**$8,681,073**
	Mark-Up (15%)	$1,302,161
	Contingency (20%)	$1,996,647
TOTAL		**$11,979,880**

Table 4: ngCFHT telescope manufacturing estimate

Telescope Manufacturing		
	PM, Engineering, DO, Travel	$2,984,111
	Azimuth Track	$437,422
	Azimuth Structure	$1,199,235
	Elevation Structure	$2,227,190
	Mechanical	$864,785
	Access Walkways	$756,391
	Utilities	$46,465
	Trial Assembly	$1,362,971
	Shipping	$787,879
Subtotal		**$10,666,449**
	Mark-Up (15%)	$1,599,967
	Contingency (20%)	$2,453,283
TOTAL		**$14,719,699**

5.2 Construction Plan

Construction of the ngCFHT is broken down into two phases: enclosure and telescope. Phase I: enclosure construction is assumed to start immediately after deconstruction of the existing enclosure and telescope. Phase II: telescope construction would ideally start after the enclosure is complete. Telescope installation may have a slight overlap with enclosure installation, since once the enclosure is secure, the telescope work could begin. Further discussion on construction schedules will be presented in subsection 5.2.4. The 250 ton

hydraulic crane used for deconstruction of the existing telescope will be used for erecting the ngCFHT. The installation sequence for the new calotte enclosure will be very similar to the sequence used on TMT. The following subsections summarize the main steps involving the construction of ngCFHT enclosure and telescope respectively.

5.2.1 Construction Assumptions

The following assumptions have been taken for enclosure construction:

1. The existing CFHT azimuth girder, bogies and drives **are not** re-used for the proposed ngCFHT enclosure and a new system is installed (this assumption can be revisited during future design and development work as it may provide cost savings).
2. Proposed enclosure has vent modules.
3. The crane remains in one location with the enclosure rotating during construction. Note this is the same 250ton crane using during deconstruction phase.
4. Falsework towers are designed to rotate with new enclosure structure during construction.

The following assumptions have been taken for telescope construction:

1. Telescope parts are fed through the aperture by the 250 ton hydraulic crane.
2. Telescope is constructed after enclosure is complete or substantially complete.
3. The telescope would be installed using special falsework and a combination of a mobile gantry crane and a dome mounted crane.
4. The telescope is constructed while pointing to zenith.

5.2.2 Enclosure Construction

The following summarizes the main steps for enclosure construction:

1. Prep summit site.
2. Prep pre-assembly site.
3. Start pre-assembly of vent, base and cap shell modules at the pre-assembly site at lower elevation. Shell modules are pre-assembled with skin plates and insulation. This is ongoing through most of the enclosure install phase, with the pre-assembly site trucking shell modules up to the summit.
4. Erect falsework towers.
5. Prep existing azimuth rail and bogies, ensure azimuth ring is set horizontal at correct elevation and get ready for vent module installation.
6. Install azimuth drives.
7. Erect ventilation modules and brace back into falsework.
8. Survey and align ventilation modules.
9. Erect base ring girder and cap bogies.
10. Erect base shell modules and brace back into falsework.
11. Align base ring girder and bogies.
12. Erect cap ring girder and align. Drive components installation is included in this step.
13. Erect shutter support structure and align.
14. Erect cap shell modules and brace back into falsework.
15. Erect shutter.
16. Perform overall survey of enclosure geometry and adjust as required.
17. Weld infill skin plates between pre-assembled modules.

18. Install infill insulation between pre-assembled modules.
19. Release enclosure from falsework towers.
20. Remove falsework towers.
21. Lower enclosure onto azimuth ring bogies.
22. Install seals.
23. Paint touch-up welded areas.
24. Install control system and electrical.
25. Site Acceptance Testing.

It should be noted that some of the steps above may be done in parallel as will be illustrated in the construction schedule in subsequent section.

5.2.3 Telescope Construction

The following summarizes the main steps for telescope construction:

1. Erect azimuth track sections and level.
2. Erect azimuth bogies/bearings.
3. Erect azimuth structure falsework.
4. Erect azimuth structures (both sides).
5. Erect mirror cell falsework.
6. Erect mirror cell structure.
7. Erect lower tube structure.
8. Survey and align mirror cell structure.
9. Survey and align lower tube structure.
10. Erect elevation journals.
11. Survey and align elevation journals.
12. Erect hex ring girders.
13. Survey and align hex ring structure.
14. Erect upper tube structure.
15. Survey and align upper tube members.
16. Erect spider ties on top of upper tube structure.
17. Install the prime focus unit support.
18. Check overall telescope geometry specially the mirror cell structure. Make adjustments as required.
19. Install hydraulic services (piping, power unit, etc)
20. Install drives, encoders and brakes.
21. Align brakes and drives.
22. Remove azimuth structure falsework.
23. Remove mirror cell falsework and transfer telescope weight to azimuth structures and azimuth bearing.
24. Install dummy mirror segments using dome mounted crane.
25. Install controls and electrical equipment.
26. Commission all drive systems.
27. Perform telescope site acceptance testing.
28. Remove dummy mirror segments and install actual mirror segments using dome mounted crane.

5.2.4 Construction Cost Estimate & Schedule

A preliminary cost estimate was developed for the construction activities and scope assumptions described above. The following outlines the estimate methodology and exclusions.

- Construction labour:
  - Due to lack of more specific information about the new enclosure and telescope, most of the construction activities and hours were adopted from detailed estimates done for TMT. For most cases, hours were scaled down by factor of 0.25 to convert from TMT hours to ngCFHT estimate. The new CFHT dome radius is approximately half of TMT's. Since typically costs are related to dome surface area which is a function of radius squared, the scale factor of 0.25 was derived to arrive at most of the labor hours. It should be noted that TMT estimated hours already included a labor efficiency factor of 1.6 to account for effects of high altitude.
  - Supervision & crane operators: includes import DSL supervision (superintendent + site engineer), local foreman, mobile crane operator, and oiler
  - Telescope & enclosure labour assumes local (Hawaiian) labour is used for all tasks described above. Labour rates are based on local union rates and a 54hr working week (6 days x 9hrs/day) with overtime and travel time applied per union agreements
  - Live-out and travel: includes daily live-out allowance, air travel, and travel time for shift turn-around for both import and local workers
  - Worker's compensation insurance is included in the estimate
- Construction equipment:
  - Large equipment: includes rental of 250t mobile crane, 25t rough-terrain crane, 2 x aerial boom lifts, and tractor trailer unit. Freight, mobilization and de-mobilization costs were included in the deconstruction phase. Therefore, these were not included. Fuel has been included for this equipment.
  - Misc. equipment, tools & falsework: includes small equipment such as tools, compressors, welding equipment, consumables, temporary power distribution, and scaffolding. This also includes 190 tonnes of falsework, including material, labour, and shipping costs.
  - Ground transport & trucking: these items were included in the deconstruction estimate. Only additional fuel and maintenance costs were accounted for the construction phase.
- Contingency: a suggested overall contingency of 20% is applied to the cost.
- **Exclusions**
  - Crane access ways (compacted, level roadways suitable for moving large cranes)
  - Water supply, toilets, and first aid facilities
  - See also scope assumptions and exclusions in sections 3.2.1 and above.
  - Permits

The cost estimate summary is given in the table below. Costs are given in 2012 US dollars.

Table 5: ngCFHT enclosure & telescope construction estimate

Enclosure Labour		
	Supervision & crane operators	$1,416,987
	Live-out & travel	$685,994
	Enclosure labour	$4,855,082
	Shipping	$979,697
	Insurance	$1,449,846
	Total Enclosure	**$9,387,605**
Telescope Labour		
	Supervision & crane operators	$1,307,988
	Live-out & travel	$534,064
	Enclosure labour	$2,392,314
	Shipping	$2,174,545
	Insurance	$1,097,082
	Total Telescope	**$7,505,993**
Construction Equipment		
	Large equipment	$4,093,665
	Misc. equipment, tools & falsework	$2,193,673
	Ground transport & trucking	$152,800
	Total equipment	**$6,440,138**
Subtotal		**$23,333,736**
	Mark-Up (15%)	$3,500,060
	Contingency (20%)	$5,366,759
TOTAL		**$32,200,556**

Enclosure construction was estimated to take approximately 12 months with a crew of 14 and 3 supervisors. Telescope construction was estimated to take approximately 12 months from start to finish with a crew of 10 and 3 supervisors. A preliminary schedule for the construction of ngCFHT enclosure is shown below, assuming a nominal start date of September 1, 2014. No explicit schedule contingency has been applied.

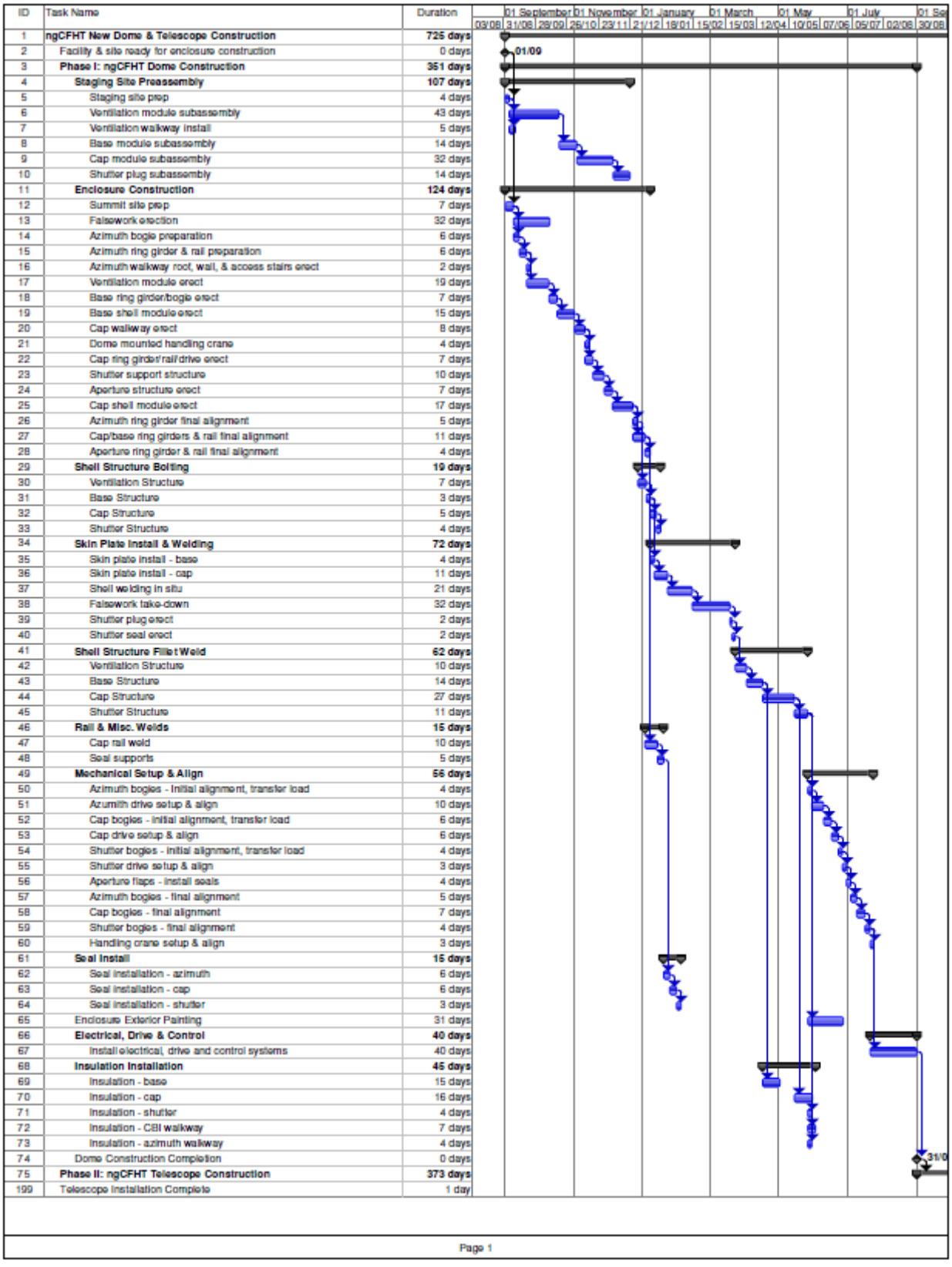

ID	Task Name	Duration
1	**ngCFHT New Dome & Telescope Construction**	**725 days**
2	Facility & site ready for enclosure construction	0 days
3	**Phase I: ngCFHT Dome Construction**	**351 days**
4	**Staging Site Preassembly**	**107 days**
5	Staging site prep	4 days
6	Ventilation module subassembly	43 days
7	Ventilation walkway install	5 days
8	Base module subassembly	14 days
9	Cap module subassembly	32 days
10	Shutter plug subassembly	14 days
11	**Enclosure Construction**	**124 days**
12	Summit site prep	7 days
13	Falsework erection	32 days
14	Azimuth bogie preparation	6 days
15	Azimuth ring girder & rail preparation	6 days
16	Azimuth walkway roof, wall, & access stairs erect	2 days
17	Ventilation module erect	19 days
18	Base ring girder/bogie erect	7 days
19	Base shell module erect	15 days
20	Cap walkway erect	8 days
21	Dome mounted handling crane	4 days
22	Cap ring girder/rail/drive erect	7 days
23	Shutter support structure	10 days
24	Aperture structure erect	7 days
25	Cap shell module erect	17 days
26	Azimuth ring girder final alignment	5 days
27	Cap/base ring girders & rail final alignment	11 days
28	Aperture ring girder & rail final alignment	4 days
29	**Shell Structure Bolting**	**19 days**
30	Ventilation Structure	7 days
31	Base Structure	3 days
32	Cap Structure	5 days
33	Shutter Structure	4 days
34	**Skin Plate Install & Welding**	**72 days**
35	Skin plate install - base	4 days
36	Skin plate install - cap	11 days
37	Shell welding in situ	21 days
38	Falsework take-down	32 days
39	Shutter plug erect	2 days
40	Shutter seal erect	2 days
41	**Shell Structure Fillet Weld**	**62 days**
42	Ventilation Structure	10 days
43	Base Structure	14 days
44	Cap Structure	27 days
45	Shutter Structure	11 days
46	**Rail & Misc. Welds**	**15 days**
47	Cap rail weld	10 days
48	Seal supports	5 days
49	**Mechanical Setup & Align**	**56 days**
50	Azimuth bogies - initial alignment, transfer load	4 days
51	Azumith drive setup & align	10 days
52	Cap bogies - initial alignment, transfer load	6 days
53	Cap drive setup & align	6 days
54	Shutter bogies - initial alignment, transfer load	4 days
55	Shutter drive setup & align	3 days
56	Aperture flaps - install seals	4 days
57	Azimuth bogies - final alignment	5 days
58	Cap bogies - final alignment	7 days
59	Shutter bogies - final alignment	4 days
60	Handling crane setup & align	3 days
61	**Seal Install**	**15 days**
62	Seal installation - azimuth	6 days
63	Seal installation - cap	6 days
64	Seal installation - shutter	3 days
65	Enclosure Exterior Painting	31 days
66	**Electrical, Drive & Control**	**40 days**
67	Install electrical, drive and control systems	40 days
68	**Insulation Installation**	**45 days**
69	Insulation - base	15 days
70	Insulation - cap	16 days
71	Insulation - shutter	4 days
72	Insulation - CEI walkway	7 days
73	Insulation - azimuth walkway	4 days
74	Dome Construction Completion	0 days
75	**Phase II: ngCFHT Telescope Construction**	**373 days**
199	Telescope Installation Complete	1 day

Page 1

A preliminary schedule for the construction of ngCFHT telescope is shown below, assuming a nominal start date of September 1, 2015.

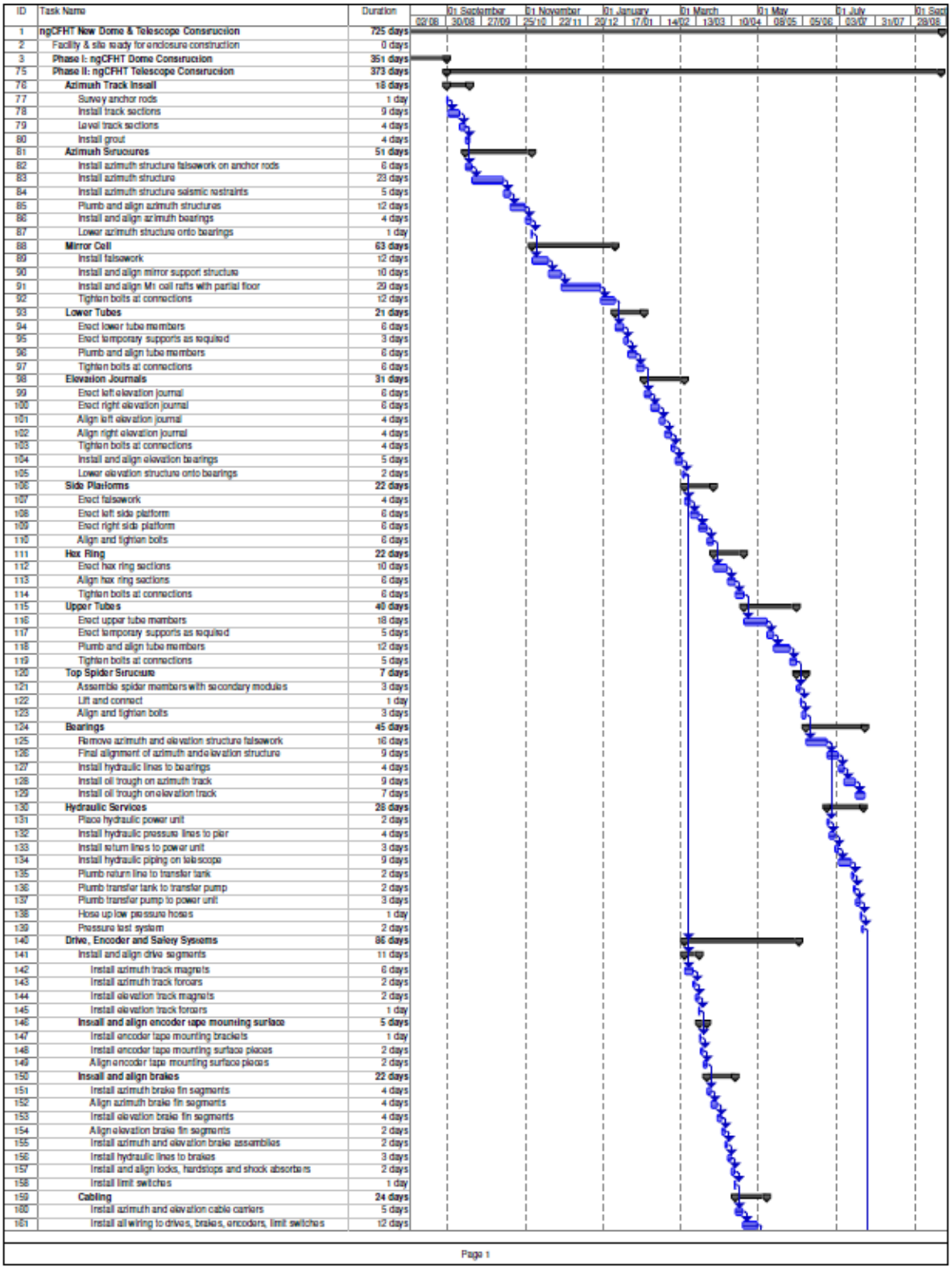

ID	Task Name	Duration
1	**ngCFHT New Dome & Telescope Construction**	**725 days**
2	Facility & site ready for enclosure construction	0 days
3	**Phase I: ngCFHT Dome Construction**	**351 days**
75	**Phase II: ngCFHT Telescope Construction**	**373 days**
76	**Azimuth Track Install**	**18 days**
77	Survey anchor rods	1 day
78	Install track sections	9 days
79	Level track sections	4 days
80	Install grout	4 days
81	**Azimuth Structures**	**51 days**
82	Install azimuth structure falsework on anchor rods	6 days
83	Install azimuth structure	23 days
84	Install azimuth structure seismic restraints	5 days
85	Plumb and align azimuth structures	12 days
86	Install and align azimuth bearings	4 days
87	Lower azimuth structure onto bearings	1 day
88	**Mirror Cell**	**63 days**
89	Install falsework	12 days
90	Install and align mirror support structure	10 days
91	Install and align M1 cell rafts with partial floor	29 days
92	Tighten bolts at connections	12 days
93	**Lower Tubes**	**21 days**
94	Erect lower tube members	6 days
95	Erect temporary supports as required	3 days
96	Plumb and align tube members	6 days
97	Tighten bolts at connections	6 days
98	**Elevation Journals**	**31 days**
99	Erect left elevation journal	6 days
100	Erect right elevation journal	6 days
101	Align left elevation journal	4 days
102	Align right elevation journal	4 days
103	Tighten bolts at connections	4 days
104	Install and align elevation bearings	5 days
105	Lower elevation structure onto bearings	2 days
106	**Side Platforms**	**22 days**
107	Erect falsework	4 days
108	Erect left side platform	6 days
109	Erect right side platform	6 days
110	Align and tighten bolts	6 days
111	**Hex Ring**	**22 days**
112	Erect hex ring sections	10 days
113	Align hex ring sections	6 days
114	Tighten bolts at connections	6 days
115	**Upper Tubes**	**40 days**
116	Erect upper tube members	18 days
117	Erect temporary supports as required	5 days
118	Plumb and align tube members	12 days
119	Tighten bolts at connections	5 days
120	**Top Spider Structure**	**7 days**
121	Assemble spider members with secondary modules	3 days
122	Lift and connect	1 day
123	Align and tighten bolts	3 days
124	**Bearings**	**45 days**
125	Remove azimuth and elevation structure falsework	16 days
126	Final alignment of azimuth and elevation structure	9 days
127	Install hydraulic lines to bearings	4 days
128	Install oil trough on azimuth track	9 days
129	Install oil trough on elevation track	7 days
130	**Hydraulic Services**	**28 days**
131	Place hydraulic power unit	2 days
132	Install hydraulic pressure lines to pier	4 days
133	Install return lines to power unit	3 days
134	Install hydraulic piping on telescope	9 days
135	Plumb return line to transfer tank	2 days
136	Plumb transfer tank to transfer pump	2 days
137	Plumb transfer pump to power unit	3 days
138	Hose up low pressure hoses	1 day
139	Pressure test system	2 days
140	**Drive, Encoder and Safety Systems**	**86 days**
141	Install and align drive segments	11 days
142	Install azimuth track magnets	6 days
143	Install azimuth track forcers	2 days
144	Install elevation track magnets	2 days
145	Install elevation track forcers	1 day
146	**Insall and align encoder tape mounting surface**	**5 days**
147	Install encoder tape mounting brackets	1 day
148	Install encoder tape mounting surface pieces	2 days
149	Align encoder tape mounting surface pieces	2 days
150	**Insall and align brakes**	**22 days**
151	Install azimuth brake fin segments	4 days
152	Align azimuth brake fin segments	4 days
153	Install elevation brake fin segments	4 days
154	Align elevation brake fin segments	2 days
155	Install azimuth and elevation brake assemblies	2 days
156	Install hydraulic lines to brakes	3 days
157	Install and align locks, hardstops and shock absorbers	2 days
158	Install limit switches	1 day
159	**Cabling**	**24 days**
160	Install azimuth and elevation cable carriers	5 days
161	Install all wiring to drives, brakes, encoders, limit switches	12 days

ID	Task Name	Duration
182	Install hydraulic lines for elevation bearings	1 day
183	Install utility distribution lines	3 days
184	Adjust cable wraps with partial cable load	3 days
185	**Dummy Masses**	**24 days**
186	Install primary mirror segment dummy masses	21 days
187	Install tertiary dummy mass	1 day
188	Install laser room dummy mass	2 days
169	**Drive System Commissioning**	**42 days**
170	**Static Test**	**8 days**
171	Test oil supply system	2 days
172	Anchor elevation top end structure with cable/winch	2 days
173	Static test elevation and azimuth bearings	2 days
174	Static test elevation and azimuth brake systems	2 days
175	**Test azimuth drive system**	**19 days**
176	Check clearances and adjust alignment	3 days
177	Set up measuring equipment	3 days
178	Apply pressure to Azimuth bearings	2 days
179	Rotate azimuth structure using winch	2 days
180	Check clearances and adjust alignments	3 days
181	Test azimuth drive system	6 days
182	**Coarse balance elevation structure**	**15 days**
183	Set up measuring equipment to monitor clearances	2 days
184	Apply pressure to elevation bearings	2 days
185	Apply force to top end structue w/ winches	5 days
186	Rotate elevation structure to horizon w/ winches	2 days
187	Check clearances and adjust alignments	4 days
188	**Telescope Acceptance Testing**	**15 days**
189	**Perform dimensional acceptance tests**	**4 days**
190	Critical axes alignments	2 days
191	M1 cell	2 days
192	**Mount control system functional and performance tests**	**8 days**
193	Range of motion tests	2 days
194	Limit switch and lock functional tests	2 days
195	Brake performance test	2 days
196	Drive and encoder performance tests	2 days
197	**Test segment handling crane**	**2 days**
198	**Test utility services**	**2 days**
199	Telescope Installation Complete	1 day

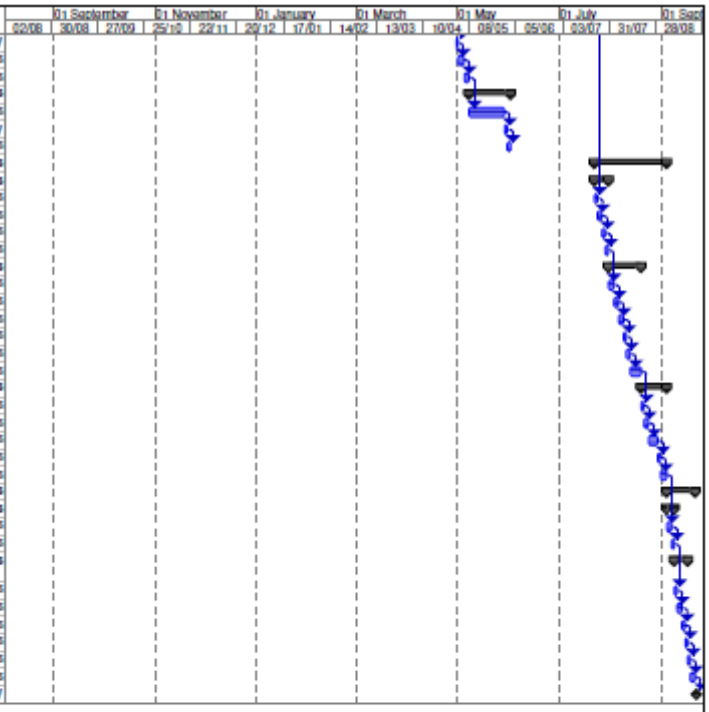

Page 2

6. Conclusions

This report outlined a programmatic study for the upgrade of the telescope structure and enclosure for the CFHT observatory. This includes the deconstruction of the existing CFHT telescope and enclosure, reinforcement of the existing outer pier structure that supports the enclosure, and the manufacture, shipping, and construction of the Next Generation CFHT enclosure and telescope structure. Further investigation of the telescope pier indicates that with the present assumptions the pier foundation will not need any remedial work to support the new telescope structure to current design codes. The next phases of design and development should focus on developing conceptual and preliminary designs for the enclosure and telescope structures.

A cost summary for the overall deconstruction, upgrade, and manufacture and construction of the enclosure and telescope structures is given in the table below. The costs shown include contingencies as outlined in the more detailed costing tables in this report.

Table 6: ngCFHT cost and schedule summary for enclosure and telescope structure

PHASE	Cost	Year 1				Year 2				Year 3				Year 4				Year 5			
	[2012 USD]	Q1	Q2	Q3	Q4	Q1	Q2	Q3	Q4	Q1	Q2	Q3	Q4	Q1	Q2	Q3	Q4	Q1	Q2	Q3	Q4
Design - Enclosure	$ 11,979,880																				
Manufacture - Enclosure																					
Design - Telescope	$ 14,719,699																				
Manufacture - Telescope																					
Deconstruction - Telescope	$ 6,602,690																				
Deconstruction - Enclosure																					
Outer Pier Upgrade	$ 2,688,556																				
Construction - Enclosure	$ 32,200,556																				
Construction - Telescope																					
Total	**$ 68,191,381**																				

APPENDIX A: ngCFHT Foundation Capacity Study (Phase II)

By Drs. Wu Di, Stiemer, Liu, and Mr. Angers

University of British Columbia

October 24rd 2012

Table of Contents

List of Tables

List of Figures

1. Executive Summary

This report presents a reappraisal study on the Next Generation Canada-France-Hawaii Telescope (ngCFHT). In Phase I of the ngCFHT work, the telescope concrete pier and the enclosure capacity were studied by the UBC team while the development of the telescope properties and azimuth track were studied by DSL.

In this report, the reappraisal of the footing and foundation of the ngCFHT Phase II work was performed by the UBC team. The objective of this report is to determine the capacity of the footing and foundation of the ngCFHT pier and enclosure by using recent design codes. This analysis was performed based on the ngCFHT Phase I work, the information, plans and reports from the original design.

1.1 Findings in Summary

1.1.1 Pier Footing and Foundation Evaluation

- The differential settlements were evaluated to be less than 10.0 mm and satisfactory.
- The soil allowable bearing capacity under gravity loads is sufficient as the estimated pressure induced by the footing was equal to the capacity.
- The bearing capacity of the soil under earthquake loads is exceeded by 33%. Since the structure having been designed in 1974, the soil capacity of existed building can increase over time. Also because of the dynamic nature of these loadings, it is common practice to increase the capacity by one-third. This allows considering the capacity as sufficient.

1.1.2 Enclosure Footing and Foundation Evaluation

The larger dome inducing higher forces to the enclosure and the new code requirements justify assessing the capacity of the outer pier. The seismic requirements were analyzed with great care since the modern codes prescribes much higher demands than the ones from the original design. The load cases and combinations were defined using the ASCE-7 2010 requirements. The capacity of the footing and foundation were evaluated. The following points were concluded:

- The footings have sufficient bending, shear and tension structural capacity to resist the demands of every load combination. The ratios of demand to capacity are under 0.50.
- The maximum bearing pressure induced by the footing to the foundation is 97% of the 161 kPa bearing capacity. The sliding capacity is also sufficient since the demand to capacity ratio is of 0.74.

1.2 Conclusion

No changes to the pier and enclosure footing and foundations are necessary. No cost and schedule estimates needed.

Figure shows the finished pier building with the enclosure steel frame walls during construction.

Figure 1: CFHT pier building during the dome support construction (CFHT, 1974, with permission)

2. Methodology and assumptions

The following steps were pursued to successfully completed during the assessment.

1. Building codes and design requirements to be used.
2. Load cases and load combinations definition.
3. Creation of a finite element model (FEM) of the structure.
4. Static and dynamic analysis of the structure.
5. Capacity checks
   a. Footing
   b. Foundation (Deflections)
6. Conclusions on the performance of the structure checked parts.

3. Pier Footing and Foundation Evaluation

3.1 Applicable Code

The loads and design requirements are defined by the International Building Code (IBC, 2006) and American Society of Civil Engineers 7 - Minimum Design Loads of Buildings and Other Structures (ASCE-7, 2005) which are the regulations in place in Hawaii. These forces were compared to the capacities of the different components that were evaluated according to the American Concrete Institute code (ACI, 2008). The evaluation of the structure and footing was done using limit state design (LSD), and the soil foundation was assessed using allowable stress design (ASD). The LSD approach insures that the different limit states are respected, for example the bending capacity of a beam, assuming a certain probability of rupture. The security associated with the limit state is dependent on the variability of the resistance and of the loads. Factors are applied to the loads and capacities to achieve that goal. The ASD philosophy is to make sure the service loads are under the elastic limit. This limit is usually reduced by a factor of safety, which is usually three (3) for foundation design.

3.2 Geometry

The pier building is a three storey reinforced concrete cylindrical pier structure. It has a 16.3 m diameter and is 14.4 m high. The walls are 304.8 mm thick over its whole height. The slabs of the first and second storey are hollow slab and 711 mm thick. The voids in the slabs are rectangular and have 914 x 914 x 356 mm dimensions. The top slab is a 304.8 mm thick slab. The first storey is 6.3 m high with an opening of 5.8 m wide and 3.2 m high. The second and third storeys are 4.0 m high and have three openings of 1020 x 2080 mm and one opening of 1800 x 2080 mm each. The foundation is a ring footing of 610 mm thickness and 2240 mm width. More details on the bar sizes and spacing are provided in the plans (CFHT, 1974).

3.3 Materials

Concrete compressive strength (f'_c) is 20.7 MPa and the elasticity modulus (E_c) was evaluated to be 21525 MPa according to the ACI (2008) with equation 1. Equation 1 has to be used with imperial units.

$$E_c = 57000\sqrt{f'_c} \quad (1)$$

The reinforcing bars have a yielding strength of 413 MPa and an elasticity modulus of 200 000 MPa.

3.4 Soil

Soil data was taken from the Foundation Investigation Report prepared by Dames & Moore (1973). The evaluated maximum soil pressure capacity was of 191 kPa. The Design Criteria & Basis of Calculations for Concrete Telescope Support states that "Dames & Moore believes the maximum safe bearing pressure under the central pier slab on unfortified soil to be 4000 psf (191 kPa), from the standpoint of bearing capacity and differential settlement of less than 10.0 mm".

Also, the report states that the water level is much below the surface. The footing top is located 2.5 m below the soil surface. The soil under the foundation consists of "sand and gravel size volcanic ash and cinders with occasional clinkers up to 152 mm. The ash is similar to furnace slag." (Dames & Moore, 1973). The density of such soil varies from 700 kg/m^3 to 2300 kg/m^3 (Dames & Moore, 1973). In the calculation, an average of 1800 kg/m^3 was assumed for simplicity.

3.5 Loads

ASCE-7 (2005) defines the load cases and combinations to be considered for the design of a new structure; these were used as the loads that have to be resisted by the existing structure.

Structural Weights

In order to assess the pier building, details on the new telescope were required. At this stage, only a simple telescope model was developed as a steel frame idealization. The telescope steel frame idealization was modeled following the recommendation by Gedig (EDS, 2011). The proposed model is shown in Figure . The location of the telescope center of gravity (H) is 7.0 meter over the top slab of the pier structure. The radius is that of the pier building and is equal to 8.15 m. The mass of the telescope (M) is approximated to 270 000 kg compared to 255 000 kg for the old telescope. The mass is attached to the pier via truss steel frame elements forming a pyramidal structure. This pyramidal frame is supported at four locations on hydraulic bearings to allow rotation of the telescope around its vertical axis. The four bearings are spaced equally at a distance (B) of 11.53 m. The bearings are idealized as linear springs with radial stiffness (K_r), tangential stiffness (K_t) and vertical stiffness (K_z). The bearings are sliding on the azimuth track that is itself supported by the ring girder. The ring girder is placed on the pier wall perimeter. The actual design of these components is beyond the scope of this project and will be done in further studies.

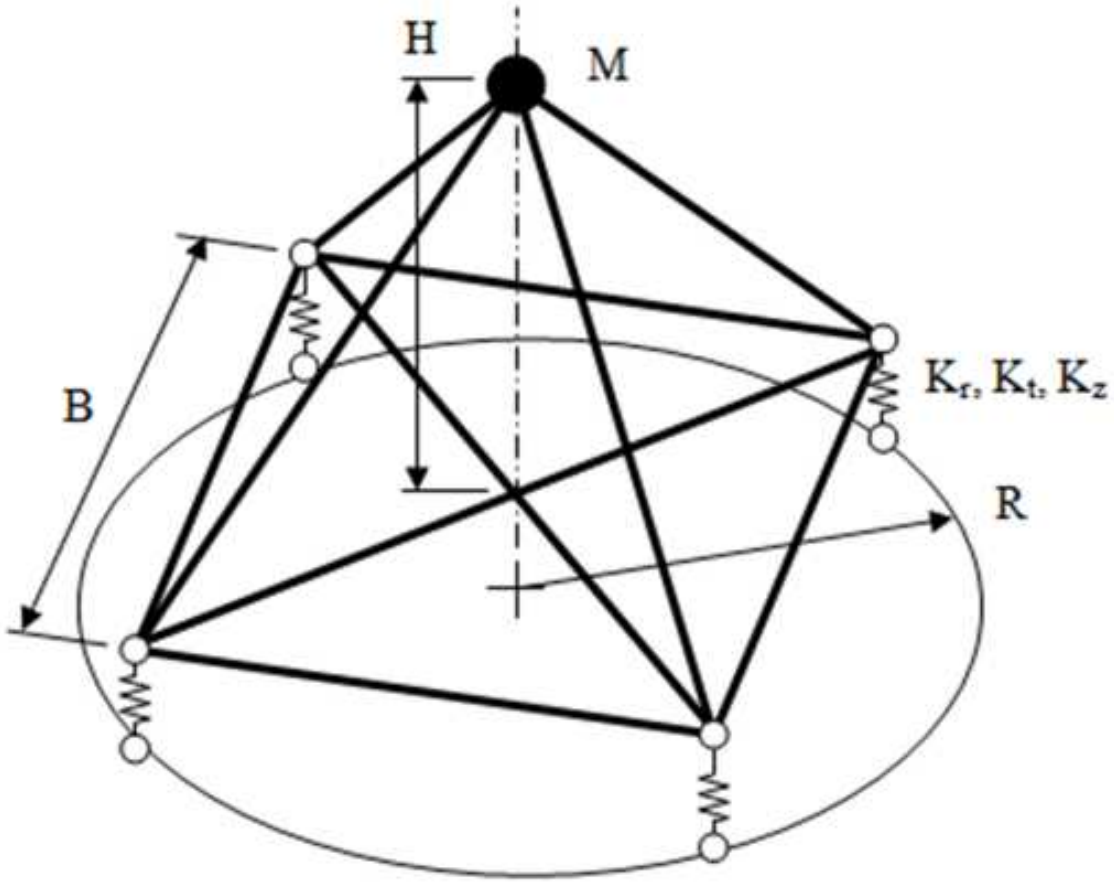

Figure 2: Idealization of the telescope frame, bearings and ring girder

3.5.1 Load Cases

It was considered that the loads to which the structure is submitted are the dead, live, and seismic loads. Wind loads were ignored because the enclosure covering the pier is isolated from the pier. The dead load includes the self weight of the structure and telescope mass. The live loads are the equipment and people loads. The live load values were taken from the document "Design Criteria & Basis of Calculations for Concrete Telescope Support" furnished by the CFHT.

Structures are subjected to different types of loadings. These loads vary more or less in time. If they are not varying excessively over time they can be considered as static, like dead loads. But, in certain cases, this assumption may not be possible or realistic. It is the case of wind, pedestrian or earthquake loadings that are dynamic loads. The response of the structure is then varying with time. The displacement, velocity and acceleration of the structure are the parameters that need to be evaluated. A structure can be analyzed either as a single degree of freedom (SDOF) or multi degree of freedom (MDOF) system.

Particular attention was paid to seismic analysis since the Mauna Kea is located in a high seismic zone and that older codes are not as severe regarding seismic requirements. For that reason, the seismic analysis is described in details in this section.

3.5.2 Load Combinations

For the evaluation of the pier walls, slabs, and footings, the limit state design procedure is used. The dead load (D), live load (L) and earthquake load (E) are factored and then combined according to the ASCE-7 (2005) requirements.

$$1.4D \tag{2}$$

$$1.2D + 1.6L \tag{3}$$

$$(0.9 - 0.2)D + 1.0E \tag{4}$$

$$(1.2 + 0.2D) + 1.0E \tag{5}$$

The combinations that include earthquake loads have a portion of their dead load added or removed to account for vertical vibration. The seismic loads were applied with different orientations to the structure. The forces, reactions and displacements were evaluated assuming the structure to remain in its elastic range. The forces induced by these factored loads were compared to the factored capacities.

The design of the foundation was realized using allowable stress design. Different load combinations were used and vertical vibration could be neglected as stated in the ASCE-7 (2005):

$$1.0D \tag{6}$$

$$1.0D + 1.0L \tag{7}$$

$$1.0D + 0.525E + 0.75L \tag{8}$$

$$1.0D + 1.0E \tag{9}$$

$$0.6D + 0.7E \tag{10}$$

The pressure induced by these loads under the footing was compared to the bearing capacity to which a safety factor was applied.

3.6 Evaluation

3.6.1 Footing

The structural capacity of the footings also needed to be assessed. The shear and flexural capacities have to exceed the forces at the supports due to the different load combinations. The evaluated foundation cross section is shown in the Figure . The footing of the pier structure was assumed to be a continuous footing. The footing was assumed to be linear between each node where the forces were evaluated. The capacity was evaluated at each of these nodes.

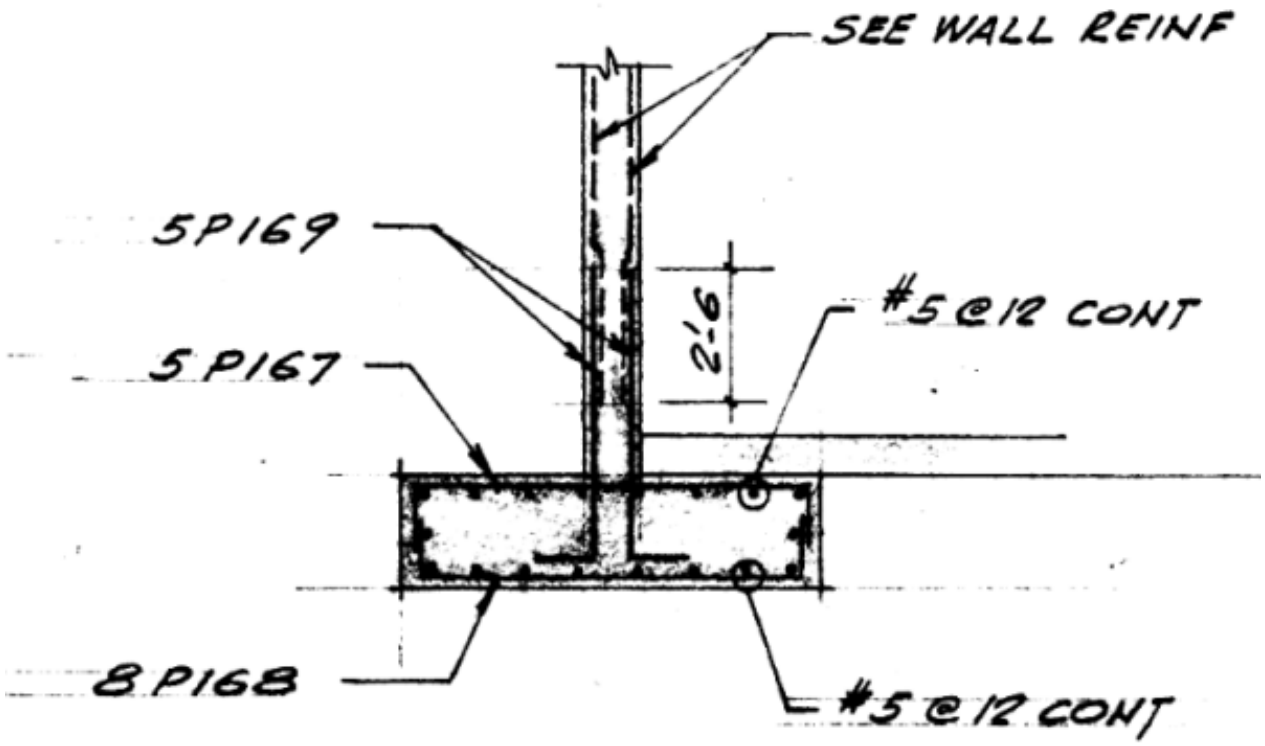

Figure 3: Foundation cross section and reinforcement detail (CFHT, 1974, with permission)

The vertical shear capacity of the footing was first evaluated. Only one-way shear needs to be checked for a continuous footing. Equation 41 has to be met in order to have a satisfactory design.

$$V_u \leq \varphi V_n \tag{11}$$

The factored shear force on critical shear surface (V_u) is described in Equation 42 (Coduto, 2001).

$$V_u = P_u\left(\frac{B-c-2d}{B}\right) \tag{12}$$

Where P_u is the factored applied compressive load, c the width of the wall, B is the width of the footing and d is the effective depth.

The capacity (V_n) is the summation of the shear load capacity of concrete (V_c) and of steel (V_s). Since there are no ties contributing to the shear capacity, the total shear capacity is that of concrete. The shear capacity is the capacity of concrete, and according to Coduto (2001) the shear capacity in a footing is equal to:

$$V_n = V_c = \frac{1}{6}2bd\sqrt{f'_c} \tag{13}$$

Where b is the length of critical shear surface. The results indicate that the shear capacity is high enough and would resist the forces induced by all load combinations. The maximum ratio of factored shear force over factored capacity was found to be 0.48.

It was also required to evaluate if the flexure design of the footing meets the requirements. First, longitudinal steel, which are the bars parallel to the wall length, should be present in sufficient quantity in the footing to resist flexural stresses from non-uniform loading and soft spots in the soil. Also, longitudinal steel should be present in sufficient amount to resist temperature and shrinkage stresses (Coduto, 2001). The minimum ratio

of steel that should be present to resist these constraints is $0.002A_g$. This criterion was found to be respected for the pier building footing since the amount of steel is $0.0026A_g$.

Transverse steel should also be assessed. The required ratios of reinforcement (A_s) were evaluated for each load combination at each section. The next equations (Equations 44 and 45) from Coduto (2001) can be used.

$$A_s = \left(\frac{f'_c b}{1.176 f_y}\right)\left(d - \sqrt{d^2 - \frac{2.353 M_{uc}}{\varphi f'_c b}}\right) \quad (14)$$

$$M_{uc} = b\left(\frac{\left(\frac{P_u}{b}\right)l^2}{2B} + \frac{2\left(\frac{M_u}{b}\right)l}{B}\right) \quad (15)$$

Where M_{uc} is the factored moment at critical section, M_u is the factored applied moment load perpendicular to wall, φ is equal to 0.9 and l is the distance from edge of the wall to the edge of the footing. These ratios were all found to be smaller than the steel ratios present in the structure. The footing was therefore considered to have enough structural shear and flexural capacity.

3.6.2 Foundation

3.6.2.1 Settlements

The "Final Investigation Report" by Dames & Moore (1974) states that the differential settlements should be kept to less than 10 mm. The settlements were evaluated using the plate bearing deflection curves. The plate load test consists of applying a loading at the height of the footing on a square steel plate to get the in-situ load-settlement data (Coduto, 2001). This method is not proven to be reliable because of the plate size that is much smaller than the foundation dimension. The depth under which the plate settles is smaller than for the real foundation and is only accounting for the soil close to the plate. Failures have been observed using this method (Terzaghi and Peck, 1967). But, because not much information on the soil properties was available to allow the use of more up-to-date methods, the plate load test results were used. The results therefore have to be considered with care.

Figure shows the curves of two tests realized at the site. For simplicity the deformations were assumed to be elastic. The pressures from the finite element model for the load case D + L were used. The maximum pressure around the ring footing was found to be 194 kPa and the minimum pressure, 153 kPa. To obtain conservative results, the maximum deflection was evaluated with the steepest curve (Test #2 on Figure) and the minimum deflection was calculated with the least steep curve (Test #1 on Figure). The maximum deflection was approximately 4.1 mm and the minimum, 0.5 mm. This gave a differential settlement of 3.6 mm. Using this method, a pressure of approximately 343 MPa would be required to achieve a 10 mm settlement.

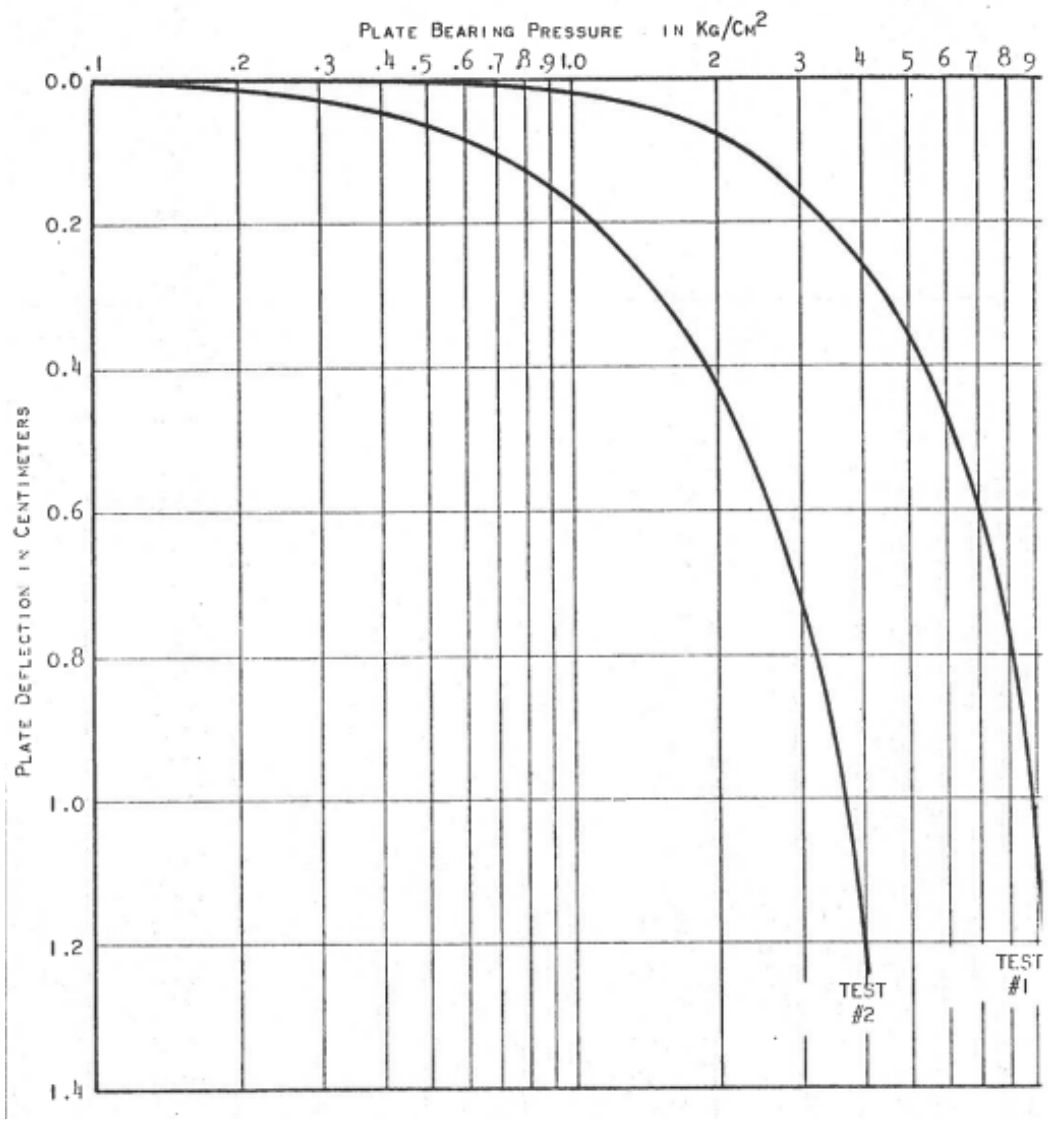

Figure 4: Plate bearing deflection curves (Dames & Moore, 1974, with permission)

It can be observed on Figure that there is significant variability in the results of both tests. This suggests that more testing would be required.

As stated earlier, even if he plate load test can lead to unconservative results, the maximum differential settlement was found to be 36% of the allowable one, which can be considered acceptable.

3.6.2.2 Soil Capacity

The allowable stress design load combinations applied to the pier building induce forces at the base of the structure. These forces are resisted to by the footings that distribute them to the soil. A bigger area of foundation results in a lower pressure applied to the soil. This bearing pressure induces compressive and shear stresses in the soil. When the shear stresses are high enough, they may exceed the shear strength of the soil, which is called a bearing failure (Coduto, 2001). Generally, three types of failure can occur: general

shear failure, local shear failure and punching shear failure. For shallow foundation, it is generally only necessary to check for general shear failure. See Figure for a representation of a general shear failure.

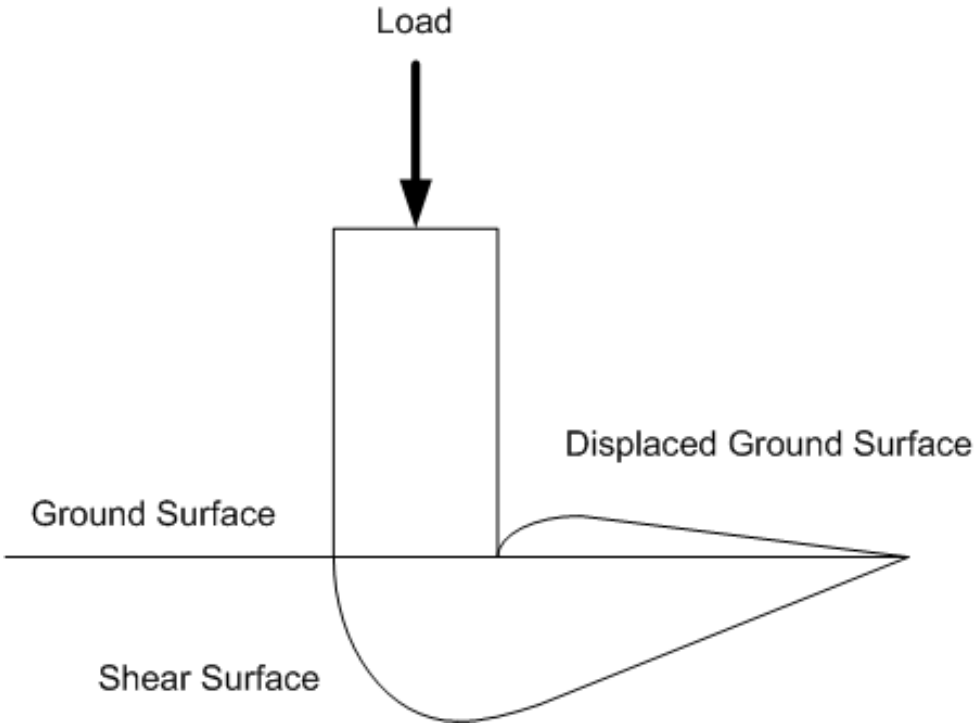

Figure 5: General shear failure of a shallow foundation

The pressure distributed by the footing at each node of the modeled structure was compared to the capacity. Different methods are available to evaluate this requirement and are described in Coduto (1999). The bearing capacity (q_{cap}) taken from Dames & Moore "Investigation soil report" was of 191 kPa.

Both vertical force (P) and moment (M) present at the support of the structure induce pressure to the soil. The moment is transformed into a force being applied with an eccentricity (e), and an equivalent pressure (q_{equiv}) can be calculated and compared to the bearing capacity. A quick way to account for this is to use an effective footing width B' (Coduto, 2001). The procedure to obtain the equivalent bearing pressure is described in Equations 46 to 48.

$$q_{equiv} = \frac{P + W_f}{B' D} - u_d < q_{cap} \tag{16}$$

$$B' = B - 2e \tag{17}$$

$$e = \frac{M}{P + W_f} \tag{18}$$

Where L is the length of the footing, W_f the weight of the foundation, u_d the pore water pressure (u_d is 0 if at a greater distance than the height of the surface to the bottom of the footing. The eccentricity has to be smaller than B/6 to prevent lifting of the footing.

The calculations suggest that uplift of the foundation would be avoided for every load case. For the load combinations D and D + L, the maximum ratios of pressure over capacity were 0.91 and 1.02, respectively. For the load combinations including earthquake loads, the maximum pressure ratio was 1.33. Coduto (2001) states that geotechnical engineers usually increase the bearing capacity of soils by 33% for earthquake load combinations. This is allowed for four reasons (Coduto, 2001): 1) The shear strength of soils under dynamic loading is higher than during static loading resulting in a greater bearing capacity, 2) Lower factor of safety can be tolerated because earthquake are rare events, 3) Under dynamic loading, settlements are generally smaller and, 4) Larger settlements can be tolerated under rare events because population can accept more visible damage. Because of the variability of the soils, not every soil type will present that type of behavior. Increasing the bearing capacity by 33% is not recommended anymore in recent codes.

Our estimates suggest that the soil under dead and live load can bear the pressure distributed by the footings. Considering that there is an important safety factor for the bearing capacity, this is acceptable. For earthquake combinations, if a 33% increase in the bearing capacity is used, the design could be considered as safe. However, advice from geotechnical experts having studied the specific site conditions would be required.

If eventually the capacity is found to be insufficient, different solutions can be considered. An easy way to decrease the pressure induced by the footing would be to increase its width. In the case of the pier building, because of the presence of the dome structure around the pier, it would only be possible to increase the footing width inside the pier. Because of the restrained space and equipment in place, this solution may be difficult to implement.

An alternate solution would be to reinforce the soil bearing capacity with post-grouting piles through drilled holes. This consists in drilling holes through the footing and soil, and to insert steel pipes filled with grouting. The problem with this option is again the restrained space to drill and the fact that the bearing stratum may be far away from the surface. Other avenues could be studied to reinforce the soil.

It should be noted that Dames & Moore (1973) recommended that the footing should be at least 3.0 m wide and that the soil should have been strengthen with cement grouting under the foundation in drilled holes. To our knowledge, the present footing is 2.24 m and the soil has not been reinforced. This may explain why the capacity is too low under earthquake load combinations.

3.7 Conclusions

A preliminary version of a telescope frame was designed and placed on top of the pier that represents the telescope static and dynamic behavior. The analysis was performed using the International Building Code and the American Concrete Institute code, and the seismic analysis was completed using an equivalent lateral force method. The foundation capacity and soil capacity were evaluated. They were then compared to the forces and steel in place. The most significant results are summarized in Table .

Table 1: CFHT pier building evaluation results summary

	Demand	Capacity	Ratio force vs capacity
Footing bending structural capacity			
Required steel ratio	0.2%	0.27%	0.74
Settlements – Plate load test evaluation			
Gravity load combination	3.6 mm	10.0 mm	0.36
Foundation allowable pressure			
Earthquake load combination	254 kPa	191 kPa	1.33
Gravity load combination	195 kPa	191 kPa	1.02

The following points were concluded:

- The differential settlements were evaluated to be less than 10.0 mm and satisfactory.
- The soil allowable bearing capacity under gravity loads is sufficient as the estimated pressure induced by the footing was equal to the capacity.
- The bearing capacity of the soil under earthquake loads is exceeded by 33%. Since the structure having been designed in 1974, the soil capacity of existed building can increase over time. Also because of the dynamic nature of these loadings, it is common practice to increase the capacity by one-third. This allows considering the capacity as sufficient.

4. Enclosure Footing and Foundation Evaluation

4.1 Applicable Code

The loads are defined by the American Society of Civil Engineers 7 - Minimum Design Loads of Buildings and Other Structures (ASCE 7) 2010. The structural and footing designs are done using limit state design (LSD) and the soil foundation is evaluated using allowable stress design (ASD). For more details please refer to ASCE-7 (2010).

4.2 Geometry

The outer pier covers the inner concrete pier building supporting the telescope. The enclosure building is a 5 storey steel structure of an overall height of 14.9 m and of an outer diameter of 28.8 m. The 1st level is referred as the ground level and the 5th level as the observation level. The inner diameter is of 16.8 m and there is a spacing of 76 mm between the inner concrete pier and the outer steel pier.

The structure is divided in 12 bays along its perimeter. Each column is numbered from 1 to 12. For each level and each bay, the typical bay framing is drawn. The main opening of the enclosure is located at the ground level between columns 1 and 12.

The height from the footing top to the ground level is 0.77 m and the interstorey height for the second and third levels is 3.91 m and 4.01 m, respectively. For both the fourth and observation levels, the interstorey

height is 3.09 m. The fifth level is the observation level and a balcony is located on its slab. The balcony is not shown on the drawings. The dome is placed on top of the observation level on the external ring girder.

The vertical load on the observatory level is distributed to the levels below using both inner and outer columns. The load is then carried by the diagonal columns and the outer columns to the foundation. The tension hangers support the ground and second levels and are attached to the beams of the third level.

Table 2: Dome modeling parameters

Vertical stiffness - K_z (kN/mm)	27.777
Radial stiffness - K_r (kN/mm)	27.777
Tangential stiffness - K_t (kN/mm)	2.777
Center of gravity height over observation level (m)	11.929
Number of spring supports	12

4.3 Materials

Steel sections material properties are defined according to CSA G40.12 - 1971 with a yield stress of 304 MPa, an ultimate stress of 448 MPa and a modulus of elasticity of 200 000 MPa. The reinforcing bars have a yield strength of 413 MPa, and a modulus of elasticity is 200,000 Mpa. Concrete compressive strength is 20.7 MPa and the elasticity modulus is evaluated to be 21,525 MPa.

4.4 Soil

Soil data is taken from the Foundation Investigation Report prepared by Dames & Moore, (1973). The density of such soil varies from 700 kg/m^3 to 2300 kg/m^3, (Dames & Moore, 1973). In the calculation, an average of 1500 kg/m^3 is assumed for simplicity.

The Structural Design Brief for the Peripheral Building (SNC, 1974) for the outer pier uses a bearing capacity of 161 kPa, this value is lower and is used for the analysis.

4.5 Loads

This section of the report presents the load cases and combinations applied to the outer pier structure. The definition of load cases and combinations are provided in details in the ASCE-7 2010. The loads acting on the outer pier include dead, live, ice, snow, wind and earthquake loads. It should be noted that the center of gravity of the dome is located at a 1 m horizontal distance from the center of dome sphere due to the opening in the dome configurations. As a result, all the dome loads are applied as combination of point load and point moments on the center of sphere, which is located at a height of 11.929 m from the observation level.

4.5.1 Load Cases

Dead load

Dead load is the structural mass of the outer pier, which includes the total weight of the construction materials. These loads are obtained from the Structural Design Brief for the Peripheral Building (SNC, 1974) as a pressure load on each floor. They are applied on the beam in the model as vertical uniformly distributed forces. Table 3 presents the dead load applied on each floor.

Table 3: Dead loads per floor

Floor	Pressure (kPa)	Weight (kN)
Ground	2.873	1182.96

2	2.873	1182.96
3	2.873	1182.96
4	2.873	1182.96
Observatory- Peripheral	6.281	2586.35
Observatory- Center	6.281	1506.42
Outer pier total		8824.644

The current dome situated on the outer pier is wished to be replaced to accommodate the new telescope. The current dome weighs 3783 kN and it is approximated that the new dome will have a weight of approximately 5000 kN due to its overall bigger size. The dome dead load is applied as a point load and a point moment on the dome center.

Table 4: Dead load for the dome

Vertical reaction (kN)	Horizontal eccentricity (m)	Moment w.r.t. dome center (kN.m)
-5000	1.0	5000

The total dead weight of the structure including the dome is 13 825 kN or 1 409 240 kg.

Live load

Live load is the load due to the use and occupancy of the building. Similar to the previous section, the live loads are obtained from the original Structural Design Brief for the Peripheral Building (SNC, 1974). It is assumed that live loads have not changed significantly over the years, and they are applied as vertiacal uniformly distributed loads on each beam. Table 5 summarizes the live loads per floor.

Table 5: Live load per floor

Floor	Pressure (kPa)	Weight (kN)
Ground	7.182	2957.42
2	4.789	1971.614
3	4.789	1971.614
4	4.789	1971.614
Observatory – Peripheral	9.576	3943.23
Observatory - Center	4.788	1148.36

Ice load

Since the structure is located on Mauna Kea where freezing ice storms occur, it is necessary to take into account ice loads. It is approximated that the pressure applied by ice load is 68 kg/m^2. For the peripheral building, the vertical force per bay is 5.031 kN/m of height. The ice load is applied over half the circumference of the outer pier. The dome also has to resist ice loads on half of its surface. The dome loads are summarized in the following table.

Table 6: Ice load on the dome

Vertical Reaction (kN)	Horizontal Eccentricity (m)	Moment w.r.t. dome center (kN.m)

-851	9.1	7740

Snow load

The pressure applied by snow is approximated to be 150 kg/m^2 on the dome. It is assumed that snow loads can be neglected for the vertical walls of the outer pier. The snow load is applied as a combination of point load and point moment on the center of gravity of the dome.

Table 7: Snow load on the dome

Vertical Reaction (kN)	Horizontal Eccentricity (m)	Moment w.r.t. dome center (kN.m)
-334	0.0	0.0

Wind load

Effect of winds on the structure has also been considered in this study. The maximum wind speed that the structure resists is evaluated to be 78 m/s. The ASCE-7 2010 procedure for dome roofs is used to compute the forces induced on the structure by the wind. This procedure is used for the dome and the outer pier walls. It evaluates a force for each node of the dome. The lateral and vertical wind forces for the dome are summed and applied at a height of 6.865 m from the observation level.

The wind loads applied to the exterior walls are concentrated at each intersection of column and a beam. This method gives a realistic assumption of the wind effects since it considers the positive and negative pressure effects over the whole perimeter of the outer pier. The forces are applied perpendicularly to the surface of the outer pier. The following table summarizes the wind loads. Two cases have to considered according to the ASCE-7 2010, cases A and B.

Table 8: Lateral wind loads cases

Bay	Lateral perpendicular force per vertical meter- Case A (kN/m)	Lateral perpendicular force per vertical meter- Case B (kN/m)
1	7.40	13.72
2	-5.23	2.05
3	-17.87	-15.43
4	-21.15	-21.15
5	-15.09	-15.09
6	-9.03	-9.03
7	-9.03	-9.03
8	-15.09	-15.09
9	-21.15	-21.15
10	-17.87	-15.43
11	-5.23	2.05
12	7.40	13.72

It should be noted that positive forces are compressive forces applied perpendicular to the surface of the outer pier and negative forces are tension forces. Table 9 presents the total lateral and vertical wind loads applied to the dome top.

Table 9: Wind loads on dome

Lateral reaction (kN)	Vertical uplift reaction (kN)	Center of lateral reaction (m)	Center of vertical reaction (m)	Moment w.r.t. dome center (kN.m)
1876	+1855	0.92	0	1718

Earthquake

The ASCE-7 2010 requires the structure to resist earthquake load for 2500 years return period. The structure is assumed to have a low ductility and energy dissipation capability. As a result, in order to have a conservative evaluation, ductility factor (R) is chosen to be equal to 2. The soil in place is evaluated to be a soil class C.

Equivalent static procedure is used to represent the effect of seismic forces on the building. It assumes the response of the structure under seismic excitation is mostly concentrated in the first lateral mode of vibration. The structure is pushed with a lateral force distribution representing the lateral deformation of the structure in its first vibration mode shape. To obtain theses forces it is first necessary to obtain the first natural period of the structure. The chosen fundamental period is of 0.5 seconds. This period is used to get the spectral acceleration at the base of the structure. The spectral acceleration is obtained using the design spectrum which is function of the emplacement and the soil parameters. For a fundamental period of 0.5 seconds and the Mauna Kea site, the design spectral acceleration is 0.5g. The spectral acceleration is then multiplied by the seismic weight which is equal to the dead weight to acquire the base shear. The base shear is distributed over the height of the structure as a triangular distribution. The base shear is equal to 50% of the seismic weight. The forces at each floor are presented in Table 10.

Table 10: Lateral force at each level for the outer pier

Floor	Lateral force (kN)
Ground	28.05
2	169.71
3	315.02
4	427.24
Observatory	1866.40
Dome	4105.88
Total base shear	6912.32

4.5.2 Load Combinations

Following the ASCE-7 requirements, the load cases are combined to represent the worst loading conditions to apply on the structure. It is important to note that no factor is applied to the dome dead load since its mass has more precision and that it is wish to evaluate the capacity with that precise mass. The capacity of the structure is compared to each of the load combination to ensure that the structure meets the requirements. The structural capacity is evaluated using limit state design and the foundations capacity is evaluated using allowable stress design. Each method uses different load combinations. The structural capacity of the beams, columns, bracings and footings are evaluated using limit state design. The following load combinations are used for the LSD, in which, D is the dead load, L the live load, S the snow load, I the ice load, W the wind load and E the earthquake load. Also, D_{Dome} is the dead load of the dome and W_A and W_B are wind load from case A and B, alternatively.

1. $1.4D + 1.0E + 0.2S + 1.2D_{Dome}$

2. $1.4D + D_{Dome}$
3. $1.2D + 1.6L + 0.5S + 0.2I + D_{Dome}$
4. $1.2D + 1.6S + 1.0L + D_{Dome}$
5. $1.2D + 1.6S + 0.5W_A + D_{Dome}$
6. $1.2D + 1.0W_A + 1.0\,L + 0.5S + 1.0I + D_{Dome}$
7. $0.9D + 1.0W_A + 1.0I + D_{Dome}$
8. $0.7D + E + 0.8D_{Dome}$
9. $1.2D + 1.6S + 0.5W_B + D_{Dome}$
10. $1.2D + 1.0W_B + L + 0.5S + 1.0I + D_{Dome}$
11. $0.9D + 1.0W_B + D_{Dome}$

The soils are evaluated using allowable stress design. The combinations used are listed below.

1. $1.0D + D_{Dome}$
2. $1.0D + 1.0L + 0.7I + D_{Dome}$
3. $1.0D + 1.0S + 0.7W_A + 0.7I + D_{Dome}$
4. $1.0D + 1.0S + 0.7W_B + 0.7I + D_{Dome}$
5. $1.0D + 0.75L + 0.75S + D_{Dome} + 0.525I + 0.525W_A$
6. $1.0D + 0.6W_A$
7. $1.0D + 0.6W_B$
8. $1.14D + 0.7E + 1.14D_{Dome}$
9. $1.0D + 0.45W_A + 0.75S + D_{Dome}$
10. $1.0D + 0.45W_B + 0.75S + D_{Dome}$
11. $1.1D + 0.75L + 0.525E + 0.75S$
12. $0.6D + 0.42W_A + 0.42I + 0.6D_{Dome}$
13. $0.6D + 0.42W_B + 0.42I + 0.6D_{Dome}$
14. $0.46D + 0.7E + 0.74D_{Dome}$
15. $1.0D + 0.75L + 0.75S + D_{Dome} + 0.525I + 0.525W_B$

The design checks are done for each of the combinations described to assess the structure and foundation performance.

4.6 Evaluation

Therefore, the footings and foundation have to be assessed. This study presents the design checks and results for each of the member types as well as the dynamic properties and the deflections under earthquake loads.

4.6.1 Footing

The structural capacity of the concrete footing is verified. It is assumed that only axial loads are transmitted to the footing and that the diagonal columns do not induces moments. The Structural Design Brief for the Peripheral Building (SNC, 1974) also made that assumption.

The bending and shear capacities in the tangential and radial directions have to be assessed as well as the tension in the hoops. The bending capacity of the section is evaluated using Response2000 and the shear capacity using CAN/CSA-A23.3-04 requirements.

The bending moment around the tangential axis of the footing is resisted by the reinforcement bars parallel to the width of the footing. The bending moment around the radial axis is resisted by the reinforcement parallel

to the length of the footing. The shear for a radial section is resisted by the concrete and steel shear stirrups. The shear for a tangential section is resisted by concrete in the tangential direction in the bottom part of the footing. Finally, the longitudinal tension in the circular footing induced by the radial horizontal forces of the columns is resisted by the longitudinal steel reinforcement bars.

The following table presents the demand to capacity to ratio for each ultimate limit state.

Table 11: Structural performance of the footing

Ultimate state	Load combination	Demand to capacity ratio
Bending around tangential axis	$1.4D + 1.0E + 0.2S + 1.2D_{Dome}$	0.24
Bending around radial axis	$1.4D + 1.0E + 0.2S + 1.2\ D_{Dome}$	0.49
Shear for tangential section	$1.4D + 1.0E + 0.2S + 1.2\ D_{Dome}$	0.44
Shear for radial section	$1.4D + 1.0E + 0.2S + 1.2\ D_{Dome}$	0.33
Tension in hoops	$1.2D + 1.6L + 0.5S + 0.2I + 1.0\ D_{Dome}$	0.41

It is concluded that the footing has sufficient capacity since the ratio of demand vs. capacity are below 1.0.

4.6.2 Foundation

The foundations have to be evaluated using allowable stress design load combinations. The bearing capacity and the sliding of the footing are checked in this section.

4.6.2.1 Bearing capacity

It is also necessary to evaluate if the soils supporting the footings can resist the loads transmitted. The pressure induced by each column to the footing is assumed to be equally distributed to the soils via the footing over its tributary area, the total area of footing divided by 12 columns. The pressure applied on the soil has to be smaller than the bearing capacity of the foundation.

The bearing capacity from the Dames & Moore Soil Report evaluates the bearing capacity to 191 kPa. Although the Structural Design Brief for the Peripheral Building (SNC, 1974) uses a bearing capacity of 161 kPa. To obtain conservative results, the value of 161 kPa is used for the checks. The pressure includes the weight of the footing and of the soil in place over the footing. The bearing capacity results for the worst column for the earthquake load combination and gravity load combination are given in the next table.

Table 12: Bearing capacity performance for earthquake and gravity loads

Bearing capacity (kPa)	Demand to capacity ratio for $1.1D + 0.75L + 0.525E + 0.75S$	Demand to capacity ratio for $1.0D + 1.0L + 0.7I + 1.0\ D_{Dome}$
161	0.97	0.66

The bearing capacity for earthquake and gravity loads is not exceeded. The capacity is concluded to be sufficient.

4.6.2.2 Sliding of the footing

The sliding of the foundation is also verified. It consists of checking if the total lateral load is smaller than the sliding capacity. The sliding capacity is the summation of the friction between the footing and the foundation and of the passive pressure soil resistance placed around the footing.

The sliding of the footing calculations procedure was taken from Coduto (2001). It assumes the sliding resistance to be dependent on the allowable coefficient of friction of the soil, the area of the footing, the axial

load applied on the foundation. The loads are also resisted by passive pressure which is dependent on the soil type and weight. The results are summarized in the next table.

Table 13: Sliding capacity performance for earthquake loads

Demand to capacity ratio for $0.46D + 0.7E + 0.74D_{Dome}$	Demand to capacity ratio for $1.14D + 0.7E + 1.14D_{Dome}$
0.74	0.60

The load combination $0.46D + 0.7E + 0.74D_{Dome}$ results in a lower ratio because of the lower axial loads compared to the load combination $1.14D + 0.7E + 1.14D_{Dome}$. The sliding capacity of the structure is sufficient to resist the loads applied.

4.6.2.3 Deflections

Deflections of the structure under earthquake loadings are needed to be evaluated to verify if the outer pier is interacting with the concrete inner pier and if the ASCE-7 2010 interstorey drifts limitations are respected. The distance at the fourth level between the outer and inner pier is 76.2 mm and the maximum interstorey drift is 2.5% according to the ASCE-7 2010. The displacements induced by the earthquake lateral forces applied are elastic deformation. To obtain the maximum inelastic displacements, the deformations need to be multiplied by the deflection amplification factor which is equal to 2. The deflections are checked for each level in X and Y directions in tables below.

Table 14: Outer pier deflections in Y direction summary

Level	Elastic displacements (mm)	Inelastic displacements (mm)	Demand to capacity ratio	Interstorey drifts
Ground	3.0	6.0	0.08	0.77%
2	18.0	35.9	0.47	0.77%
3	34.5	68.9	0.90	0.82%
4	47.0	94.0	1.23	0.81%
Observation	50.6	101.1	-	0.23%

Table 15: Outer pier deflections in X direction summary

Level	Elastic displacements (mm)	Inelastic displacements (mm)	Demand to capacity ratio	Interstorey drifts
Ground	2.4	4.9	0.06	0.63%
2	14.5	29.1	0.38	0.62%
3	27.9	55.7	0.73	0.66%
4	38.1	76.2	1.00	0.66%
Observation	41.8	83.5	-	0.24%

It is observed that the deflections in Y direction are higher than in X direction. The first principle approach of the bracings design taught us that more bracings are participating in X direction than in Y directions which permits us to expect higher deflections in Y direction. This confirms again that it was a good decision to perform the analysis in Y direction.

The interstorey drifts are all under 2.5% meaning the structure is stiff enough for the ASCE-7 requirements. The deflections in Y direction are higher than the space between the concrete internal pier and the outer steel pier which makes us conclude that interaction between both structures can be expected during major earthquake events. It should also be noted that the pier will also sustain deflections that are not necessary in the same direction as the outer pier because they have different vibration periods. The deflections in X direction are smaller that the allowable space between the two structures.

4.7 Conclusions

The larger dome inducing higher forces to the enclosure and the new code requirements justify assessing the capacity of the outer pier. The seismic requirements were analyzed with great care since the modern codes prescribes much higher demands than the ones from the original design. The load cases and combinations were defined using the ASCE-7 2010 requirements. The capacity of the footing and foundation were evaluated. The following points were concluded:

- The footings have sufficient bending, shear and tension structural capacity to resist the demands of every load combination. The ratios of demand to capacity are under 0.50.
- The maximum bearing pressure induced by the footing to the foundation is 97% of the 161 kPa bearing capacity. The sliding capacity is also sufficient since the demand to capacity ratio is of 0.74.

References

1. ACI 318-08. (2008). “Building Code Requirements for Structural Concrete and Commentary.” American Concrete Institute, Farmington Hills, Michigan, USA.
2. ACI 371R-98. (1998). “Guide for the Analysis, Design, and Construction of Concrete-Pedestal Water Towers.” American Concrete Institute, Farmington Hills, Michigan, USA.
3. American Institute of Steel Construction, (2005). “Specification for Structural Steel Buildings (ANSI/AISC 360-05)” American National Standards Institute.
4. American Society of Civil Engineers, (2010). “Minimum Design Loads of Buildings and Other Structures – ASCE 7”. Reston Virginia, USA.
5. American Society of Civil Engineers. (1999). “Guideline for Structural Condition Assessment of Existing Buildings - ASCE 11.” Reston, Virginia, USA.
6. American Society of Civil Engineers. (2005). “Minimum Design Loads of Buildings and Other Structures – ASCE 7.” Reston, Virginia, USA.
7. Bentz E. and Collins M.P. (2000), “Response-2000, Version 1.0.5, Reinforced Concrete Sectional Analysis using the Modified Compression Field Theory”. University of Toronto, Ontario, Canada.
8. Bracci, J. M., Kunnath, S. K., Reinhorn, A. M. (1997) “Seismic Performance and Retrofit Evaluation of Reinforced Concrete Structures.“ Journal of Structural Engineering, Vol. 123, No. 1.
9. CAN/CSA-A23.3-04, (2004) “Design of Concrete Structures”. Canadian Standard Association.
10. Cantell, S. F. (2005). “The Adaptive Reuse of Historic Industrial Buildings: Regulation Barriers, Best Pratices and Case Studies.“ Virginia Polytechnic Institute and State University, blacksburg, Virginia, USA.
11. CFHT. (1974). “Pier Building Drawings.” Surveyer Nenniger and Chênevert Inc.
12. Chopra, A. (2007). “Dynamics of Structures – Theory and Applications to earthquake Engineering.” Prentice-Hall, New Jersey, USA.

13. Coduto, D.P. (2001). "Foundation Design – Principles and Practices". Prentice-Hall, Upper Saddle River, New Jersey, USA.
14. Computers and Structures, Inc., Berkley. (1998). "SAP2000 - Basic Analysis Reference." Berkley, California, USA.
15. Computers and Structures, Inc., Berkley. (1999). "ETABS User's Manual." Berkley, California, USA.
16. Computers and Structures, Inc., Berkley. (2006). "Concrete Shell Reinforcement Design Technical Note and Design Information." Berkley, California, USA.
17. Computers and Structures, Inc., Berkley. (2009). "Structural Analysis Program – SAP2000 Version 14." Berkley, California, USA.
18. Dames and Moore. (1973). "Foundation Investigation Report." Hawaii, USA.
19. Dames and Moore. (1974), "Final Investigation Report." Hawaii, USA.
20. Day, R. W. (1999). "Geotechnical and Foundation Engineering: Design and Construction." McGraw-Hill, New York, USA.
21. Grundmann, W. (1997). "A Canada-France-Hawaii 12-16m Telescope Study."
22. IBC, (2003). "International Building Code". International Code Council, Country Club Hills, Illinois, USA.
23. IBC. (2006). "International Building Code." International Code Council, Country Club Hills, Illinois, USA.
24. Langston, C., Wong, F. K. W., Hui, E. C. M., Shen, L-Y. (2008) "Strategic Assessment of Building Adaptive Reuse Opportunities in Hong Kong." Building and Environment, Vol 43, pp. 1709-1718.
25. Pillai, S. U., Marie-Anne Erki, and D. W. Kirk. (2008). "Reinforced Concrete Design." Tata McGraw-Hill, Toronto, Ontario, Canada.
26. Priestley, M. J. N., Seible, F. and Calvi, G. M. (1996). "Seismic Design and Retrofit of Bridges." John Wiley and Sons, Inc. New York, NY, USA.
27. SAP2000, Computers and Structures, Inc., Berkley. (2009). "Structural Analysis Program". Version 14. Berkley. California, USA.
28. SNC, (1974). "Structural Design Brief for the Peripheral Building", Canada-France-Hawaii Telescope.
29. Stavridis, L. T. (2000) "Simplified Analysis of Layered Soil-Structure Interaction." Journal of Structure Engineering, ASCE, February: 224-230.
30. Terzaghi, K. and Peck, R. (1967). "Soil Mechanics in Engineering Practice 2nd ed.." John Wiley, New York, New York, USA.
31. Vion, P. and Deschamps, D. (2010). "L'expertise et la réparation du pont en arc de Maamelten (Liban)." 17e Colloque sur la progression de la recherche québécois sur les ouvrages d'art, Québec, Canada, 10-11 May 2010.
32. Winkler, E. (1867). "Die Lehre von der Elasticitaet und Festigkeit." 1867, Prag, Dominicus

APPENDIX G. NGCFHT PRELIMINARY OPTICAL DESIGN CONCEPTS FOR THE 2010 CFHT USERS MEETING IN TAIPEI

Herzberg Institute of Astrophysics/
Institut Herzberg d'astrophysique

ngCFHT
Preliminary Optical Design Concepts for the 2010 CFHT users meeting in Taipei

John Pazder

REVISION 1.0

12/14/2010

Scope

This report is limited optical design of wide field telescopes for a fibre feed spectrograph to replacing CFHT with 'ngCFHT'.

Summary

This report outlines some results of some Zemax results from exploring the concept of replacing CFHT with a telescope dedicated to wide field fibre fed spectroscopy. This would be a project similar to the WFMOS project, but with 100% time. Feasibility of a 10m WFMOS is shown but more work is needed to investigate specific risk areas such as fibre feed focal ratios.

1 WFMOS background

WFMOS is a wide-field optical multi-object spectrograph proposed for Subaru. The instrument has 2400 fibres at the focus of the 1.5 degree FOV HyperSuprime corrector. The fibres feed three identical VPH spectrographs. Two major studies have been done, one lead by JPL and completed in Jan of 2009 and a second lead by AAO, completed in March of 2005. The ngCFHT proposal is essentially the WFMOS proposal on a 10m telescope as a replacement for the current CFHT telescope. ngCFHT plans to leverage the previous WFMOS work, shamelessly copying from these proposals where possible.

The WFMOS reports are available on the internet, the 2005 AAO report is located at:
http://www.gemini.edu/files/docman/science/aspen/WFMOS_feasibility_report_public.pdf

and the 2009 JPL report located at:
http://member.ipmu.jp/masahiro.takada/WFMOS_Study_Summary_Jan30_2009.pdf

The major change from WFMOS is the corrector on the larger telescope, this report specifically targets the problem of the feasibility a 1.5 degree corrected FOV on a 10m telescope.

2 Design Requirements

The preliminary top level design requirements for the science goals are:

Table 1: Top Level Requirements

Top Level Requirements for Science Goal	
Aperture	> 8m (exposure times up to 4h)
Multiplexing	> 3000
Field of view	> 1.5 sq. degrees
Spectral resolutions	R1500 to R20,000

Wavelength range	400nm to 1000nm

As this study was primarily to look at the feasibility of a 1.5 degree corrector on a 10m telescope, corrector designs were investigated with the following requirements:

Table 2: WFC study requirments

Wide Field Corrector Requirements used for Study	
Aperture	10m, segmented
Field of view	1.5 degrees field diameter (circular format)
Wavelength range	400nm to 10,000nm
Image quality (at fibre)	< 0.3" – 0.4" (rms spot size diameter)
Vignetting	< 15%
Fibre feed focal ratio	f/2.3 goal (f/2 requirement)
Exit pupil	Near telecentric (within a degree or two)
Primary mirror Focal Length	< 17.5m (as fast or faster than Keck)

3 Design considerations

The goal of a wide field spectroscopic survey is to maximize the light grasp and multi-object multiplexing, while minimizing the cost. An additional consideration for these science goals is to get on sky as soon as possible to maximize the first light science impact.

To get on-sky quick the current concept is to replace the existing CFHT dome with a calotte dome on the current pier. This limits the dome size to ~18m radii, which fits a Keck telescope (f/1.75 primary). Push back to the mechanical engineer looking into the dome (Kei Szeto) for larger dome to fit a longer focal length primary mirror was a no-go, indicating that the dome is size near the maximum size practical.

Competing with the drive to fast primary to minimize dome size is the focal ratio to feed the fibres. The leading fibre optics supplier for astronomy is Polymicro Technologies. The standard numerical aperture for astronomical fibres is a NA of 0.22+/-0.02. Consultation with Polymicro indicated that custom fibres could be developed as fast as 0.25 NA to 0.27 NA. The equivalent to fibre feed focal ratio is approximately f/2.3 with current fibres and as fast as f/1.85 to f/2 with custom fibres.

The focal ratio requirements require the field corrector on the f/1.75 primary to operate both as a corrector and focal extender. Three element Wynne prime focus correctors, the classic design for a field corrector, are theoretically designed as zero power correctors. As zero power correctors colour correction is not needed, allowing the corrector to be built with just fused silica or crown glasses such as Bk7. In practice, Wynne type correctors are mild focal extenders, extending the focal ratio approximately 10%. The focal extending property works to our advantage, but it was

found classical three element Wynne corrector would not give enough focal extension and more complicated multiple element field corrector designs are probably required both for the focal ratio requirements and for image quality.

Glass size is an important constraint in the design; better image quality can be obtained by allowing larger corrector lens. In exploring designs it was found the problem was very challenging if the largest lens was limited to 1m diameter as no usable solution was found. If a maximum element size of 1.5m diameter was allowed suitable solutions could be found.

Schott information circular "TIE-41 Large Optical Blanks" gives considerable information on optical blanks. Table 1 from that report is reproduced below. It gives a summary of glass availability as a function of size. As indicated in the table, 1.5m sized blanks can be produced with development. Schott has produced N-Bk7 up to diameters of 1.6m but the required homogeneities my not have been produced to this size. Fused silica is also available in the 1.5m diameter range. The largest LSST corrector element is a 1.55m in diameter element. It is anticipated that fused silica will be considerable more expensive than bk7. For this reason, bk7 was used as the baseline for the designs but bk7 or fused silica can be used for the design with similar performance.

Glass Type Family	Melting Technology Min Prod*	Max Dim present capabilities	Max Dim with development	Restricted by	Preferred Glass Types
BK	Cont. Tank 5 tons	∅1000 x 300	∅1500 x 500 or equiv. Vol	CT, CS, ES	N-BK7
LLF, LF, F, SF	Cont. Tank 5 tons	∅1000 x 300	∅1500 x 500 or equiv. Vol	CT, CS, ES	LLF1, LF5, F2, SF6
FK, PK	Discont. Pot	∅360 x 60	∅460 x 100	Cryst, VS	N-FK51A
LAK, LAF, LASF	Discont. Pot	300 x 160 x 43 GD	360 x 280 x 80 GD	Cryst, VS	LAK8, LAK9
KZFS	Discont. Pot	300 x 160 x 43 GD	360 x 280 x 80 GD	Cryst, VS	KZFSN4

Table 1: Glass types and their associated production information

Min Prod*	Minimum production amount needed for high quality
CT:	Casting Time
CS:	Center-
ES:	Edge-
VS:	Volume Striae
Cryst:	Crystallization
GD:	Gross diameter

15% Vignetting was allowed at the edge of the field in the design. This 0.15 magnitude loss is generally viewed as acceptable in astronomical systems, and allows a larger field with smaller lens, with minimal impact on science.

4 Preliminary Designs

4.1 Design presented in Taipei report

The design presented at Taipei in the "A Next Generation CFHT: technical" power point was a intended to show feasibility of a 1.5 degree wide field corrector on a 10m, not to present an optimal design. The design used the prescription for HyperSuprime in the 2005 WFMOS feasibility report as the starting point, removing the ADC's, and redesigning for a 10m telescope. All glasses are bk7, but fused silica could have been used equally well. Layout and spot diagrams and vignetting are shown in figures 1 to 4.

The field of view is 1.5 degrees diameter, or 1.7 sq. degrees. Image quality is 0.4" RMS spot diameter at the edge of the field and 0.34" at the centre of the field. The design is telecentric to within 2.5 degrees. The largest element is 1.54m. The design uses many more element than would usually be considered necessary for a WFC. These elements allow the corrector to work as a focal length extender, providing an output focal ratio of f/2.06. The design utilizes 6 elements, in the next section it is shown that a simpler solution can be found with fewer elements.

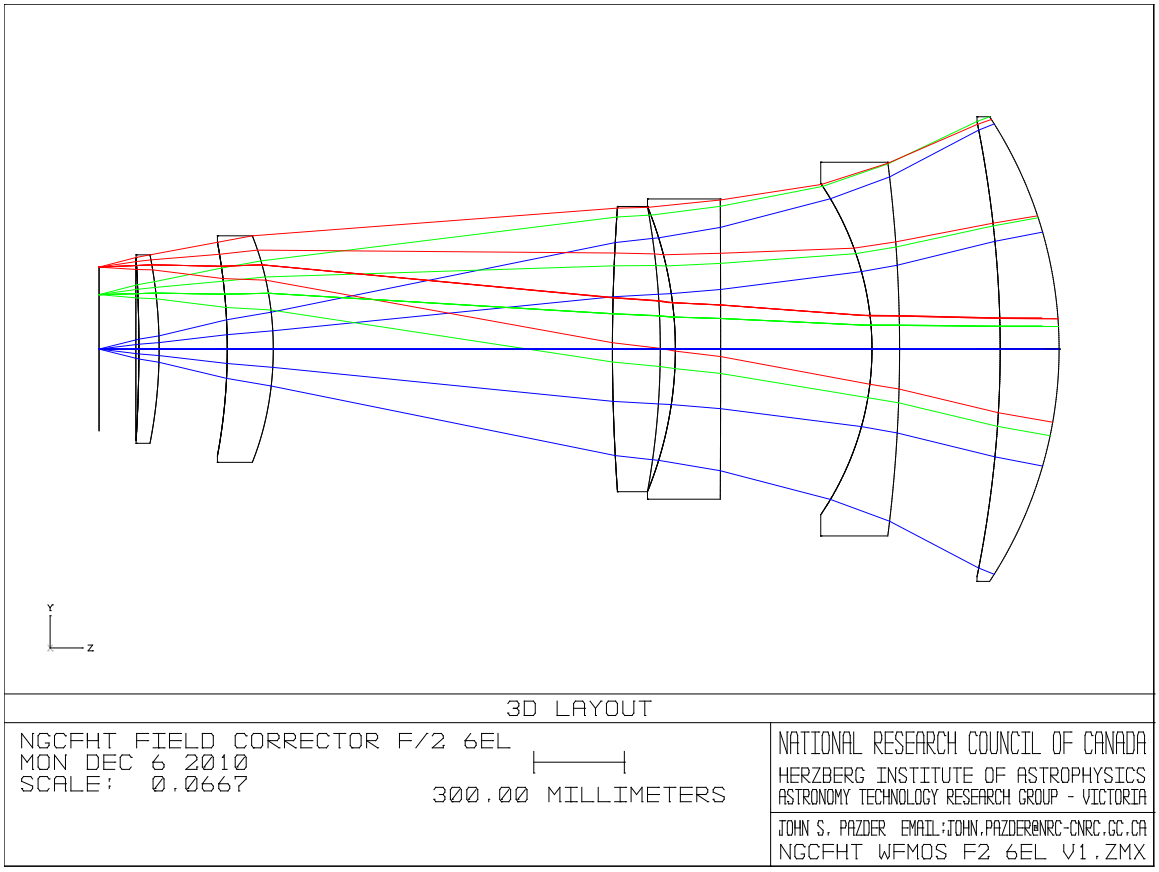

Figure 1: ngCFHT field corrector presented at Taipei

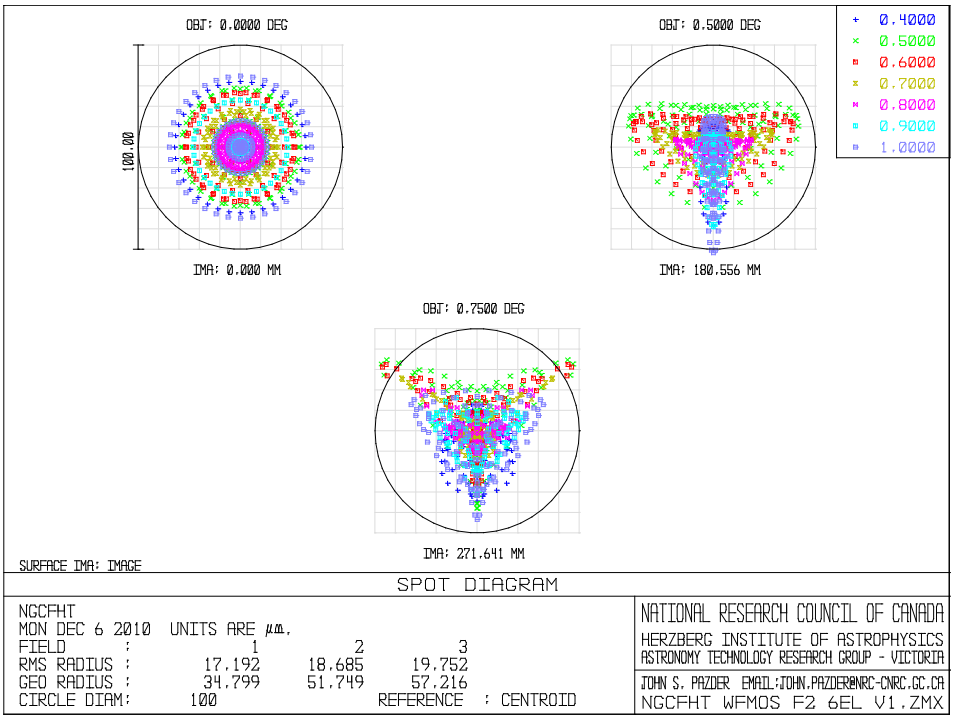

Figure 2: Spot diagrams for Taipei design (circle is 1")

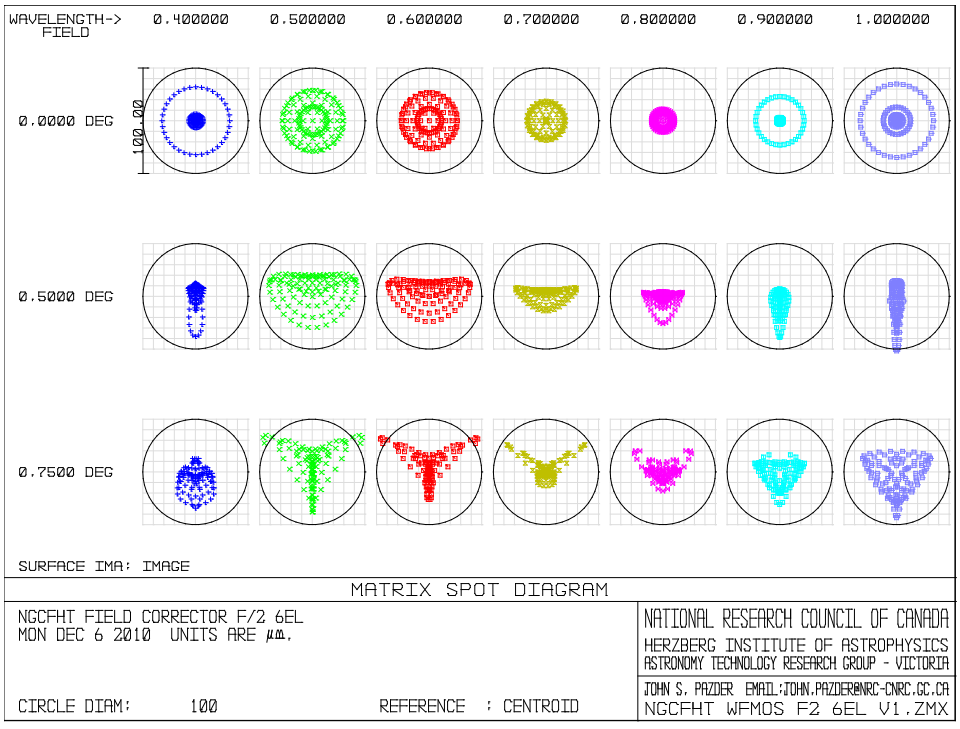

Figure 3: Spot matrix for Taipei design (circle is 1")

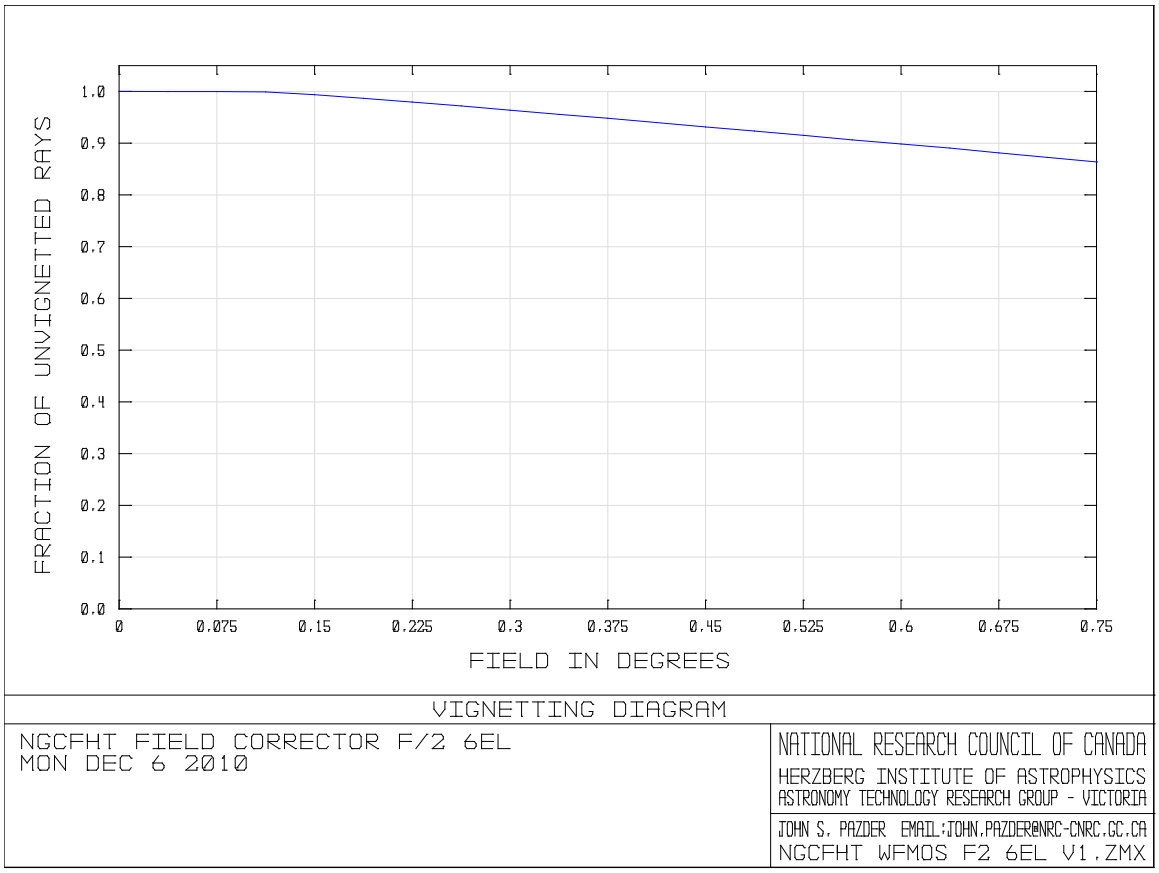

Figure 4: Vignetting for Taipei design

4.2 Five element corrector design

The Taipei design can be simplified by removing one of the elements near the detector making the corrector a 5 element system. The performance is virtually the same, with 0.37” RMS diameter spots at the edge of the field and 0.32” at the centre of the field. Telecentricity is the slightly better being within 2.1 degree. The largest element remains unchanged and the focal ratio is slightly faster at f/2.04. The design is shown in figures 5 through 8.

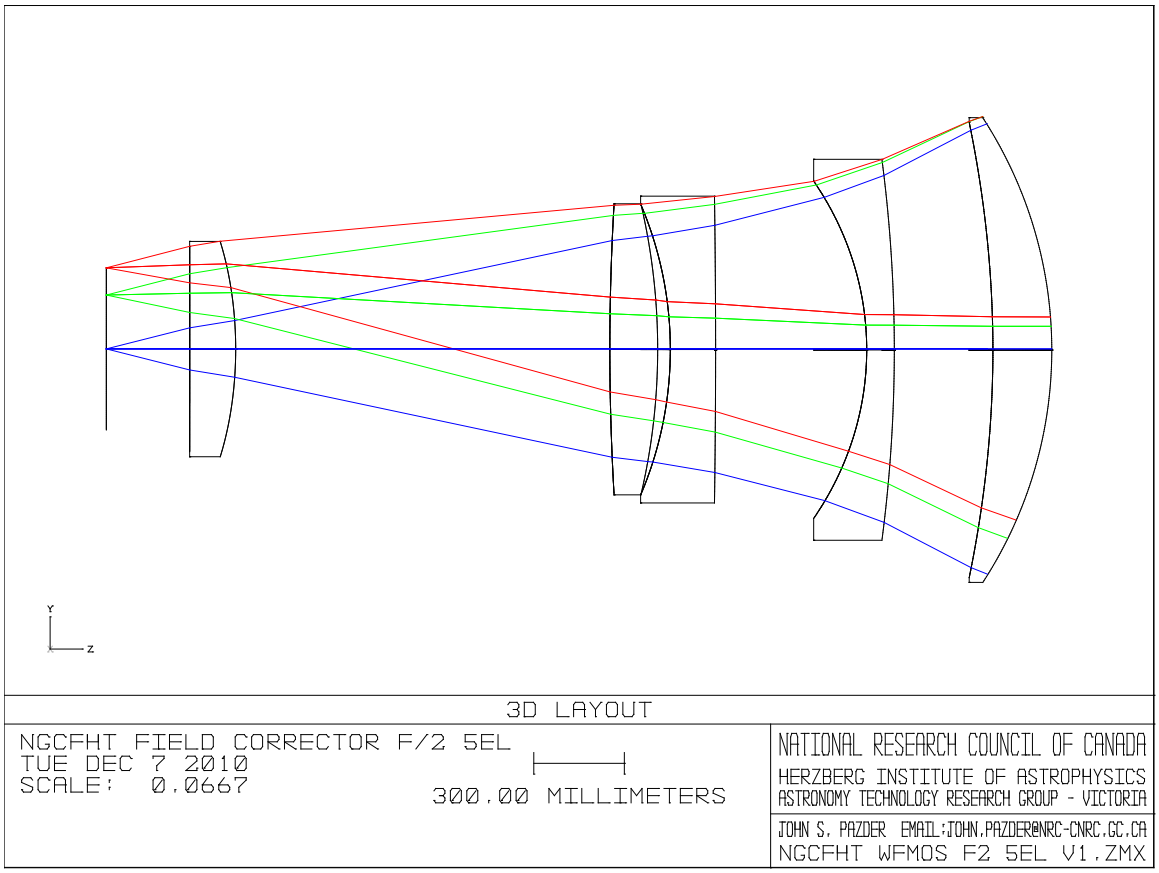

Figure 5: 5 element ngCFHT corrector

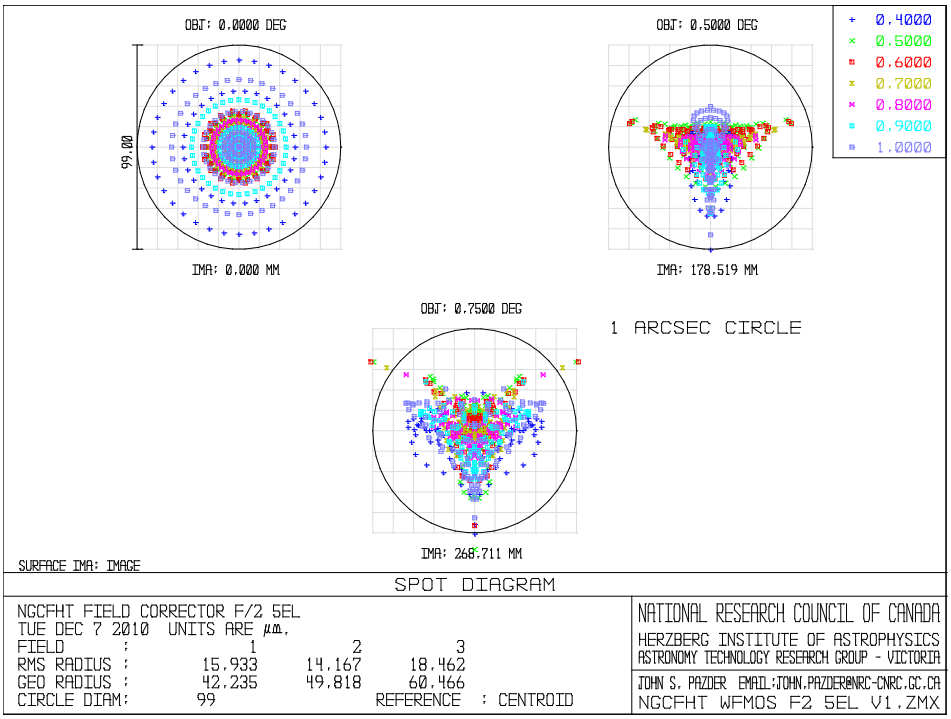

Figure 6: Spot diagram for 5 element design (circle is 1")

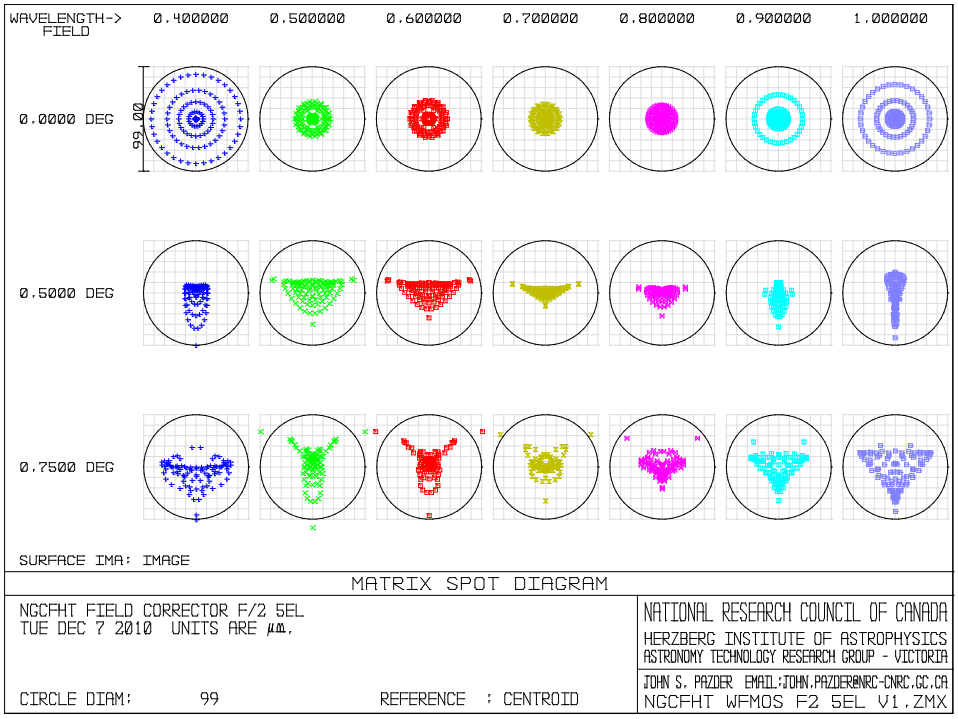

Figure 7: Spot matrix for 5 element design (circle is 1")

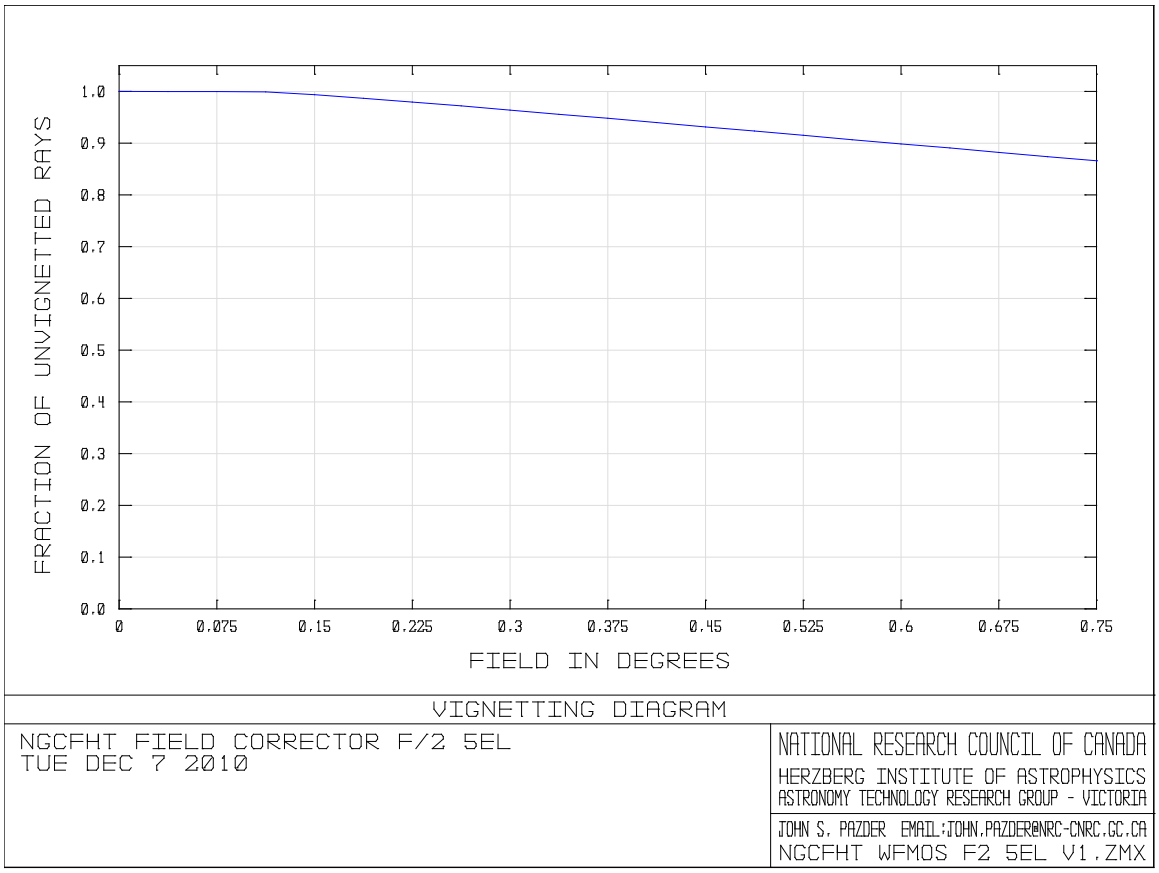

Figure 8: Vignetting for 5 element design

4.3 Four element design

A brief attempt at a simpler 4 element design was made. As anticipated, with fewer elements it becomes harder to both lengthen the focal length and correct the field with using just n-bk7 glass. The result is not conclusive that it cannot be done but it is consistent with experience in that image quality would be poorer and better image quality the focal ratio would be closer to the primary mirrors focal ratio. The output focal ratio is f/1.85 and the image quality is 0.57" RMS spot diameter at the edge of the field and 0.3" at the centre. The largest element remains at 1.54m. The show stopper for this design is the focal ratio is faster than what we understand that fibres can be made to accept. A more detailed study is necessary to determine the feasibility of a four element design. A layout and spot diagram is show below in figures 9 & 10.

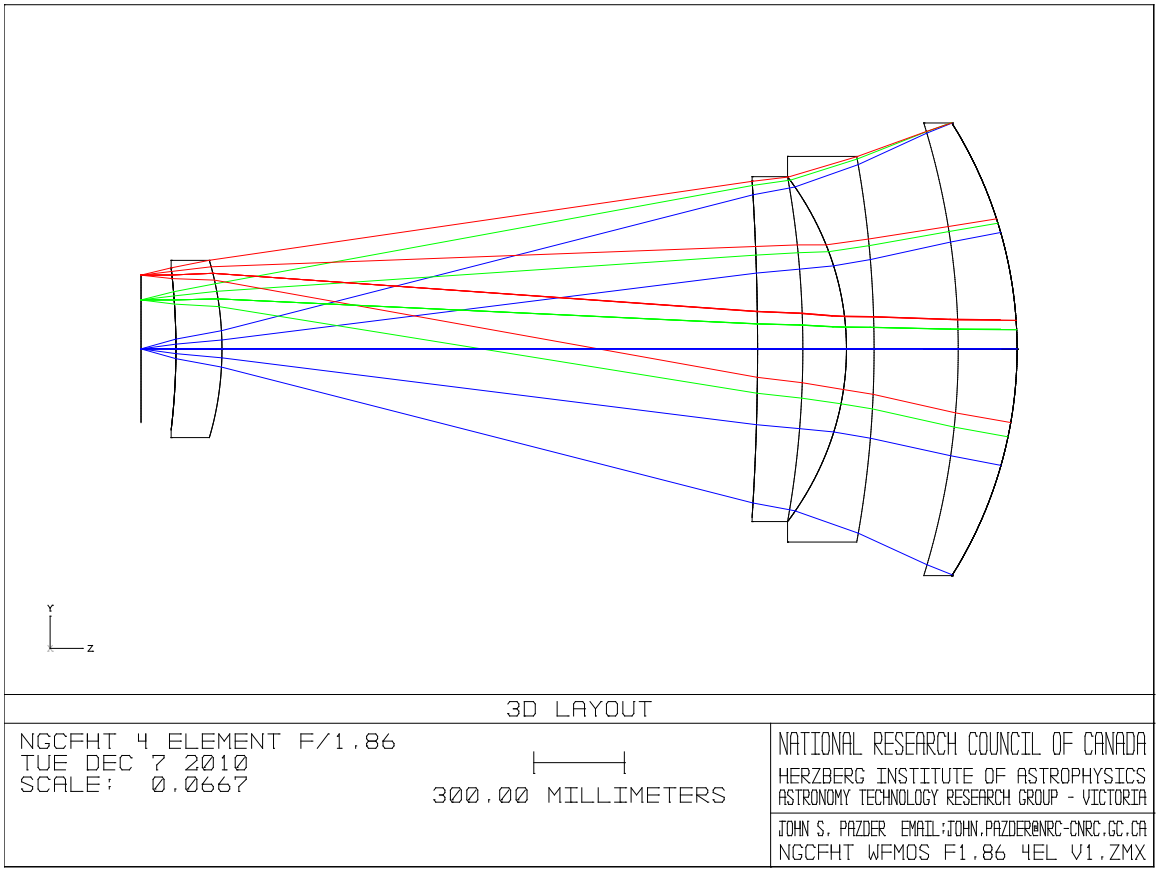

Figure 9: ngCFHT 4 element field corrector

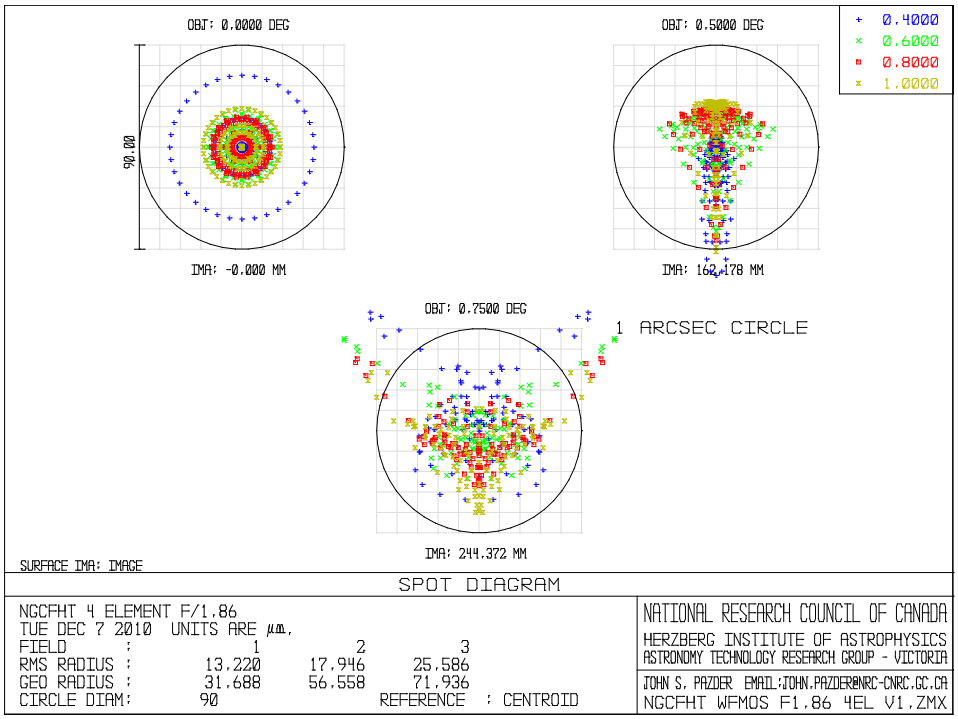

Figure 10: Spot diagram for 4 element design

5 Three Mirror Anastigmat design

A Three Mirror Anastigmat (TMA) design similar to the LSST but without the refractive corrector was explored. This TMA design form is often referred as a Rumsey or Korsh design, for this report we simply use the general term TMA. The LSST was used as the starting point and the refractive corrector was removed, the focal ratio targeted to f/2.5 (to use existing fibre technology) and the focal plane was placed so it was at the secondary mirror to make a convenient fibre location. As this concept was envisioned to be based on the LSST mirror polishing process of two curvatures on the same primary substrate the aperture was kept the same as LSST at 8.36m. The design is shown in figures 11, 12 & 13.

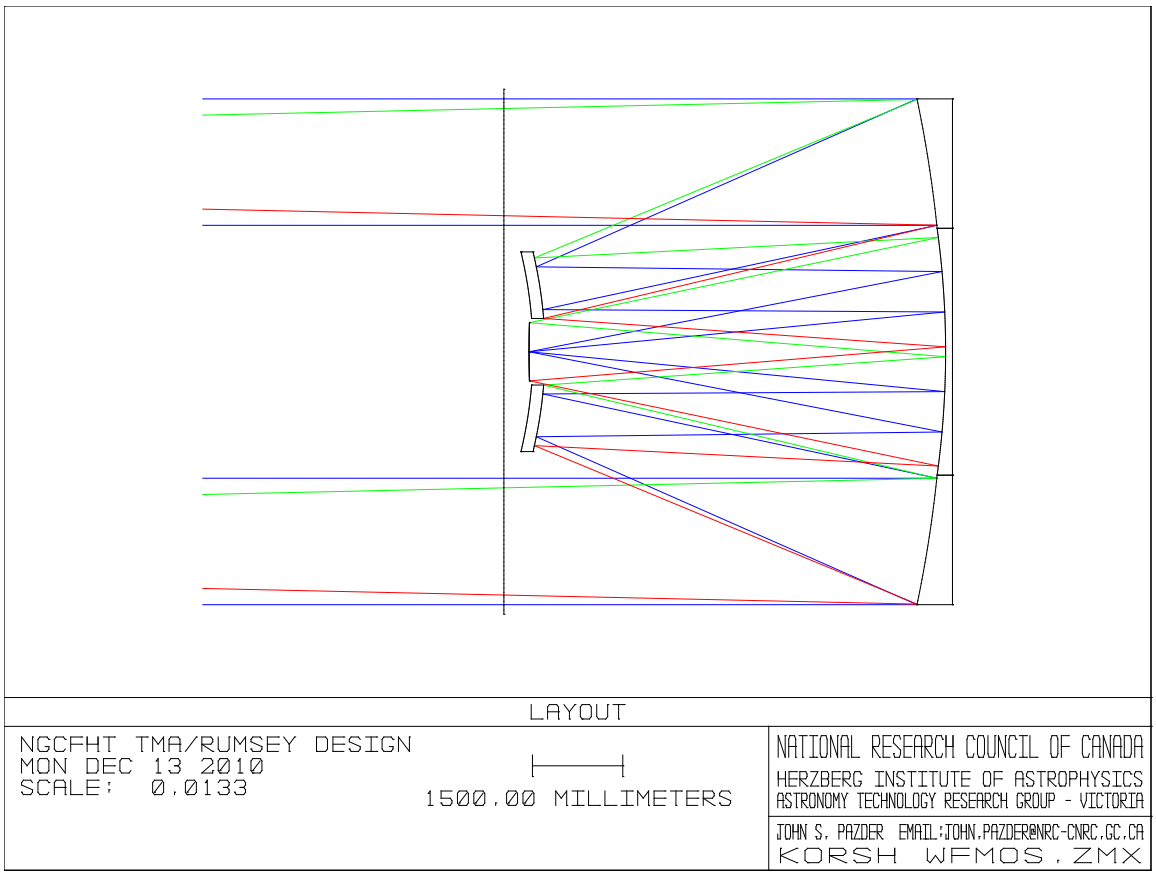

Figure 11: ngCFHT TMA design f/2.5, 8.36m, 2.5 degree FOV

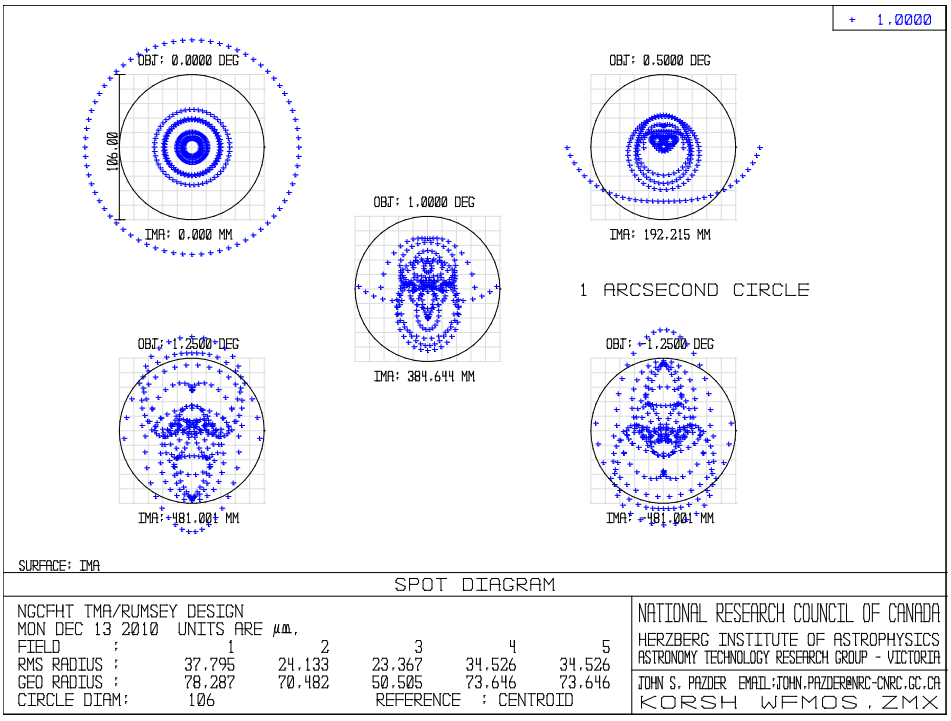

Figure 12: Spot diagram for TMA design

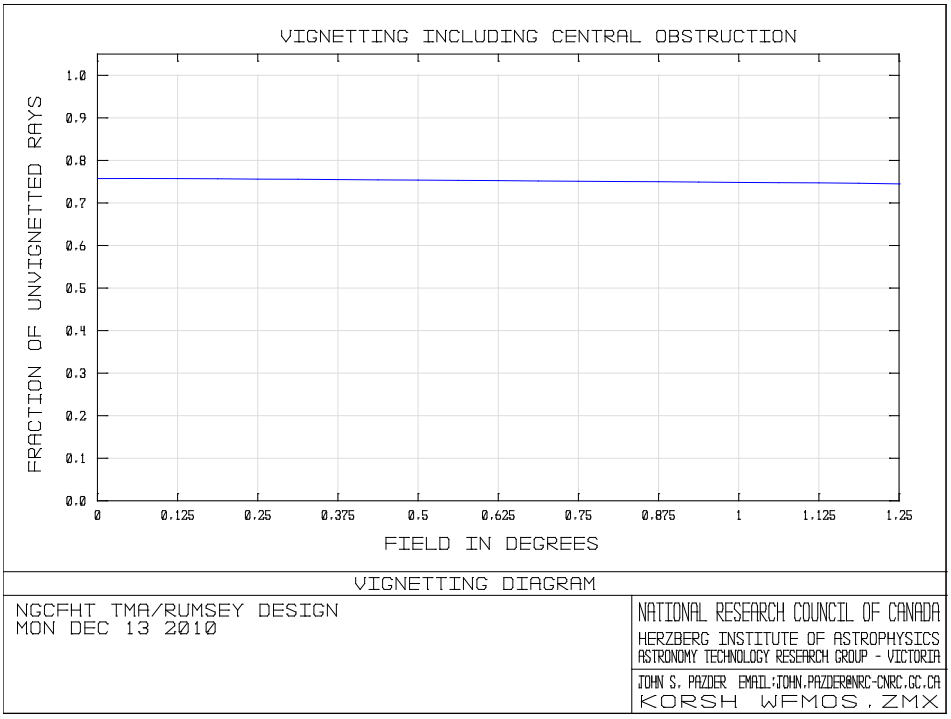

Figure 13: Vignetting for TMA design

The system was optimized to a 2.5 degrees diameter field of view (circular format) or 4.9 sq degrees. The design has an image quality of 0.7" RMS spot diameter at the centre of the field, 0.5" in the middle area and 0.7" at the edge. The central obstruction in this design is 4m so the effective unobstructed aperture is 7.34 meters. The primary is currently fairly fast, f/1.2, the speed of the LSST primary.

The image quality is not quite to specification but it can be improved by lengthening the system with a slower primary or reducing the field of view. This was not explored due to time constraints in the study.

The design is attractive in that the field of view is not limited by the size of refractive corrective optics (~1.5m) but only by the optical aberrations. The wider field of view gives a larger A-Omega. For the design A-Omega is 207 m^2-deg^2. The equivalent aperture to get the same A-Omega with 1.7 sq. degree field (as before) is a 12.2m telescope, thus it is competitive with the pervious 10m designs for some science programs.

A TMA design is an interesting option for the ngCFHT. A very limited amount of time was spent on this and the author feels that more time would be warranted. It is possible to apply the same design form to a segmented primary by placing the ~4m tertiary mirror in front of the segmented primary. Conceptually this design form can be viewed as two element reflective field corrector with a hyperbolic primary.

6 Fibre Numerical Aperture

Existing optical fibres for astronomy, such as the Polymicro FBP, have a numerical aperture of 0.22+/-0.02 which corresponds to f/2.27. With tolerances, the f/# range is f/2.5 to f/2.08. As discussed in section 4, to fit the design into the dome we want ~f/2, which is on the lower end of the stock f/# tolerance range. A discussion with Polymicro indicated that the fibre numerical aperture can be increased with greater fluorine doping in the cladding. It was speculated that NA's of 0.25 to 0.27 (f/2 to f/1.85) can be achieved. The effect on Focal Ratio Degradation (FRD) is hard to estimate. FRD can be caused by non-uniformity in the cladding. It is possible increasing the doping in the cladding may have an effect on FRD. Polymicro is able to proto-type a FBP fibre with enhanced fluorine doping and the author advises to move ahead with a proto-type given the impact on the overall design. Fibres can be feed close to the NA of the fibre, but some margin must be left for fibre bending. If the angle of incidence of the light exceeds the NA of the fibre light loss will occur as coupling into the cladding occurs. Further investigation is needed to determine safe margins between the feed NA and fibre NA.

7 Thin-Thick Fiber concept

The 2005 WFMOS feasibility study considered an alternative concept to developing high NA astronomical fibres. A two fibre system with A high-NA **thin** fibre (NA >0.28) used at the telescope feed and this would be coupled to a **thick** "conventional astronomical' fibre fed at f/4. The thin fibre would be a very short run, order of meters, thus would not be constrained in terms of having as good blue transmission as the thick fibre. In the report it appears that a specific thin fibre has not been identified, and fibres with reasonable blue transmission were being sought from fibre manufactures.

This concept requires a some what complex thin to thick fibre coupler as show in Figure 14. This type of coupler was used in FMOS, but with any fibre coupler, losses occur.

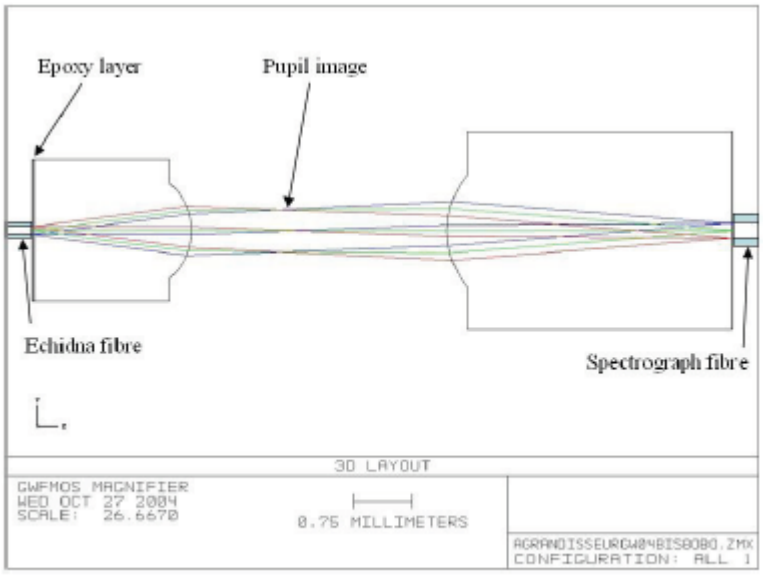

Figure 125. FMOS type design of the Gemini WFMOS connectors.

Figure 14: Thick thin fibre coupler concept from 2005 WFMOS report.

8 Spectrograph design changes

This report has focused on the telescope design. Modifications are also required to the spectrographs. With the larger 10m aperture the spectrographs as described in the WFMOS reports will have to be either scaled up in size for a larger collimator beam diameter or a larger included angle (and greater grating line frequency) to keep the same resolution. A larger included angle will result in lower diffraction efficiency, assuming the gratings in the WFMOS report were sized for optical cost and efficiency. The 2009 WFMOS study had a 500mm grating size, and a simple scale up to 10m from 8.2m would result in a 610mm grating, increasing the complexity and cost of the spectrographs.

9 Conclusions

A WFMOS which fits in a dome on the CFHT pier is possible. Critical to the designs is feeding fibre at f/2 or faster. As an immediate propriety feeding fibres at f/2 or faster must be verified as viable by pro-typing higher NA fibres or the thick-thin fibre concept should be explored further. TMA design look intriguing should be explored in the feasibility stage. The designs presented in this report are simple demonstrations of proof of concept. They are preliminary concept and further optimization will improve the designs and reduce cost. Ghosting effects must also be considered as the designs are advanced.